TWO-STEP HYDROTHERMAL SYNTHESIS OF MANGANESE OXIDE IMPREGNATED FRUIT WASTE DERIVED ADSORBENT FOR CATIONIC DYE REMOVAL

FATHIMATH AFRAH SOLIH

FACULTY OF ENGINEERING
UNIVERSITI MALAYA
KUALA LUMPUR

2025

TWO-STEP HYDROTHERMAL SYNTHESIS OF MANGANESE OXIDE IMPREGNATED FRUIT WASTE DERIVED ADSORBENT FOR CATIONIC DYE REMOVAL

FATHIMATH AFRAH SOLIH

THESIS SUBMITTED IN FULFILMENT OF THE REQUIREMENTS FOR THE DEGREE OF DOCTOR OF PHILOSOPHY

FACULTY OF ENGINEERING
UNIVERSITI MALAYA
KUALA LUMPUR

2025

UNIVERSITI MALAYA

ORIGINAL LITERARY WORK DECLARATION

Name of Candidate: Fathimath Afrah Solih

Matric No: 17013869/2

Name of Degree: Doctor of Philosophy

Title of Thesis: Two-Step Hydrothermal Synthesis of Manganese Oxide Impregnated Fruit Waste Derived Adsorbent for Cationic Dye Removal.

Field of Study: Heath, Safety and Environment (Chemical and Process)

I do solemnly and sincerely declare that:

(1) I am the sole author/writer of this Work.
(2) This Work is original.
(3) Any use of any work in which copyright exists was done by way of fair dealing and for permitted purposes and any excerpt or extract from, or reference to or reproduction of any copyright work has been disclosed expressly and sufficiently and the title of the Work and its authorship have been acknowledged in this Work.
(4) I do not have any actual knowledge, nor do I ought reasonably to know that the making of this work constitutes an infringement of any copyright work.
(5) I hereby assign all and every right in the copyright to this Work to the Universiti Malaya ("UM"), who henceforth shall be owner of the copyright in this Work and that any reproduction or use in any form or by any means whatsoever is prohibited without the written consent of UM having been first had and obtained;
(6) I am fully aware that if in the course of making this Work, I have infringed any copyright whether intentionally or otherwise, I may be subject to legal action, or any other action as may be determined by UM.

Candidate's Signature Date:11/4/2025

Subscribed and solemnly declared before,

Witness's Signature Date: 11/4/2025

Name:

Designation:

TWO-STEP HYDROTHERMAL SYNTHESIS OF MANGANESE OXIDE IMPREGNATED FRUIT WASTE DERIVED ADSORBENT FOR CATIONIC DYE REMOVAL

ABSTRACT

The global production of biomass waste is significant, with an estimated 180 billion tonnes generated yearly. In recent years, research has increasingly focused on resource recovery from non-toxic biomass waste due to its high carbon content, renewability, and abundant availability. Therefore, considering the notable characteristics of agricultural waste biomass, this study aims to develop a low-cost fruit-waste-based adsorbent to remove the cationic dye from aqueous solutions. Unlike conventional biomass-based adsorbents, this study introduces a novel hybrid synthesis combining avocado seeds and banana peels, chemically modified to optimize adsorption performance. These inexpensive, carbon-rich biomass materials have mesoporous surfaces and contain oxygenated functional groups, which are crucial for dye removal. Furthermore, hydrothermal carbonization is an innovative and energy-efficient thermochemical process that enhances the yield of adsorbent materials. To further enhance its performance, the adsorbent underwent phosphoric acid activation and manganese oxide impregnation. Chemical activation enhances the physicochemical characteristics of the biomass materials, while manganese oxide impregnation reduces agglomeration and facilitates electrostatic attractions for removing cationic dyes. The physicochemical analysis revealed the metal-impregnated adsorbent (HA/Mn) and acid-activated adsorbent (HA) from avocado seed and banana peel (RA) demonstrated a significant increment in surface area (666 m^2/g) compared to activated HA (535 m^2/g) and unmodified RA (1.19 m^2/g). The functional group analysis indicates that HA/Mn is an efficient adsorbent as the modification introduces additional hydroxyl, carboxyl, carbonyl, phosphate, and manganese functional groups. Adsorption study also revealed that HA/Mn completely

removed the colour, which is 37% to 33% higher than that of the raw avocado seed (63%) and raw banana peel (67%), respectively. HA/Mn also shows 29 % increase in adsorption capacity (199 mg/g) compared to the raw adsorbent banana peel (112 mg/g) and 18 % higher than raw avocado seed (181 mg/g). The validation study demonstrated that HA/Mn is the most efficient with a COD removal of 85 % with 18 % more colour removal and 23 % increased adsorption capacity compared to RA. Besides, kinetic and isotherm studies confirmed that HA/Mn fitted well with the pseudo-second-order kinetic model and the Redlich-Peterson isotherm model with a β value of 0.9412, suggesting a dominantly homogenous chemisorption process. This study also integrated machine learning in biomass-based dye removal, significantly improving large-scale predictability and efficiency. The Random Forest Regression Model demonstrated high accuracy in predicting dye removal efficiency, both at the laboratory and large-scale application levels, enhancing the scalability of this approach. The reusability study revealed that HA/Mn has a 48 % higher regeneration capacity, leading to an over 80 % reduction in adsorption costs, making it a highly economical alternative to commercial adsorbents. Additionally, HA/Mn has a higher removal colour efficiency of 6-18 % in industrial wastewater than in commercial AC with a surface area of >100 m^2/g. In summary, these findings advance adsorption science by introducing a novel, scalable, and economically viable hybrid adsorbent, reinforcing the role of biomass-based solutions in sustainable dye wastewater treatment and circular economy initiatives.

Keywords: *Avocado Seed; Banana Peel; Hybrid Adsorbent; Adsorption Process; Optimization*

SINTESIS ADSORBEN BERASASKAN SISA BUAH-BUAHAN MELALUI PROSES HIDROTERMAL DUA LANGKAH YANG DIIMPREGNASIKAN DENGAN MANGAN OKSIDA BAGI PENYINGKIRAN PEWARNA KATIONIK DARI LARUTAN AKUEUS.

ABSTRAK

Pengeluaran sisa biojisim global sangat besar, dengan anggaran 180 bilion tan dihasilkan setiap tahun. Dalam beberapa tahun kebelakangan ini, penyelidikan menumpukan pada pemulihan sumber daripada sisa biojisim tidak toksik disebabkan kandungan karbonnya yang tinggi, kebolehbaharuan, dan ketersediaan melimpah. Oleh itu, dengan mempertimbangkan ciri-ciri penting sisa biojisim pertanian, kajian ini bertujuan membangunkan adsorben berasaskan sisa buah berkos rendah bagi menyingkirkan pewarna kationik daripada larutan akueus. Berbeza dengan adsorben biojisim konvensional, kajian ini memperkenalkan sintesis hibrid baharu yang menggabungkan biji avokado dan kulit pisang diubah suai secara kimia untuk mengoptimumkan prestasi penjerapan. Bahan biojisim ini murah dan kaya karbon mempunyai permukaan mesopori serta kumpulan berfungsi beroksigen yang penting untuk penyingkiran pewarna. Selain itu, karbonisasi hidrotermal merupakan proses termokimia inovatif dan cekap tenaga yang meningkatkan hasil bahan adsorben. Bagi meningkatkan prestasi, adsorben ini menjalani pengaktifan asid fosforik dan pemendapan mangan oksida. Pengaktifan kimia meningkatkan ciri fizikokimia bahan biojisim, manakala pemendapan mangan oksida mengurangkan penggumpalan serta memudahkan daya tarikan elektrostatik bagi menyingkirkan pewarna kationik. Analisis fizikokimia menunjukkan adsorben yang diubah suai dengan logam (HA/Mn) dan adsorben diaktifkan dengan asid (HA) daripada biji avokado dan kulit pisang (RA) menunjukkan peningkatan luas permukaan (666m^2/g) berbanding HA (535m^2/g) dan RA yang tidak diubah suai (1.19m^2/g). Analisis kumpulan berfungsi menunjukkan HA/Mn adalah adsorben berkesan kerana pengubahsuaian ini memperkenalkan kumpulan hidroksil, karboksil, karbonil, fosfat, dan mangan. Selain itu, kajian penjerapan juga menunjukkan HA/Mn berjaya menyingkirkan warna sepenuhnya,

iaitu 37% hingga 33% lebih tinggi daripada biji avokado mentah (63%) dan kulit pisang mentah (67%). HA/Mn juga menunjukkan peningkatan kapasiti penjerapan sebanyak 29% (199mg/g) berbanding kulit pisang mentah (112mg/g) dan 18% lebih tinggi daripada biji avokado mentah (181mg/g). Kajian pengesahan menunjukkan HA/Mn adalah adsorben hibrid paling cekap dengan penyingkiran COD sebanyak 85%, serta 18% lebih tinggi dalam penyingkiran warna dan peningkatan 23% dalam kapasiti penjerapan berbanding RA. Selain itu, kajian kinetik dan isoterm mengesahkan HA/Mn sesuai dengan model kinetik pseudo-tersusun kedua dan model isoterm Redlich-Peterson dengan nilai β sebanyak 0.9412, menunjukkan proses kemisorpsi dominan dan homogen. Kajian ini juga mengintegrasikan pembelajaran mesin dalam penyingkiran pewarna berasaskan biojisim, meningkatkan kebolehramalan dan kecekapan dalam skala besar. Model Random Forest Regression menunjukkan ketepatan tinggi dalam meramalkan kecekapan penyingkiran pewarna, baik pada peringkat makmal mahupun aplikasi berskala besar, sekali gus meningkatkan kebolehskalaan pendekatan ini. Kajian kebolehgunaan semula menunjukkan HA/Mn mempunyai kapasiti regenerasi 48% lebih tinggi, membawa kepada lebih daripada 80% pengurangan kos penjerapan, menjadikannya alternatif menjimatkan berbanding adsorben komersial. Selain itu, HA/Mn juga menunjukkan kecekapan penyingkiran warna 6-18% lebih tinggi dalam air sisa industri berbanding arang aktif komersial (AC) dengan luas permukaan melebihi 100m^2/g. Kesimpulannya, penemuan ini memajukan bidang sains penjerapan dengan memperkenalkan adsorben hibrid baharu yang berskala, berdaya ekonomi, dan cekap, mengukuhkan peranan penyelesaian biojisim dalam rawatan air sisa berwarna serta ekonomi kitaran.

Kata kunci: *Biji Avokado; Kulit Pisang; Adsorben Hibrid; Proses Penjerapan; Pengoptimuman*

ACKNOWLEDGMENTS

Alhamdulillah. Praise be to Allah the Almighty God, the most gracious and the most merciful. I am deeply grateful to my research supervisors Prof. Ir. Dr. Abdul Aziz Abdul Raman and Chm. Dr. Archina Buthiyappan for their support and guidance during my Ph.D. journey. Their dedication, sincerity, and passion for research have been a major source of inspiration to me. It has been a truly privileged experience to conduct research under their mentorship. I would also like to express my sincere gratitude to Dr. Kyaw Myo Aung, whose invaluable guidance and advice significantly contributed to the completion of my research.

I am grateful to my fellow lab mates in Unit Lab Operations, Department of Chemical Engineering for making my Ph.D. journey more enjoyable and meaningful. Especially, Adila, Yan Yin, Zainab, Zhang, and Pu Wei for the continuous discussions, all the fun, and endless support to reach the very end together. I would also like to thank the constant support system of my life: Ziya, Sama, Zainath, and Haleemath for all the long-distance talks when in need of a moral boost.

Furthermore, I would like to thank my family, my parents Solih and Shafia, and my sister Aisha for their prayers, love, and guidance. A special thanks to my precious daughter, Maya, who has given me extra courage throughout this journey. Finally, I am so grateful to my husband, Safwan, for all the love, support, encouragement, and pushing me to grow outside of my comfort zone. I dedicate this thesis to my husband and daughter.

TABLE OF CONTENTS

LIST OF FIGURES

LIST OF TABLES

LIST OF SYMBOLS AND ABBREVIATIONS

°C	:	Degree Celsius
2D	:	Two dimensional
AI	:	Artificial intelligence
ANOVA	:	Analysis of Variance
BET	:	Brunauer-Emmett-Teller
C=C	:	Alkene and aromatic functional groups
C_2H_6O	:	Ethanol
Cf	:	Final concentration
C-H	:	Aliphatic functional group
C_i	:	Initial concentration
CNN	:	Convolutional Neural Network
C-O	:	Carboxyl functional group
CO_2	:	Carbon dioxide
COD	:	Chemical Oxygen Demand
COD_f	:	Final chemical oxygen demand
COD_i	:	Initial chemical oxygen demand
COM-AC	:	Commercial activated carbon
Conc	:	Concentration
DOE	:	Design of Experiment
DT	:	Decision Tree
FTIR	:	Fourier Transform Infrared Spectroscopy
g/L	:	Gram per litre
GDP	:	Gross domestic product
H_2SO_4	:	Sulphuric acid

H_3PO_4	:	Phosphoric acid
HA	:	Acid-activated hybrid adsorbent
HA/Mn	:	Metal-impregnated hybrid adsorbent
HCL	:	Hydrochloric acid
hr	:	Hour
HTC	:	Hydrothermal carbonization
HTC/RA	:	Hybrid adsorbent hydrochar
m (g)	:	Mass in grams
MB	:	Methylene blue dye
mf (g)	:	Final mass in grams
mg/g	:	Milligram per gram
min	:	Minute
ML	:	Machine learning
MnO	:	Manganese Oxide
Mn-O	:	Manganese functional group
MPa	:	Mega pascal
MSE	:	Mean squared error
NaOH	:	Sodium hydroxide
-OH	:	Hydroxyl functional group
OOB	:	Out of bag
pH	:	Potential of hydrogen
pH_{pzc}	:	Point of Zero Charge
PKS	:	Palm kernel shell charcoal
P-OH	:	Phosphoric functional group
POME	:	Palm oil mill effluent
Q_{max}	:	Maximum adsorption capacity

R	:	Correlation coefficient
R^2	:	Root mean squared error
RA	:	Raw hybrid adsorbent
RAS	:	Raw avocado seed
RBP	:	Raw banana peel
RF	:	Random Forest
RF 20%	:	Random forest, 80% for training 20% for testing
RF 30%	:	Random forest, 70% for training 30% for testing
RNN	:	Recurrent Neural Network
RSM-CCD	:	Response Surface Methodology – Central Composite Design
SDG	:	Sustainable development goals
SEM- EDX	:	Scanning Electron Microscopy - Energy Dispersive X-Ray
SP	:	Slow pyrolysis
V	:	Volume
λmax	:	Maximum wavelength

CHAPTER 1: INTRODUCTION

1.1 Background

The rapid global population growth has significantly increased the generation of agricultural waste, with approximately 180 billion tonnes of global biomass waste produced annually (Mujtaba et al., 2023). In Malaysia alone, 1.2 million tonnes of agricultural waste are disposed of in landfills each year. Despite the agricultural sector contributing 7.4 % to the GDP of Malaysia in 2020 and an export value of RM 115.5 billion in 2019, managing agricultural waste remains challenging. Thus, agricultural waste can be converted into valuable resources like compost, biosorbents, and biofuels through microbial transformation, offering both economic and environmental benefits and aligning with the principles of a circular economy (Pocha et al., 2022). Among various types of agricultural waste, fruit waste such as orange bagasse (de Miranda Ramos Soares et al., 2020), papaya bark (Nipa et al., 2023), banana peel (Muhamad et al., 2023) and avocado seed (Haki et al., 2022) have shown potential for dye removal from aqueous solutions. Fruit wastes, in particular, are economically attractive, non-toxic, and sustainable, making them promising adsorbents due to their significant availability, ease of handling, and low-cost nature (Sivaranjanee et al., 2024).

Annually, 2.4 million tonnes of avocado waste and over 57.6 million tonnes of banana waste are generated globally (Chen et al., 2023; Nyakang'i et al., 2023). Both avocado seeds and banana peels are low-cost precursors with mesoporous surfaces and high carbon content. Besides, avocado seeds and banana peels contain oxygenated functional groups, which are crucial for pollutant removal. Furthermore, avocado seeds contain phenol groups, while banana peel has amine functional groups, both of which are highly effective for dye adsorption (Avalos-Viveros et al., 2023; Maheshwari et al., 2023). However, unmodified raw avocado seed and banana peel often exhibit insufficient adsorption capacity and low colour removal efficiency due to their hydrophilic properties, lignin

content, and organic sticky compounds (Kumar et al., 2024; Watwe et al., 2023). Furthermore, unmodified adsorbents tend to agglomerate in the adsorption process, decreasing the adsorption performance (W. Zhang et al., 2020).

Modifying these biomass-based adsorbents through processes such as carbonization and activation can significantly enhance their adsorption efficacy by improving surface porosity, increasing carbon content, and enhancing oxygenated functional groups (Waghmare et al., 2023). In addition, functionalization with metal impregnations can enhance the porosity while reducing the agglomeration (Jiao et al., 2021; Li et al., 2017). Recent literature primarily focuses on individual biosorbent studies but lacks research on adsorbents derived from mixed waste materials for dye removal. Mixing two fruit wastes can enhance the physicochemical properties of the hybrid adsorbent while improving the adsorption performance and reducing waste generation.

In this study, a low-cost hybrid adsorbent was synthesized from mixed fruit wastes, avocado seeds, and banana peels through two-step hydrothermal carbonization for methylene blue dye removal. Hydrothermal carbonization enhances surface area, structural porosity, and higher carbon yield while reducing energy consumption and increasing the production yield (Sivaranjanee et al., 2024). Manganese oxide was impregnated into the phosphoric acid-activated hybrid adsorbent to improve porosity, increase active binding sites, and improve agglomeration, thereby enhancing cationic dye adsorption (Liu et al., 2021). Moreover, the Design of the Experiment and a machine learning algorithm, the Random Forest Regression Model, were used for more precise predictions for dye removal. The study compares the adsorption performance and regeneration of the developed hybrid adsorbent with a commercially available adsorbent. Additionally, an economic analysis for hybrid adsorbent production is conducted to determine the feasibility of using fruit wastes as adsorbents.

1.2 Problem statement

The usage of carbon-rich porous materials in the adsorption process, like activated carbon, entails substantial investment costs for large-scale operations (Shahrokhi-Shahraki et al., 2021). Commercially available adsorbents synthesized from slow pyrolysis consume more energy in production and have poor regeneration quality, resulting in overall cost escalation (Abdulhameed et al., 2021). Hence, recent studies have focused on finding alternative carbonization methods, such as hydrothermal carbonization (HTC), to minimize adsorbent production costs and energy consumption (Mahalaxmi & Kumar, 2024).

Also, researchers are additionally focused on developing an environmentally friendly and affordable adsorbent from a variety of waste materials. This has led to a growing need for alternative adsorbents derived from low-cost waste materials, such as fruit waste, to provide cost-effective, sustainable solutions for the adsorption process (Yusuff et al., 2022). Fruit waste holds potential as an adsorbent due to significant availability, ease of handling, and the low-cost nature of underutilized waste materials (Sivaranjanee et al., 2024). However, the use of raw biomass waste materials for adsorption has its limitations, such as low adsorption capacity due to the limited surface area, which restricts the active binding sites (Kumar et al., 2024; Watwe et al., 2023). Combining different waste materials to produce a green adsorbent can enhance the physicochemical properties, improve the efficiency of the adsorbent, and reduce the environmental impacts from waste generation. Moreover, the modification of the adsorbents derived from fruit waste improves the surface porosity, increases the carbon content, and improves the oxygenated functional group, resulting in enhanced adsorption performance (Waghmare et al., 2023).

Additionally, achieving optimal efficiency in the adsorption process relies on identifying the best-performing adsorbent for different pollutants at optimal operational

conditions (Watwe et al., 2023). The traditional methods used for optimizing the adsorption process require extensive experimentation and are time-consuming (Yusuff et al., 2021). Statistics and predictive tools such as Design of Experiment (DOE) and Machine Learning (ML) can efficiently optimize and predict the adsorption performance (Ecer & Yılmaz, 2024; Fetimi et al., 2021; Oluwasina et al., 2020). DOE is a statistical tool used to reduce the number of experiments and minimize the use of chemicals and analysis, thereby lowering the overall cost of the adsorption process. Furthermore, Response Surface Methodology- Central Composite Design (RSM-CCD) is an advanced statistical technique using DOE to design and optimize the adsorption process and understand the effect of the parameters on the adsorption process (Tharayil & Chinnaiyan, 2024). However, when dealing with a greater number of process parameters or variables, more experimental data and processing are required for higher accuracy. Integrating ML algorithms into statistical optimization methods offers a promising solution for mitigating process variability and resource demands (de Miranda Ramos Soares et al., 2020; Rosly et al., 2022). Using ML algorithms to predict adsorption efficiency simplifies experimental intricacies by reducing their number and duration while establishing nonlinear connections between input and output variables (Wang & Yao, 2023).

1.3 Research questions

The relevant research questions that are going to be addressed in this study are as follows:

1. Could efficient adsorbent be developed by mixing different types of fruit waste through two-step HTC with MnO impregnation, and how does it affect the physicochemical properties of developed adsorbent?
2. How do contact time, adsorbent dosage, initial pH of solution, and initial dye concentration influence the adsorption efficiency of unmodified and modified hybrid adsorbents?

3. Which kinetic and isotherm models best characterize the adsorption behaviour of a hybrid adsorbent for dye removal from aqueous solutions, and what are the dye removal mechanisms of the hybrid adsorbent?
4. Does integrating RSM-CCD with a machine learning algorithm improve prediction efficiency for dye removal performance?
5. What are the feasibility and cost implications of producing hybrid adsorbent to commercial carbon-based adsorbent?

1.4 Aim and objectives

The present study aims to synthesize a low-cost hybrid adsorbent from fruit wastes to remove recalcitrant contaminants from aqueous solutions. Thus, the objectives of this study are:

1. To synthesise and characterise hybrid adsorbent from fruit wastes, specifically banana peel and avocado seed, via two-step hydrothermal carbonization.
2. To optimize the adsorption performance of synthesized adsorbents by assessing the effects of contact time, adsorbent dosage, initial solution pH, and initial dye concentration on colour removal, adsorption capacity, and COD removal.
3. To study the adsorption kinetics and isotherm and kinetic of the methylene blue dye from aqueous solution using hybrid adsorbent.
4. To predict the adsorption performance of the hybrid adsorbent using Response Surface Methodology - Central Composite Design and a machine learning algorithm.
5. To evaluate the economic feasibility of hybrid adsorbent for industrial wastewater application.

1.5 Scope of the study

In this study, avocado seeds and banana peels were selected as precursors for developing hybrid adsorbent through a two-step hydrothermal carbonization process for dye removal in aqueous solutions. The physicochemical properties of the hybrid adsorbents, including their chemical functional groups, elemental composition, surface area, surface morphology, and point of zero charges, were analysed. Methylene blue, a cationic dye, was selected as a model dye to evaluate the performance of the adsorbents and evaluate the effect of operational parameters, including the initial pH of the solution, adsorbent dosage, initial dye concentration, and contact time. The adsorption process was designed and optimized using Design-Expert and Response Surface Methodology (RSM), while a machine learning algorithm, Random Forest (RF) regression model, was used to enhance the predictability and accuracy of dye removal. Adsorption kinetics and isotherms were also studied to understand the behaviour between the adsorbent and adsorbate. Finally, a regeneration study and economic analysis were performed to determine the feasibility and commercial viability of the newly developed hybrid adsorbent.

1.6 Thesis outline

The thesis is structured to comprehensively present the study on biomass-based adsorbents for dye removal from wastewater. It begins with an abstract, followed by an introduction, a detailed methodology, an analysis and discussion of results, and a conclusion summarizing key findings. Supporting information, including references and appendices, is provided to reinforce the research.

Chapter 1: Introduction

The introduction chapter includes background information on fruit wastes and water pollution from dye wastewater, as well as a brief outlook on developing adsorbents from banana peels and avocado seeds to remove dye from wastewater. Additionally, Chapter

1 includes the problem statement, research questions, aim, and objectives of the study, along with the scope and significance of the research. The thesis outline is also included in this section.

Chapter 2: Literature review

This chapter provides a comprehensive literature review of recently published studies on biomass waste-derived adsorbents for wastewater treatment, especially for removing dyes and recalcitrant pollutants through the adsorption process. This chapter explores various types of adsorbents derived from biomass-base, which was utilized for dye removal, addressing the limitations and challenges associated with the conventional commercial adsorbents used for dye removal. Furthermore, Chapter 2 discusses optimization tools utilized to improve the performance and accuracy of the adsorption process using fruit-waste-derived adsorbents for dye removal while considering the effects of operational parameters.

Chapter 3: Methodology

This chapter describes the methodology of the research activities used to achieve the objectives of this study. Chapter 3 includes the materials, methods, development of adsorbents, and characterization methods of the adsorbents. Furthermore, this chapter covers the evaluation and validation of the adsorbents for methylene blue dye removal, along with analysis techniques and optimization tools for the adsorption process. Lastly, this chapter also includes safety precautions.

Chapter 4: Results and discussion

The Results and Discussion chapter presents the results of preliminary experiments for raw avocado seed and raw banana peel adsorbent followed by the results of the adsorbent synthesis process. Chapter 4 also includes a physiochemical analysis of hybrid adsorbents BET, FTIR, SEM-EDX, and pH_{pzc}. The chapter reports on the adsorption performance and comparison of hybrid adsorbents: RA (raw adsorbent from avocado seed and banana peel), acid-activated adsorbent (HA), and metal-impregnated adsorbent (HA/Mn). Moreover, it covers optimized adsorption processes using the design of experiments and machine learning techniques. Finally, economic analysis, along with a regeneration study, is included in this chapter for interpretation.

Chapter 5: Conclusion and Recommendations

This chapter summarizes the key research findings, including the modification of the adsorbents through hydrothermal carbonization, acid activation, and functionalization using metal oxide impregnation. It also includes a summary of the optimization of the dye removal process for the newly developed hybrid adsorbent and its potential for industrial applications. This chapter also provides future research recommendations and the knowledge contributions from this study.

CHAPTER 2: LITERATURE REVIEW

2.1 Introduction

This chapter outlines the use of biomass waste materials to produce promising adsorbents for dye wastewater treatment. Besides, this chapter also includes different biomass-based adsorbents and their limitations in removing pollutants. Furthermore, the chapter discusses adsorbent synthesis methods, modification techniques, and the characteristics of adsorbents. Additionally, the effects of different operational parameters on adsorption performance are included, and the chapter concludes with a summary of the literature review highlighting the research gaps.

2.2 Conventional treatment methods for dye wastewater treatment

The uncontrolled discharge of wastewater is a major global environmental concern. Wastewater treatment plays a crucial role in protecting public health and the environment by removing or neutralizing pollutants before water re-enters the natural cycle. Industrial wastewater contains a variety of contaminants, including organic matter, heavy metals, and various pathogens. Among these, industrial dye wastewater is a significant environmental concern due to its complex, toxic, and non-biodegradable nature.

The extensive use of synthetic dyes in industries is driven by their high solubility, stability against photodegradation, and resistance to microbial breakdown. Since the early 20th century, synthetic dyes have largely replaced natural dyes, with over 100,000 commercial variants and a global production exceeding 700,000 tons annually. Of this, approximately 150,000–200,000 tons enter industrial wastewater streams(Singh, 2017; Subbaiah Munagapati et al., 2021; Xue et al., 2022). The major contributors to dye wastewater, as illustrated in Figure 2.1, include the textile, printing, paper, food processing, and tannery industries, with the textile sector alone responsible for 54% of total dye discharge (Solayman et al., 2023).

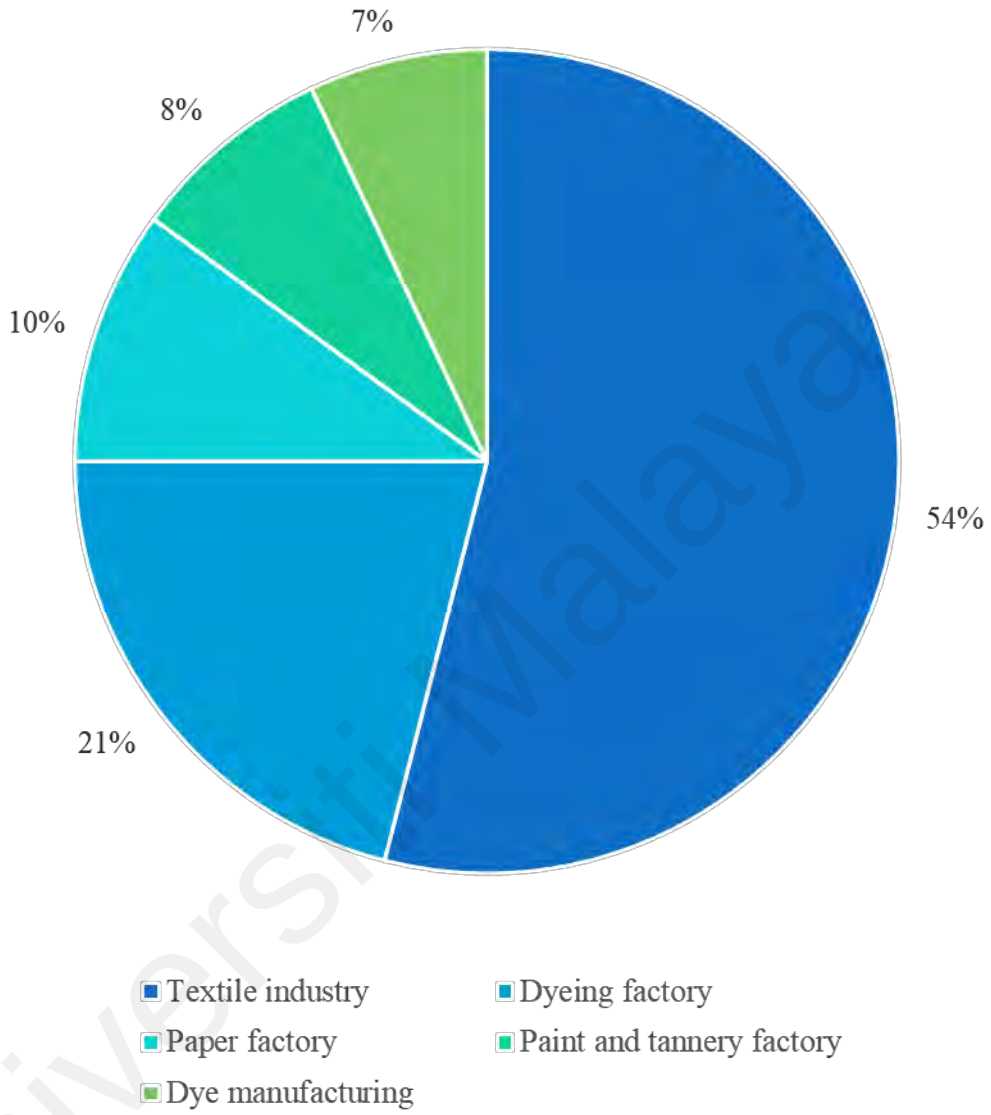

Figure 2.1 : Sector-wise dye wastewater contributing industries

Textile processes such as dyeing, printing, and finishing generate vast amounts of dye-contaminated effluents, often discharged untreated, leading to the accumulation of dyes, dye by-products, and heavy metals in water bodies (Batool & Valiyaveettil, 2021; Rezk et al., 2019). Concentrations in textile effluents can reach up to 800 mg/L, contributing over 280,000 tons of dyestuff annually (Solayman et al., 2023; Sridhar et al., 2022).Table 2.1 outlines the conventional dye removal technologies, highlighting their advantages and limitations. These traditional methods include physical, chemical, and biological processes, each with its own set of strengths and challenges in effectively treating dye-contaminated wastewater (Tuli et al., 2020a).

Chemical dye removal methods offer simplicity and effectiveness but often result in secondary waste or by-products, such as sludge or aromatic amines (Tchobanoglous et al., 2003). Biological methods, while capable of degrading dyes using enzymes or microorganisms, are hindered by unreliable enzyme production and inefficiency in metabolizing certain dyes, such as azo dyes (Henze et al., 2008).

Physical treatments, including ion exchange and coagulation, are generally cost-effective but may not be suitable for all dyes and can generate sludge. Among these, the adsorption process stands out as the most promising method for dye removal due to its high efficiency, versatility in removing a wide variety of dyes, and minimal waste generation, despite challenges such as the high cost of activated carbon. Besides, within the complex wastewater treatment system, due to the presence of a variety of solid and chemical pollutants in the aqueous solution, adsorption has garnered increasing attention as a versatile and high-efficiency treatment method (Tharayil & Chinnaiyan, 2024).

Table 2.1 : Dye removal treatment methods

	Methods	Advantages	Disadvantages
Chemical treatment	Oxidative process	Simplicity of application	Activating agent required
	Fenton's reagent	Fenton's reagent is a suitable chemical means	Sludge generation
	Photochemical	No sludge and foul odours are produced	Formation of by-products
	Sodium hypochlorite	Increases azo bond creation	Release aromatic amines
	Ozonation	No increase for wastewater and sludge volume	Short half-life (20mins)
	Electrochemical destruction	No usage of chemicals and no sludge build-up	Flow rates cause a direct decrease in dye removal
Biological treatment	Decolourization (white rot fungi)	Able to degrade dyes using enzymes	Enzyme production was unreliable
	Mixed bacterial	Decolourized in 24–30 h	Azo dyes are not readily metabolized
	Dye bioremediation	Azo dyes can be decolourized	Yields methane and hydrogen sulphide
Physical treatment	Adsorption	Efficient removal of a wide variety of dyes	Activated carbon is expensive
	Ion exchange	Higher regeneration	Not effective for all dyes
	Membrane separation	Efficiently removes a variety of inorganic and organic matter	High energy consumption, expensive.
	Coagulation	Simple to operate and cheap. Preferred for vat or sulphur dyes	Sludge generation and not suitable for acidic or azo dyes.

The adsorption process is a successful approach among the preceding methods due to its high efficiency, operational simplicity, low starting cost, reusability, resistance to contaminants, and minimal waste generation (Kaewtrakulchai et al., 2024). The effectiveness of adsorption is primarily influenced by the specific characteristics of both the adsorbent and the adsorbate (Crini & Lichtfouse, 2019). For instance, efficient adsorption of perfluorooctanoic phosphonate occurs at mesoporous structure between 29-109 nm, whereas for dye molecules such as methylene blue, adsorbent with a pore size of more than 2 nm is preferred.

In summary, adsorption is the most effective method for dye removal due to its high efficiency and minimal waste production among the conventional treatment methods for dye wastewater. However, commercial adsorbents remain expensive and have limited regeneration capacity. Therefore, developing low-cost alternative adsorbents is essential to enhance the economic feasibility of adsorption-based treatment systems.

2.2.1 Dye adsorption from aqueous solution

Most synthetic dyes contain organic and inorganic chemicals, cyclic compounds, and high molar mass molecules, making them highly resistant to degradation (Ay et al., 2012). An estimated 10–50% of globally produced dyes ultimately end up in aquatic ecosystems, where they pose a severe threat to marine life and water quality. Dyes reduce sunlight penetration, disrupting photosynthesis and decreasing dissolved oxygen levels, which in turn increases chemical oxygen demand (COD) (Alorabi et al., 2020; Kabiru Bello et al., 2018; C. Liu et al., 2012; Rainert et al., 2021; Tuli et al., 2020a). Additionally, prolonged human exposure to synthetic dyes has been linked to skin diseases, respiratory complications, cardiovascular disorders, diabetes, and even carcinogenic and mutagenic effects due to the presence of benzidines and naphthalene derivatives (Kabiru Bello et al.,

2018). Therefore, the long-term effects of synthetic dyes may lead to genetic mutations in living organisms (Liu et al., 2021).

Cationic (basic) dyes, commonly used for dyeing acrylic, wool, nylon, and silk, are among the most problematic dyes in wastewater due to their bright, intense colours and resistance to degradation (Zafar et al., 2022). These dyes contain positively charged ions and include cationic azo dyes, anthraquinone dyes, and phthalocyanine dyes. Cationic dyes are water-soluble, carrying a positive charge and yielding coloured cations in solution, as summarized in Table 2.2. They include cationic azo dyes, di- and tri-arylcarbenium, phthalocyanine dyes, methane dyes, anthraquinone, and various solvent and polycarbocyclic dyes. Basic dyes are known for their high visibility, brilliance, and intensity of colours, making them extensively used as models in dye adsorption studies, including dyes like Crystal Violet (Ismail et al., 2024), Methylene Blue (Vinayagam et al., 2024), Basic Blue 41(Zafar et al., 2022), and Rhodamine B (Vasconcelos et al., 2023). These dyes are toxic and can cause harmful effects such as allergic dermatitis, skin irritation, difficulty breathing, nausea, vomiting, excessive perspiration, mutations, cancer, mental disorientation, and methemoglobinemia (Zayed et al., 2023). The stability of these dyes against light, heat, and biological breakdown makes them highly challenging to remove from water, posing risks to both ecosystems and human health (Mehmandost et al., 2023).

Among cationic dyes, Methylene Blue (MB) is one of the most commonly detected pollutants in industrial wastewater due to its extensive use in textiles, plastics, paper, leather, and food industries (Munonde et al., 2023). MB, a thiazine-based dye with the chemical formula $C_{16}H_{18}N_3ClS$, exhibits a maximum absorbance wavelength of 663 nm. Its high-water solubility and chemical stability make MB a preferred dye for various applications, particularly in textile industries processing wool, silk, and cotton (Oladoye

et al., 2022; Xue et al., 2022). Several studies have documented MB concentrations in industrial effluents, with reported values ranging from 2.34 mg/L to 86.5 mg/L in textile wastewater (Fito et al., 2020; Munonde et al., 2023). Due to its stability and widespread use, MB is often chosen as a model dye in adsorption studies to evaluate the effectiveness of adsorbents derived from biomass (Jiang et al., 2022; Ramutshatsha-Makhwedzha et al., 2022; M. C. Silva et al., 2021).

Although MB is not classified as a highly toxic dye, it can still cause significant health issues upon prolonged exposure, including skin irritation, nausea, vomiting, respiratory distress, and even neurological disorders (Amela et al., 2012). Therefore, efficient removal of MB from industrial wastewater is crucial to minimizing its environmental and health impacts.

In summary, the discharge of synthetic dyes, particularly cationic dyes like MB, into aquatic environments poses severe ecological and health risks. These dyes persist due to their resistance to natural degradation processes, leading to reduced light penetration, disrupted aquatic ecosystems, and increased COD. Moreover, prolonged exposure to MB can have adverse effects on human health. Given its widespread industrial use and frequent presence in wastewater, the effective removal of MB is essential for reducing water pollution and ensuring environmental sustainability. Adsorption has emerged as a promising method for MB removal due to its cost-effectiveness, efficiency, and environmental friendliness.

Table 2.2 : Types of dyes used in industries

Type of dye	Properties	Applications	Toxic effects	Ref.
Acid dye: Acid yellow 36, Acid orange 7, Acid blue 83, Acid blue 7	Water-soluble anionic compounds	Textile, leather, and pharmaceutical	Vomiting, nausea, diarrhoea, carcinogenic and mutagenic effects	(dos Santos Escobar et al., 2021; Shirzad-Siboni et al., 2014)
Basic dye: Methylene blue, Basic red 1 or rhodamine 6G, Basic yellow 2	Water-soluble, applied in weakly acidic dyebaths; bright dyes	Paper, nylons, and modified polyester, textile	Toxic to aquatic life; affect respiratory and mental health, and carcinogenic	(Rima et al., 2022; salah omer et al., 2022; Xue et al., 2022)
Direct dye: Congo red, Direct red 28, Direct black 38	Water-soluble, can be applied directly without mordants	Rayon, cotton, leather, paper	Toxic to aquatic organisms, carcinogenic, mutagenic, and dermatitis	(Edokpayi & Makete, 2021; Farghali et al., 2022)
Reactive dye: C.I. reactive red 120, C.I. reactive red 147, C.I. reactive blue 19	Water-soluble, anionic compounds; largest dye class	Cotton, cellulose, nylon, silk and wool	Allergic reaction in eyes, skin, and the upper respiratory tract	(Aragaw & Alene, 2022)
Dispersive dye: Disperse red 9, Disperse violet 1, Disperse red 60	Not water-soluble	Polyester, nylon, synthetic fibres, cellulose acetate, and acrylic fibres	Mutagenic; carcinogenic; causes soil and water pollution	(Sridhar et al., 2022)
Azo dye: Direct Black 22, Disperse Yellow 7, Methyl red, Methyl orange, Trypan blue	Water-soluble	printing, cosmetics, leather, textiles paper, food process	Carcinogenic. Irritates the eye and skin and affects aquatic life	(Seyyedi & Jahromi, 2014; Shirzad-Siboni et al., 2014; Zayed et al., 2023)
Vat dye: Vat blue 1, Vat acid blue 74	Water-insoluble; oldest dyes; more chemically complex	Natural fibres and cellulosic material	Dermatitis, allergic conjunctivitis, rhinitis,	(Sridhar et al., 2022)
Sulphur dye: Sulphur brilliant green, Sulphur blue, Sulphur Black 1, Leuco Sulphur Black 1, Phthalic anhydride	Organic compounds containing sulphur or sodium sulphide	Cellulosic materials or blends, cotton, silk, paper, leather	Skin irritation; blocked noses; sneezing and sore eyes; carcinogenic	(Sridhar et al., 2022)

2.3 Commercial adsorbents utilised in dye wastewater treatment

There are various types of adsorbents utilised in dye wastewater treatment due to their capability to effectively remove a broad spectrum of pollutants, including synthetic dyes that are often toxic, non-biodegradable, and resistant to conventional treatment methods. Adsorbents in commercial applications in dye removal are summarized in Table 2.3, which includes activated carbon (Shahrokhi-Shahraki et al., 2021), zeolites (Inglezakis et al., 2023), ion exchange resins (Zagklis et al., 2015), chitosan (Shukla et al., 2024), carbon nanotubes, graphene-based materials (Zourou et al., 2022), silica-based materials(Ramalingam et al., 2024), iron oxide-based adsorbents, modified clays (Ecer et al., 2023), and biochar (Imad Rabichi et al., 2025)

However, some materials have limited commercial applications due to various imitations and challenges. For instance, adsorbents derived from chitosan have significant adsorption performance due to the abundance of amino and hydroxyl groups, allowing it to form hydrogen bonds with a wide spectrum of molecules, including dyes (Shukla et al., 2024). Nonetheless, they are used in pilot scale application and not widely commercialized due to their extensive modification and low durability (Roy et al., 2023). Carbon nanotubes and graphene oxide are highly effective in dye removal, but they have some challenges as their expensive nature limits feasibility in industrial applications (Ullah et al., 2024). Biochar, particularly derived from coconut shells or palm kernel shells, is an emerging low-cost alternative to more expensive adsorbents (Kiani Ghaleh sardi et al., 2021). While biochar holds promise for sustainable dye removal, it is not yet widely used in commercial dye wastewater treatment due to variability in its adsorption efficiency and the need for further modification and optimization (Iwar et al., 2021).

Table 2.3: Types of commercial adsorbents used in dye wastewater treatment.

Adsorbent	Application in dye removal	Remarks
Activated carbon	Removal of synthetic dyes, organic compounds, taste, odour, and some inorganic contaminants from aqueous solutions	High adsorption capacity due to high surface area and porosity. Widely used but expensive due to poor regeneration
Zeolites	Removal of cationic dyes, heavy metals, ammonia, and some organic contaminants through iron exchange.	well-defined porous structure for targeted dyes such as cationic dyes.
Ion exchange resins	removal of anionic dyes, cationic dyes, and heavy metals.	Contains specific functional groups and better selectivity for targeted dye removal
Modified clays	Removal of reactive dyes, basic dyes, organic pollutants, and heavy metals	Cost-effective and significant adsorption capacity
Chitosan	Removal of reactive dyes and organic contaminants.	Biodegradable, high adsorption capacity for anionic dyes and organic contaminants.
Carbon nanotubes	Removal of azo dyes, organic dyes, and heavy metals.	High surface area and strong adsorption properties, expensive production
Biochar (coconut shell and palm kernel shell)	Removal of organic dyes	High reusability, high surface area, low-cost alternative.
Graphene-based materials	Removal of synthetic dyes and heavy metals.	Adsorption capabilities for various contaminants.

Activated carbon is the most widely used commercial adsorbent for dye wastewater treatment due to its high porosity, large surface area, and strong adsorption affinity for organic pollutants (Asfaram et al., 2014; Sivaranjanee et al., 2024). A recent study by Umeh et. al. (2023) compared the efficiency of activated carbon and surface-modified organoclay and reported that activated carbon has a 30 % higher efficiency in removal. This finding can be supported by a study conducted by Ahmadi et. al. (2022), which compared the performance of activated carbon with hyperbranched polymer. However, synthetic polymers are also expensive, have energy-intensive production, and have

limited usage time. Therefore, activated carbon is the most widely used and readily available for dye wastewater treatment due to its cost-effectiveness, high porosity, and adsorption efficiency.

However, despite its high adsorption capacity, activated carbon is typically derived from non-renewable sources such as lignite, bituminous coal, and petroleum coke, making it expensive and less environmentally sustainable (Sulaiman et al., 2018). The global market for activated carbon was valued at USD 4.4 billion in 2023 and is projected to reach USD 7.0 billion by 2028, with a growth rate of 9.5% (marketsandmarkets, 2023). Additionally, about 45% of the global activated carbon production is used for industrial and municipal wastewater treatment (Reyes Molina et al., 2023).

Despite the high demand for activated carbon, they have several limitations and challenges, including lower environmental friendliness due to the use of non-renewable raw materials, limited regeneration, high manufacturing costs and energy requirements, poor stability, and low selectivity (Khan et al., 2023b). As a result, researchers are actively exploring alternative and cost-effective adsorbents derived from natural materials and agro-industrial by-products (Ying et al., 2016). Agricultural biomass-derived biosorbents offer cost-effectiveness, biodegradability, and reusability, making them a promising alternative for dye removal (Hameed, 2009; Sivaranjanee et al., 2024). Additionally, biosorbents contribute to environmental and economic sustainability by utilizing waste materials for pollutant removal while potentially generating energy (Ramalingam et al., 2024).

In summary, activated carbon is widely used for dye wastewater treatment due to its high adsorption efficiency, but it faces challenges such as high costs, energy-intensive production, limited regeneration, and low selectivity. While activated carbon can be sourced from both renewable and non-renewable materials, industrial applications still

primarily rely on non-renewable sources. As a low-cost, renewable alternative, biochar derived from coconut and palm kernel shells shows promise for dye removal, though its adsorption efficiency varies and requires further optimization for large-scale applications. To enhance sustainability, biomass-based adsorbents from agro-industrial waste are gaining attention as cost-effective, biodegradable, and reusable alternatives, offering excellent adsorption properties while promoting waste valorisation in dye wastewater treatment.

2.4 Biomass-based adsorbent

General food waste among solid waste has emerged as a useful resource primarily due to its large availability and low cost. Most of the food waste is contributed by fruits and vegetables (42 %) followed by dairy products, grains, and cereals (Sridhar et al., 2022). Hence, researchers have explored the use of agricultural waste resources to create low-cost, effective adsorbents with higher regeneration quality. To be an effective biosorbent, these materials must have excellent physicochemical characteristics, including high surface area and porosity to provide accessible binding sites for pollutants, as well as selectivity, stability, and appropriate chemical composition with functional groups for effective chemical interactions with pollutants (Shelke et al., 2022). Thus, biomass-based adsorbents can be considered an effective material for environmental applications, especially for removing highly soluble dyes from aqueous solutions, due to their excellent physicochemical characteristics (Thomas et al., 2023).

Various agro-industrial wastes such as almond leaves, avocado seed (Haki et al., 2022), banana peel (Hu et al., 2021), cassava stem (Obele et al., 2021), chitosan (Chen et al., 2020), rice husk (Nwabanne et al., 2022), crops (Hong & Yang, 2017), egg waste (Pakalapati et al., 2020) coconut shell, spent coffee grounds, eucalyptus, (Correia et al., 2018) and corn cob (Iheanacho et al., 2021) have been successfully used in previous

studies to synthesize adsorbents for the treatment of dyes, as summarized in Table 2.4. The optimum conditions of biomass waste material achieving the highest colour removal and adsorption capacity can be seen in this table. Furthermore, the modified and unmodified adsorbents are used in dye removal, though modified adsorbent show higher removal efficiencies.

Common biomass wastes such as fruit and vegetable peels are usually disposed of, which makes them economically attractive, environment-friendly, and inexpensive materials to be used in the development of low-cost adsorbents. Biomass-based adsorbents are becoming increasingly popular in wastewater treatment methods due to their ease of production, operational convenience, performance effectiveness, and cost-effectiveness in eliminating harmful contaminants from wastewater (Zhu et al., 2017). Lignocellulose biomass-based adsorbents are advantageous in adsorption due to their easy availability, physicochemical characteristics, chemical stability, and feasibility.

The use of adsorbents derived from biomass waste for wastewater treatment is in line with some of the Sustainable Development Goals (SDG) (Kumar et al., 2024). Specifically, it contributes to SDG 3, Good Health and Well-being, by minimizing exposure to pollutants, and SDG 6, Clean Water and Sanitation, through the effective removal of dyes from wastewater. Additionally, the application of biomass-based adsorbents supports SDG 7 in Affordable and Clean Energy, SDG 11 in Sustainable Cities and Communities, and SDG 12 for Responsible Consumption and Production. It promotes renewable energy goals, effective waste management and pollution remediation, and responsible consumption by recycling biomass waste to reduce solid waste generation.

In summary, different types of biomass waste materials can be converted into carbo-rich adsorbent as shown in Figure 2.2. Most biomass-based adsorbents are effective for

pollutant removal and can be used in both unmodified and modified forms. However, unmodified biomass-based adsorbents often require larger dosages to achieve high adsorption performance, simultaneously increasing the overall treatment cost. In contrast, modified adsorbents offer improved adsorption efficiency, requiring lower dosage, reaching equilibrium faster, and demonstrating greater adsorption capacity and colour removal percentage. Additionally, wastewater treatment using biomass-based adsorbents supports the circular economy and aligns with several sustainable development goals, providing a more sustainable approach to environmental management.

Figure 2.2 : Biomass-based adsorbents

Table 2.4: Biomass-based adsorbents for dye wastewater treatment

Adsorbent	Pollutants	Operational parameters	Adsorption capacity	Removal efficiency	Ref.
Wattle bark biochar	Anionic dye: Methyl orange	Dosage: 5 g/L pH: 2-7 Time: 120 min Conc: 20 mg/L	12.26 mg/g	95%	(Cuong Nguyen et al., 2021)
Mimosa plant biochar	Anionic dye: Methyl orange	Dosage: 5 g/L pH: 2-7 Time: 120 min Conc: 20 mg/L	12.33 mg/g	96%	(Cuong Nguyen et al., 2021)
Coffee husk biochar	Anionic dye: Methyl orange	Dosage: 5 g/L pH: 2-7 Time: 120 min Conc: 20 mg/L	12.34 mg/g	80%	(Cuong Nguyen et al., 2021)
Sodium chloride modified honeycomb gelatine biosorbent	Anionic dye: Methyl orange	Dosage: 0.2g pH: 7 Time: 30 min Conc: 100 mg/L	1107.20 mg/g	61 %	(Dang et al., 2022)
Phosphoric acid modified rockrose shell biochar	Anionic dye: Reactive red 23	Dosage: 140 mg Time: 40 min Conc: 400 mg/L	892.9 mg/g	98%	(El Farissi et al., 2021)

Table 2.4 Continued

Adsorbent	Pollutants	Operational parameters	Adsorption capacity	Removal efficiency	Ref.
Banana peel activated carbon	Cationic dye: Malachite green	Dosage: 0.2 g/L pH: 5 Conc: 1 g/L Time: 120 min	2298 mg/g	100 %	(Chen et al., 2023)
Sodium hydroxide modified rockrose shell biochar	Anionic dye: Reactive red 23	Dosage: 140 mg Time: 40 min Conc: 400 mg/L	1020.4 mg/g	97%	(El Farissi et al., 2021)
Zinc chloride and cetyltrimethylammonium bromide modified orange peel biochar	Anionic: Congo red	Dosage: 1 g/L pH: 5-7 Time: 120 min Conc: 25 mg/L	666.7 mg/g	98 %	(Karaman et al., 2021)
Hydrochloric acid modified palm leaf adsorbent	Cationic dye: Basic red-18	Dosage: 1g pH: 9 Time: 120 min Conc: 100 mg/L	-	100%	(Ozdemir et al., 2023)
Filamentous algae activated carbon	Cationic dye: Basic blue 41	Dosage: 1 g/L pH: 10 Time: 90 min Conc: 100 mg/L	125 mg/g	94%	(Afshin et al., 2018)
Sodium hydroxide modified peanut shell biochar	Cationic dye: Basic red 46	Dosage: 10 mg pH: 8 Time: 10 min Conc: 150 mg/L	687.5 mg/g	93 %	(Du et al., 2022)

Table 2.4 Continued

Adsorbent	Pollutants	Operational parameters	Adsorption capacity	Removal efficiency	Ref.
Potassium carbonate modified palm frond and palm kernel shell	Cationic dye: methylene blue	Dosage: 0.06 g pH: 10 Time: 20 min Conc: 10 mg/L	331.6 mg/g	99%	(Jasri et al., 2023)
Iron oxide modified date palm frond biochar	Cationic dye: methylene blue	Dosage: 0.02 g pH: 8 Time: 200 min Conc: 250 mg/L	189.5 mg/g	-	(Eniola et al., 2023)
Unmodified date palm frond biochar	Cationic dye: methylene blue	Dosage: 0.02 g pH: 8 Time: 200 min Conc: 250 mg/L	98.8 mg/g	-	(Eniola et al., 2023)
Unmodified water hyacinth biochar	Cationic dye: methylene blue	Dosage: 10mg Time: 24 hours Conc: 50-300ppm	462.98mg/g	-	(Phonlam et al., 2023)
Potassium hydroxide modified water hyacinth activated carbon	Cationic dye: methylene blue	Dosage: 10mg Time: 24 hours Conc: 50-300ppm	587.92mg/g	-	(Phonlam et al., 2023)
Unmodified eucalyptus biochar	Cationic dye: methylene blue	Dosage: 10mg Time: 24 hours Conc: 50-300ppm	453.52mg/g	-	(Phonlam et al., 2023)

Table 2.4 Continued

Adsorbent	Pollutants	Operational parameters	Adsorption capacity	Removal efficiency	Ref.
Potassium hydroxide modified eucalyptus activated carbon	Cationic dye: methylene blue	Dosage: 10mg Time: 24 hours Conc: 50-300ppm	552.16mg/g	-	(Phonlam et al., 2023)
Sodium chloride modified honeycomb gelatine biosorbent	Cationic dye: Methylene blue	Dosage: 0.2g pH: 7 Time: 30 min Conc: 100 mg/L	1551.5 mg/g	96 %	(Dang et al., 2022)
Sodium hydroxide modified peanut shell biochar	Cationic dye: Methylene blue	Dosage: 10 mg pH: 10 Time: 10 min Conc: 150 mg/L	538.3 mg/g	91 %	(Du et al., 2022)
Iron Oxide functionalized avocado peel hydrochar	Cationic dye: Methylene blue	Dosage: 1 g/L pH: 8 Conc: 0.015 mg/L Time: 120 min	62 mg/g	99 %	(Prabakaran et al., 2022)
Sodium carbonate activated avocado seed adsorbent	Cationic dye: Methylene blue	Dosage: 1 g/L pH: 10 Conc: 1 mg/L	103 mg/g	72 %	(Dhaouadi et al., 2020)
Iron modified banana peel adsorbent	Cationic dye: Methylene blue	Dosage: 2.5 g/L Conc: 0.05 mg/L Time: 50 min	25 mg/g	92 %	(Cathoglu et al., 2021)

Table 2.4 Continued

Adsorbent	Pollutants	Operational parameters	Adsorption capacity	Removal efficiency	Ref.
Unmodified banana peel adsorbent	Cationic dye: Malachite Green dye	Dosage: 2.5 g/L pH: 8 Time: 120 min Conc: 100 mg/L	41.0 mg/g	76 %	(Maheshwari et al., 2023)
Unmodified orange peel adsorbent	Cationic dye: Malachite Green dye	Dosage: 2.5 g/L pH: 8 Time: 120 min Conc: 150 mg/L	42.6 mg/g	74 %	(Maheshwari et al., 2023)
Sodium hydroxide, epichlorohydrin and diethylenetriamine modified banana peel adsorbent	Anionic dye: Congo red	Dosage: 2 g/L pH: 3 Time: 60 min Conc: 50 mg/L	31.6 mg/g	77 %	(Rose et al., 2023)
Phosphoric acid modified moringa olefera	Cationic dye: Crystal violet	Dosage: 0.2 g/L pH: 5 Time: 240 min Conc: 10mg/L	469.6 mg/g	96 %	(salah omer et al., 2022)
Hydrochloric acid activated avocado seed adsorbent	Cationic dye: Crystal violet	Dosage: 50 g/L pH: 7 Conc: 100 mg/L Time: 120 min	3.33 mg/g	100 %	(Ukpong et al., 2023)

Table 2.4 Continued

Adsorbent	Pollutants	Operational parameters	Adsorption capacity	Removal efficiency	Ref.
Oyster mushroom biosorbent	Real wastewater (swine): Ammonium	Dosage: 2 mg/L pH: 8 Time: 360 min	1631.8 mg/g	-	(Feng et al., 2020)
Unmodified Ficus benjamina biosorbent	Cationic dye: Rhodamine B	Dosage: 2 g/L pH: 2 Conc: 100 mg/L	10 mg/g	-	(Watwe et al., 2023)
Unmodified Ficus benjamina biosorbent	Cationic dye: Malachite green	Dosage: 2 g/L pH: 2 Conc: 100 mg/L	40 mg/g	-	(Watwe et al., 2023)
Unmodified Ficus benjamina biosorbent	Cationic dye: Crystal violet	Dosage: 2 g/L pH: 4 Conc: 100 mg/L	11 mg/g	-	(Watwe et al., 2023)
Unmodified Ficus benjamina biosorbent	Cationic dye: Methylene blue	Dosage: 2 g/L pH: 6 Conc: 100 mg/L	25 mg/g	-	(Watwe et al., 2023)
Avocado seed activated carbon	Industrial wastewater	Dosage: 5 g/L pH: 3 shaking speed: 100 rpm	-	COD: 94.5 %	(Atiyah et al., 2024)

2.4.1 Fruit waste-based adsorbents

Fruit waste is abundantly available, comprising 6.8-33 % of total fruit production (640 million metric tonnes per year), and is discarded as peels and seeds (Mahato et al., 2020). These fruit wastes can be utilized as biomass-based adsorbents for dye removal without extensive modifications, reducing production costs and energy consumption while avoiding the use of toxic chemicals. Consequently, green adsorbents obtained from bio-waste and agricultural byproducts have been developed as effective alternatives to conventional adsorbents for dye removal (Ying et al., 2016). However, the raw fruit waste materials exhibit relatively poor adsorptive performance compared to the modified biomass-based adsorbents, as the raw adsorbents tend to agglomerate and have a lower surface area due to the presence of sticky organic matter (Batool & Valiyaveettil, 2021). As a result, researchers are modifying the fruit waste-based adsorbents through physical or chemical methods to improve their adsorption performance and overcome the limitations of raw biomass-based adsorbents. Furthermore, modified biomass-based adsorbents often possess specific surface properties, such as micropores, which increase the available surface area for pollutant binding (Bisiriyu & Meijboom, 2020; Pakalapati et al., 2020; T. Zhang et al., 2020).

2.4.1.1 Avocado-based adsorbent

Avocado (*Persea Americana*) is a tropical and subtropical fruit native to Mexico and Central America. The demand for avocados has increased due to their growing popularity and nutritional benefits, leading to a rise in their harvest rate (Prabakaran et al., 2022). As one of the most widely traded tropical fruits globally, the processing of avocados by industries and households generates a substantial amount of waste. The avocado seed is not edible, so only the flesh is utilized, while the skin and seed, which account for approximately 21-30% of the fruit, are discarded (Araújo et al., 2018). Large quantities of avocado shells, seeds, and other wastes are generated from avocado processing

industries as only the pulp is used for oil, guacamole, and pastes (Haki et al., 2022). Although avocado waste is not inherently harmful to the environment, the global production of avocado peels and seeds results in a significant amount of solid waste, estimated at 2.4 million tons each year (Salazar-Lópeza et al., 2020). The avocado seed contains 6-40% cellulose, 3-47% hemicellulose, and 1-15% lignin (Vargas et al., 2020). Furthermore, avocado waste contains phenol, carboxyl, and hydroxyl functional groups, which contribute to its higher adsorption efficiency for heavy metals and cationic dyes (Haki et al., 2022; Prabakaran et al., 2022)

Researchers are always finding new and better alternatives for low-cost adsorbents, and they are using avocado seeds to make adsorbents to remove different pollutants from aqueous solutions (Zhu et al., 2017). While some researchers used the biomass obtained from avocado seeds to remove fluoride from wastewater by using CO_2 for activation, (Negrete et al., 2018) other researchers used the adsorbent developed from avocado to remove toxic materials and carcinogenic substances like phenolic compounds in industrial wastewater (Leite et al., 2017; Sellaoui et al., 2021). Besides, metal ions such as chromium, lead (S. P. Boeykens et al., 2019b), copper, cadmium (Wanja et al., 2016), ammonium (Zhu et al., 2017), and fluoride (Negrete et al., 2018) are also removed using adsorbents developed from an avocado seed. In addition to the above heavy metal removal, avocado seed-based adsorbents are used in studies to remove dyes from aqueous solutions, such as crystal violet (Haki et al., 2022; Ukpong et al., 2023) and methylene blue (Dhaouadi et al., 2020; Prabakaran et al., 2022) and trypan blue (Tamer et al., 2020). Most often, the adsorbents are made by making activated carbon using a high-temperature furnace, which increases the porosity of the adsorbent (Negrete et al., 2018; Wanja et al., 2016). The removal rate and optimum operational conditions used for biosorbent for wastewater treatment are provided in Table 2.4.

Acid modification is done on avocado seeds as the seed consists of physicochemical properties of a pH value of 5.8, functional groups of acidic 2036 mmol/g, and basic 1.92 mmol/g (Muñoz et al., 2016). A study by Munoz et. al. (2016) reported that acid modification overcomes the limitation of insufficient adsorption capacity in raw biomass with a maximum of 5.6 mg/g of metal uptake, while acid-treated avocado adsorbents showed a 21.8 mg/g. However, a limited number of studies have been done on dye removal using avocado seed adsorbents. The most recent studies conclude that the physical modification of raw avocado seed powder improves the adsorption process, which can remove more than 96 % of phenolic compounds due to the increase in pore volume of more than 80 % (Leite et al., 2017). Furthermore, studies show that the adsorption of avocado seed is endothermic and pH-dependent (Negrete et al., 2018). Moreover, previous studies also stated that adsorbent synthesized from avocado also works best in the first 30 minutes to one hour of contact time, after which adsorption steadily decreases (Wanja et al., 2016).

In conclusion, avocado seed adsorbents achieved higher adsorption performance when their surface is modified, enhancing their physical and chemical characteristics. Studies have shown that modified adsorbents derived from avocado seeds can effectively remove metal ions and dye molecules from wastewater. The acid modification of avocado seeds significantly enhances their adsorption capacity, with treated seeds exhibiting superior adsorption performance compared to raw biomass. Furthermore, the modified adsorbent derived from avocado seeds exhibits increased phenolic O-H stretching, leading to greater hydrogen bonding.

2.4.1.2 Banana-based adsorbent.

Bananas (*Musa*), one of the most widely consumed fresh fruits, generate a substantial amount of waste, estimated at up to 412.6 million tons annually (Jiang et al., 2022). This

large quantity of banana production waste often ends up in landfills and freshwater bodies after harvest, as there has been limited commercial utilization of this waste material so far. However, banana peels and stems can be utilized as high-quality adsorbents for treating wastewater dyes due to their favourable surface properties. The banana peel contains between 43-47 % cellulose, 13-20 % hemicellulose, 55 % holocellulose, and 13-27 % lignin (Silva et al., 2021). Besides, Banana peel adsorbents have a high performance due to their heterogeneous, rough, and porous surface, which traps pollutants in their crater-like pores in the adsorption process (Pandharipande & Deshpande, 2013; Sun et al., 2023). In addition, recent studies show evidence that banana peel has chemical functional groups such as amide, carboxyl, and hydroxyl, which results in higher adsorption efficiency (Avila et al., 2016; Batool & Valiyaveettil, 2021; Cathoglu et al., 2021; C Liu et al., 2012).

Banana peels have been frequently used to remove heavy metal ions like cadmium (Chen et al., 2018) copper (Pandharipande & Deshpande, 2013; Sun et al., 2023), lead (Hu et al., 2021), and chromium (Selimin et al., 2022). In addition, adsorbents derived from banana waste has also been employed to remove dyes such as methylene blue (Lee et al., 2021), reactive black 5, congo red, and reactive red from aqueous systems (Abdulfatai et al., 2013; Misran et al., 2022; V. Munagapati et al., 2018; Temesgen et al., 2018). Recent studies show that raw banana peel can be used as an adsorbent simply by removing the excess moisture and making it into a powder form without further modification (Chen et al., 2018; V. Munagapati et al., 2018). On the other hand, some studies show making modified activated carbon from the banana peel is better to remove dyes in aqueous solutions than using raw banana peel (Misran et al., 2022). Researchers developed a more efficient adsorbent by making activated carbon from raw banana peel powder by heating the materials at 450°C (Abdulfatai et al., 2013). While raw banana peel, activated banana peel and banana peel activated carbon are promising adsorbents

for pollutant removal, their optimum condition to achieve their maximum performance need to be taken into consideration. A study by Maheshwari et. al. (2022) used raw banana peel adsorbent, requiring 20 g/L to achieve 76% pollutant removal. In contrast, a study by Tolkou et. al. (2024) using activated banana peel adsorbent achieved 96 % removal efficiency with just 0.6 g/L. Furthermore, a study by Sun et. al. (2023) using metal oxide-impregnated banana peel attained a removal efficiency of 99 % using only 1 g/L. From an economic and environmental standpoint, these findings indicate that modified and functionalized adsorbents require 95-97% less adsorbent dosage compared to raw adsorbent, making them a more cost-effective solution.

In conclusion, banana peels have been used as effective adsorbents to remove recalcitrant pollutants including heavy metal ions and dyes. While raw powdered banana peel can be utilized as an adsorbent, studies suggest that chemically activated and functionalized adsorbents derived from banana peel are even more effective for removing dyes from aqueous solutions. When modified, banana peel materials have shown increased efficiency in dye removal, as the activation process improves their surface area and active binding sites. Additionally, banana peel contains a fibrous surface area and a high concentration of O-H and amine functional groups, which contribute to its effectiveness as an adsorbent for cationic dye removal.

2.5 Limitations of fruit waste-based adsorbents

Raw biomass-based adsorbents derived from fruit wastes can be utilized without any modification for pollutant removal. Literature studies show that raw biosorbent from agricultural wastes has a low adsorption rate and it has also been observed that these biomass-based adsorbents require further modifications by physical modification or chemical modification to increase the number of active binding sites and increase the surface area (Abdulfatai et al., 2013; Ranasinghe et al., 2018). Adsorbents derived from

clay (Obayomi & Auta, 2019), plant residues (Duan et al., 2022), agricultural waste (Phouthavong et al., 2023), and other renewable sources show great potential for the effective removal of dyes and heavy metals in wastewater treatment. However, to be effective, these biomass-based adsorbents must possess specific properties, including high surface area and porosity to provide accessible binding sites for pollutants, selectivity, stability, and appropriate chemical composition with functional groups for chemical interactions with pollutants. Additionally, abundance and reusability are important factors for reducing procurement and production costs. Several studies are conducted to find the efficiency of biomass-based adsorbents to enhance the efficiency, such as drying temperature and time, the final size of the adsorbents, amount of dosage used, contact time, and the concentration of the contaminant solutions used (C. Liu et al., 2012; Muñoz et al., 2016).

In summary, unmodified fruit-waste-derived adsorbents can be utilized for dye treatment. However, it frequently necessitates further physical or chemical modification to enhance the adsorption performance. Modified adsorbents exhibit promising potential for effectively removing dyes due to the high surface area, porosity, selectivity, and stability after modification. Hence, the synthesis process, method of surface modification, and the type of functionalization influence the effectiveness of biomass-based adsorbents.

2.6 Adsorbents synthesis methods

Thermochemical processes such as pyrolysis, torrefaction, hydrothermal carbonization, and gasification convert biomass into adsorbent (Raninga et al., 2023; Reyes Molina et al., 2023). The synthesis of adsorbents involves the use of heat, which reduces the biomass weight by 40-50%. This reduction results from the loss of oxygen compounds through the melting of cellulose, hemicellulose, and lignin, ultimately producing a carbon-rich material (Reyes Molina et al., 2023). Thus, carbonization converts cellulose

and lignin to CO_2, forming porous surfaces on the adsorbent by breaking down unstable chemical bonds and releasing the volatile fraction of the precursor material (Neolaka et al., 2023).

2.6.1 Pyrolysis

The pyrolysis process involves the thermal decomposition of biomass under anaerobic conditions or with limited oxygen in higher temperatures (< 800 °C) (Jjagwe et al., 2021). In the case of slow pyrolysis, the process takes place at temperatures ranging from 300 to 1000 °C, with a gradual heating rate of 5-10 °C per minute (Negrete et al., 2018) . On the other hand, fast pyrolysis is utilized to convert biomass rapidly into biochar and other products. It involves starting temperatures around 500 °C and can reach up to 1000 °C, with a heating rate of 300 °C per minute (Ding et al., 2023). By carefully controlling the temperature and operating time of the reactor along with the dosage amount used, higher biochar yields can be achieved. Fast pyrolysis is commonly employed for large-scale production of biochar, which can then be used as an adsorbent to remove heavy metals from water and soils. Whereas slow pyrolysis is used to produce activated carbon, it is commonly used to remove pollutants such as dye and produce biochar as a primary product along with bio-oil and syngas. Pyrolysis can be conducted under nitrogen flow along with physical activation such as a gas flow like carbon dioxide (Negrete et al., 2018). In addition to dry pyrolysis, hydrothermal carbonization (HTC), known as wet pyrolysis, has the potential to become an environmentally sound conversion method to exploit extracted biomass, as it has the advantage of converting wet materials without the need for an energy-intensive drying pretreatment.

2.6.2 Hydrothermal carbonization

Hydrochar is the term used to describe adsorbents obtained from the hydrothermal carbonization (HTC) of carbon-based precursors such as biomass materials. HTC has

gained interest as a promising method for processing biomass and waste into hydrochar adsorbents because it generates a higher yield and carbon rate, is energy-dense, and adds value to solid waste sources. This method involves subcritical water conditions, typically at mild temperatures ranging from 180 to 350 °C and autogenous pressures between 2 and 6 MPa, thereby reducing carbon dioxide emissions (Avalos-Viveros et al., 2023; Pauletto et al., 2021). Hydrochar is created chemically through reactions that include hydrolysis, dehydration, and decarboxylation (Ding et al., 2023). The duration of the HTC process can range from 30 minutes to 3 days, depending on the material used. One advantage of using HTC to convert trash is that it avoids the need to dry typically damp feedstocks. Subsequently, this decreases the pre-treatment time, cost, and energy usage in the adsorbent production. HTC decreases greenhouse gas emissions since a substantial percentage of the carbon in the initial feedstock is retained inside the biochar (Flora et al., 2013). Furthermore, the HTC process releases a small amount of carbon dioxide and does not involve processing any hazardous waste.

HTC is getting more attention to turning biomass and waste streams into hydrochar, a carbon-rich, energy-dense, value-added solid material. The HTC process occurs in water as a green reaction solvent, resulting in three kinds of products: gases, an aqueous phase, and solid hydrochar. HTC needs a lower temperature where the reaction is done under water and pressure. Additionally, the HTC process involves several thermochemical reactions such as hydrolysis, dehydration, decarboxylation, aromatization, and condensation polymerization, resulting in three kinds of products: gases, an aqueous phase, and solid hydrochar (Sivaranjanee et al., 2024). Consequently, various molecules (phenols, acids, ketones, aldehydes, etc.) are obtained through the degradation of cellulose, hemicellulose, and lignin, with the process being heavily influenced by temperature and contact time. HTC simulates natural coalification, producing a solid

material with increased energy density and carbon content relative to the initial feedstock and decreased oxygen and volatile content.

Recent studies show that treating a material with HTC before activating it chemically or physically makes the pores bigger and improves its ability to adsorb (Jiang et al., 2022). Although HTC has been used for several years for energy production applications, its use for obtaining hydrochar from fruit waste as an alternative to commercial adsorbents is being investigated. Furthermore, the low-temperature reaction for HTC in water and pressure conditions makes it a greener and efficient process for synthesizing value-added materials from biomass.

In summary, two common biomass carbonization techniques for producing adsorbents are direct pyrolysis and hydrothermal carbonization. Pyrolysis requires higher temperatures and longer processing times compared to HTC, which involves lower temperatures and shorter carbonization periods. Additionally, the hydrothermal method tends to yield higher adsorbent production rates than conventional pyrolysis. As a result, HTC can decrease the overall cost of adsorbent production.

2.7 Adsorbent modification techniques

Using the right modification method, biomass-based adsorbents can be activated to produce an effective porous structural adsorbent with a high adsorption capacity. Carbonization and activation of biomass wastes are crucial processes that transform the biosorbent improve the functionalities by removing the organic lignocellulosic organic matter on the surface of the adsorbent(Mahmood Al-Nuaimy et al., 2023). Carbonization of adsorbent can be obtained by pyrolysis or hydrothermal carbonization, while activation of adsorbent can be accomplished through a physical activation process or a chemical activation process. Furthermore, the type of biomass, processing time, heating rate, and

carbonization temperature can all influence the quality and performance of the synthesized adsorbents (Mujtaba et al., 2023).

2.7.1 Physical and chemical activation

The two types of adsorbent activation are chemical and physical activation of the adsorbents. The physical process involves heating the organic raw material to high temperatures of 600 and 1000 °C in an inert atmosphere, then activating the resulting carbon material in the presence of oxidizing agents like CO_2, steam, and air (Brazil et al., 2022; Genuino et al., 2018; Negrete et al., 2018). Whereas, in chemical activation as summarized in Table 2.5, adsorbents react with salt bases or chemicals such as H_3PO_4, H_2SO_4 $ZnCl_2$, KOH, NaOH, H_2SO_4, and HNO_3, at 450 to 900◦C in an inert or oxygen environment (Dhaouadi et al., 2020; Georgin et al., 2018; Haki et al., 2022; Prastuti et al., 2019; Sellaoui et al., 2021). In the study conducted by Negrete et. al. (2018), physical activation with CO_2 (600°C to 1000°C) after carbonization with N_2 flow (600°C to 1000°C) for 20 samples provided low yield in the range of 12 % to 25 % (Negrete et al., 2018). However, a study conducted by Pauletto et. Al. (2021) produced a higher yield of 59 % activated carbon after acid activation. Besides, low activation temperatures and time are required for the preparation of activated adsorbent in the chemical process when compared to the physical activation method.

Physical activation consists of two stages, where both stages take place separately. In the case of biomass, carbonization occurs first to convert the oxygen-rich biomass into a carbon-rich biochar. Typically, this carbonization is conducted under an inert atmosphere using N_2 or CO_2-rich gas at temperatures between 400 and 600 °C, followed by activation of the biochar at temperatures between 600 and 850 °C (Reyes Molina et al., 2023). Thermal activation is obtained from heating the biomass materials in an isolated heating chamber to provide heat and maintain the temperature of the cylindrical stainless-steel

reactor constantly. In the study conducted by Molin et. al. (2023), the carbonization and activation took place at higher temperatures between 500 °C to 800 °C, respectively. On the other hand, Rodrigues et. al. (2011), reported carbonization using Argan flow for 1 hour at 800°C, gas changed to carbon dioxide and increased the temperature to 900°C for 3 hours. Emerging trends involve the adoption of microwave activation instead of traditional thermal activation in pyrolysis processes. Microwave irradiation induces hot spots that impact the yield and properties of pyrolysis products. Under microwave activation, solids demonstrate increased heating values and specific surface areas, resulting in higher gas and solid yields compared to conventional pyrolysis. However, the liquid yield obtained is lower. Additionally, nearly half of the biomass can be converted into a high-energy gas product, leading to significant yields (Vargas et al., 2020).

Chemical activation requires lower reaction temperatures compared to physical activation. Commonly, the temperature ranges for chemical activation are between 300 and 700 ℃, versus 600 – 800 ℃ for physical activation (Francis & Abdel Rahman, 2016; Raninga et al., 2023). However, for chemical activation, acids, alkaline, or salt base can be used for the activation. When chemical modification is done on raw material, it increases the mean pore diameter due to swelling during the activation and modification process.

Among the chemical agents frequently used in chemical activation techniques, H_3PO_4 has superior properties due to its feasibility, recyclability, environmental friendliness, and low corrosion effect on activator devices (Alam et al., 2023). H_3PO_4 as a chemical activating agent boosts the adsorption capacity of activated adsorbent as a result of introducing an oxygenated phosphoric functional group on the surface of the adsorbent (J. Jabar et al., 2022). Furthermore, with recently published studies, H_3PO_4 increases the surface area significantly. For example, a study conducted by Kumar and Gupta (2020),

raw saw dust was soaked in H_3PO_4 (60%) for 12 hrs before carbonizing (250°C) and activation (600°C), which was report to significantly increase the surface area to 1409 m^2/g (Kumar & Gupta, 2020). Weak acids like H_2O_2 have also been used recently, which shows increased oxygen-containing functional groups on the surface for enhanced adsorption (Zuo et al., 2016). For the avocado seed, the raw biomass shows potential as it is, however, the acid activation improves the adsorption capacity and surface area of the adsorbents. For example, the study conducted by Boeykens et. al. (2019) used natural biomass, activated biomass, and activated carbon from avocado seeds. Carbonization was achieved via pyrolysis, which resulted in a low yield, leading the researchers to use natural biomass and activated biomass for heavy metal removal. Natural biomass has a maximum adsorption capacity of 19 mg/g, while H_3PO_4-activated biomass recorded a slight increase with 27 mg/g for lead adsorption. In the same study, chromium adsorption was also tested on natural biomass and activated biomass using the same chemical, H_3PO_4, which has a lower adsorption at 3 mg/g for natural biomass and 5 mg/g for activated biomass (S. P. Boeykens et al., 2019b).

NaOH modified avocado shell had increased porosity, more cracks, and a rougher surface morphology than the raw materials (Haki et al., 2022). Moreover, oxygen and carbon elements were homogenously scattered in NaOH modified adsorbent than the raw adsorbents. Looking into the dye removal efficiency of NaOH modified avocado waste, the adsorption capacity was 179.8 mg/g while a study conducted by Dhaouadi et.al. (2020) for methylene blue dye removal using raw avocado seed with 10 different salt bases concluded that the presence of salts did not improve the adsorption capacity. the adsorption capacity of salt activated adsorbents had similar results to the adsorbent without the salt activation. For example, Na_2CO_3-activated adsorbent had a 103.1 mg/g maximum adsorption capacity, while raw avocado seed adsorbent had a slightly lower adsorption capacity of 99.8 mg/g. On the other hand, compared to raw avocado seed

adsorption capacity (pp.8 mg/g) activated adsorbent using salts such as NaCl, Na_2SO_3, $C_6H_5Na_3O_7$, $NaHSO_3$, and Na_2HPO_4 achieved and adsorption capacity of 92.9 mg/g, 94.3 mg/g, 80.4 mg/g, and 86.6 mg/g, respectively. Nonetheless, the comparable outcomes observed in the adsorption capacity of certain salts mentioned above can be attributed to the steric hindrance effect and the aggregation of dye molecules, both of which interfered with the adsorption of the dye (Dhaouadi et al., 2020).

In summary, one of the fundamental steps to modify adsorbents from fruit wastes is chemical or physical activation, as summarized in Table 2.5. Chemically activated biomass-based adsorbents achieve higher adsorption performance than unmodified raw biomass-based adsorbents in dye removal. Hence, chemical activation is a common practice in biosorbent synthesis to enhance the chemical properties by introducing more oxygenated functional groups, which are essential for the removal of recalcitrant pollutants, especially in industrial dye wastewater treatment.

Table 2.5 : Activation of adsorbents

Adsorbent	Activation Process	Adsorbate	Adsorption Capacity (mg/g)	Ref.
Tea waste	H_3PO_4 (Phosphoric acid)	Methylene blue dye	238.1	(Tuli et al., 2020b)
Tea waste	KOH (Potassium hydroxide)	Methylene blue dye	357.1	(Tuli et al., 2020b)
Tea waste	$ZnCl_2$ (Zinc chloride)	Methylene blue dye	147.1	(Tuli et al., 2020b)
Saw dust	H_3PO_4 (Phosphoric acid)	Naphthalene	370.8	(Kumar & Gupta, 2020)
Avocado seed	$ZnCl_2$ (Zinc Chloride)	2-Nitrophenol	761.0	(Pauletto et al., 2021)
Avocado seed	$ZnCl_2$ (Zinc chloride)	2-Nitrophenol	562.0	(Pauletto et al., 2021)
Avocado seed	NaCl (Sodium chloride)	Methylene blue dye	92.7	(Dhaouadi et al., 2020)
Avocado seed	$NaHCO_3$ (Sodium bicarbonate)	Methylene blue dye	103.1	(Dhaouadi et al., 2020)
Avocado seed	$C_6H_5Na_3O_7$ (Sodium citrate)	Methylene blue dye	99.5	(Dhaouadi et al., 2020)
Avocado seed	$Na_2S_2O_3$ (Sodium thiosulfate)	Methylene blue dye	101.5	(Dhaouadi et al., 2020)
Avocado seed	$NaNO_2$ (Sodium nitrite)	Methylene blue dye	86.6	(Dhaouadi et al., 2020)
Sugarcane bagasse	Physical: heat	Copper	9.5	(C. Liu et al., 2012)
Watermelon rind	Physical: heat	Copper	5.7	(C. Liu et al., 2012)
Eucalyptus bark	Physical: heat	Zinc (II)	128.2	(Afroze et al., 2016)
Forest residue	Physical: heat	Toluene	716.0	(Reyes Molina et al., 2023)
Avocado seed	Ar: 1 hour and CO_2: 3hours	Phenol	90.0	(Rodrigues et al., 2011)

2.7.2 Metal oxide impregnation

Functionalization of adsorbents through impregnation is a process in which other materials are loaded onto the surface of the adsorbent to enhance its adsorption performance (Brazil et al., 2022). In this regard, metal impregnation can improve the physical and chemical functionality of the adsorbent by increasing the number of active binding sites and introducing more oxygenated functional groups. While metal oxides can be used as independent adsorbents for pollutant removal, they often have low stability and high agglomeration. Functionalizing biomass-based adsorbents with metal impregnation can help overcome these limitations by increasing stability, reducing agglomeration, and improving the overall physicochemical properties (Shelke et al., 2022).

Metal oxide impregnation of biomass-based adsorbents has been studied using a variety of nanosized organic or inorganic metallic oxides or hydroxides, including cerium hydroxide, manganese oxide, ferric oxide, zirconium oxide, and activated alumina oxides (Keikavousi Behbahan et al., 2021; Maheshwari et al., 2023). However, the field application of nano-sized sorbents has several problems, such as excessive pressure drop if used in incomplete solid-liquid separation. In addition, biomass nanoparticles such as adding different waste materials tend to aggregate in solution and thus lose sorption capacity (Feng et al., 2020). Furthermore, manganese oxide impregnated adsorbents are getting attention in dye removal due to their unique properties. Manganese oxide can be used as an individual adsorbent for contaminants removal. However, the use of nano-sized adsorbents in wastewater treatment faces several challenges, such as incomplete solid-liquid separation in fluid-bed systems and significant agglomeration in aqueous solution, leading to a low adsorption performance. To overcome these issues, nano-sized metallic oxides have been impregnated on porous materials, like biomass adsorbents (Wan et al., 2018).

2.7.2.1 Manganese oxide

Manganese oxides exhibit a range of attractive qualities, including their redox activity, electrochemical properties, large surface area, porosity, stability under diverse environmental conditions, low cost, and environmental friendliness. Thus, impregnating manganese oxide nanoparticles into the porous structure of biomass material, like activated carbon, hydrochar, and biomass-based adsorbents, enhances the adsorption performance due to the unique properties of manganese oxide (Brocza et al., 2024). Manganese oxide-impregnated adsorbents have better adsorption performance for a variety of pollutants such as dye, heavy metals, and organic compounds, increasing the performance and the selectivity of the adsorbent (Li et al., 2022). Besides, manganese oxide enhances the adsorption performance, acting as a catalyst in the adsorption process (Victor et al., 2019). A study conducted by Liu et al. (2024), achieved 95% methylene blue dye removal using lignin biochar, while a study conducted by Alalid et al. (2020) removed arsenic and lead successfully using manganese oxide impregnated on date tree waste biomass adsorbent.

Manganese oxide is considered harmless and cost-effective, which can subsequently reduce the production cost and increase the environmental friendliness of the adsorbent by impregnating it with manganese oxide. While manganese oxide-impregnated adsorbents exhibit enhanced adsorption performance by facilitating the breakdown of pollutants and are considered cost-effective functionalized adsorbents, there are limitations to their effectiveness in dye removal applications, such as uniform distribution of the metal oxides and clumping of nanoparticles on the surface (Patil et al., 2016). These challenges can be overcome by careful control over the synthesis procedure. Moreover, manganese oxide impregnations address the challenges faced by biomass adsorbents, including agglomeration of adsorbents, low porosity, and low surface area. Hence, nano-sized metallic oxides have been immobilized on porous materials to eliminate these

technical obstacles. Hence, functionalizing biomass-based adsorbents by impregnating the porous material with metal oxide will enhance the adsorption performance (Liu et al., 2021).

2.8 Significant characteristics of adsorbents

Characteristics of the adsorbents are studied before and after modification to understand the changes on the surface as well as the changes in the adsorption process for dye removal. This is crucial because the overall adsorption process encompasses three primary mechanisms: diffusion, surface chemical reactions, and surface complexation (Della-Flora et al., 2020). These mechanisms are influenced by the properties of both the adsorbent and the adsorbate. The activated carbon derived from avocado seeds exhibits a nearly neutral surface pH of 6.1-6.8, along with hydrophobicity- hydrophilicity ratio values below 1.0, signifying the predominantly hydrophilic character of this material (Della-Flora et al., 2020). The majority of the biomass-based adsorbents from fruit waste have the highest surface element for carbon, followed by hydrogen, nitrogen and oxygen. However, in some cases, a higher amount of oxygen is recorded in unmodified adsorbents due to the moisture content of the adsorbent (Murugesan et al., 2019).

The point of zero charge (pH_{pzc}) is studied to understand the pH values on the surface of the adsorbents surface, which exhibits a positive charge when the pH is below the point of zero charge and a negative charge when the pH exceeds the pH_{pzc} (Rodrigues et al., 2011). The pH_{pzc} is measured by the pH value ΔpH of zero by calculating the difference between the initial and final pH of the solutions. For cationic and anionic dye removal, the point pHpzc is essential to understanding how the pH affects

the adsorption process. Recent studies conducted on biosorbent for dye removal reported that cationic dye removal was observed above the pH_{pzc} of the adsorbent, while

anionic dyes favoured pH below the pH_{pzc} of the adsorbent (Chen et al., 2023; Mahalaxmi & Kumar, 2024; Schadeck Netto et al., 2019).

Surface morphology enables researchers to see the changes in porosity, while surface area analysis gives detailed information on the surface area, pore size, and the category of the adsorbent (micropore, mesopore, and macropore). A study conducted by Gonza´lez et. al. (2007), have reported mesopores were formed at 1000 °C under nitrogen flow for pyrolysis without chemical activation, whereas with chemical activation, carbonization at 800°C without nitrogen flow presented heterogeneity of the micropore size and microporosity (Elizalde-González et al., 2007). However, using HTC in recent studies, researchers were able to develop microporosity at lower temperatures of >350 °C, reducing the cost of production by decreasing the consumption of energy and time. Similar high surface areas have been reported for physically activated and functionalized biomass-based adsorbents.

Besides, the chemical functional groups with wavelengths ranging from 4000 - 400 cm^{-1} give specific chemical groups on the surface of the adsorbent. Avocado by-products (avocado oil, avocado seed and avocado peel) has several chemical functional groups such as hydroxyl (-OH, 3200-3500 cm^{-1}), carboxyl (C-O,1000-1300 cm^{-1}), C=C, alkene (1630 cm^{-1}) or aromatic (1475-1600 cm^{-1}) and C-H, $-CH_3$ and $-CH_2-$, alkane (2850-3000 cm^{-1}, 1375-1450 cm-1, 1465 cm^{-1}), aromatic (900- 960 cm^{-1} and 3050 – 3100 cm^{-1}) or aldehyde (2750 -2850 cm^{-1}) (*Typical IR Absorption Frequencies for Common Functional Groups*). However, the most important for activated carbons among these functional groups found in avocado are O-H groups from alcohols and phenols, aromatic rings, C=O from esters and carboxylic groups, and finally CH groups from aromatic and aliphatic (Leite et al., 2018b)

In summary, the modification of the adsorbents affects the physicochemical characteristics of the adsorbents, which enhance the adsorption performance. Thus, the limitations of raw adsorbents are overcome by the chemical and physical modification of the adsorbents. While the carbonization of adsorbents increases the surface area of the adsorbent by removing the organic matter on the surface of the adsorbents, the chemical activation increases the oxygenation functional groups. Besides, the functionalization of the adsorbents using metal oxides also enhances the physicochemical properties by increasing the surface area, resulting in efficient dye removal.

2.9 Modelling and optimization methods

The traditional methods used for optimizing the adsorption process require extensive experimentation and are time-consuming (Yusuff et al., 2021). Furthermore, it has proven difficult to achieve efficient optimum conditions using traditional methods, as they did not consider the interactions between the parameters that affect the adsorption process. Statistics and predictive tools such as Design of Experiment (DOE) and Machine Learning (ML) can efficiently optimize and predict the adsorption performance (Ecer & Yılmaz, 2024; Fetimi et al., 2021; Oluwasina et al., 2020). The optimization of process parameters is a crucial step in determining how to increase process efficiency. The use of statistical optimization methods in the development of adsorption processes can result in lower process variability and lower resource requirements, such as raw materials, equipment, and time. The number of factors influencing adsorption impacts the required number of experiments for process optimization. A higher number of process parameters necessitates a larger number of experiments to determine the efficiency of dye removal across all possible combinations of influencing factors (Yusuff et al., 2021). Hence, most articles in the literature focus solely on the pollutant's removal efficiency. On the contrary, the utilization of machine learning and artificial intelligence algorithms within statistical optimization methods for modelling and optimizing adsorption processes can reduce

process variability and resource requirements (such as raw materials, effort, and experimental time)(Rosly et al., 2022). Previous studies have employed response surface methodology (RSM) to investigate factor interactions, which proves more efficient than traditional approaches that focus on one parameter at a time. Hence, including random forest (RF) and decision tree (DT) algorithms via machine learning can be the approach to achieve cost reduction and minimize the consumption of valuable resources like energy and materials.

Design of Experiment (DOE) is a statistical tool used to reduce the number of experiments and minimize the use of chemicals and analysis, thereby lowering the overall cost of the adsorption process. Furthermore, Response Surface Methodology (RSM) is an advanced statistical technique using DOE to optimize the adsorption process and understand the effect of the parameters on the adsorption process. Central Composite Design (CCD) is a commonly used design in RSM, allowing researchers to specifically design experiments to understand the impact of variables on the adsorption process (Tharayil & Chinnaiyan, 2024). RSM-CCD uses mathematical and statistical techniques to develop empirical models based on the experimental data (Ecer et al., 2020; Van Thuan et al., 2017). It aims to optimize analysis by combining the effects of various variables into minimal test runs, thereby reducing the number of experiments needed to evaluate the relationship between design responses and factors (Ecer & Yılmaz, 2024; Kumari et al., 2023). Thus, when evaluating the relationship between independent variables, RSM-CCD is used to maximize performance yield, which can be influenced by the independent variables (Ecer & Yılmaz, 2024; Ecer et al., 2020, 2023).

2.9.1 Machine learning algorithm

Machine learning is an artificial intelligence-based approach that empowers computers to learn from complex, multidimensional data sets and develop predictive models. This

technology has proven to be a potent solution for tackling practical challenges across a wide range of industries, drawing substantial interest and attention. Thus, ML algorithms can be used effectively to predict the adsorption performance of adsorbent to remove recalcitrant pollutants in waste water treatment (Ismail et al., 2024). Its application in water treatment and desalination has gained prominence, as it offers practical solutions to combat water pollution and scarcity. In recent years, AI techniques have been utilized to optimize these processes, leading to improved efficiency. Moreover, the application of AI is anticipated to reduce operational costs in water treatment by optimizing chemical usage and decreasing overall expenses (Alam G et al., 2022). Hence, AI is being increasingly applied in water treatment to overcome the limitations of traditional methods. The water industry is investing in AI, with an estimated investment of $10.8 billion by 2030, and this technology is expected to reduce operational costs by 20 to 30% through optimized chemical usage and cost reduction.

AI offers simplicity, flexibility, and ease of implementation, making water treatment processes more efficient. Commonly used AI techniques in water treatment include Random Forest, Recurrent Neural Network, Convolutional Neural Network, Decision Tree, Feed Forward Back Propagation Neural Network, and Adaptive Network Based Fuzzy Inference System. However, a major challenge is the availability of sufficient data for AI to predict future outcomes and enhance system performance. ML models significantly reduce material and labor consumption in future experimentation and research by using regression models to predict adsorption performance.

The expanding array of ML models, such as random forest (RF), has effectively demonstrated their ability to simulate complex relationships between influencing elements and dependent outcomes (de Miranda Ramos Soares et al., 2020; Ghaedi et al., 2014). Random Forest models create numerous diverse decision trees that randomly train

a selected subset of the data and a limited set of randomly chosen features. This intentional use of randomness helps minimize overfitting and cultivate diversity, enabling the model to navigate complex relationships and effectively uncover hidden patterns within the data (Mehmandost et al., 2022).

Decision trees are straightforward hierarchical models that use recursive partitioning to similar data groups, and they are categorized as classification or regression trees based on the predicted output (Hassan et al., 2017). Each internal node applies a condition on an input variable, directing the process. The process ends at a leaf node, where the predicted value, which serves as the output of the model, is determined for the specific input values that traversed through the tree (Alpaydin, 2020). Large regression trees are prone to overfitting, while smaller trees may not adequately capture the underlying patterns in the data. Researchers aim to construct the most compact tree that can generalize well to new data with minimal error (Hastie et al., 2009). This involves employing pruning strategies before and after to refine the structure of the tree and enhance its generalization ability.

Decision trees have advantages like interpretability and low computational demands, but they can be limited in accuracy, such as overfitting, sensitivity to irrelevant features, and instability to training data changes. However, ensemble techniques like combining multiple decision trees, such as a random forest regression model, can help mitigate the limitations of individual decision trees as shown in Figure 2.2. By leveraging the strengths of each tree while averaging out their weaknesses, ensemble methods result in more robust and accurate models (Cha Zhang, 2012). Random Forest models are highly effective for predicting dye adsorption onto adsorbent materials. They can reliably forecast the adsorption potential of new adsorbents by learning the relationships between adsorbent properties and dye uptake, even with limited data or complex material

structures. Additionally, Random Forest models provide valuable insights into the key factors driving dye adsorption by analysing the importance of different features within each tree (Ghaedi et al., 2014). This deeper understanding enables more accurate prediction of dye removal, accelerating the development of effective dye removal technologies (de Miranda Ramos Soares et al., 2020)

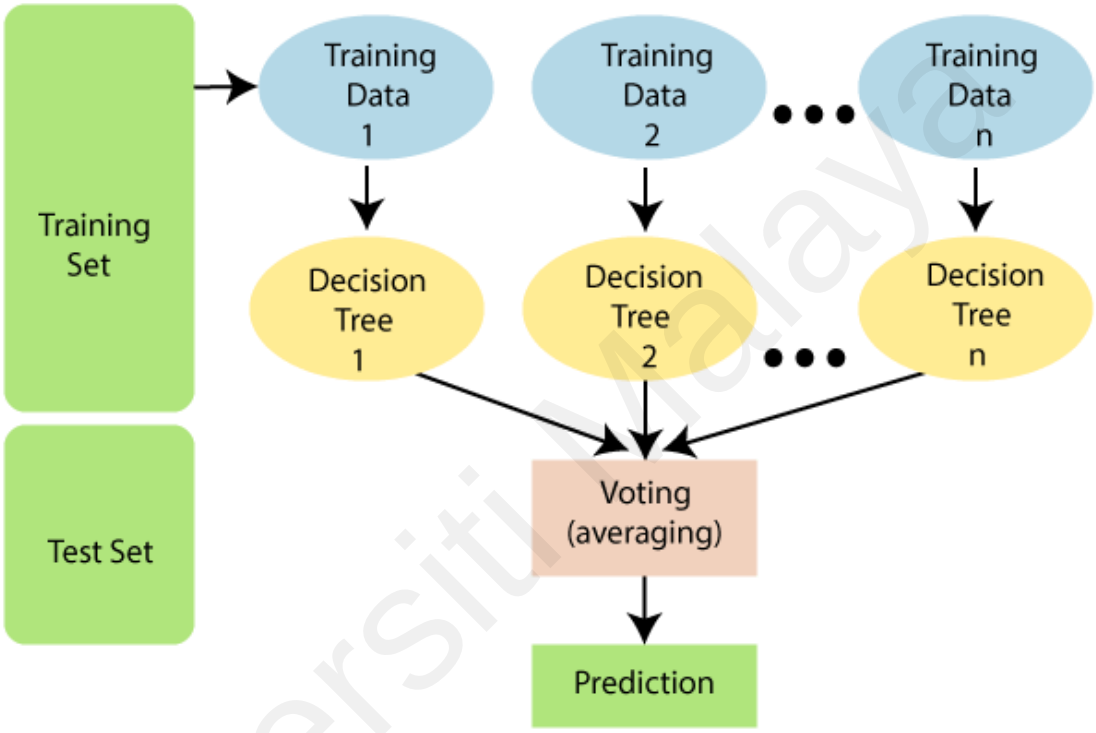

Figure 2.3 : Training and testing in random forest regression model

2.9.1.1 Random forest modelling

Random Forest modelling is a supervised learning method that is versatile in handling both regression and classification tasks with labelled target variables. While individual decision trees exhibit high variance, their collective utilization significantly reduces overall variance by training on specific data samples. The final output relies on insights from multiple trees rather than a single tree. In classification, a majority voting classifier determines the ultimate decision, while regression problems produce an output representing the mean value of all individual outputs.

This process of combining outputs, called "Aggregation," is illustrated in Figure 2.3. However, when dealing with a greater number of process parameters or variables, more experimental data and processing are required for higher accuracy. Integrating ML and AI algorithms into statistical optimization methods offers a promising solution for mitigating process variability and resource demands (de Miranda Ramos Soares et al., 2020; Rosly et al., 2022).

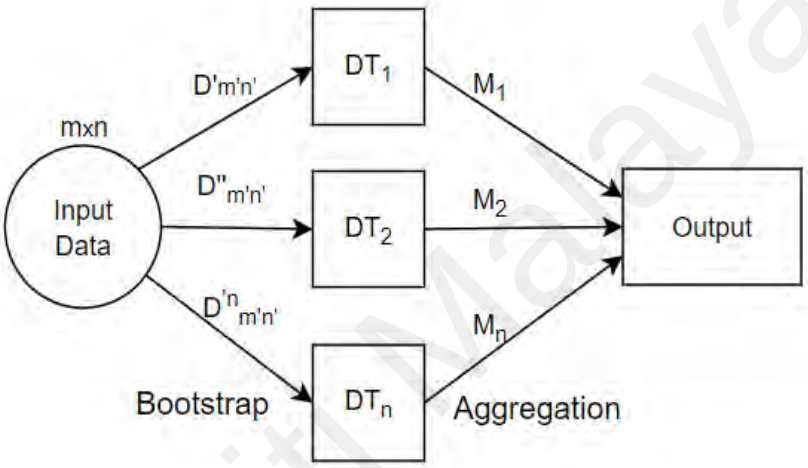

Figure 2.4 : Flowchart of random forest regression.

Using ML algorithms to predict adsorption efficiency simplifies experimental intricacies by reducing their number and duration while establishing nonlinear connections between input and output variables (Wang & Yao, 2023).The combination of RSM with this soft computing technique can overcome the limitations of RSM and accurately predict results by including non-controllable parameters in modelling. Additionally, this approach works on a smaller number of experiments, allowing for a more realistic solution to be achieved for unseen behaviours of post-process parameters.

In summary, the Response Surface Methodology-Central Composite Design and machine learning techniques for dye removal in industrial wastewater offer significant

advantages over traditional methods. Machine learning models, such as Random Forest, enhance predictive accuracy, enabling quicker and more cost-effective optimizations. Thus, combining these approaches can efficiently optimize and predict the adsorption process by considering the interactions between multiple parameters, reducing the need for extensive experimentation, and lowering resource consumption. This combination of advanced techniques leads to a more sustainable and effective approach to the removal of dye from wastewater with improved process efficiency and reduced operational costs.

2.10 Factors affecting the adsorption performance

2.10.1 Initial pH of the solution

The pH of the solution plays a vital role in the adsorption process, which depends heavily on both adsorbents being used and the pollutants being treated. Some adsorbents work best in acidic pH, while others work best in neutral or alkaline pH (Pandiarajan et al., 2018). The pH value is an influence on the surface charge of the adsorbent material and further affects the removal of cationic dyes and antibiotics from the aqueous solution. Studies show that when the pH of the solution has increased, the adsorption of heavy metals in an aqueous solution gradually increases until they reach the optimum operational value (Chen et al., 2018). Similarly, studies show that the adsorption capacity increases when the pH is increased from 2 and higher. The low adsorption capacity in lower initial pH values is due to the surface of the adsorbent being surrounded by the ions H+, inducing repulsive forces and decreasing the interaction of the ions of the dyes with the sites of the adsorbent. Thus, reduction in the adsorption rate at low pH values can be due to the high concentration and the mobility of the ions H+ (Amela et al., 2012). On the other hand, at high pH, the concentration of H+ decreases, and the total surface of the adsorbent becomes negatively charged, enhancing the sorption of the ions' dye through electrostatic interactions.

The optimum pH of the solution for a biosorbent depends on the adsorbate and the point of zero charge. For cationic dyes, higher pH values are optimal, as the cationic dyes are positively charged, and when the pH is higher than the point of zero charge for the adsorbent, the surface of the adsorbent will be negatively charged, attracting the cationic dye molecules. However, some research indicates that the highest adsorption occurs at lower pH values, as low as pH 1.5, since a highly acidic medium exhibits a significant electrostatic attraction between the biosorbent's positively charged surface and the acidic, anionic dye. As the pH value of the biosorption system increases, the number of negatively charged sites grows, while the number of positively charged sites decreases (Ay et al., 2012). Furthermore, due to electrostatic repulsion, a negatively charged surface site on the biosorbent does not encourage dye anion biosorption.

2.10.2 Adsorbent dosage

Studying the effect of adsorbent dosage provides insight into the effectiveness of adsorbent and the efficiency of dye adsorption at minimal dosages, helping to evaluate the economic feasibility of the adsorbent process. A study conducted by Maheshwari et al. (2023), used unmodified adsorbent derived from banana peel and orange peel for cationic dye removal, which required an adsorbent dosage of 2.5 g/L. On the other hand, a study conducted by Salah et. Al. (2022) used phosphoric acid-activated adsorbent derived from plant biomass for cationic dye, which required an optimum adsorbent dosage of 0.2 g/L. These studies indicate that the amount of optimum adsorbent dosage significantly decreases with the modification of the biomass-based adsorbents, which will lead to an overall cost reduction.

Furthermore, due to the availability of the binding sites on the adsorbent, the adsorption process increases with the increase of adsorbent dosage until the equilibrium is reached (Inbaraj et al, 2004). After a specific adsorbent dose, the adsorption decreases

gradually, this may be because the active sites are saturated with accumulated particles, which result in repulsion between the dye molecules and the adsorbent (Roy et al., 2018). A study conducted by Prabakaran et. Al. (2022) used a dosage range of 10-80 mg, where the highest dye removal was recorded when the dosage was increased from 10 to 50 mg. However, it was also reported that a slight decrease was noticed when the dosage was increased further from 60-80 mg; this may be due to agglomeration of the adsorbents (Prabakaran et al., 2022).

2.10.3 Initial concentration of the pollutants

The percentage of dye removal is highly dependent on the initial dye concentration. As the initial dye concentration increases, the percentage of dye removal typically decreases due to the saturation of adsorption sites on the adsorbent surface (Khamwichit et al., 2022). At lower concentrations, more active sites are available for adsorption, but as the concentration increases, these sites become insufficient. However, a higher initial dye concentration can increase the loading capacity of the adsorbent due to a stronger driving force for mass transfer (Duan et al., 2022; Inyinbor et al., 2023).

The initial concentration of the dye solution significantly impacts the adsorption process by affecting the ratio of dye molecules to available active sites and overcoming the resistance to mass transfer between the liquid phase (pollutants) and the solid phase (adsorbent) (Mahalaxmi & Kumar, 2024; Shalaby et al., 2016). Furthermore, real textile wastewaters contain higher dye concentrations than those typically used in literature studies. Therefore, researchers employ empirical design procedures based on adsorption equilibrium conditions to predict the adsorber size and performance.

2.10.4 Contact time

Contact time is the duration required for the adsorption process to reach equilibrium, which plays a crucial role in maximizing adsorption efficiency in industrial applications.

Initially, adsorption performance increases rapidly with contact time, due to the available active binding sites (Hambisa et al., 2022). As time progresses, these increases slow down due to various factors such as collisions between dye molecules, repulsive forces between the adsorbent and adsorbate, and decreased collisions among dye molecules once equilibrium is achieved (Jasri et al., 2023). However, over time, the uptake rate slows due to increased steric hindrance and a decrease in available active sites, which limits the diffusion of dye molecules onto the adsorbent surface (Hambisa et al., 2022; Sivaranjanee et al., 2024).

In conclusion, as contact time increases, the adsorption increases at first, then the dye removal becomes stable, and no more adsorptions can be observed. This is because at the beginning of the adsorption process, all the active binding sites of the adsorbent will be vacant, and with allowed time, there will be fewer sites available (V. S. Munagapati et al., 2018).

2.11 Summary

The adsorption process is a highly efficient method for removing dyes from aqueous solutions due to its simplicity, ease of operation, and flexibility. However, current commercial adsorbents are expensive and have limited regeneration ability. Biomass-based adsorbents present a promising alternative as they offer cost-effective solutions and enhanced regeneration capacity, making the overall treatment process more sustainable. Derived from biomass waste, these adsorbents exhibit excellent physicochemical properties, reducing both production costs and the need for toxic chemicals.

Underutilized fruit waste, such as banana peels and avocado seeds, can be used as biomass-based adsorbents for dye removal with minimal modification, further reducing energy consumption and production costs. While these materials show promise, their adsorption performance often requires enhancement. Modified adsorbents, with increased

surface area, porosity, selectivity, and stability, demonstrate greater efficiency in dye removal. Hydrothermal carbonization (HTC), compared to conventional pyrolysis, offers a more environmentally friendly and energy-efficient alternative. HTC also produces a higher mass yield, making it more cost-effective for large-scale applications. Additionally, chemically activating biomass-based adsorbents and impregnating them with metal oxides significantly enhances their adsorption performance.

Despite these advancements, several research gaps remain. While individual biomass materials like banana peels and avocado seeds have been explored for dye removal, limited research exists on hybrid adsorbents combining both materials. This gap can be addressed by developing a hybrid adsorbent synthesized via a two-step hydrothermal carbonization process, which could offer improved dye removal efficiency. Furthermore, while the optimization of adsorption parameters such as contact time, adsorbent dosage, pH, and dye concentration has been studied for individual adsorbents, their effects on hybrid adsorbents remain underexplored. Additionally, the adsorption mechanism of mixed biomass waste adsorbents requires further investigation.

There is also a lack of research integrating machine learning techniques, such as Random Forest, with traditional optimization methods like Response Surface Methodology (RSM) to predict and enhance the dye removal process. While both approaches have been used separately, their combined application could significantly improve the efficiency and scalability of dye removal processes, reducing the need for extensive experimentation. Another notable knowledge gap is the economic feasibility of producing hybrid adsorbents from fruit waste compared to commercial carbon-based adsorbents, which remains underexplored, particularly for large-scale industrial applications. This research will address this gap by evaluating the cost-effectiveness and economic viability of hybrid adsorbents in real-world wastewater treatment systems.

In conclusion, the current literature highlights several knowledge gaps, including the synthesis of hybrid adsorbents from mixed biomass materials (especially avocado seeds and banana peels), the optimization of adsorption conditions, a comprehensive understanding of the adsorption mechanism, the integration of machine learning for predictive modelling, and a thorough economic evaluation. Thus, in this research, addressing these gaps will advance the use of biomass-based adsorbents in sustainable wastewater treatment and support circular economy initiatives.

CHAPTER 3: METHODOLOGY

3.1 Introduction

This chapter outlines the materials and methods used to develop and investigate the performance of adsorbents derived from banana peels and avocado seeds, focusing on five main objectives. The methodology for Objective 1 involves the synthesis of the adsorbent through a two-step hydrothermal carbonization process. The first step includes HTC, followed by activation transforming the biomass into a porous, carbon-rich adsorbent. The second step involves the functionalization of the activated biomass adsorbent via manganese oxide impregnation. The adsorbents were characterized for surface morphology, elemental composition, chemical functional groups on the surface, and the point of zero charge for the raw unmodified adsorbent, the adsorbent derived from the first step of synthesis involving HTC with phosphoric acid activation, and the adsorbent derived from the second step of synthesis involving the metal oxide impregnation.

The methodology for Objective 2 covers the experimental design used to analyse the effects of operational parameters and optimize the adsorption performance in terms of colour removal and adsorption capacity. This section also includes the selection and justification of the operational conditions, such as initial pH, contact time, adsorbent dosage, and initial dye concentration. Additionally, the methodology for validating the adsorbent's performance in COD removal and comparing the newly developed hybrid adsorbent with a commercial decolourizing adsorbent is described. Objective 3 focuses on the use of nonlinear models to conduct adsorption kinetic and isotherm studies using the best-performing hybrid adsorbent for methylene blue dye removal. This section also highlights the potential adsorption mechanism of the hybrid adsorbent in cationic dye removal.

The methodology for Objective 4 involved the application of machine learning models, specifically random forest regression, to analyse the experimental data obtained from the adsorption study. Different training and testing configurations were utilized to develop the predictive model, which was then used to estimate the dye removal efficiency in terms of colour removal, adsorption capacity, and COD removal. Additionally, this objective included the validation of the predictive model for scale-up applications using 3L and 5L of simulated methylene blue dye wastewater.

Finally, Objective 5 focused on evaluating the economic viability and feasibility of the adsorbent, detailing the methods used for the regeneration study and production cost analysis. Additionally, the newly developed hybrid adsorbent was tested on various industrial wastewaters to investigate its industrial applicability and performance in real-world wastewater treatment applications, comparing its effectiveness to commercial adsorbents. The overall methodology for this project is illustrated in Figure 3.1.

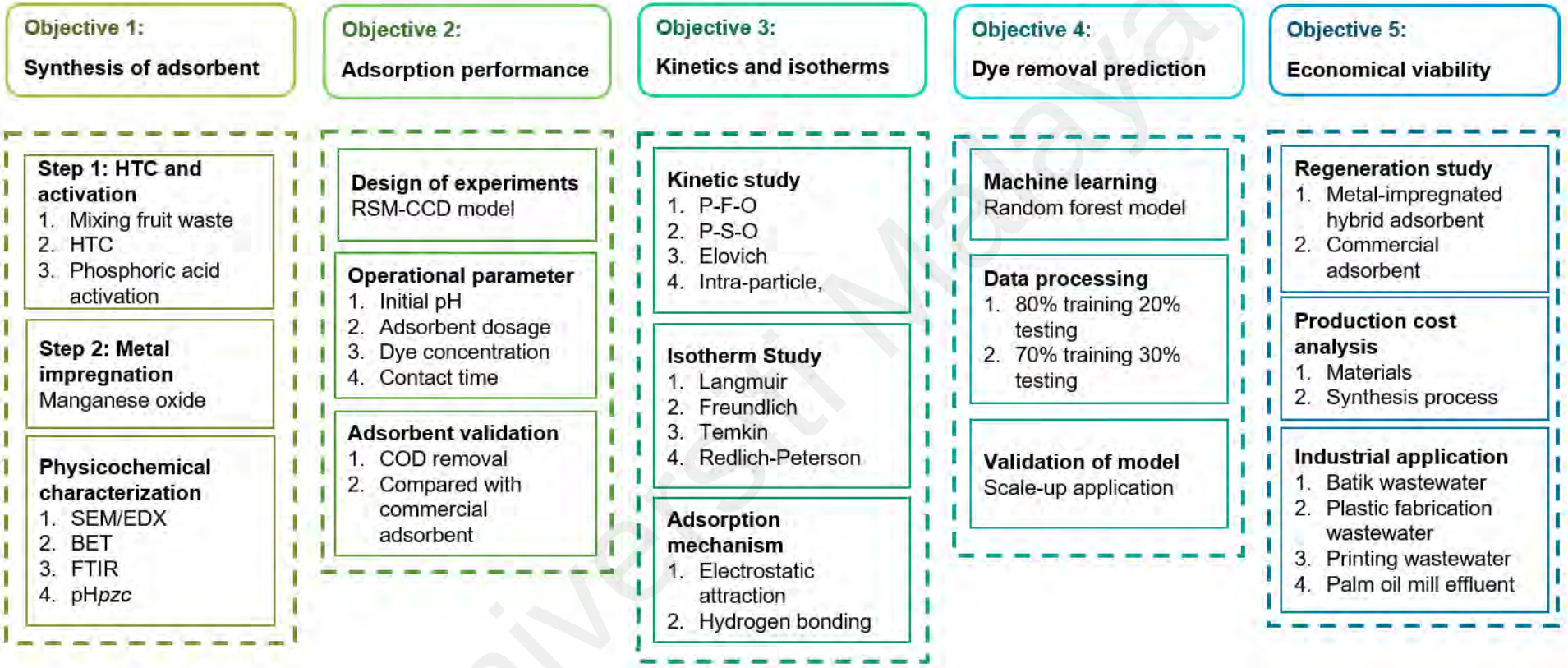

Figure 3.1 : Overall methodology of research

3.2 Chemicals and materials

The chemicals for the experiments were purchased from Sigma-Aldrich (Malaysia). Hydrochloric acid (HCL) and sodium hydroxide (NaOH) were used for pH adjustment, while phosphoric acid (H_3PO_4, 85%) was used in the chemical modification of adsorbents. Manganese oxide (Mn_3O_4) was used in the metal impregnation of the adsorbents, while Methylene blue (MB), a cationic dye, was used as an adsorbate for experiments. Sodium hydroxide (NaOH) was used in the characterization of the adsorbents for the point of zero charge, while sulphuric acid (H_2SO_4) and ethanol (C_2H_6O) were used in the regeneration study. Distilled water was used in the preparation process to clean the materials used.

As for the adsorbent precursors, banana peels were collected locally from stalls free of charge, while avocado seeds were purchased in Bangsar, Malaysia. The industrial wastewater was collected from local factories in Malaysia, including batik wastewater from a factory in Kuala Lumpur, printing wastewater from a local factory in Cheras, plastic fabrication wastewater from a factory in Selangor, and palm oil mill effluent from a mill in the Klang Valley.

3.3 Synthesis of adsorbent

Sun-dried avocado seeds and banana peels were thoroughly washed with distilled water to remove impurities. Each material was then oven-dried separately at 60 °C for 24 hours to eliminate excess moisture. The dried samples were ground into a fine powder using an electric grinder (Xinanbangle, 3000W) in small batches and then sieved through a 150 µm (No. 45) mesh for uniformity. The powdered samples were stored in labelled airtight containers for further use as raw avocado seeds (RAS) and raw banana peels (RBP).

3.3.1 Fruit-waste mixing ratio

Experiments were conducted using RAS and RBP to evaluate their adsorption performance for methylene blue dye removal. A raw hybrid adsorbent (RA) was then developed by optimizing the RAS-to-RBP ratio using Response Surface Methodology – Central Composite Design (RSM-CCD) to achieve the best adsorption performance in terms of colour removal, COD reduction, and adsorption capacity. The hybrid adsorbent synthesis was optimized for a total of 10 g of RA, with the RAS-to-RBP ratio varying from 25% to 75% as per the RSM-CCD design. The specific mixing ratios are summarized in Table 3.1. The optimized RA composition was then selected for further processing and subjected to the two-step hydrothermal carbonization process to enhance its adsorption properties.

Table 3.1 : Optimization of raw hybrid adsorbent

Mixing ratio	Weight of RAS	Weight of RBP
0% RAS to 100% RBP	0 g	10 g
75% RBP to 25% RAS	2.5 g	7.5 g
50% RBP to 50% RAS	5 g	5 g
25% RBP to 75% RAS	7.5 g	2.5 g
100% RAS to 0% RBP	10 g	0 g

3.3.2 Hydrothermal carbonization and activation

Two-step hydrothermal carbonization was divided into carbonization and activation in Step one and metal oxide impregnation in Step two, as illustrated in Figure 3.2. This division structures the synthesis process into material preparation and functionalization, ensuring optimal development of the adsorbent's properties before metal incorporation. In the first step, hydrothermal carbonization was carried out by filling 80% of the autoclave tube with 15.00 g of the optimized raw hybrid adsorbent and 65 mL of distilled water. The autoclave system was placed inside a pre-heated oven at a varied temperature from 180 °C to 220 °C and heated for 2.0 h to check the yield of the materials. After 2.0 h, the autoclave was removed immediately and quenched in water. The resulting carbonized material was washed repeatedly with distilled water, filtered thoroughly till the filtrate was clear in colour, and dried at 100 °C overnight. The yield was calculated for each of the temperatures and was calculated using the following Eq (3.1). Where *m* (g) is the initial mass of HA. The m_f (g) is the final mass of the hybrid adsorbent (HTC/HA).

$$\%Yeild = \left(\frac{m}{m_f}\right) x\ 100 \tag{3.1}$$

The dried hydrochar, HTC/HA, was used in the chemical activation process performed using 1:1 (wt./v) with raw materials and 85 % phosphoric acid (H_3PO_4) (M. C. Silva et al., 2021). 10.0 g of HTC/HA were mixed with 10.0 mL of H_3PO_4. A clumpy mixture was formed, as in Figure 3.2, for all samples, and 60 ml of distilled water was added to each beaker to produce a smooth, thick paste. The beakers were sealed with paraffin and were left for 24 hrs at room temperature. The samples turned dark brown after 24 hrs and were heated at 60 °C overnight, it was then sieved and stored until further use. The materials were activated using a furnace temperature ranging from 250 °C to 550 °C at a

heating rate of 5 °C/min. 20.0 g of each sample was placed in a covered porcelain crucible for activation by heating at 250 °C, 350 °C, 450 °C, and 550 °C for 120 min. Once the furnace had cooled down, the resultant material was purified with an aqueous NaOH solution to remove the excess H_3PO_4, followed by rinsing the activated hybrid adsorbent with distilled water until it reached a neutral pH. Finally, the activated hybrid adsorbent was dried at 100°C overnight. The samples were sieved to prevent clumping before being stored in airtight containers.

3.3.3 Metal oxide impregnation

The metal impregnation was conducted using manganese oxide and activated hybrid adsorbent derived from the banana peel and avocado seed. The impregnation preliminary experiments were conducted using manganese oxide and hybrid adsorbent at 0.1:1, 0.5:1, and 1:1 (Mn_3O_4: HA). From the preliminary study, the 0.1:1 ratio was used to impregnate activated hybrid adsorbent (HA) in a beaker. 1.0 g of manganese oxide was dissolved in 50 mL of distilled water, followed by adding 10 g of activated hybrid adsorbent into the beaker. The mixture was stirred at 300 rpm for 2 hours on a magnetic stirrer, and the beakers were left undisturbed on the counter for an additional 2 hours. The impregnated activated hybrid adsorbent was dried at 100°C for 12 hrs in an oven. The impregnated hybrid adsorbent was then washed several times to eliminate any excess MnO and further dried in an oven. The final adsorbent was carefully collected, stored in an airtight container and labelled as HA/Mn.

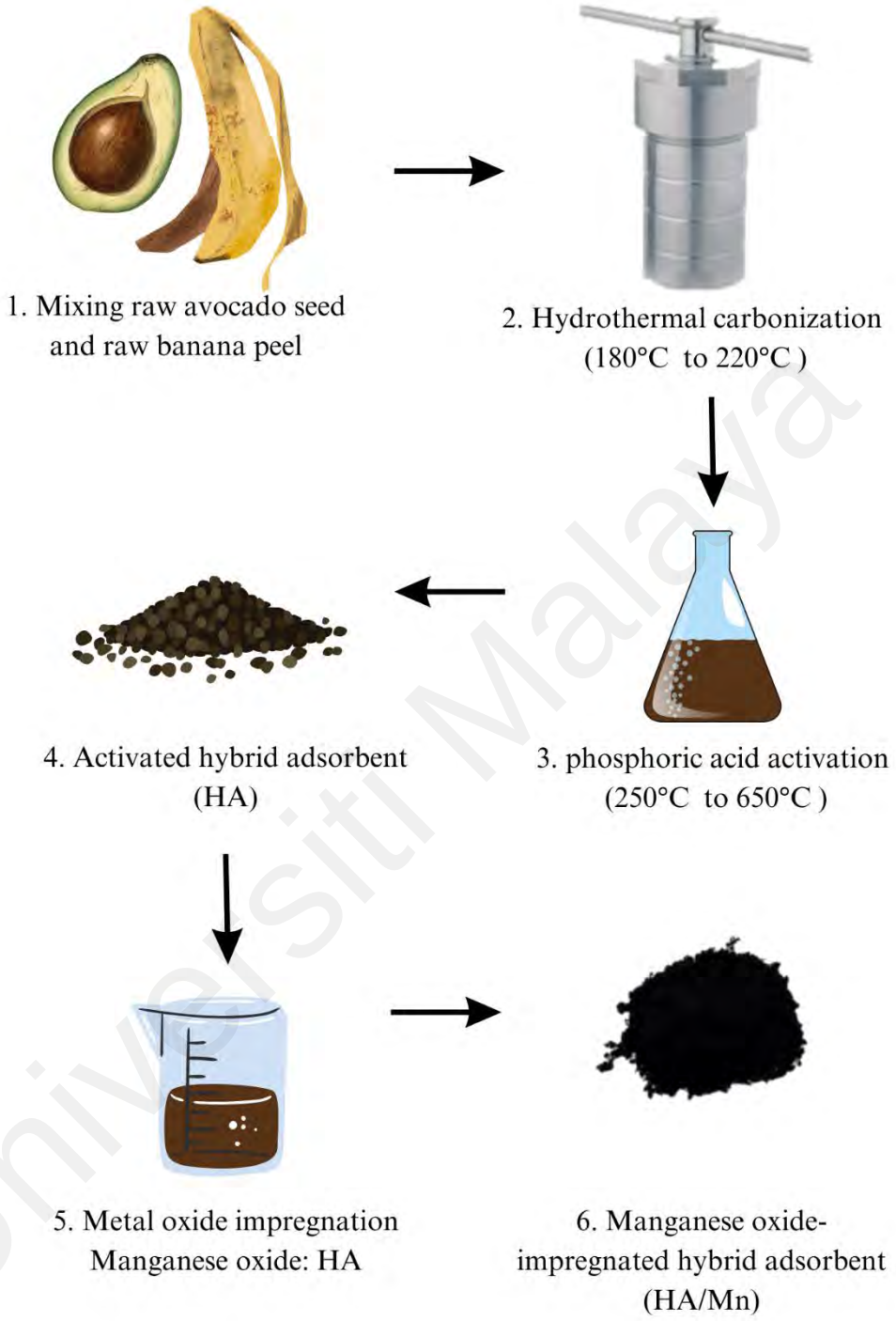

Figure 3.2 : Synthesis of hybrid adsorbent

3.4 Adsorbent characterization

The point of zero charge (pH_{pzc}) was determined for raw adsorbent (RA), activated hybrid adsorbent (HA), and metal-impregnated hybrid adsorbent (HA/Mn) in pH ranging from 2 to 11. Fourier Transform Infrared Spectroscopy (FTIR) analysis was performed with a Perkin Elmer Spectrum Version 10.4.2 FTIR spectrometer, providing unique insights into the chemical functional groups of the hybrid adsorbents (RA, HA, and HA/Mn) using Perkin Elmer Frontier FTIR with wave numbers in the range of 500 cm^{-1}-4000 cm^{-1}. The specific surface area was analysed through Brunauer-Emmett-Teller (BET) (TriStar II-Micromeritics) for the hybrid adsorbents. BET provided the pore size, surface area, and pore volume for RA, HA, and HA/Mn. The morphological patterns and the elemental composition of hybrid adsorbents were characterized by Scanning Electron Microscopy/ Energy Dispersive, SEM/EDX using the equipment PHENOM ProX, and the software used for analysis was PhenomProSuite. SEM/EDX imaging provided visual data on the porosity of the adsorbents and identified elements along with their respective weight percentages present on the surface after adsorbent modification.

3.5 Experimental design

The adsorption process was designed and optimized using the Response Surface Methodology-Central Composite Design (RSM-CCD) in Design-Expert 12. Independent variable values were selected based on preliminary experiments, industrial wastewater characteristics, and relevant scientific literature. Industrial dye wastewater typically contains dye concentrations ranging from 0.05 to 0.25 g/L, with pH values between 6 and 10, though some dyeing processes can lower the pH to 5 (Yaseen & Scholz, 2018). In batch adsorption treatments, the contact time generally varies from 1 to 4 hours when using powdered adsorbents, whereas continuous adsorption processes can extend from 12 to 120 hours (Mohd Hanafiah et al., 2024).

The literature reports various optimal conditions for cationic dye removal as summarized in Table 2.4. For instance, Cathoglu et al. (Cathoglu et al., 2021) achieved optimal adsorption using 2.5 g/L adsorbent, 0.5 g/L dye concentration, and a 50-minute contact time. Similarly, Waghmare et al. (Waghmare et al., 2023) reported maximum colour removal with 0.6 g/L adsorbent, 0.01 g/L dye concentration, 90-minute contact time, and pH 6. Besides, Prabakaran et al. (Prabakaran et al., 2022) achieved highest performance in optimal conditions, including pH 8, 1.0 g/L adsorbent, 120-minute contact time, and 0.3 g/L dye concentration.

While most literature suggests that cationic dye removal is favoured under alkaline conditions, recent studies indicate that optimal removal can also occur in acidic environments. Salah et al. (2022) reported that crystal violet was effectively removed at pH 5 using 0.2 g/L of phosphoric acid-activated Moringa oleifera, with an optimum contact time of 240 minutes. Similarly, Watwe et al. (2023) achieved the highest removal efficiency for malachite green at pH 2, crystal violet at pH 4, and methylene blue at pH 6 using unmodified Ficus benjamina adsorbent. In contrast, anionic dyes such as methyl red and methyl orange exhibit optimal removal in highly acidic conditions between pH 2 to 4 (Salih et al., 2022). Rose et al. (2023) further reported that Congo red was effectively removed at pH 3 using sodium hydroxide-modified banana peel. These findings highlight the influence of pH on dye adsorption efficiency, emphasizing the need for pH-specific optimization.

Considering industrial wastewater characteristics and prior research using biomass-based adsorbent for dye removal, this study selected the following parameter ranges for the experimental design: pH 2–10, adsorbent dosage 0.5–5.0 g/L, dye concentration 0.1–0.5 g/L, and contact time 10–180 minutes. These parameters were optimized using DOE, as summarized in Table 3.2.

Table 3.2 : Ranges of independent variables used in the RSM-CCD

Code	Variable	Unit	Levels		
			-1	**0**	**+1**
A	Initial pH	-	2	6	10
B	Adsorbent dosage	g/L	0.5	2.8	5.0
C	Dye Concentration	g/L	0.1	0.3	0.5
D	Contact time	min	10	100	180

The experimental design consisted of a three-level (+1, 0, -1) RSM-CCD with four numerical parameters: A (Initial pH), B (Adsorbent dosage in g/L), C (Dye concentration in g/L), and D (Contact time in min). The RSM-CCD generated an experimental design with 30 runs, minimizing experiment repetition while maximizing parameter interactions, as given in Table 3.2. The number of experiments for RSM-CCD design can be calculated using Eq.3.2, where 'c' represents centre-point replicas, 'n' is the numerical components, and 'N' is the total experimental runs.

$$N = 2n + 2n + nc \tag{3.2}$$

The RSM-CCD model was used to evaluate the effect of the independent variables used in the experiments by combining statistical and mathematical approaches. Thus, providing a comprehensive understanding of the relationship between operational parameters and their corresponding outcomes, adsorption capacity, and colour removal. ANOVA statistical analysis was used to evaluate the applicability of the model. At the same time, residual plots and regression coefficients were assessed to indicate the validity of the fitted model and evaluate the relevance and suitability of actual and predicted runs.

3.6 Adsorption study

Batch adsorption experiments were conducted using the experimental design in Table 3.3, with different adsorbent dosages of adsorbent in a 50 mL pH-adjusted dye solution of known dye concentration as given in Table 3.2. The dye solution was stirred in a shaker (Lab Companion SI-300) at 150 rpm for predetermined contact times, as shown in Figure 3.3. The supernatant was filtered with a 0.22 μm syringe filter, and its absorbance was measured at the maximum wavelength of the MB dye (λmax 663 nm) using a spectrophotometer (Spectroquant® Pharo 300) without any additional reagents. For COD removal, Spectroquant COD Cell Test kits (25 -1500 mg/L) were used in the spectrophotometer to determine the COD levels before and after the adsorption experiments. The efficiency of the adsorbents for MB dye removal was calculated for the percentage of COD removal, percentage of colour removal, and adsorption capacity. The percentage of colour removal was calculated using the following Eq. (3.4), and the adsorption capacity was calculated by using Eq (3.5).

$$\%\ COD\ removal = \frac{COD_i - COD_f}{COD_i} x\ 100 \tag{3.3}$$

$$\%\ Colour\ removal = \frac{C_i - C_f}{C_i} x\ 100 \tag{3.4}$$

$$Adsorption\ capacity = \frac{C_i - C_f}{m} V \tag{3.5}$$

Where COD_i and COD_f are the initial COD concentration (mg/L) and the final COD concentration (mg/L) after the adsorption experiment, respectively. In Eq (3.4), C_i and C_f are the initial concentration (g/L) and the final concentration (g/L) of the dye, respectively; V is the solution volume (L); and m is the mass (g) of the adsorbent dosage, respectively.

Table 3.3: Experimental design for dye removal

Run	Initial pH	Adsorbent Dosage (g/L)	Dye Concentration (g/L)	Contact Time (min)
1	2	2.8	0.3	95
2	2	5.0	0.1	180
3	10	5.0	0.1	180
4	6	1.8	0.3	95
5	6	2.8	0.3	95
6	6	2.8	0.3	95
7	2	0.5	0.1	180
8	2	0.5	0.5	180
9	6	2.8	0.3	95
10	10	5.0	0.1	10
11	10	0.5	0.5	180
12	10	0.5	0.1	10
13	2	0.5	0.1	10
14	10	5.0	0.5	10
15	6	2.8	0.3	75
16	10	5.0	0.5	180
17	6	2.8	0.3	95
18	6	2.8	0.3	265
19	6	2.8	0.3	95
20	10	0.5	0.1	180
21	10	0.5	0.5	10
22	6	2.8	0.3	95
23	2	0.5	0.5	10
24	2	5.0	0.5	180
25	6	2.8	0.1	95
26	6	7.8	0.3	95
27	2	5.0	0.1	10
28	14	2.8	0.3	95
29	2	5.0	0.5	10
30	6	2.8	0.7	95

Figure 3.3 : Schematic diagram of adsorption study

3.7 Adsorption kinetics and isotherm

Adsorption kinetics and isotherm studies were conducted to evaluate the mechanism and behaviour of the hybrid adsorbent in cationic dye removal. The kinetics study was performed under optimal conditions for adsorbent dosage, initial dye concentration, and initial pH of the solution. Adsorption performance was monitored at 20-minute intervals until the contact time reached 240 minutes. Thus, the adsorption was recorded for the following contact times: 20, 40, 60, 80, 100, 120, 140, 160, 180, 200, 220, and 240 mins. The kinetic study was analysed by fitting the experimental data to three non-linear kinetic models: Pseudo-first-order in Eq. (3.6), Pseudo-second-order in Eq. (3.7), and Elovich in Eq. (3.8).

$$q_e = q_e - q_e\, e^{(K_1 t)} \tag{3.6}$$

$$q_t = \frac{k_2\, q_e^2\, t}{1 + k_2\, q_e\, t} \tag{3.7}$$

$$q_t = \frac{1}{\beta}\ln(1 + \alpha\beta t) \tag{3.8}$$

Where $K_1(min^{-1})$ and $K_2(g.mg^{-1}.min^{-1})$ are the Pseudo-First-Order and Pseudo-Second-Order constants, respectively, $q_e(mgg^{-1})$ is the adsorption capacity at equilibrium while $q_t(mgg^{-1})$ is the adsorption at any time, t (min) is the contact time. Besides, α ($mg/g.min$) is the initial adsorption rate, and β ($mgmg^{-1}$) is the desorption constant.

The isotherm study was conducted with dye concentrations ranging from 0.025 g/L to 0.3 g/L, under optimized conditions for adsorbent dosage, contact time, and initial pH. Therefore, the adsorption isotherm experiments were conducted at different concentrations, as the following 0.025, 0.050, 0.075, 0.100, 0.125, 0.150, 0.175, 0.200, 0.225, 0.250, 0.275, and 0.300 g/L. Experimental data were fitted to four non-linear isotherm models: Temkin in Eq. (3.9), Freundlich in Eq (3.10), Langmuir in Eq in (3.11), and Redlich-Peterson in Eq. (3.12) to assess adsorption capacity and surface interactions.

$$q_e = B \ln(A_T C_e) \tag{3.9}$$

$$q_e = K_f C_e^{\frac{1}{n}} \tag{3.10}$$

$$q_e = \frac{q_{max} k_L C_e}{1 + k_L C_e} \tag{3.11}$$

$$qt = \frac{\alpha_T C_e}{1 + \beta C_e^n} \tag{3.12}$$

Where $q_e\ (mg/g)$ is the adsorption at equilibrium, $q_{max}(mg/g)$ is the maximum adsorption capacity. $A_T\ (l/g)$ is the Temkin isotherm model equilibrium binding constant while $B = \frac{RT}{b}\ (J/mol)$ is the heat of adsorption with the gas constant of 8.314 $(J/mol.K)$. Besides, K_f and k_L are the Freundlich adsorption constant and Langmuir constant (L/mg), respectively. $C_e\ (mg/L)$ is the equilibrium concentration of the adsorbate, whereas n is the heterogeneity factor. Lastly, $\alpha_T\ (L/g)$ and $\beta\ (L/g)$ are the Redlich-Peterson constants with n as the Redlich-Peterson exponent within 0 to 1.

3.8 Machine learning model

The random forest modelling technique comprises an ensemble of various decision trees that handle both regression and classification tasks, which is crucial for this experiment's numeric output parameters (Abdi et al., 2021; de Miranda Ramos Soares et al., 2020). Each decision tree is equipped with a fitting function tailored to the random selection of features. Each tree in this "random" forest is built using input vectors that are randomly selected during the training process (Fathalian et al., 2022). The regression models combine decision trees from diverse data subsets, acting as unique classification experts. Python libraries, Pandas for managing data, NumPy for efficient computations, and Sklearn for pre-processing supported the RF regression model, primarily using the "RandomForestRegressor" function. The predictors underwent normalization and evaluation using diverse metrics to ensure accurate predictions of removal efficiency. The analysis focused on metrics such as mean squared error, correlation coefficient (R), R^2, adjusted R^2, and root mean squared error to assess the performance of the regression model (de Miranda Ramos Soares et al., 2020; Ma et al., 2023; Peng & Karimi Sadaghiani, 2023). The equations for calculating the R^2 and MSE are as follows in Eq. (3.13) and Eq. (3.14), respectively.

$$R^2 = 1 - \frac{\sum_{i=1}^{N}(y_{p,i} - y_{o,i})^2}{\sum_{i=1}^{N}(y_{p,i} - y_m)^2} \tag{3.13}$$

$$MSE = \frac{1}{N}\sum_{i=1}^{N}(|y_{p,i} - y_{o,i}|)^2 \tag{3.14}$$

The experimental data obtained through RSM-CCD of HA/Mn for methylene blue dye removal underwent processing using a Python ML algorithm model, random forest (Python Software Foundation, Beaverton, OR USA). Prior to regression, the predictors

were normalized by calculating their mean and standard deviation to remove the measurement unit. Additionally, the combination of random forest (RF) and RSM-CCD was utilized to predict removal efficiency with greater precision. The experimental dataset from RSM-CCD was used for regression models, with RF 20 % for 80 % training and RF 30 % for 70 % testing. For regression, the recommended setting for the number of randomly selected predictors (entry or 'k') is one-third of the number of predictors. At the same time, for classification, it is the square root of the number of predictors (Mehmandost et al., 2022). Another crucial tuning hyperparameter is the decision tree depth, affecting overfitting and ensemble learning performance, typically ranging from 1 to 10 (de Miranda Ramos Soares et al., 2020; Mehmandost et al., 2023).

In this study, default settings in Python were sufficient due to the limited input features of four independent variables. Lastly, using the results obtained from the process optimization via RSM-CCD and the predictions from ML, Random Forest 20% the validation of the hybrid adsorbent was conducted. The validation of adsorbent was evaluated on a large scale for 3L and 5L, using the methylene blue dye removal prediction model from the RSM-CCD-RF.

3.9 Feasibility and economic viability

To evaluate both feasibility and economic viability, a 10-cycle regeneration study was conducted, comparing the performance of the hybrid adsorbent with a wood-based commercial decolourizing adsorbent. The first cycle for both adsorbents was performed under their respective optimum conditions. After each cycle, desorption was carried out using equal parts of NaOH and ethanol as elution solvents. The adsorbents were then rinsed with distilled water until the pH stabilized between 6 and 7, followed by oven drying at 115°C for 30 minutes. This process was repeated for each subsequent cycle.

The economic viability was evaluated by comparing the production costs of the hybrid adsorbent and the commercial adsorbent. The cost analysis included synthesis expenses, covering material and processing costs. The cost in this research is represented as the amount required per litres of wastewater treated in US dollars (USD). The economic feasibility was analysed and compared between the newly developed adsorbent and the commercial adsorbent in terms of the overall cost, including the cost of treating 1,000 L of wastewater with the regeneration study. To validate the findings of the economic analysis, the hybrid adsorbent and commercial adsorbent were tested on real industrial wastewater, such as from batik, printing, POME, and plastic fabrication facilities. The adsorption performance of the hybrid adsorbent on the industrial wastewater was analysed using COD test kits and spectrophotometer to determine the COD removal, colour removal, and adsorption capacity.

3.10 Safety precautions

The safety precautions for all chemicals and materials used in this study are detailed in Table 3.4. Standard safety protocols were followed during the preparation of chemical solutions, which were used in a fume chamber. Utilizing personal protective equipment, exposure to hazardous substances was avoided. All prepared chemicals or materials were stored in properly labelled, airtight containers. Additionally, all waste generated from experimental activities, including leftover or unused samples, was collected and discarded using the appropriate disposal methods.

Table 3.4 : Safety precautions

Chemical	Risks	Precautions
Hydrochloric acid (HCl)	1. may cause ulcer in respiratory tract. 2. May cause pulmonary infection. 3. May cause nausea, diarrhoea, and vomiting. 4. May cause corrosion of mucous membrane. 5. May cause lung problems, gastritis, and skin problems.	1. Store it in a tightly sealed container in a well-ventilated place. 2. Wear PPE when handling chemical. 3. Use the chemical in fume chamber. 4. Practice proper chemical disposal. 5. Keep it away from metals and acids.
Sodium hydroxide (NaOH)	1. May cause severe skin burns. 2. Can cause serious eye damage. 3. May cause gastrointestinal tract burns. 4. Cause severe irritation of respiratory tract.	1. Provide adequate ventilation. 2. Keep metals and acids away. 3. Store it in a tightly sealed container in a well-ventilated place. 4. Practice proper chemical disposal.
Manganese Oxide (Mn_3O_4)	1. High concentrations will cause damage to the foetus. 2. May cause skin and eye irritation. 3. Toxic to aquatic organisms.	1. Wear proper PPE. 2. Store it in a tightly sealed container in a well-ventilated place. 5. Practice proper chemical disposal.
Sulphuric Acid (H_2SO_4)	1. May cause severe skin burns. 2. Can cause serious eye damage. 3. Corrosive when exposed to materials for a longer time. 4. Too much inhalation may cause respiratory problems.	1. Wear proper PPE. 2. Store it in a tightly sealed container in a well-ventilated place. 3. Practice proper chemical disposal. 3. Keep from freezing temperatures and physical damage

Table 3.4 Continued

Chemical	Risks	Precautions
Ethanol (C_2H_6O)	1. May cause dermatitis. 2. May cause damage to the foetus. 3. Too much inhalation may lead to respiratory problems. 4. May cause nervous system issues.	1. Wear proper PPE. 2. Store it in a tightly sealed container in a well-ventilated place. 3. Keep it away from all sources of ignition. 4. Practice proper chemical disposal.
Methylene Blue dye	1. May cause methaemoglobin. 2. May cause dermatitis. 3. May cause nausea, diarrhoea, and vomiting.	1. Wear proper PPE. 2. Store it in a tightly sealed container in a well-ventilated place. 3. Keep it away from all sources of ignition. 4. Practice proper chemical disposal.

CHAPTER 4: RESULTS AND DISCUSSION

4.1 Introduction

This chapter discusses the experimental results for the developed hybrid adsorbents. The results of the preliminary experiments for the mixing ratio, two-step hydrothermal carbonization, and metal oxide impregnation of the raw hybrid adsorbent were also discussed. The chapter discusses the physicochemical characteristics of the hybrid adsorbents, including the unmodified raw adsorbent (RA), acid-activated hybrid adsorbent (HA), and metal-impregnated hybrid adsorbent (HA/Mn). Additionally, it presents the experimental and statistical analysis of the adsorption performance of the hybrid adsorbents. This chapter also discusses the optimization study, the validation of adsorbent efficiency, and the accuracy of dye removal prediction obtained from the Design of Experiment and machine learning approaches. Moreover, this chapter discusses the results obtained for the adsorption kinetics and isotherms, the regeneration study, and the cost estimation for the hybrid adsorbent.

4.2 Preliminary experiments

Preliminary experiments are a crucial step in this study for developing a novel adsorbent. The initial phase focused on evaluating the dye removal efficiency of raw avocado seed and raw banana peel adsorbents. Following this, the experiments aimed to determine the optimum mixing ratio of raw avocado seed to raw banana peel to develop the hybrid adsorbent, RA. Subsequently, the synthesis process was optimized, beginning with the optimization of hydrothermal carbonization temperature, acid activation temperature, and the manganese oxide impregnation ratio. Finally, based on the findings from these preliminary investigations, the optimum conditions for adsorbent development were selected. These steps provided essential insights into maximizing adsorption performance and refining the preparation of the adsorbent for cationic dye removal.

4.2.1 Optimization of mixing ratio of raw hybrid adsorbent

The preliminary experiments evaluated the performance of raw avocado seed adsorbent (RAS) and raw banana peel adsorbent (RBP) for removing a cationic dye, methylene blue dye, which was used to determine the ratio for the raw hybrid adsorbent. The standard experimental procedure and the experimental design in Section 3.5 were used to investigate the efficiency of colour removal and adsorption capacity for dye removal using RAS in Table 4.1 and RBP in Table 4.2. Figures 4.1, 4.2, 4.3, and 4.4 show RAS and RBP for colour removal and adsorption capacity, respectively.

The colour removal and adsorption capacity were maximum when the initial pH was in alkaline conditions for RAS with increased colour removal from 50 % to >80 % and adsorption capacity increased from 80 mg/g to 180 mg/g. Similarly, RBP shows an increase in colour removal from 40% to 100% when the pH levels are increased from 2 to 10 and an increase in the adsorption capacity from 200 mg/g to over 400 mg/g. The colour removal increased to 85 % when the pH was increased to 10 using 0.6 g of RAS at 300 mg/L of initial dye concentration. Under similar operating conditions, complete colour removal was achieved for RBP when the initial pH increased from 2 to 10. This is in line with published literature using avocado and banana peels as adsorbent for cationic dye removal. A study conducted by Maheshwari et. al. (2023) achieved 76 % colour removal and 41 mg/g adsorption capacity at the optimum initial pH of 8 using raw banana peel adsorbent for a cationic dye. Similarly, a study conducted by Netto et. al. (2019) used raw avocado seed to remove methylene blue dye, which reported an optimum pH of 10 for a maximum of 103 mg/g.

Table 4.1: Experimental results for dye removal using raw avocado seed.

Experimental Run					Performance Efficiency	
Run	pH	Adsorbent dosage (g/L)	Dye concentration (g/L)	Contact time (min)	% Colour removal	Adsorption capacity (mg/g)
1	2	2.8	0.3	95	49.7	54.3
2	2	5.0	0.1	180	63.2	12.6
3	10	5.0	0.1	180	98.4	19.7
4	6	1.8	0.3	95	65.8	112.8
5	6	2.8	0.3	95	70.9	77.4
6	6	2.8	0.3	95	71.6	78.1
7	2	0.5	0.1	180	38.5	77.1
8	2	0.5	0.5	180	46.5	465.3
9	6	2.8	0.3	95	70.9	77.3
10	10	5.0	0.1	10	99.4	19.9
11	10	5.0	0.5	180	99.7	99.7
12	10	0.5	0.1	10	99.8	199.7
13	2	0.5	0.1	10	66.8	133.6
14	10	5.0	0.5	10	99.9	99.9
15	6	2.8	0.3	75	68.5	74.7
16	10	0.5	0.5	180	54.3	542.9
17	6	2.8	0.3	95	72.3	78.9
18	6	2.8	0.3	265	77.5	84.6
19	6	2.8	0.3	95	70.4	76.8
20	10	0.5	0.1	180	99.5	199.0
21	10	0.5	0.5	10	41.0	410.2
22	6	2.8	0.3	95	67.9	74.0
23	2	5.0	0.5	10	48.8	48.8
24	2	5.0	0.5	180	97.6	97.6
25	6	2.8	0.1	95	96.1	35.0
26	6	7.3	0.3	95	98.4	40.7
27	2	5.0	0.1	10	70.6	14.1
28	14	2.8	0.3	95	100.0	109.1
29	2	0.5	0.5	10	33.3	333.3
30	6	2.8	0.7	95	41.7	106.2

Table 4.2: Experimental results for dye removal by raw banana peel

Experimental Run					Performance Efficiency	
Run	pH	Adsorbent dosage (g/L)	Dye concentration (g/L)	Contact time (min)	% Colour removal	Adsorption capacity (mg/g)
1	2	2.8	0.3	95	11.9	13.0
2	2	5.0	0.1	180	12.1	2.4
3	10	5.0	0.1	180	98.8	19.8
4	6	1.8	0.3	95	98.7	169.3
5	6	2.8	0.3	95	98.7	107.7
6	6	2.8	0.3	95	90.3	98.5
7	2	0.5	0.1	180	15.6	31.2
8	2	0.5	0.5	180	0.5	5.3
9	6	2.8	0.3	95	98.7	107.6
10	10	5.0	0.1	10	98.5	19.7
11	10	5.0	0.5	180	99.5	99.5
12	10	0.5	0.1	10	99.2	198.3
13	2	0.5	0.1	10	57.3	114.7
14	10	5.0	0.5	10	99.5	99.5
15	6	2.8	0.3	75	98.1	107.0
16	10	0.5	0.5	180	54.3	542.9
17	6	2.8	0.3	95	92.6	101.0
18	6	2.8	0.3	265	99.1	108.1
19	6	2.8	0.3	95	98.7	107.7
20	10	0.5	0.1	180	95.2	190.5
21	10	0.5	0.5	10	99.1	991.2
22	6	2.8	0.3	95	96.7	105.5
23	2	5.0	0.5	10	1.6	1.6
24	2	5.0	0.5	180	3.2	3.2
25	6	2.8	0.1	95	91.9	33.4
26	6	7.3	0.3	95	99.1	41.0
27	2	5.0	0.1	10	15.3	3.1
28	14	2.8	0.3	95	99.7	108.8
29	2	0.5	0.5	10	14.2	142.1
30	6	2.8	0.7	95	99.4	253.1

Figure 4.1 illustrates the colour removal efficiency of raw avocado seed (RAS) and raw banana peel (RBP) adsorbents under varying conditions. RAS exhibited better colour removal at a lower dye concentration of 100 mg/L and a higher adsorbent dosage of 250 mg, increasing from 50% to 63%. In contrast, RBP achieved superior colour removal (80%) at a higher dye concentration of 500 mg/L with the same adsorbent dosage. The improved performance at lower concentrations is attributed to the availability of more active sites for dye adsorption, whereas at higher concentrations, limited active sites result in reduced removal efficiency (Khamwichit et al., 2022). The result is in line with studies reported previously for dye removal (Baloo et al., 2021; Khiam et al., 2022).

The effect of contact time on colour removal further supports this trend. Both RAS and RBP exhibited increased colour removal with longer contact times, from 10 to 180 minutes. RAS improved from 49% at 10 minutes to 52% at 180 minutes at pH 2, while at pH 10, colour removal exceeded 85% at 180 minutes. Similarly, RBP achieved complete colour removal at pH 10 with extended contact time.

The adsorption capacity was highest when the adsorbent dosage was lowest at 25 mg and when the concentration was highest at 500 mg/L for both adsorbents. RAS adsorption capacity increased with the increase in time, while RBP adsorption capacity was lower when the time was increased. These findings align with study conducted by Danish and others (2018) reported adsorption capacity increased with increasing adsorbent dosage for removal of methylene blue dye using banana waste. Similarly, study conducted by Prabakaran et. al (2022) using activated avocado seed, dye removal was increased attaining 95 % colour removal with the increase in adsorbent dosage up to 1.5 g/L. The effect of adsorbent dosage for both RAS and RBP revealed that higher removal efficiency at higher adsorbent dosages due to the presence of more active sites available for adsorption (Jiang et al., 2021).

As for the contact time, both RAS and RBP show colour removal was increased when time was increased from 10 min to 180 min. RAS shows an increment from 49 % at 10 min to 52 % at 180 mins at pH 2, while at pH 10 (180 min) > 85% colour removal was achieved. Likewise, RBP achieved complete colour removal in higher contact time in pH 10. Adsorption capacity was highest for RAS in higher contact time in alkaline condition, resulting in 200mg/g adsorption capacity at 180 mins in pH 10. However, RBP exhibits higher adsorption capacity in lower contact time with 400mg/g at 44mins (pH10), while 200 mg/g adsorption capacity was recorded for 180mins at pH 3. The increases in contact time led to a decrease in adsorption capacity, indicating the adsorption equilibrium was reached (Tang et al., 2021). This is in line with previous studies, as all the active binding sites of the adsorbent are unoccupied at the start of the adsorption process, and as contact time increases, fewer vacant sites are available for the adsorption process to occur (V. S. Munagapati et al., 2018; Prabakaran et al., 2022)

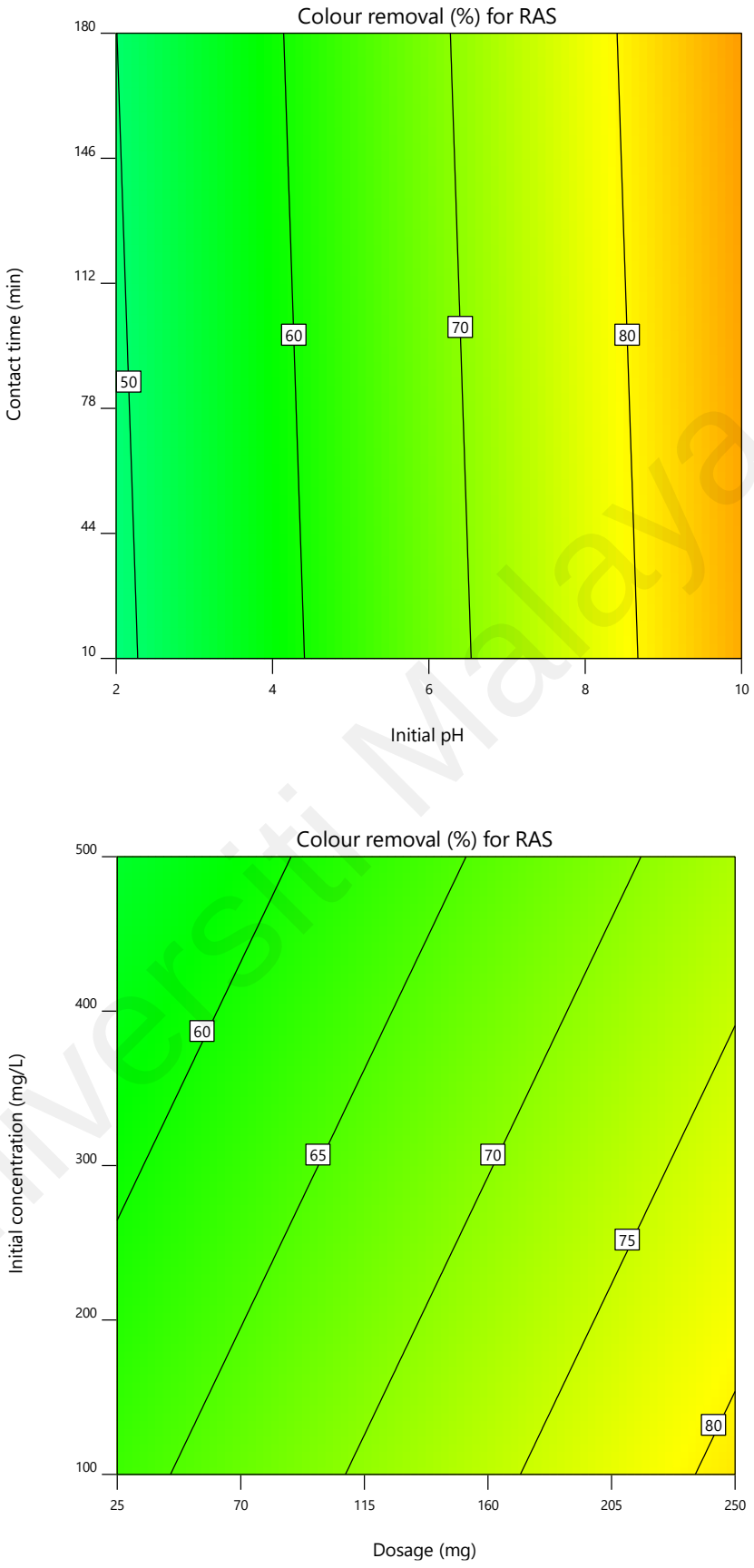

Figure 4.1 : 2D Contour for effect of parameters on colour removal for raw avocado seed.

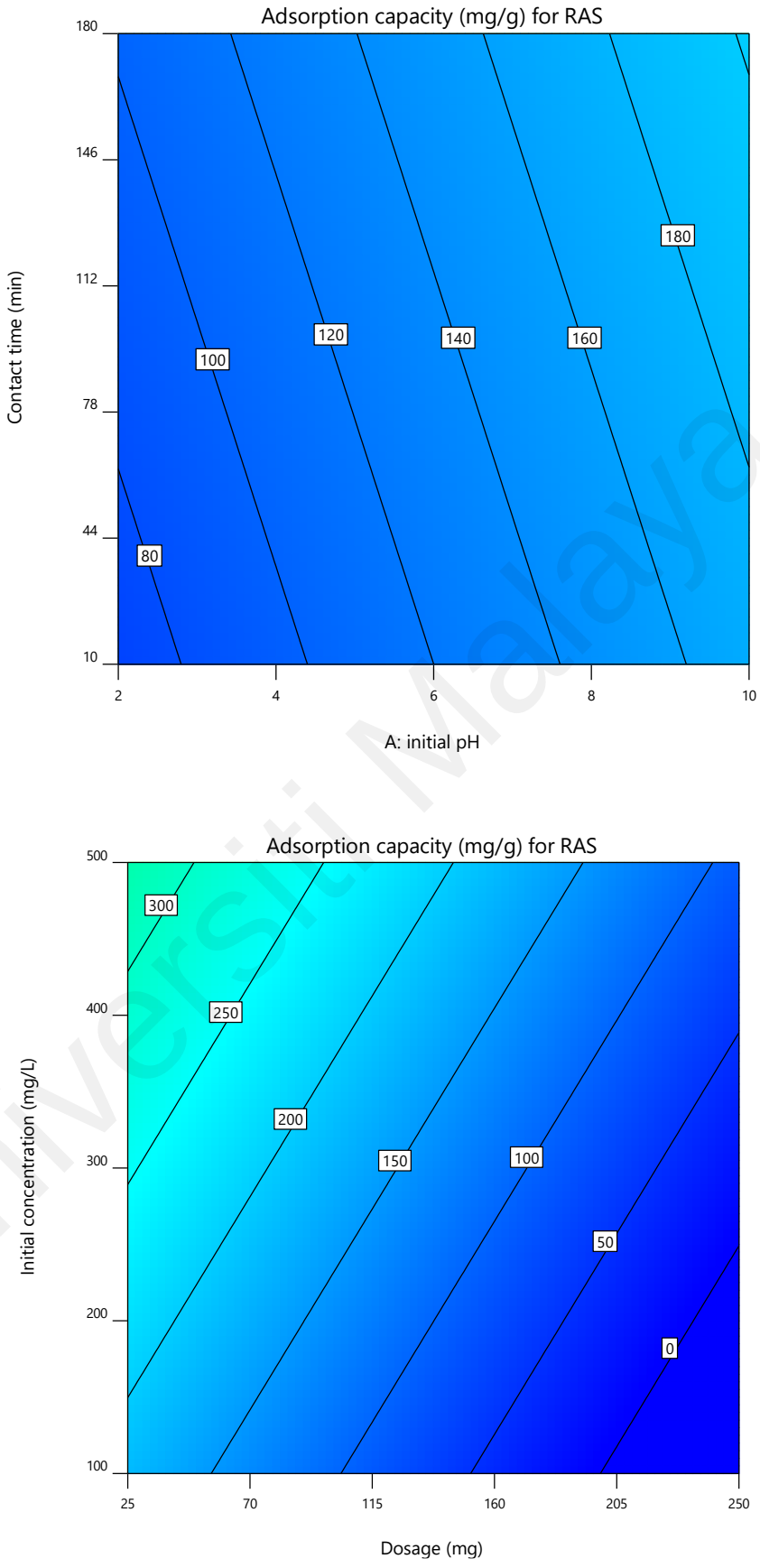

Figure 4.2 : 2D contour for effect of parameters on adsorption capacity for raw avocado seed.

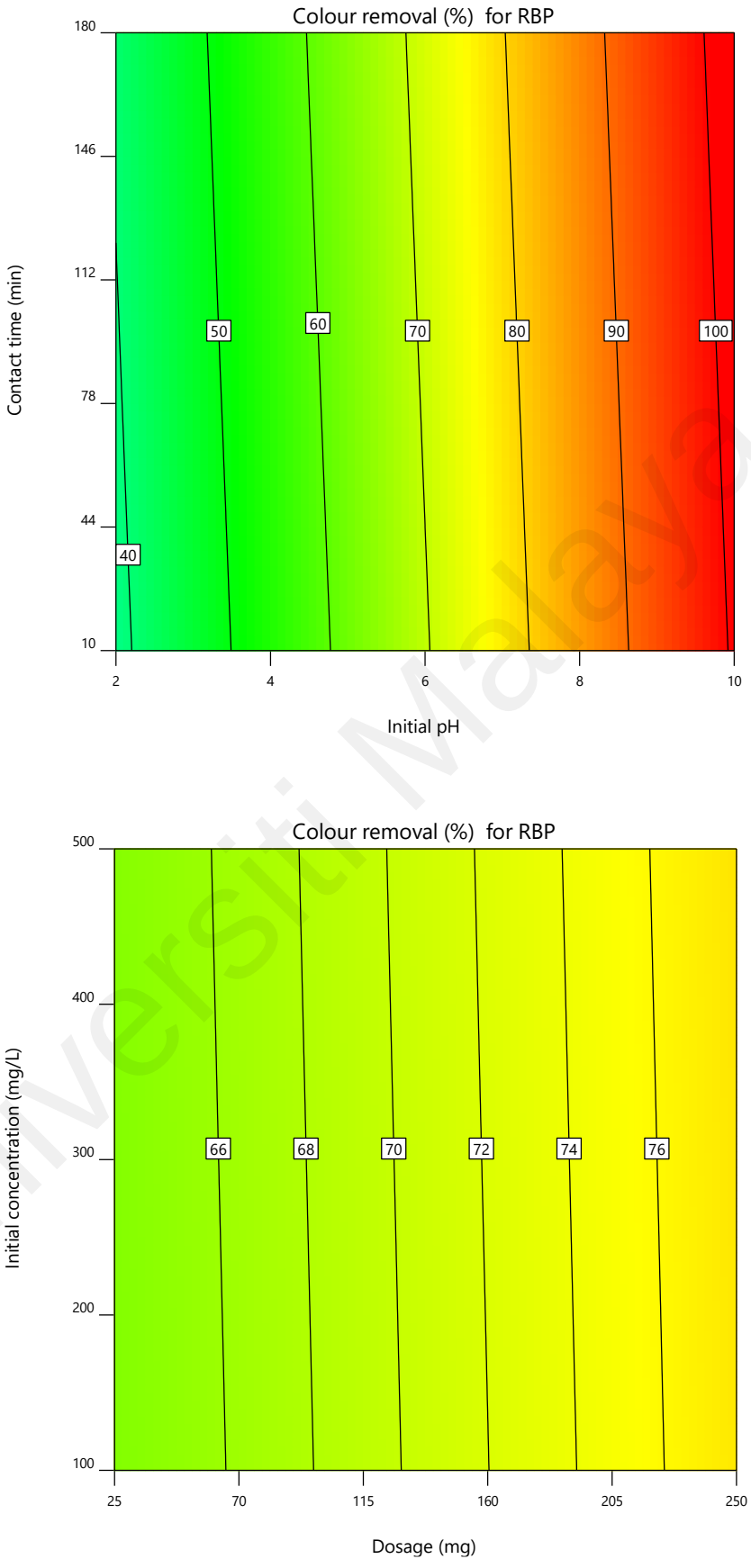

Figure 4.3 : 2D Contour for effect of parameters on colour removal for raw banana peel.

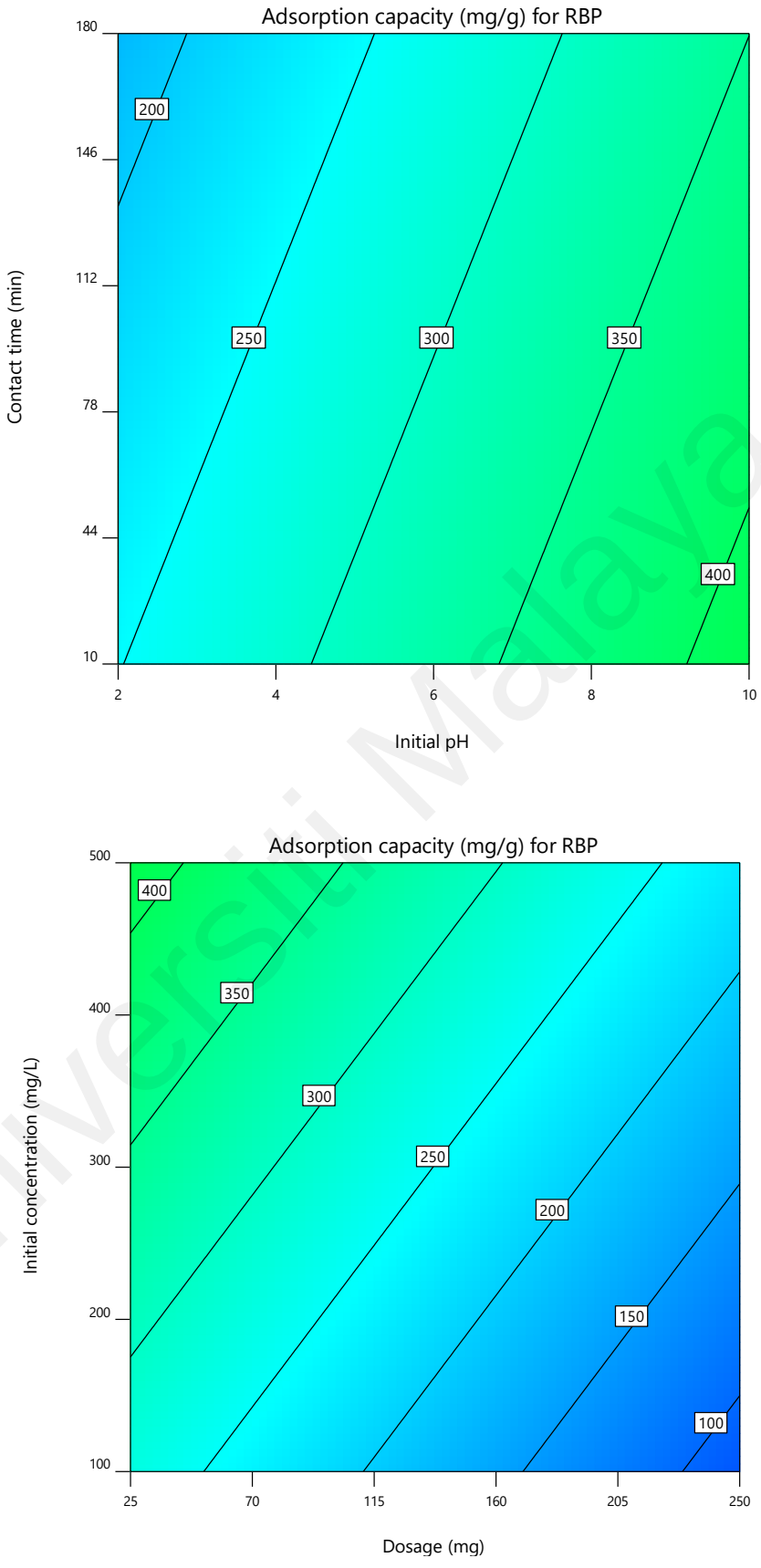

Figure 4.4 : 2D Contour for effect of parameters on adsorption capacity for raw banana peel.

Figures 4.1 to 4.4 show RAS and RBP with maximum adsorption performance achieved in alkaline conditions, where increased negative charge on the adsorbent surface enhanced electrostatic attraction with the positively charged methylene blue dye. RAS achieved over 80% colour removal and 180 mg/g adsorption capacity at pH 10, while RBP reached 100% colour removal and over 400 mg/g adsorption capacity. Besides, adsorption capacity was highest at the lowest adsorbent dosage (25 mg) and highest dye concentration (500 mg/L) due to the high dye-to-site ratio. At lower dye concentrations, excess active sites improved adsorption efficiency, but as concentration increased, site saturation reduced efficiency. RAS showed a steady increase in adsorption, reaching 200 mg/g at 180 minutes, indicating gradual diffusion of dye molecules into micropores. In contrast, RBP achieved 400 mg/g in 44 minutes, suggesting faster equilibrium due to more accessible adsorption sites.

The optimization study, conducted using the RSM-CCD numerical tool, identified optimum operational parameters based on experimental data. The four operation parameters were kept within the range while maximizing the colour removal and adsorption capacity. Under these optimization conditions, the best performance was achieved at initial pH 9, 3 g/L adsorbent dosage, 0.5 g/L dye concentration, and 120 minutes contact time. RAS achieved 63.6% colour removal and 181.2 mg/g adsorption capacity, while RBP removed 67.1% of dye with an adsorption capacity of 112.0 mg/g. Furthermore, Figures 4.1 to 4.4 visually show the effects of independent variables, showing improved performance within optimized ranges. Since RAS exhibited lower colour removal but higher adsorption capacity than RBP, hybrid adsorbent ratios were explored to enhance overall performance. Using RSM-CCD, the experimental design was conducted for various ratios as given in Table 4.3, with a fixed adsorbent dosage of 3g/L.

Table 4.3 : Experimental results for varying percentages of RAS to RBP

Experimental Run				Performance Efficiency		
Run	**pH**	**Contact time (min)**	**Percentage of RAS to RBP (%)**	**COD removal (%)**	**% Colour removal**	**Adsorption capacity (mg/g)**
1	8	140	75	42.4	69.5	161.8
2	2	95	50	33.1	58.4	132.3
3	6	95	50	63.5	79.7	206.9
4	10	95	50	61.9	89.9	219.4
5	4	50	25	48.1	79.5	184.5
6	6	95	100	40.1	62.0	147.6
7	8	50	75	41.9	69.5	161.0
8	6	180	50	55.4	82.9	199.9
9	6	95	50	46.4	79.7	182.2
10	6	95	50	46.9	79.6	182.8
11	6	95	50	46.9	79.6	182.9
12	4	140	25	47.4	79.7	183.8
13	6	95	50	45.5	79.6	180.8
14	6	95	50	44.8	79.8	180.1
15	6	10	50	46.6	54.3	145.9
16	8	140	25	45.6	79.5	180.9
17	4	50	75	41.5	69.4	160.3
18	6	95	0	34.4	64.0	142.2
19	8	50	25	42.5	79.5	176.4
20	4	140	75	40.9	69.5	159.6

Adsorption experiments with varying mixing ratios showed COD removal ranging from 33 % to 63 %, colour removal ranging from 54 % to 90 %, with adsorption capacities between 132 mg/g and 219 mg/g. In figure 4.5, the effect of mixing ration on COD shows 47% COD removal at lower percentage of RAS (25%) to higher percentage of RAS (75%) in alkaline condition of pH 8. A gradual increase in COD removal can be noticed from 37 % to 65 % (RAS to RBP), however a decrease is noticed from 65 % to 75 % RAS. Furthermore, the highest COD removal was recorded in the range of 45 % to 55% of RAS percentage in initial pH of 8 for contact time of 95mins.

Looking into the colour removal of mixing ratio in Figure 4.6, when the RAS to RBP percentage is lower at 25 %, the colour removal is 82%, compared to 75 % of RAS in the mixture which achieved 76 % removal in pH of 8. Moreover, the highest colour removal was achieved around the percentage of 45 % of RAS to RBP with a colour removal efficiency of 84%. These results for colour removal indicates that more RAS in the mixture achieves higher colour removal than more RBP in the mixture. Similarly, adsorption capacity in Figure 4.7, follows the same trend, with lower values at 25% and 75% RAS and a peak of 193 mg/g at a 45% to 55% RAS to RBP ratio. The 2D contour plots further confirm that the optimal mixing ratio for adsorption performance lies between 45% and 55% RAS to RBP.

Thus, to determine the optimal ratio for COD removal, colour removal and adsorption capacity, numerical optimization was performed, maximizing adsorption performance while maintaining operational conditions within range. The optimization study results indicated that a 3 g/L dosage of raw hybrid adsorbent (RA), consisting of 50% raw avocado seed (RAS) and 50% raw banana peel (RBP) (1.5 g/L each), achieved the highest performance, with 53 % COD removal, 84% colour removal and an adsorption capacity of 198 mg/g.

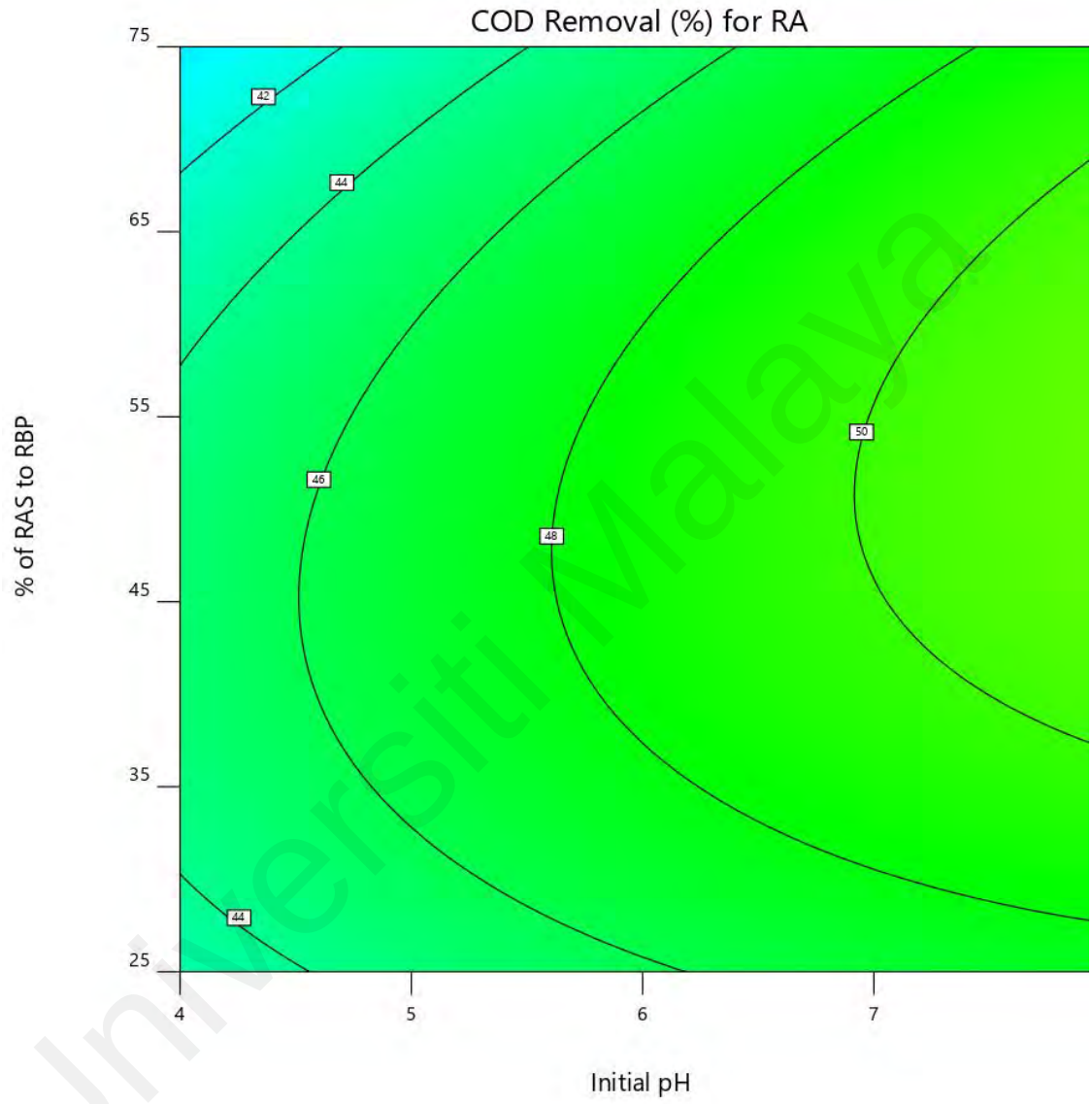

Figure 4.5 : 2D Contour for the effect of the percentage for mixing ratio on COD removal

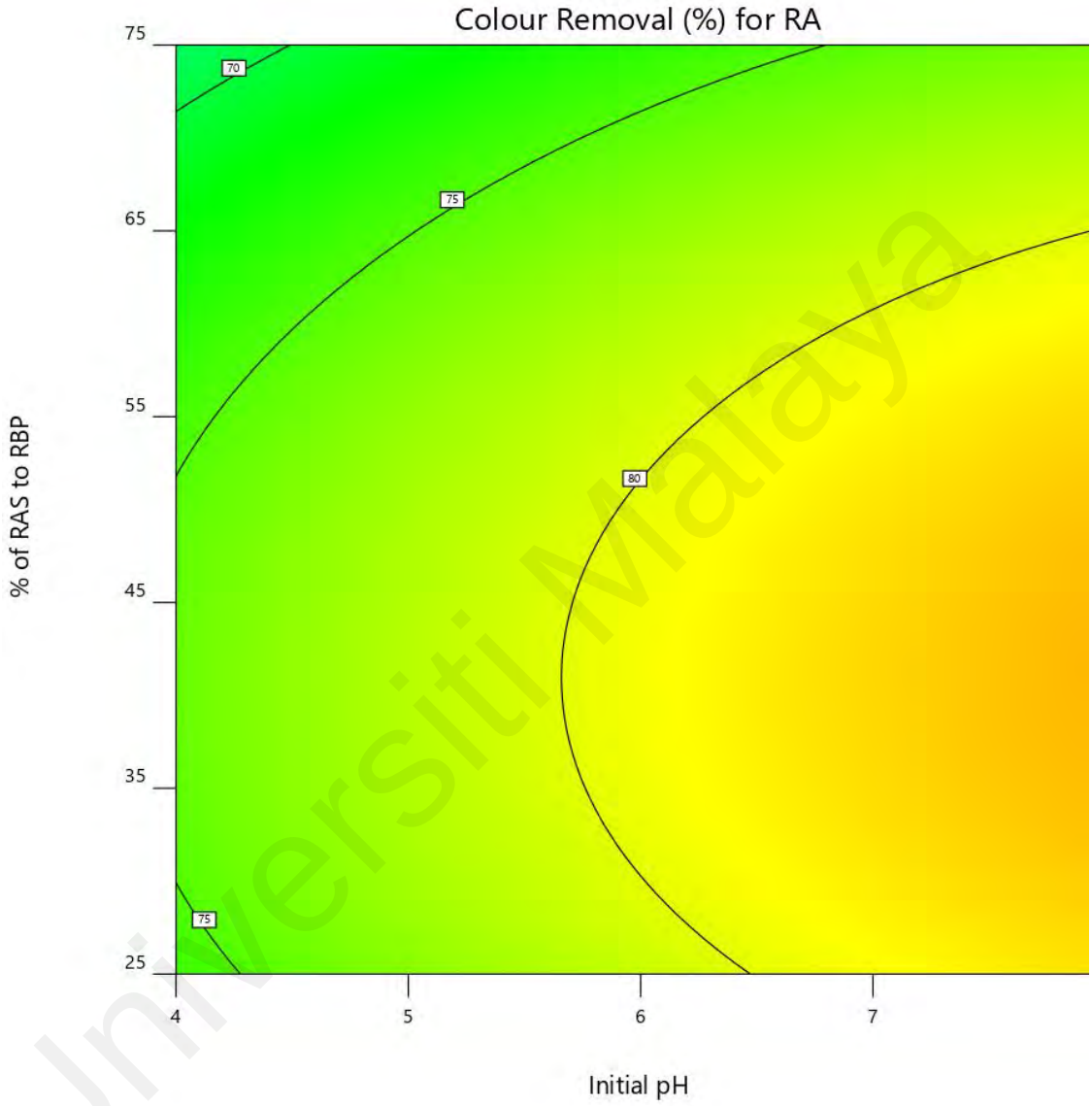

Figure 4.6 : 2D Contour for the effect of the percentage for mixing ratio on colour removal

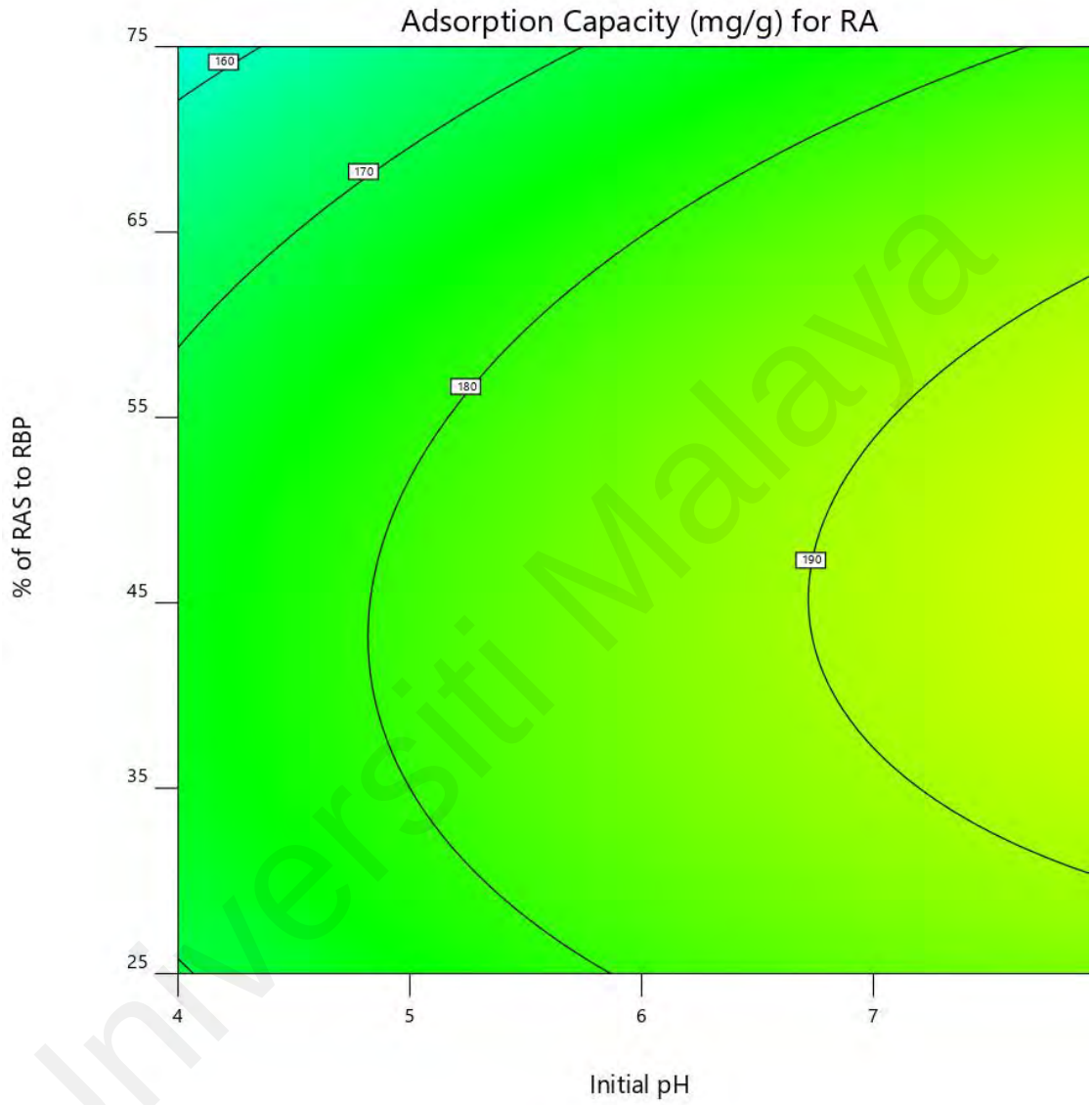

Figure 4.7 : 2D Contour for the effect of the percentage for mixing ratio on adsorption capacity

These findings confirm the potential of RAS and RBP for cationic dye removal, with their combination of mixing 50 % RAS (1.5 g) with 50 % RBP (1.5 g) outperforming individual adsorbents with an adsorbent dosage of 3 g. This optimal synthesis ratio aligns with a recent study on hybrid adsorbents using equal parts of orange and lemon peels, which removed 98% of Methylene Blue dye (Ramutshatsha-Makhwedzha et al., 2022). Consequently, the 1:1 RAS: RBP ratio was adopted for further modification procedures in this study. The hybrid adsorbent improved performance by 13% and 17% compared to RAS and RBP, respectively, likely due to increased binding sites, enhanced stability, and improved point of zero charge, facilitating more efficient cationic dye removal. Moreover, the mixing of both fruit wastes may have increased the adsorption performance due to the increased oxygenated functional groups combining both materials.

4.2.2 Optimization of hydrothermal carbonization temperature

To improve the performance of raw hybrid adsorbent, two-step hydrothermal carbonization (HTC) followed by metal oxide impregnation was conducted. To investigate the effect of hydrothermal HTC and slow pyrolysis (SP), both synthesis methods were used to carbonize the hybrid adsorbent to find the best route regarding higher mass production and higher performance for dye removal. SP was conducted at a range of 200 °C to 600 °C for 4 hours, using 20 g of raw hybrid adsorbent (10 g of RAS and 10 g RBP) in a covered porcelain crucible in a muffled furnace. The hydrothermal carbonization was carried out using 15 g of raw hybrid adsorbent (7.5 g of RAS and 7.5 g of RBP) with distilled water in an autoclave and heated for 2 hours at a range of 180 °C to 220 °C in a laboratory oven. The yield percentage is calculated to evaluate the economic performance of the mass-produced (Jiang et al., 2022).

The yield of the final mass obtained from the HTC of RA between 180 °C and 220 °C was calculated and is presented in Figure 4.8. The lower yield (49 %) at 180°C is likely due to insufficient temperature, leading to incomplete biomass decomposition. As the temperature increased to 200 °C, the yield and adsorption performance improved to 51 % and 87 %, respectively. The higher yield and performance at 200 °C, can be attributed to the completion of key decomposition processes such as hydrolyzation, polymerization, and secondary char formation (Nguyen et al., 2022; Yan et al., 2023). At temperatures beyond 200°C, the yield declined due to intensified biomass decomposition, dehydration, and over-carbonization, which resulted in excessive volatile matter loss (Avalos-Viveros et al., 2023; Liu et al., 2025).

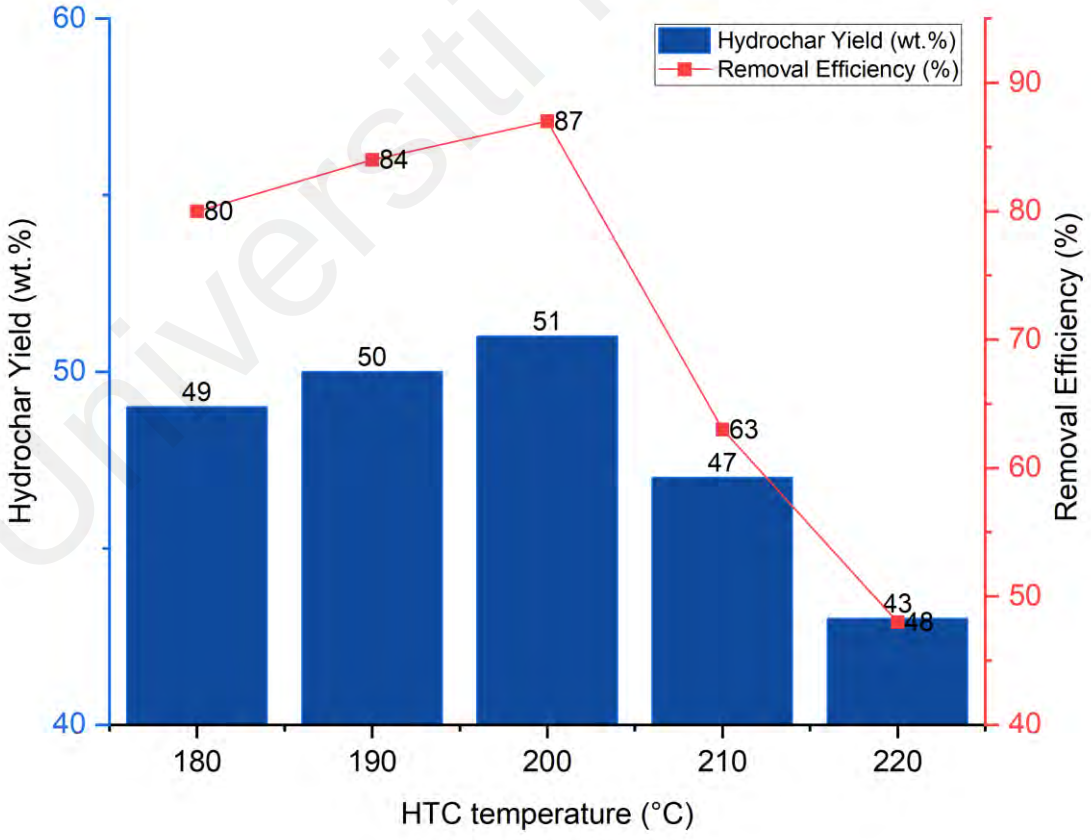

Figure 4.8 : Effect of HTC temperature on hydrochar yield and removal efficiency

Excessive carbonization at higher temperatures may lead to pore collapse or reduced surface functionality, negatively affecting dye removal efficiency. Therefore, 200°C balances both high yield and optimal adsorption performance, making it the most suitable HTC temperature for producing effective adsorbents. The adsorbents with the highest yield were selected for preliminary studies on methylene blue dye removal. Under fixed operational conditions (pH 6, MB concentration of 0.3 g/L, 95 minutes of contact time, and adsorbent dosage of 2.8 g/L), HTC-derived adsorbent exhibited 10.3% higher colour dye removal efficiency and 14 % higher mass yield than SP, as summarized in Table 4.4. The higher performance of HTC-based adsorbent in both mass yield and adsorption efficiency highlights its potential for practical applications in dye wastewater treatment. Thus, based on these findings, hydrothermal carbonization was performed using 15 g of raw adsorbent at 200°C, followed immediately by acid activation to enhance adsorption properties in the hybrid adsorbent.

Table 4.4 : Comparison of HTC and SP

Parameters	**Hydrothermal Carbonization**	**Slow Pyrolysis**
Temperature	200 °C	400 °C
Time	2 hr	4 hr
Mass Yield	51 %	37 %
Colour removal	83 %	65 %
Adsorption capacity	91 mg/g	71 mg/g
COD removal	73 %	56 %

4.2.3 Optimization of acid activation of adsorbent

This study investigates a newly developed hybrid adsorbent derived from avocado seeds and banana peels, for which no prior literature has specified the optimal activation temperature during the activation process. Therefore, the acid activation temperature was varied from 250 °C to 650 °C for 2 hours to determine the most effective temperature for enhancing the adsorption performance and the physicochemical properties of the hybrid adsorbent. Acid activation of the materials obtained from HTC was done using H_3PO_4 85 % with a 1:1 ratio (Brazil et al., 2022). Additional studies conducted on acid activation without HTC resulted in a 7.3% lower colour removal efficiency and a 6.8 mg/g lower adsorption capacity, highlighting the importance of HTC in the synthesis. The preliminary tests were conducted with fixed operational parameters (pH 6, concentration of MB 0.3 g/L, 95 mins of contact time, and adsorbent dosage of 2.8 g/L).

Preliminary experiments conducted using the adsorbent obtained from 450 °C removed the highest percentage of the colour with 99.7 % with 107.6 mg/g adsorption capacity as shown in Figure 4.9. The gradual increase in adsorption performance from 250°C to 450°C indicates that higher temperatures enhance mesoporous surface development through depolymerization via hydrolysis and oxidation (Imad Rabichi et al., 2025). As shown in Figure 4.9, this temperature range also enhances the colour removal and adsorption capacity by preventing excessive biomass shrinkage and the release of volatile matter peaking around 400°C to 500°C. However, beyond 450°C, a decline in adsorption efficiency is observed, likely due to pore shrinkage caused by the decomposition of chemical functional groups and dehydrogenation above 500°C (Fan et al., 2025). Thus, the optimized hybrid adsorbent, activated at 450°C with 85% H_3PO_4, was subsequently used for manganese oxide impregnation.

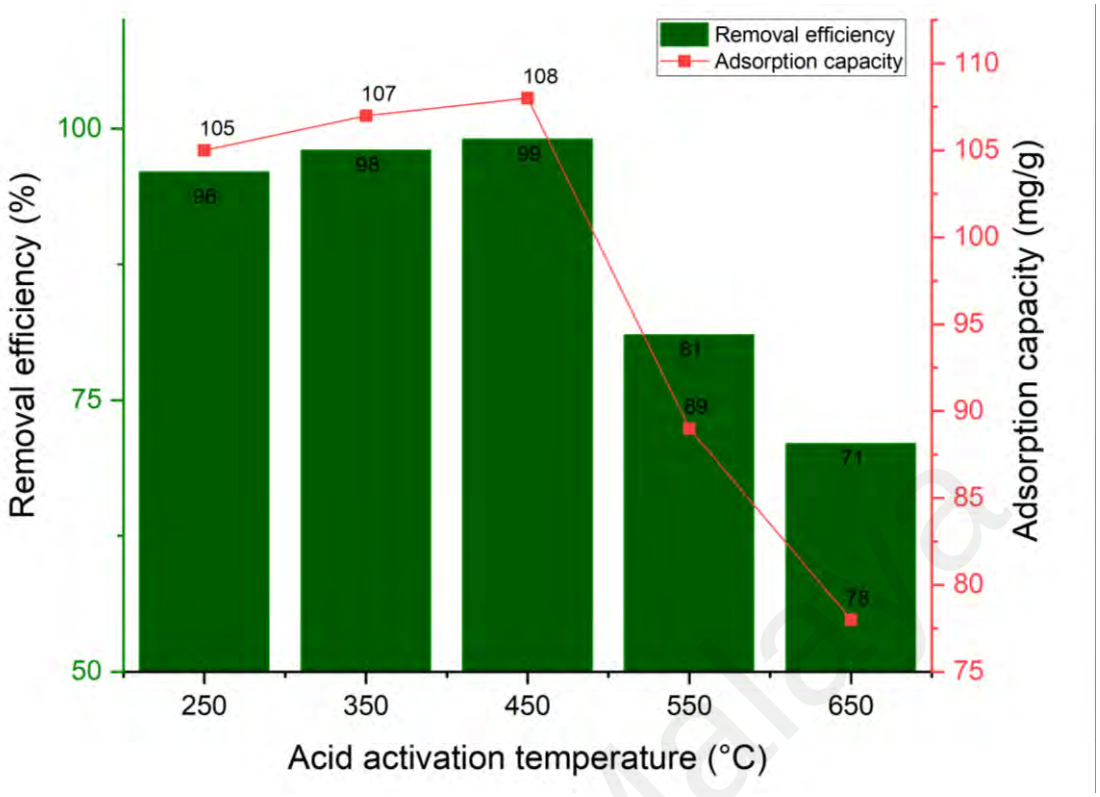

Figure 4.9 : Effect of activation temperature on the adsorbent

4.2.4 Optimization of impregnation material

The impregnation preliminary experiments were conducted using manganese oxide and hybrid adsorbent at 0.1:1, 0.5:1, and 1:1 (Mn_3O_4: HA) measured in grams. From the preliminary study Figure 4.10, it was revealed that the 0.1:1 achieved highest removal efficiency with 99.1 % colour removal and 88.9 mg/g adsorption capacity followed by 0.5:1 and 1:1. Therefore, 1.0 g of manganese oxide was dissolved in 50 mL of distilled water, followed by adding 10 g of HA into the beaker. The mixture was stirred at 400 rpm for 2 hours on a magnetic stirrer and the beakers were left undisturbed on the counter for additional 2 hours. The impregnated activated hybrid adsorbent was dried at 100°C for 12 hrs in an oven. The final adsorbent was carefully collected, stored in airtight container and labelled as HA/Mn.

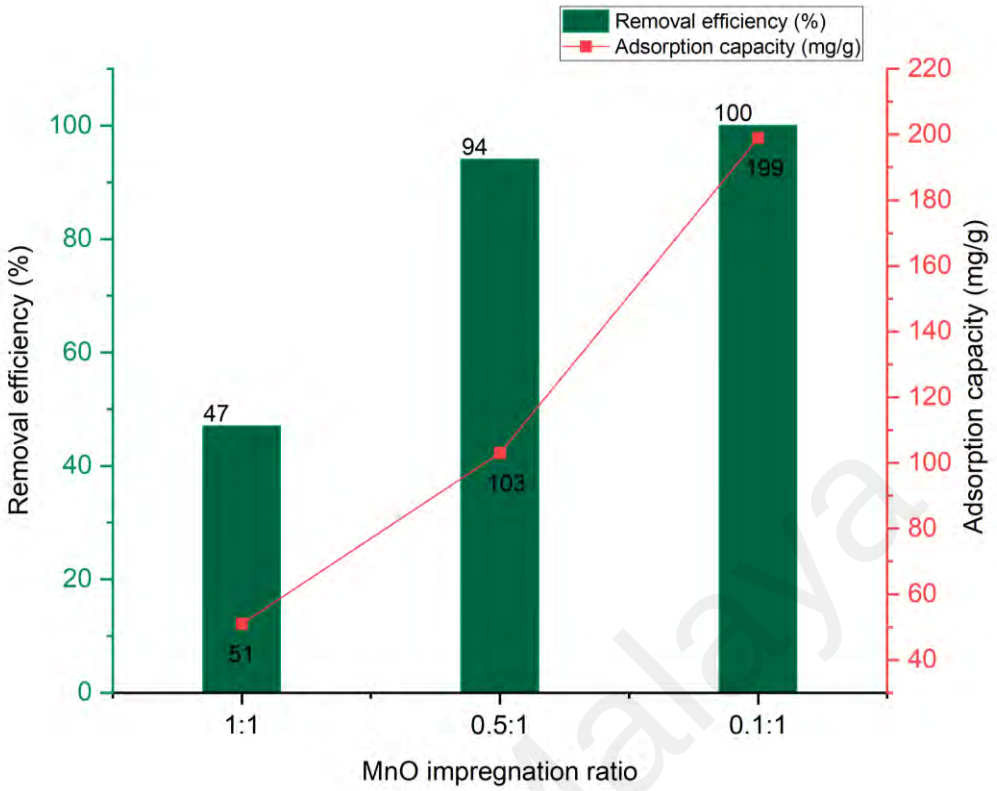

Figure 4.10 : Adsorption performance for manganese oxide impregnation

4.2.5 Selection of optimum conditions

The preliminary tests conclude that a mixture of avocado seed and banana peel can be successfully used to synthesize hybrid adsorbents. Two-step hydrothermal carbonization is step one for the carbonization and acid activation followed by step two, the functionalization using metal impregnation. Thus, this study synthesized three hybrid adsorbents: RA, a raw hybrid adsorbent at a 1:1(RAS:RBP) ratio; HA, a hydrothermal carbonized (200 °C) and acid activated adsorbent (450 °C); and HA/Mn, a functionalized adsorbent with metal oxide impregnation at a ratio of 0.1:1 (Mn_3O_4:HA). Furthermore, the preliminary experiments under fixed operating conditions (initial pH of 7, adsorbent dosage of 2.8 g/L, initial dye concentration of 0.3 g/L, and contact time of 95 mins) for colour removal and adsorption capacity were conducted. The manganese oxide-impregnated hybrid adsorbent has the highest removal efficiency for colour removal and

adsorption capacity (100.0 %, 109.1 mg/g) followed by an acid-activated hybrid adsorbent at 450 ℃ (99.7 %, 108.6 mg/g) and the raw hybrid adsorbent at the ratio 1:1 (80.3 %, 104.9 mg/g). The metal impregnation and acid activation enhanced the adsorption performance compared to the unmodified raw hybrid adsorbent.

4.3 Physiochemical characteristics of adsorbents

4.3.1 Surface functional groups

Figure 4.11, the raw adsorbent (RA) and acid-activated hybrid adsorbent (HA) displayed broad peaks corresponding to O-H stretching at 3267.5 cm^{-1} and 3177.1 cm^{-1} , C-O stretching at 1013.7 cm^{-1} and 1339.9 cm^{-1}. RA and HA have a band at 1607.4 $cm^{-1}$and 1571.1 cm^{-1}, respectively, corresponding to C=C stretching and C-H stretching at 2920.7 cm^{-1} and 2268.5 cm^{-1}, respectively. Furthermore, decreasing peak intensity was observed in HA compared to the RA, which can be related to the decarboxylation and dehydration of the adsorbent structure after modification and activation processes (Jiang et al., 2022). The functional groups in the adsorbents developed in this study are similar to those identified in previously reported works using avocado seeds and banana peel (S. P. Boeykens et al., 2019a; Mbarki et al., 2022; V. Munagapati et al., 2018; Salomón et al., 2020; Wanja et al., 2016; Xue et al., 2022) Additionally, for HA, the bands detected between 900 and 950 cm^{-1} indicate the presence of the P-OH bond after acid activation using phosphoric acid. Furthermore, the peaks representing P-OH are in line with other studies using H_3PO_4 as the activating agent. For example, a study conducted by Song and others (2022), after H_3PO_4 modification phosphate groups were present between 800 to 1000 cm^{-1}. Another study conducted by Khan et. al (2022) using phosphoric acid-activated Indian jujube for cationic dye removal reported a broad peak around 1000 $cm^{-1,}$ suggesting phosphate group.

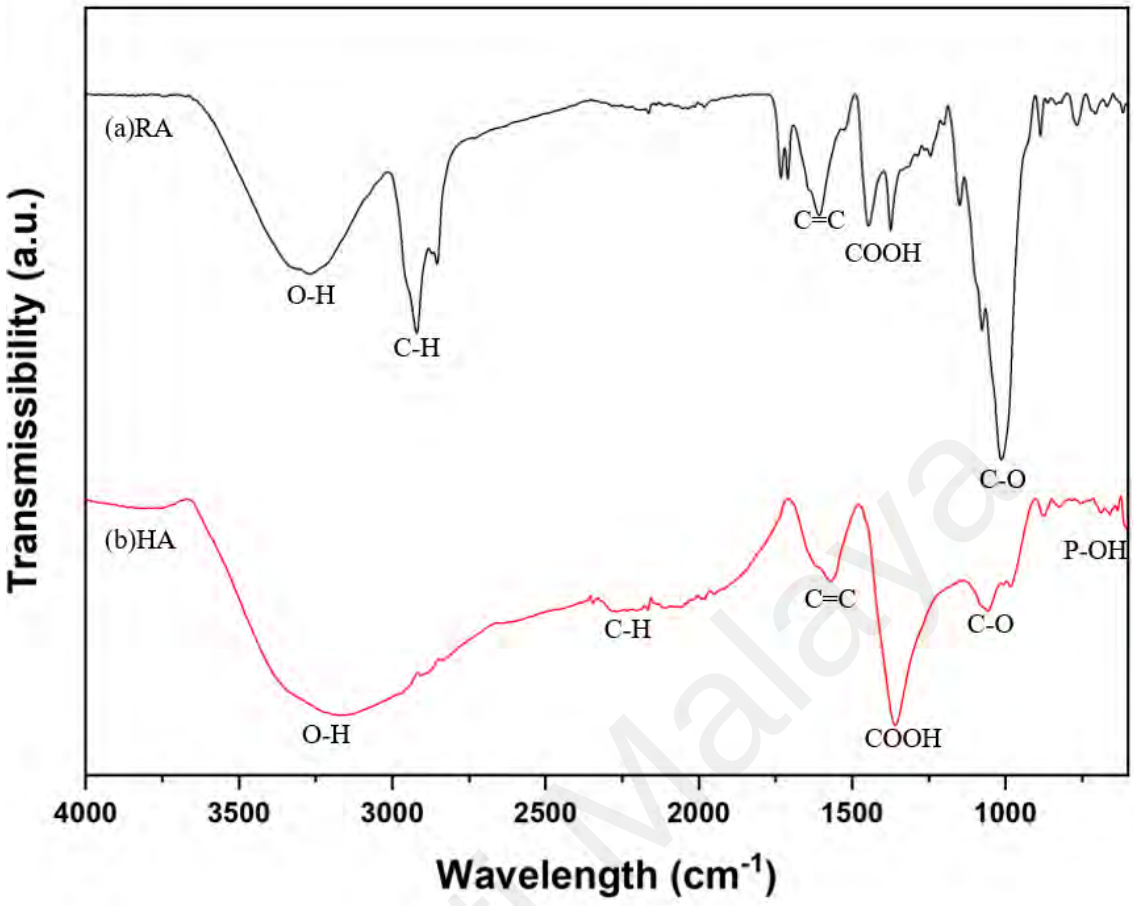

Figure 4.11 : FTIR Spectra for (a) RA and (b) HA.

The functional groups of HA/Mn are provided in Figure 4.12. HA/Mn showed the presence of hydroxyl, carboxyl, and carbonyl functional groups based on the FTIR analysis. The band observed at 3400cm^{-1} arises from chemically adsorbed water and vibrations originating from the hydrogen-bonded O–H groups present in cellulose, pectin, and lignin (Raji et al., 2023). On the other hand, the band observed at 1173 and 1554 cm^{-1} corresponds to the stretching vibrations of C–O and C=O, reflecting the conversion of the biomass's cellulosic component. Additionally, the bands detected at 930 and 892 cm^{-1} indicate the presence of the P-OH bond, indicating the presence of H_3PO_4 and confirming successful chemical activation. The results obtained in the FTIR analysis are consistent with research conducted on avocado waste (T Ahmad & M Danish, 2022) and banana

peel (Rose et al., 2023) by Ahmad and Danish (2022) and Rose and others (2023), respectively. Avocado seed or avocado skin-based studies have mostly reported the functional groups such as phenol, hydroxyl, carbonyl, and aromatic alkene groups (Haki et al., 2022; Ibrahim et al., 2023; Prabakaran et al., 2022). Similarly, banana-waste-based studies also have reported the presence of hydroxyl, carboxylic acid, aromatic, cellulose, hemicellulose, lignin polymer, amine, and amide (Hu et al., 2021; Maheshwari et al., 2023; Sun et al., 2023). Besides, studies reported that symmetrical P-O-P vibration of phosphate and polyphosphate bridges (Khan et al., 2022; Song et al., 2022). An additional peak can be noticed after metal impregnation between 500 cm^{-1} to 700 cm^{-1} at 604 cm^{-1}, indicating successful Mn-O stretching (Alalid et al., 2020; Brocza et al., 2024). This is in line with previous studies that used Manganese oxide impregnated adsorbents. A study conducted by Qu et. at. (2023), reported successful metal oxide impregnation with an additional peak at 574 cm^{-1}, and a study conducted by Alalid et. al. (2020), reported Mn-O vibrations at 542 cm^{-1}.

In summary, the raw hybrid adsorbent, acid-activated adsorbent, and metal impregnated adsorbent consist of O-H, C-O, and C=C functional groups. Additional functional groups were found after the modification of the adsorbent, which shows successful acid activation with P-O vibrations and the Mn-O vibrations. The increased oxygenated functional groups will enhance the adsorption of positively charged dye molecules in cationic dyes.

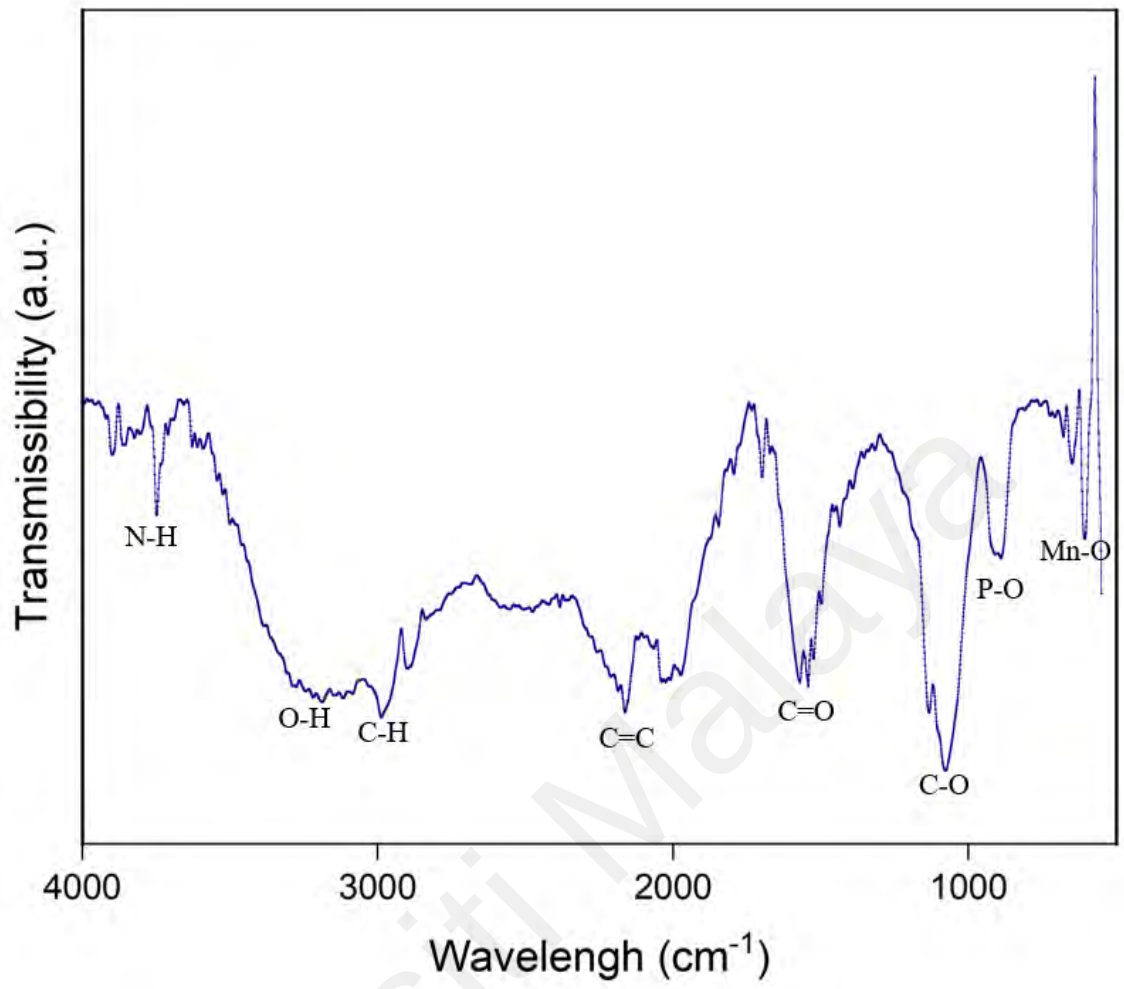

Figure 4.12 : FTIR Spectra for HA/Mn

4.3.2 Surface area analysis

To investigate the impact of the modification on hybrid adsorbents, BET surface area analysis was conducted for RA, HA, and HA/Mn, as summarised in Table 4.5. The results show a substantial increase in surface area, with HA exhibiting a 450-fold increase from 1.19 m^2/g (RA) to 535.97 m^2/g. This enhancement is attributed to the decomposition of organic matter during hydrothermal carbonization and phosphoric acid activation. The surface area was further increased to 666.36 m^2/g for HA/Mn, a 590-fold increase compared to RA, due to manganese oxide impregnation, which promoted further biomass

decomposition, reduced carbon agglomeration, and facilitated mesopore formation. The mesoporous structure of HA/Mn is large enough to adsorb methylene blue dye molecules of 1.7 × 0.76 × 0.33 nm (M. Arias et al., 1999). For comparison, wood-based commercial activated carbon typically has a surface area greater than 100 m^2/g, confirming that the modified hybrid adsorbents have a significantly larger surface area suitable for dye removal. Specifically, the surface area of HA is 5.36 times greater than the commercial adsorbent, while HA/Mn shows a 6.66-fold increase.

Preliminary experiments under fixed conditions (pH 7, 2.5 g/L adsorbent dosage, 0.2 g/L dye concentration, and 90 min contact time) demonstrated 15–18% higher colour removal for HA and HA/Mn than RA. Additionally, HA and HA/Mn exhibited higher adsorption capacities than RA, with 24 mg/g and 45 mg/g, respectively. The increase in surface area confirms successful modification via phosphoric acid activation and manganese oxide impregnation, leading to enhanced adsorption performance. The low surface area of unmodified adsorbents is attributed to lignocellulosic particles obstructing pore development. A study by Patra et al. (2021) reported similar findings, where unmodified chitosan had a surface area of 5 m^2/g, while modification with a weak acid (methanol) increased it tenfold to 53 m^2/g.

In summary, the modified hybrid adsorbents exhibited significantly higher surface area than the raw adsorbent, with HA/Mn reaching 666 m^2/g, demonstrating effective surface modification. The mesoporous structure further enhances its ability to adsorb methylene blue dye molecules, confirming its potential as an efficient adsorbent.

Table 4.5 : Surface area analysis for biomass-based adsorbents.

Adsorbent	S_{BET} (m^2/g)	Pore size (nm)	Ref.
HA/Mn	666.36	2.486	This study
HA	535.97	2.500	
RA	1.19	5.260	
Avocado seed hydrochar	25.98	13.010	(Prabakaran et al., 2022)
Avocado seed biochar	299.90	0.670	(Salomón-Negrete et al., 2018)
Banana peel biochar	112.57	3.840	(Hu et al., 2021)
Cocoa leaves biochar	957.02	7.210	(J. M. Jabar et al., 2022)
Chitosan	5.03	3.150	(Patra et al., 2021)
Modified chitosan	53.90	97.430	
Wattle bark biochar	393.15	1.980	(Cuong Nguyen et al., 2021)
Mimosa biochar	285.53	2.160	
Coffee husk biochar	2.62	11.720	

4.3.3 Surface morphology

The surface morphology of RA, HA, and HA/Mn in Figure 4.13, 4.14 and 4.15, respectively displays distinct characteristics before and after modification. The raw adsorbents displayed a smoother surface with few pores and an uneven structure with visible sticky organic matter and fibrous particles attached, as seen in Figure 4.9. This reflects to the biomass material's lignocellulosic surface properties (Xue et al., 2022). After H_3PO_4 activation, the adsorbent (HA) in Figure 4.10 exhibits a porous surface with deep crater-like and hexagonal pores. The Mn_3O_4, impregnated hybrid adsorbent, HA/Mn shown in Figure 4.11, exhibits a rough texture with increased porosity and irregular rough cavities throughout the surface. Besides, in Figure 4.11 (b), the flaky substance on the surface of the HA/Mn are manganese particles, indicating successful metal impregnation

of the adsorbent. It was observed that the porosity of the adsorbents gradually increased with chemical modification and metal impregnation.

A study conducted by Georgin et al. (2018) observed increased porosity and minor cavities in the internal structure of avocado shell after H_2SO_4 activation. Another study by Rose et al. (2023) on banana peel adsorbents showed limited porosity in raw adsorbents, which increased significantly with deep ledges after NaOH acid activation. Similarly, a study by Munagapati et al. (2018) using banana peel shows a similar porous surface with HA, while Pauletto et al. (2021) reported avocado seed to have hexagonal pores like HA. The differences in pore structure might be due to the presence of lignocellulosic materials commonly found in biomass.

In summary, the SEM analysis revealed that adsorbents show an increase in porosity after chemical modification. Additionally, a rougher texture was observed after metal impregnation, consistent with previous studies using fruit waste biomass adsorbents (T Ahmad & M Danish, 2022; Misran et al., 2021; Prabakaran et al., 2022; M. Silva et al., 2021).

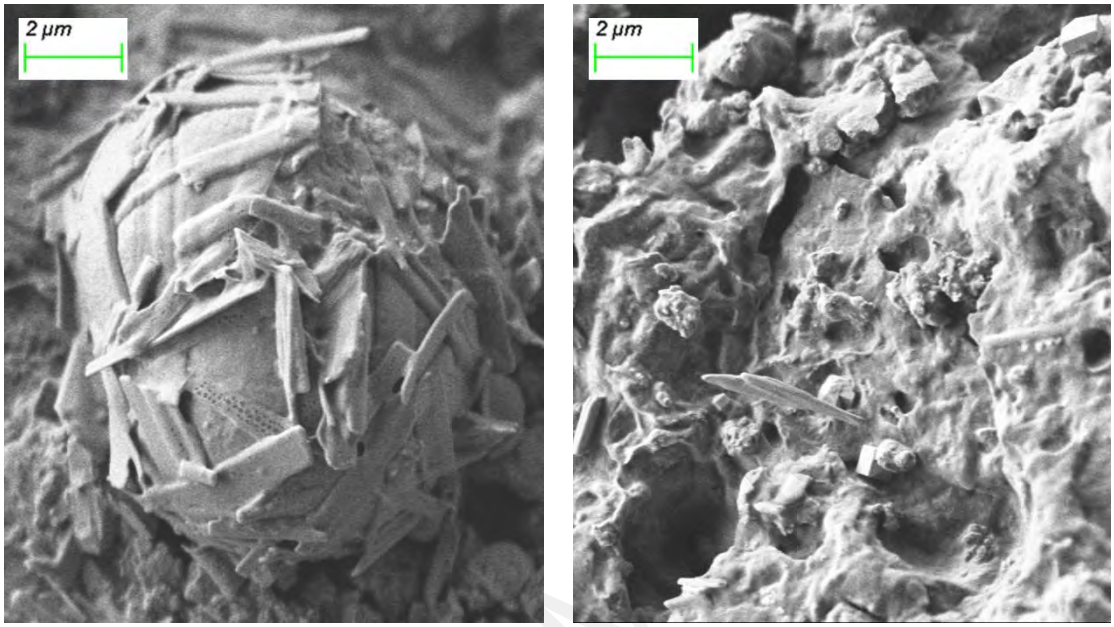

(a) (b)

Figure 4.13 : SEM Images of RA with a magnification of 5000x.

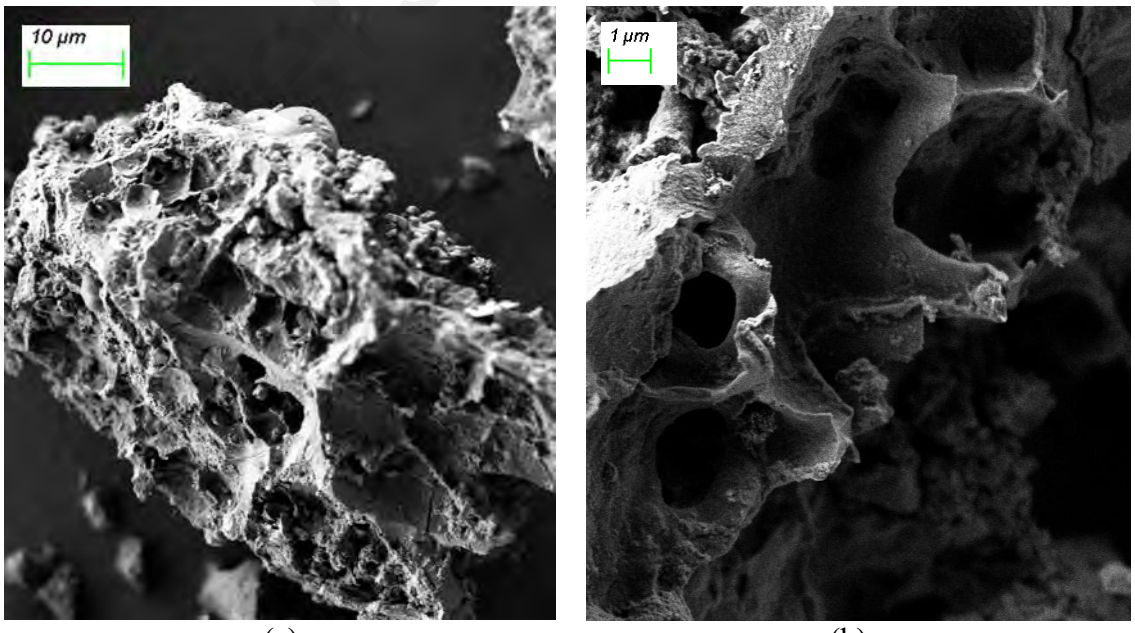

(a) (b)

Figure 4.14 : SEM Images of HA with a magnification of (a) 1000x and (b) 5000x.

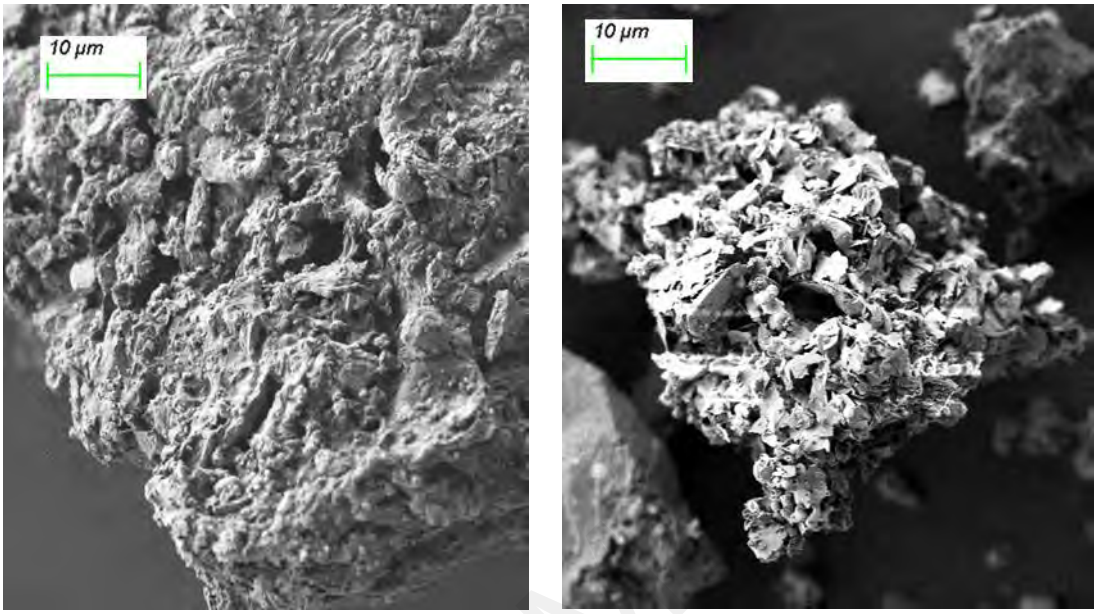

(a) (b)

Figure 4.15 : SEM Images of HA/Mn with a magnification of (a) 5000x and (b) 1000x.

4.3.4 Elemental analysis

The elemental analysis was conducted for the three-hybrid adsorbent: RA, HA, and HA/Mn, in Figure 4.16, 4.17 and 4.18, respectively. The elemental analysis reveals that the raw adsorbent, RA, consists of 71 % carbon and 27 % oxygen, as shown in Figure 4.16. In contrast, the acid-activated adsorbent, HA (Figure 4.17), exhibits increased carbon content to 84 %, reduced oxygen to 12 %, and the presence of phosphorus 2 % and sodium 2 %. The presence of phosphorus after modification is due to the activation of adsorbents with H_3PO_4. Similarly, the study conducted by Pawar et. al. (2023) on banana peels concluded that the two main elements are carbon and oxygen. A study conducted by Prabakaran et. al. (2022) reported that after iron activation of the avocado

seed, the adsorbent had a carbon content of 72 % and the presence of oxygen along with Iron. Moreover, in Figure 4.18 for HA/Mn, the carbon and oxygen content on the surface were 18 % and 28 %, respectively. Conversely, the phosphorus content increased to 10 %, along with 40 % manganese.

In summary, after acid activation, the carbon content of HA increased compared to the raw unmodified adsorbent. However, after metal impregnation, the carbon content decreases while manganese on the surface increases. Besides, compared to the HA adsorbent, the decrease in carbon content and increase in oxygen for HA/Mn is attributed to the metal impregnation of manganese oxide, which covers the surface of the adsorbent.

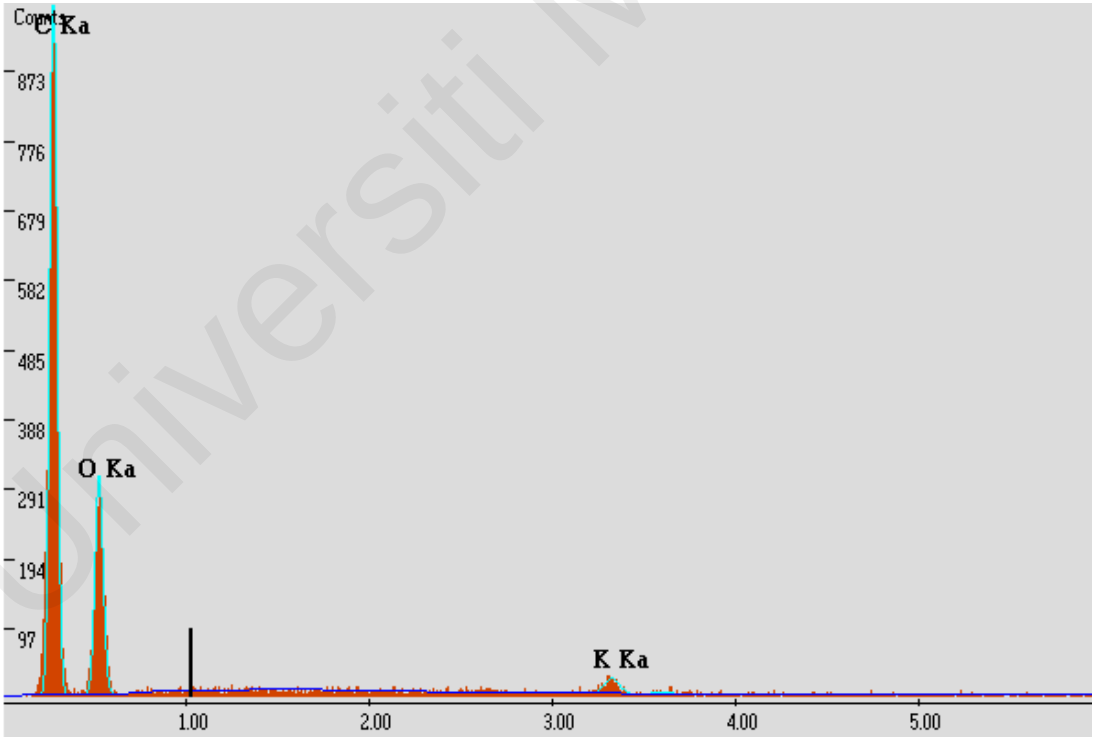

Figure 4.16 : EDX Image of RA.

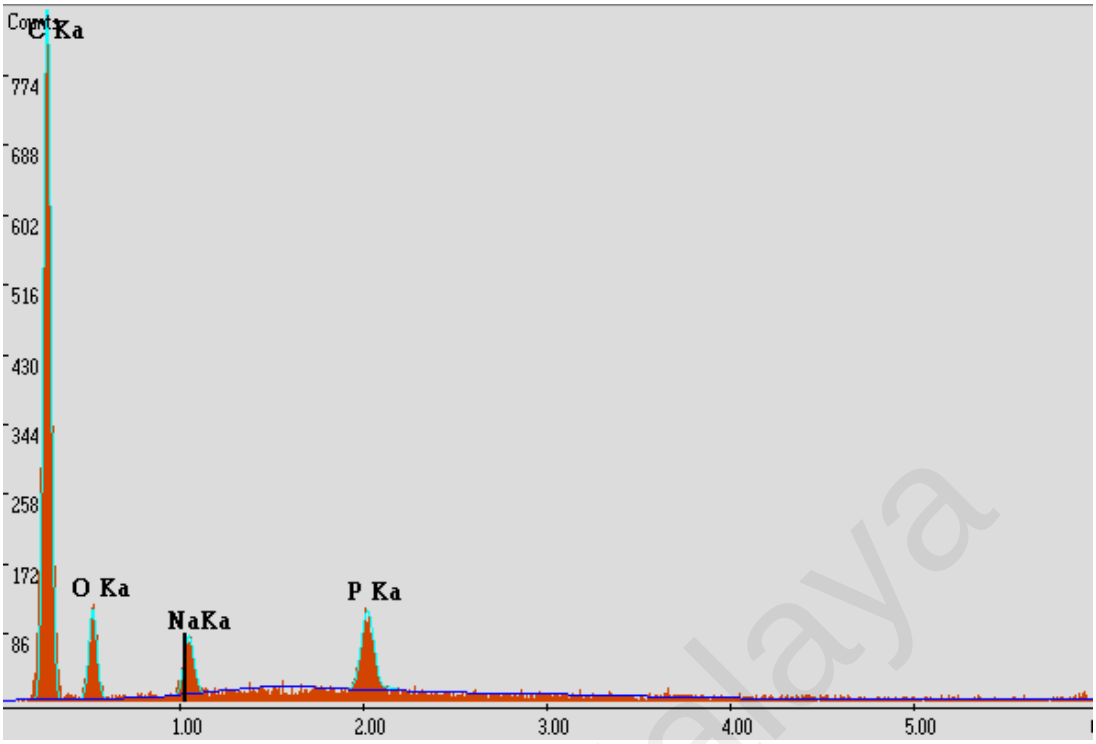

Figure 4.17 : EDX Image of HA.

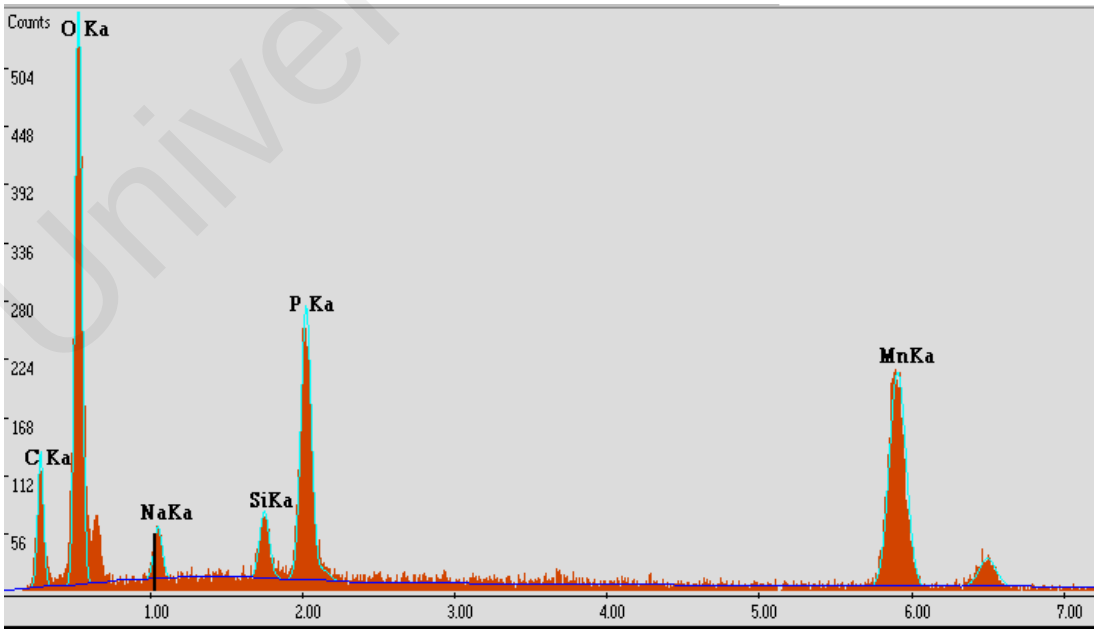

Figure 4.18 : EDX Image of HA/Mn.

4.3.5 Point of zero charge

The point of zero charge (pH_{pzc}) was determined using the method by Postai et al. (2016). In this method, 0.05 g of adsorbent was added to 20 mL of 0.1 M NaCl solution, with the pH adjusted from 2 to 11 using 0.1 M HCl or NaOH (Postai et al., 2016). After shaking the solution for 24 hours at 150 rpm, the final pH was recorded. The pHpzc was measured by calculating the difference between the initial and final pH of the solutions. Figures 4.19, 4.20, and 4.21 show that RA, HA, and HA/Mn have pH_{pzc} values of 6.0, 6.2, and 6.6, respectively.

The pH_{pzc} indicates the preferred pH level of the dye solutions for optimal performance. For HA/Mn, it suggests that the adsorbent will be positively charged when the initial pH is below 6.6 and negatively charged when the initial pH is above 6.6 (Gonzales-Condori et al., 2023; Rose et al., 2023). The point of zero charge results aligns with previous pH_{pzc} characterizations. Gonzales-Condori et al. (2023) found avocado-based adsorbents have a pH_{pzc} of 5.5, while Rose et al. (2023) reported banana peel adsorbents with a pH_{pzc} of 6.6. These studies reported that cationic dye removal was observed above the pH_{pzc} of the adsorbent, while anionic dyes favoured a pH below the pH_{pzc} of the adsorbent (Chen et al., 2023; Mahalaxmi & Kumar, 2024; Schadeck Netto et al., 2019).

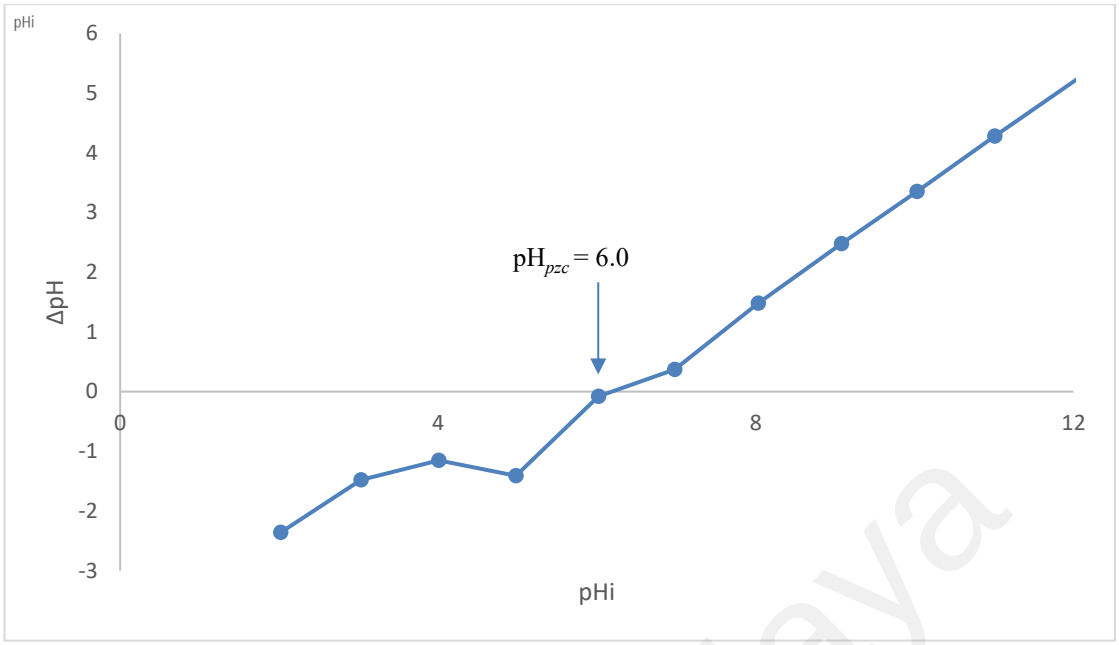

Figure 4.19 : Determination of point of zero charge for RA.

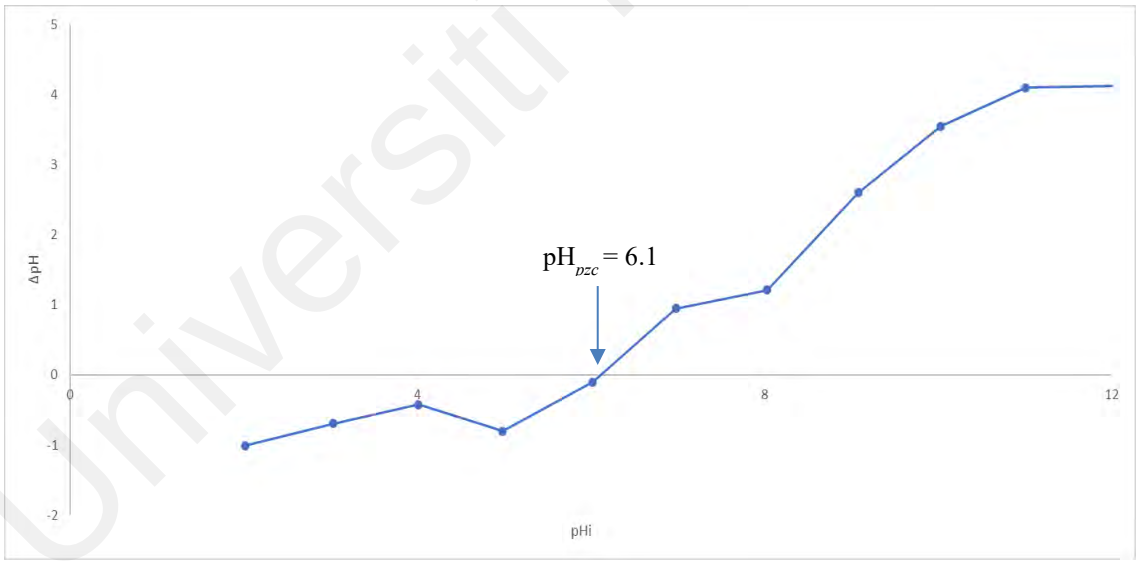

Figure 4.20 : Determination of point of zero charge for HA.

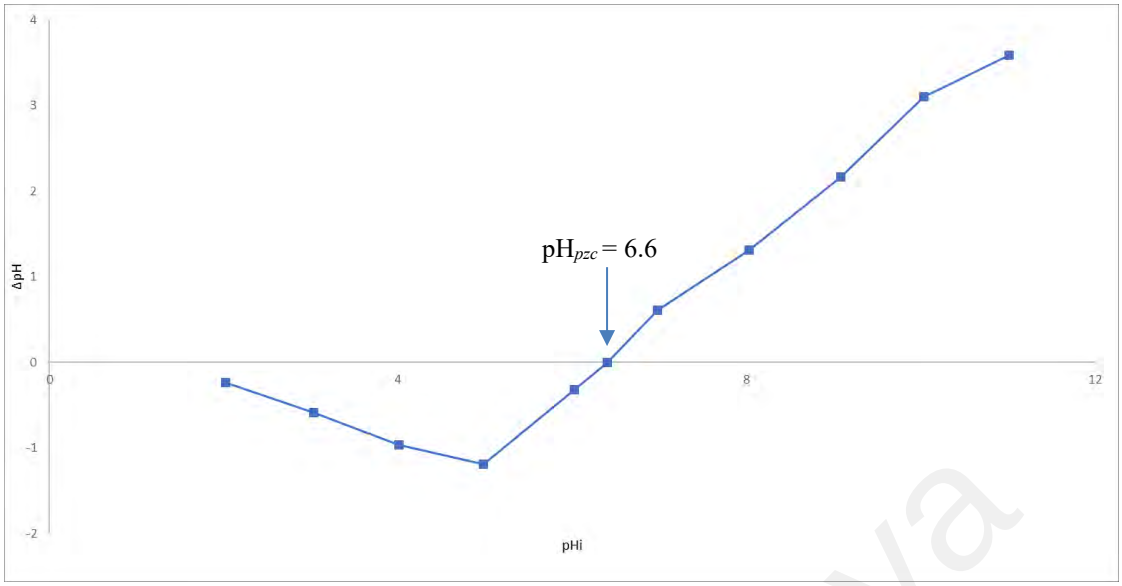

Figure 4.21 : Determination of point of zero charge for HA/Mn.

4.3.6 Summary of physicochemical characteristics

In summary, the modification of the hybrid adsorbent has significantly enhanced its physicochemical properties, as shown in Table 4.6. Among the adsorbents, HA/Mn exhibited superior physicochemical properties compared to RA and HA. It had the highest surface area with mesoporous porosity, making it highly suitable for methylene blue adsorption. The improved morphology and surface area enhance physical adsorption of dye molecules, while the increase in oxygenated functional groups facilitates chemical adsorption through hydrogen bonding. Additionally, the point of zero charge indicates that at a solution pH above 6–6.6, electrostatic attraction is more favourable, collectively improving adsorption performance. Moreover, elemental analysis and chemical characterization confirmed successful surface modification with H_3PO_4 activation and Mn_3O_4 impregnation. Furthermore, the increased oxygenated functional groups from phosphorus and manganese after metal impregnation enhance cationic dye removal, making RA, HA, and HA/Mn highly effective adsorbents.

Table 4.6 : Physicochemical characteristics of the hybrid adsorbents

Adsorbent	Surface morphology	Surface elemental	Pore diameter (nm)	Surface area (m^2/g)	pH_{pzc}	Chemical functional groups
Unmodified raw adsorbent, RA	• Compact smooth surface with few pores • Sticky organic matter on the surface	C: 72 % O: 28 %	5.26	1.19	6.0	OH (3268 cm^{-1}) C-O (1014 cm^{-1}) COOH (1554 cm^{-1})
Acid-activated hybrid adsorbent, HA	• Well-developed crater-like and hexagonal pores • Rough texture	C: 85 % O: 13% P: 2 %	2.50	535.98	6.2	OH (3177 cm^{-1}) C-O (1340 cm^{-1}) COOH (1455 cm^{-1}) P-OH (892 cm^{-1})
Metal oxide impregnated hybrid adsorbent, HA/Mn	• Deep pores with rough texture • Manganese particles attached to the surface of adsorbent.	C: 33 % O: 39% P: 7 % Mn: 16 %	2.49	666.36	6.6	OH (3400 cm^{-1}) C-O (1573 cm^{-1}) COOH (1500 cm^{-1}) P-OH (930 cm^{-1}) Mn-O (604 cm^{-1})

4.4 Adsorption performance evaluation of hybrid adsorbents

Raw hybrid adsorbent (RA), phosphoric acid-activated hybrid adsorbent (HA), and manganese oxide impregnated hybrid adsorbent (HA/Mn) were used to investigate methylene blue dye removal. three of the hybrid adsorbents were compared with each other to find the best performing adsorbent for cationic dye removal. preliminary experiments conducted shows that the adsorption performance also increased after surface modification through acid action and metal impregnation.

The experimental results, statistical analysis, and the effect of parameters are discussed in this section. The experimental results for RA, HA, and HA/Mn are tabulated in Tables 4.7. 4.8 and 4.9, respectively, for colour removal and adsorption capacity. The experimental results were used for the statical analysis to identify the significance of the operating parameters. Besides, using the respective experimental results for the hybrid adsorbents, the effect of each parameter, including the initial pH, adsorbent dosage, dye concentration, and contact time, was analysed and compared.

4.4.1 Statistical analysis

Analysis of Variance (ANOVA) was used to determine the statistical analysis for RA, HA, and HA/Mn, indicating the significance of the operation parameters for colour removal and adsorption capacity. The F-value and P-value from ANOVA analysis are statistical measures to determine the significance of the independent variables. While the F-value is the variation within the samples, the p-value is the calculation for the probability of the hypothesis testing. When the p-value is < 0.05, it indicates that the independent variable is significant in the study. If the p-value is greater than 0.1, it indicates that the variables are insignificant in the regression model. The insignificant variables are removed to improve the model.

Table 4.7: Experimental results for dye removal by unmodified hybrid adsorbent

Experimental Run					Performance Efficiency	
Run	**Initial pH**	**Adsorbent dosage (g/L)**	**Dye concentration (g/L)**	**Contact time (min)**	**% Colour removal**	**Adsorption capacity (mg/g)**
1	2	2.8	0.3	95	42.1	45.9
2	2	5.0	0.1	180	78.9	15.8
3	10	5.0	0.1	180	99.0	19.8
4	6	1.8	0.3	95	67.2	115.2
5	6	2.8	0.3	95	97.1	105.9
6	6	2.8	0.3	95	96.2	104.9
7	2	0.5	0.1	180	14.2	28.5
8	2	0.5	0.5	180	40.4	404.0
9	6	2.8	0.3	95	96.7	105.5
10	10	5.0	0.1	10	97.0	19.4
11	10	5.0	0.5	180	99.4	99.4
12	10	0.5	0.1	10	96.4	192.9
13	2	0.5	0.1	10	63.3	126.6
14	10	5.0	0.5	10	99.2	99.2
15	6	2.8	0.3	75	95.5	104.2
16	10	0.5	0.5	180	97.3	973.2
17	6	2.8	0.3	95	96.3	105.1
18	6	2.8	0.3	265	99.8	108.9
19	6	2.8	0.3	95	99.6	108.6
20	10	0.5	0.1	180	80.3	160.6
21	10	0.5	0.5	10	38.4	384.0
22	6	2.8	0.3	95	96.5	105.3
23	2	5.0	0.5	10	57.0	57.0
24	2	5.0	0.5	180	13.0	13.0
25	6	2.8	0.1	95	98.3	35.7
26	6	7.3	0.3	95	97.8	40.5
27	2	5.0	0.1	10	64.9	13.0
28	14	2.8	0.3	95	99.0	108.0
29	2	0.5	0.5	10	16.0	160.2
30	6	2.8	0.7	95	99.2	252.5

Table 4.8: Experimental results for dye removal by acid-activated hybrid adsorbent.

Experimental Run					Performance Efficiency	
Run	**Initial pH**	**Adsorbent dosage (g/L)**	**Dye concentration (g/L)**	**Contact time (min)**	**% Colour removal**	**Adsorption capacity (mg/g)**
1	2	2.8	0.3	95	95.7	104.4
2	2	5.0	0.1	180	98.6	19.7
3	10	5.0	0.1	180	98.6	19.7
4	6	1.8	0.3	95	97.2	166.7
5	6	2.8	0.3	95	99.5	108.6
6	6	2.8	0.3	95	99.4	108.4
7	2	0.5	0.1	180	91.6	183.3
8	2	0.5	0.5	180	97.2	972.4
9	6	2.8	0.3	95	99.4	108.4
10	10	5.0	0.1	10	92.0	18.4
11	10	5.0	0.5	180	99.7	99.7
12	10	0.5	0.1	10	92.6	185.3
13	2	0.5	0.1	10	97.9	195.7
14	10	5.0	0.5	10	99.7	99.7
15	6	2.8	0.3	75	99.3	108.3
16	10	0.5	0.5	180	99.7	996.6
17	6	2.8	0.3	95	99.3	108.4
18	6	2.8	0.3	265	99.5	108.6
19	6	2.8	0.3	95	99.4	108.4
20	10	0.5	0.1	180	98.4	196.9
21	10	0.5	0.5	10	99.6	995.7
22	6	2.8	0.3	95	99.4	108.4
23	2	5.0	0.5	10	99.6	99.6
24	2	5.0	0.5	180	97.2	97.2
25	6	2.8	0.1	95	98.6	35.9
26	6	7.3	0.3	95	99.5	41.2
27	2	5.0	0.1	10	98.6	19.7
28	14	2.8	0.3	95	95.4	104.1
29	2	0.5	0.5	10	97.3	972.7
30	6	2.8	0.7	95	98.0	249.6

Table 4.9: Experimental results for dye removal by metal-impregnated hybrid adsorbent

Experimental Run					Performance Efficiency	
Run	**Initial pH**	**Adsorbent dosage (g/L)**	**Dye concentration (g/L)**	**Contact time (min)**	**% Colour removal**	**Adsorption capacity (mg/g)**
1	2	2.8	0.3	95	100.0	100.0
2	2	5.0	0.1	180	100.0	100.0
3	10	5.0	0.1	180	97.7	167.5
4	6	1.8	0.3	95	99.9	109.0
5	6	2.8	0.3	95	100.0	109.1
6	6	2.8	0.3	95	99.9	109.0
7	2	0.5	0.1	180	99.8	99.8
8	2	0.5	0.5	180	99.9	109.0
9	6	2.8	0.3	95	99.9	109.0
10	10	5.0	0.1	10	99.7	36.2
11	10	5.0	0.5	180	99.9	109.0
12	10	0.5	0.1	10	99.9	109.0
13	2	0.5	0.1	10	100.0	41.4
14	10	5.0	0.5	10	99.9	109.0
15	6	2.8	0.3	75	99.7	108.8
16	10	0.5	0.5	180	96.4	96.4
17	6	2.8	0.3	95	100.0	109.1
18	6	2.8	0.3	265	100.0	200.0
19	6	2.8	0.3	95	99.9	20.0
20	10	0.5	0.1	180	84.3	214.6
21	10	0.5	0.5	10	100.0	20.0
22	6	2.8	0.3	95	99.9	20.0
23	2	5.0	0.5	10	99.7	19.9
24	2	5.0	0.5	180	99.0	197.9
25	6	2.8	0.1	95	87.6	175.2
26	6	7.3	0.3	95	51.2	512.2
27	2	5.0	0.1	10	58.0	116.0
28	14	2.8	0.3	95	37.9	378.9
29	2	0.5	0.5	10	14.7	147.4
30	6	2.8	0.7	95	15.8	157.9

ANOVA analysis results for the colour removal suggest reduced quadratic models for RA, HA, and HA/Mn as detailed in Table 4.10 to 4.12 with an R^2 value of 0.6785, 0.9167, and 0.9409, respectively, for colour removal. The raw hybrid adsorbent shows initial pH and adsorbent dosage as the significant variables with a p-value of < 0.0001 and 0.0075, respectively. The HA shows the most significant variables for colour removal to be the initial concentration and adsorbent dosage with both p-values < 0.0001. Besides, HA used for colour removal also identified initial pH and contact time as significant variables with p-values of 0.0389 and 0.0020, respectively. However, HA/Mn identified adsorbent dosage and initial dye concentration as the most significant variables, with both p-values < 0.0001. Moreover, the reduced quadratic models for RA, HA, and HA/Mn show a precision ratio exceeding 4, with an adequate precision of 10.3481, 18.5724, and 26.9786, respectively, for colour removal.

ANOVA analysis results for adsorption capacity for RA, HA, and HA/Mn suggest reduced quadratic models as well with R^2 value of 0.8235, 0.8798, and 0.9493, respectively. The raw hybrid adsorbent, RA, indicates three of the operational parameters being significant with p-values of <0.0001 for adsorbent dosage and 0.0002 for initial concentration, while initial pH has a p-value of 0.0111. The acid-activated adsorbent, HA, suggests all the operational parameters are significant with p-values of 0.0026 for contact time, 0.0117 for initial pH, and <0.0001 for both adsorbent dosage and initial concentration. The most significant operational parameters for HA/Mn in the adsorption capacity model were adsorbent dosage and dye concentration, both with p-values < 0.0001, like the colour removal model. The precision ratio for adsorption capacity exceeded 4, with an adequate precision of 15.6409, 16.8810, and 27.0849 for RA, HA, and HA/Mn, respectively.

In summary, adsorbent dosage and initial concentration are the significant operational parameters for the methylene blue dye. Comparing the R^2 value of the models, HA/Mn has the highest values for both colour removal and adsorption capacity. Thus, the analysis implies the reduced quadratic model is significant for MB dye removal, as evidenced by the HA/Mn model with an F-value of 71.17 (p-value < 0.0001) for colour removal. Similarly, for adsorption capacity, the HA/Mn model demonstrates significance with an F-value of 57.59 (p-value < 0.0001). Moreover, the adequate precision over 4 for all the reduced quadratic models for HA/Mn suggests that the model is suitable within the given design space.

Table 4.10: ANOVA results for colour removal and adsorption capacity using RA.

(a) **Reduced Quadratic Equation for Colour Removal**					
Source	**Sum of Squares**	**df**	**Mean Square**	**F-value**	**p-value**
Model	16578.88	4	4144.72	13.19	< 0.0001
A-Initial pH	11731.97	1	11731.97	37.33	< 0.0001
B-Adsorbent Dosage	2656.52	1	2656.52	8.45	0.0075
A^2	3516.57	1	3516.57	11.19	0.0026
B^2	1096.82	1	1096.82	3.49	0.0735
R^2	0.6785				
Adjusted R^2	0.6270				
Predicted R^2	0.3279				
Adeq Precision	10.3481				
Equation	$92.4 + 25.07\,A + 12.37B - 14.83A^2 - 8.35B^2$				

(b) **Reduced Quadratic Equation for Adsorption Capacity**					
Source	**Sum of Squares**	**df**	**Mean Square**	**F-value**	**p-value**
Model	8.07E+05	9	89636.44	10.37	< 0.0001
A-Initial pH	67685.4	1	67685.4	7.83	0.0111
B-Adsorbent Dosage	3.11E+05	1	3.11E+05	35.94	< 0.0001
C-Dye Concentration	1.75E+05	1	1.75E+05	20.19	0.0002
AB	45413.74	1	45413.74	5.25	0.0329
AC	31746.33	1	31746.33	3.67	0.0698
BC	91821.12	1	91821.12	10.62	0.0039
BD	34519.78	1	34519.78	3.99	0.0595
CD	52489.1	1	52489.1	6.07	0.0229
B^2	53759.98	1	53759.98	6.22	0.0215
R^2	0.8235				
Adjusted R^2	0.744				
Predicted R^2	0.3438				
Adeq Precision	15.6409				
Equation	$106.5 + 56.85A - 133.03B + 85.29C - 53.28AB + 44.54AC - 75.75BC - 46.45BD + 57.28CD + 57.83B^2$				

Table 4.11: ANOVA results for colour removal and adsorption capacity using HA.

(a) **Reduced Quadratic Equation for Colour Removal**					
Source	**Sum of Squares**	**df**	**Mean Square**	**F-value**	**p-value**
Model	20639.54	8	2579.94	19.9	< 0.0001
A-Initial pH	629.22	1	629.22	4.85	0.0389
B-Adsorbent Dosage	9100.98	1	9100.98	70.2	< 0.0001
C-Dye Concentration	3796.84	1	3796.84	29.29	< 0.0001
D-Contact time	1618.64	1	1618.64	12.48	0.002
BC	2542.82	1	2542.82	19.61	0.0002
BD	407.78	1	407.78	3.15	0.0907
B^2	3277.6	1	3277.6	25.28	< 0.0001
D^2	918.34	1	918.34	7.08	0.0146
R^2	0.8835				
Adjusted R^2	0.8391				
Predicted R^2	0.7005				
Adeq Precision	18.5724				
Equation	96.8 + 5.48A + 22.95B – 12.58C + 9.72D + 12.61BC -5.05BD – 14.6B^2 - 7.68D^2				

(b) **Reduced Quadratic Equation for Adsorption Capacity**					
Source	**Sum of Squares**	**df**	**Mean Square**	**F-value**	**p-value**
Model	87095.05	9	9677.23	16.27	< 0.0001
A-Initial pH	4577.3	1	4577.3	7.69	0.0117
B-Adsorbent Dosage	43784.66	1	43784.66	73.59	< 0.0001
C-Dye Concentration	13996.52	1	13996.52	23.53	< 0.0001
D-Contact time	7055.61	1	7055.61	11.86	0.0026
AB	3831.34	1	3831.34	6.44	0.0196
AC	2463.02	1	2463.02	4.14	0.0554
BC	7376.74	1	7376.74	12.4	0.0021
BD	4256.26	1	4256.26	7.15	0.0146
D^2	1983.08	1	1983.08	3.33	0.0829
R^2	0.8798				
Adjusted R^2	0.8257				
Predicted R^2	0.6874				
Adeq Precision	16.881				
Equation	114.69 + 14.78A -46.73B + 24.15C + 20.11D -15.47AB + 12.41AC -21.47BC –16.31BD – 11.06D^2				

Table 4.12: ANOVA results for colour removal and adsorption capacity using HA/Mn

(a) **Reduced Quadratic Equation for Colour Removal**					
Source	**Sum of Squares**	**df**	**Mean Square**	**F-value**	**p-value**
Model	19841.56	5	3968.31	71.17	< 0.0001
B-Adsorbent Dosage	8769.57	1	8769.57	157.28	< 0.0001
C-Dye Concentration	5019.15	1	5019.15	90.02	< 0.0001
BC	193.92	1	193.92	3.48	0.0745
A^2	2945.38	1	2945.38	52.82	< 0.0001
B^2	5019.15	1	5019.15	90.02	< 0.0001
R^2	0.9368				
Adjusted R^2	0.9237				
Predicted R^2	0.8225				
Adeq Precision	26.9786				
Equation	98.7 + 22.44B - 15.49C + 18.02BC - 5.31A^2- 13.45B^2				

(b) **Reduced Quadratic Equation for Adsorption Capacity**					
Source	**Sum of Squares**	**df**	**Mean Square**	**F-value**	**p-value**
Model	1.17E+05	6	19516.21	57.59	< 0.0001
B-Adsorbent Dosage	88454.53	1	88454.53	261.03	< 0.0001
C-Dye Concentration	18659.73	1	18659.73	55.07	< 0.0001
AC	1080.77	1	1080.77	3.19	0.0873
BC	2850.38	1	2850.38	8.41	0.0081
BD	1094.69	1	1094.69	3.23	0.0854
B^2	5396.59	1	5396.59	15.93	0.0006
R^2	0.9376				
Adjusted R^2	0.9213				
Predicted R^2	0.8804				
Adeq Precision	27.0849				
Equation	112.01 - 70.83B + 31.05C - 10.27 AC + 13.35BC - 8.27BD +18.00B^2				

4.4.2 Effect of operating parameters

4.4.2.1 Initial pH of the solution

*(a) **Colour removal***

Figures 4.22, 4.23, and 4.24 show the effect of initial pH on colour removal using RA, HA, and HA/Mn. The colour removal of RA increased from 65 % to 76 % when the pH was increased from 2 to 10 at 180 mins. An increment in the colour removal was also recorded for a lower contact time of 10 with the increased colour removal of 80 % from 69 %. The highest colour removal from Figure 4.22 can be seen as 80 % at 10 min of contact time and in alkaline condition of pH 10. This is in line with the pH_{pzc} for RA with a pH_{pzc} of 6, indicating the cationic dye removal takes place in alkaline conditions. Based on the ANOVA analysis for colour removal for RA, the initial pH is a significant variable, resulting in higher colour removal under alkaline conditions. A study conducted by Eniola et. al. (2023) achieved high performance in alkaline conditions of pH 8 using unmodified date seed, while a study conducted by Maheshwari et. al. (2023) reported that raw banana peel and raw orange peel for cationic dye removal was achieved at pH 10.

In Figure 4.23, HA showed an increment in colour removal from 74 % to 85 % when pH was increased from 2 to 10 at the lowest contact time of 10 min. At pH 2, when the contact time was increased to 180 min, colour removal increased to 93 %. When the pH was increased to 10 at 180 mins, complete colour removal was achieved. Hence, colour removal for HA performed well in higher pH values ranging from 7 to 10. This is in line with the pH_{pzc} of the adsorbent as HA has a point of zero charge of 6.2. Previous studies reported that the optimum pH for avocado seed adsorbent and banana peel adsorbent for methylene blue dye removal was reported as an alkaline condition (Dhaouadi et al., 2020; Maheshwari et al., 2023; Nallapan Maniyam et al., 2020; Schadeck Netto et al., 2019). ANOVA analysis for colour removal for HA, the initial pH is a significant variable which is in line as the effect of initial pH on the colour removal of MB dye using HA.

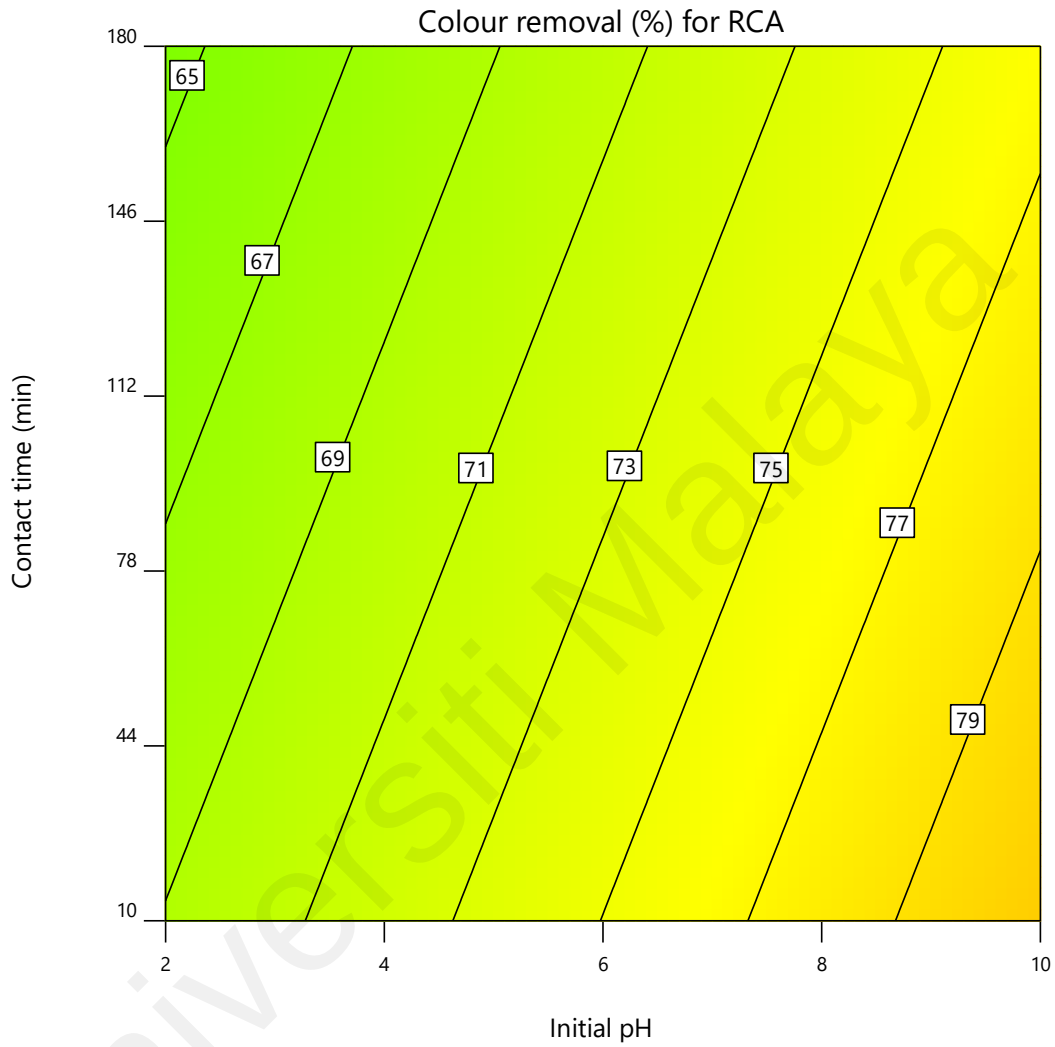

Figure 4.22 : 2D Contour for effect of contact time against initial pH on colour removal for RA.

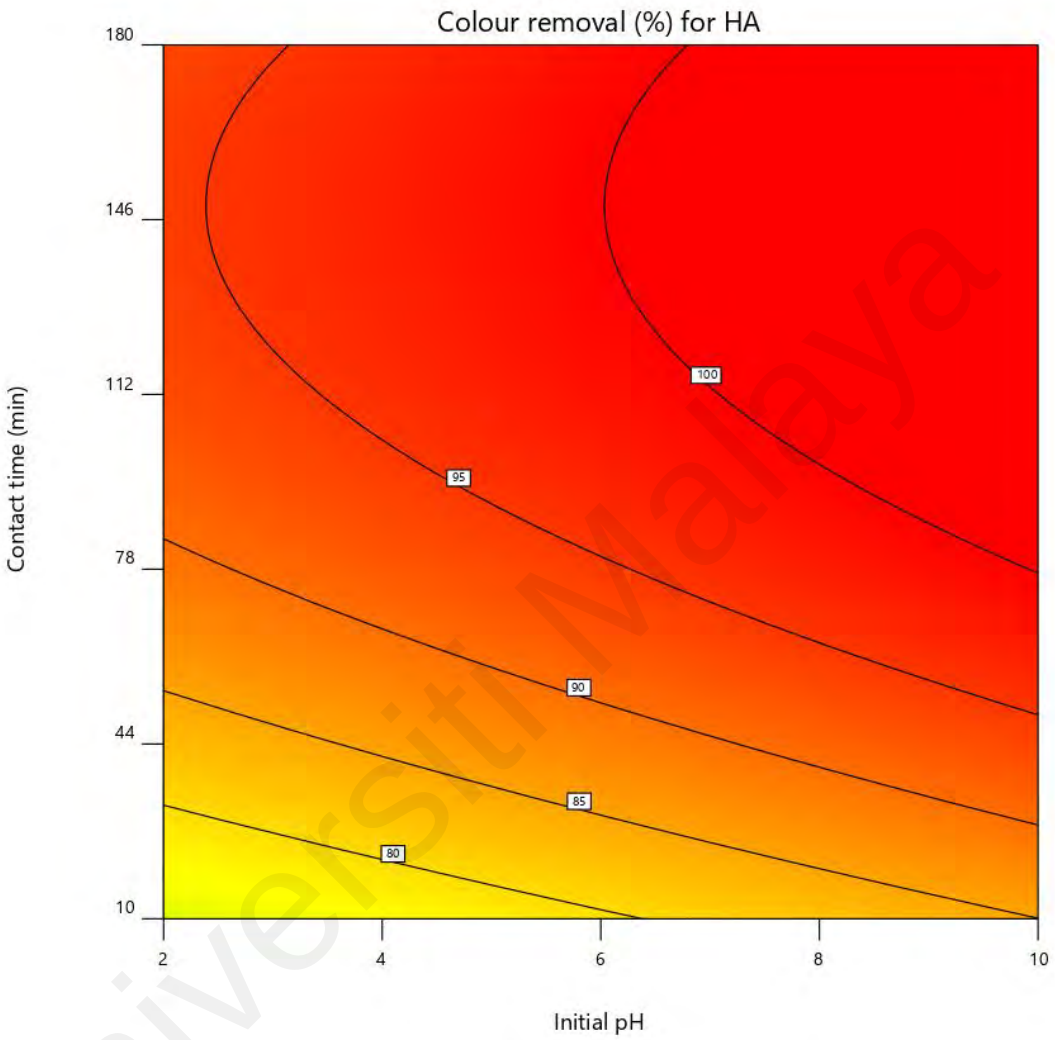

Figure 4.23 : 2D Contour for effect of contact time against Initial pH on colour removal for HA.

HA/Mn, as shown in Figure 4.24, achieves the highest colour removal under alkaline conditions, which is consistent with the pH_{pzc} indicating higher removal for cationic dye above the pH_{pzc} of 6.4. Increasing the pH resulted in an increase in MB dye colour removal from 83.4 % to 92.5 % at an adsorbent dosage of 2.8 g/L and a concentration of 0.3 g/L. The effect of initial pH for the colour removal is in line with previous studies for cationic dye removal using biomass material. The removal efficiency for HA/Mn is highest at alkaline conditions at pH 8 for avocado seed hydrochar for methylene blue removal (Prabakaran et al., 2022) and pH 11 for papaya bark fibre for methylene blue dye removal (Nipa et al., 2023). Although, based on the ANOVA analysis, the initial pH is regarded as an insignificant variable, HA/Mn works best under alkaline conditions with a higher removal efficiency.

(b) ***Adsorption capacity***

The effect of initial pH on adsorption capacity for RA, HA, and HA/Mn are shown in Figures 4.25, 4.26, and 4.27. Furthermore, in ANOVA analysis, initial pH was a significant variable for RA and HA. However, for HA/Mn, it was an insignificant variable. The adsorption capacity of RA in Figure 4.25 shows the highest adsorption capacity was achieved at pH 10 with 233.7 mg/g compared to pH 2 with 82.4 mg/g at 10 mins of contact time. However, when the time was increased to 180 mins, the adsorption capacity was 53.2 mg/g and 205 mg/g at pH 2 and 10, respectively. As presented in Figure 4.26, the adsorption capacity for HA was highest at pH 10 with 98.8 mg/g compared to pH 2 with 69.8 mg/g at 10 mins of contact time. Additionally, when the time was increased to 180 mins, the adsorption capacity was 109.3 mg/g and 138.3 mg/g at pH 2 and 10, respectively.

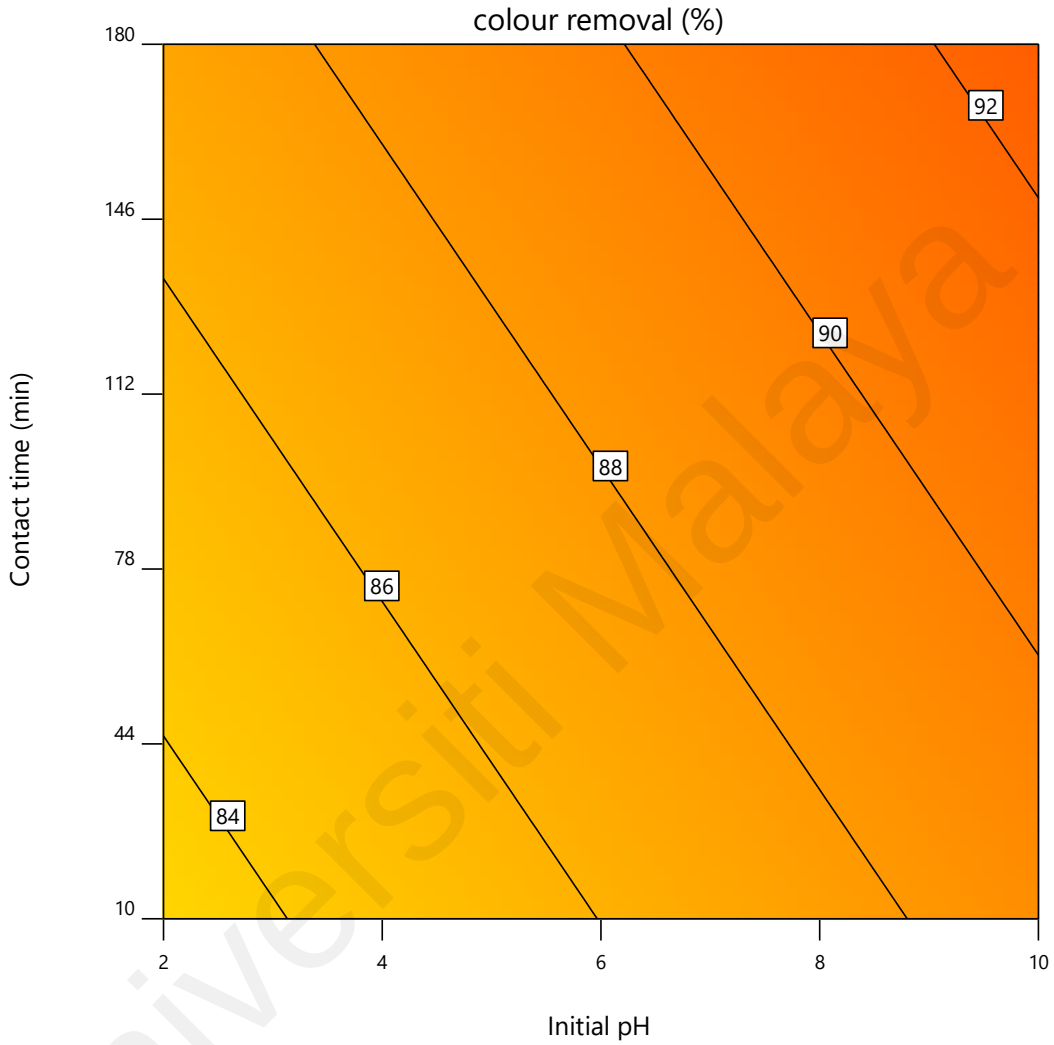

Figure 4.24 : 2D Contour for effect of contact time against initial pH on colour removal for HA/Mn

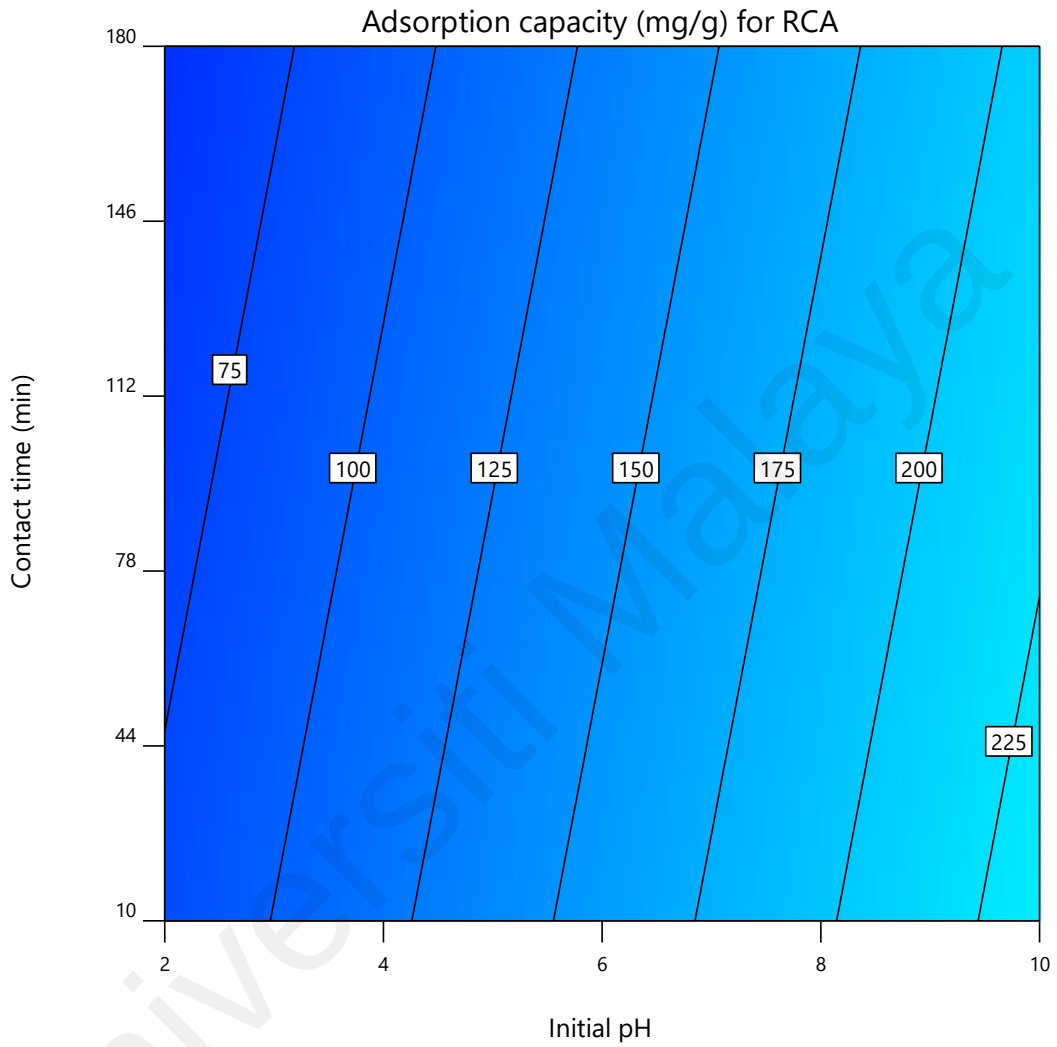

Figure 4.25 : 2D Contour for effect of contact time against initial pH on adsorption capacity for RA.

In Figure 4.27, it is evident that in alkaline conditions, higher adsorption capacity was achieved for HA/Mn. Thus, the adsorption capacity was found to increase from 84.72 mg/g to 128.05 mg/g at alkaline conditions after 10 min of contact time. The effect of initial pH for the MB dye removal is in line with previous studies for cationic dye removal using biomass material. The high adsorption in alkaline conditions can be from the elimination of protons from the surface functional groups of the hybrid adsorbent, influenced by different pH conditions, along with the properties of the cationic dye being targeted. These findings are in line with studies using banana stem (M. Silva et al., 2021), avocado seeds (S. Boeykens et al., 2019), banana peel (Chen et al., 2023) and avocado shells (Georgin et al., 2018).

In summary, the effect of pH on adsorption performance for RA, HA, and HA/Mn suggests higher efficiency in alkaline conditions. All three adsorbent have a point of zero charge between 6 to 6.6, which shows the highest adsorption performance under alkaline conditions, which is consistent with results obtained for RA, HA and HA/Mn. It is in line with previous studies using avocado seed and banana peel for cationic dye removal; such activated avocado seed removed 81 % at alkaline conditions (Prabakaran et al., 2022), Another study using iron-modified banana peel achieved 92 % colour removal in alkaline conditions (Cathoglu et al., 2021)

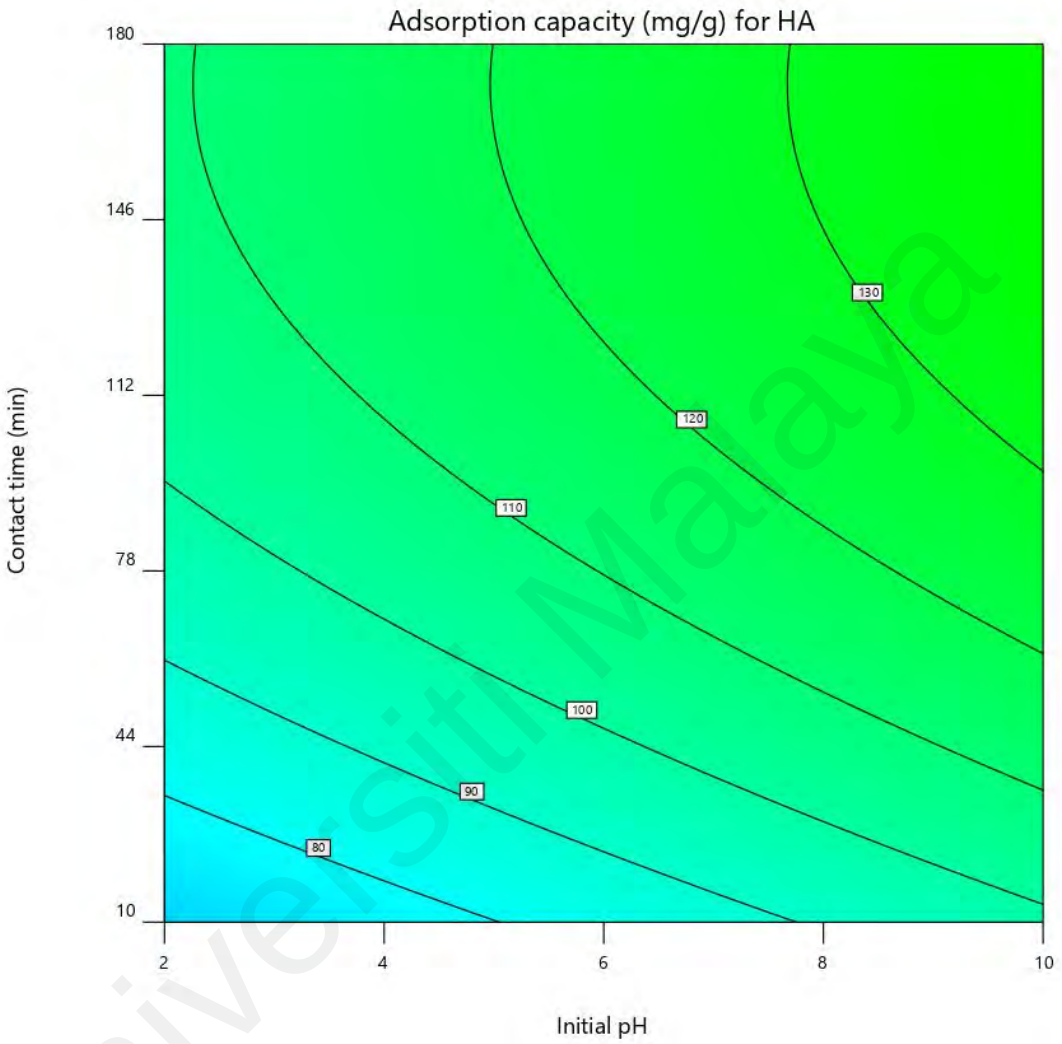

Figure 4.26 : 2D Contour for effect of contact time against initial pH on adsorption capacity for HA.

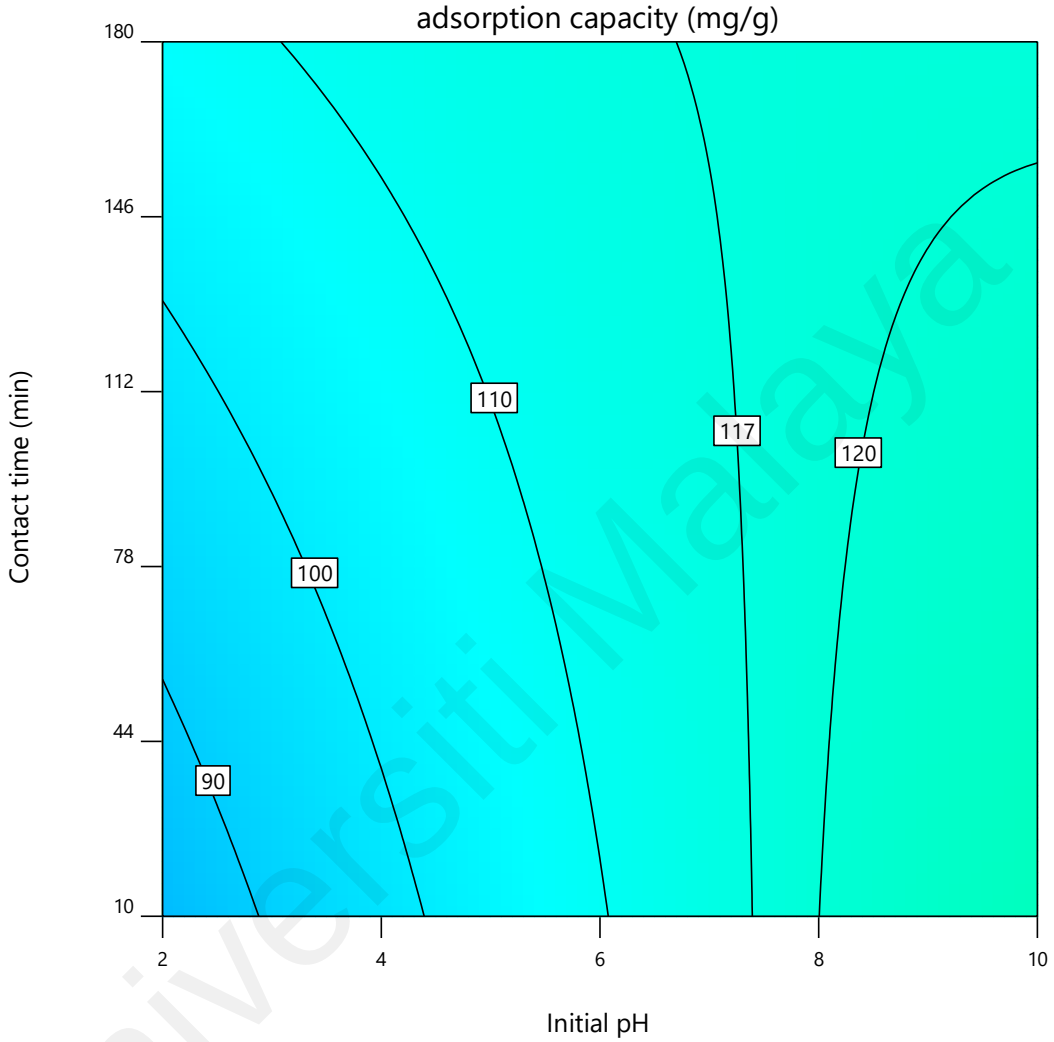

Figure 4.27 : 2D Contour for effect of contact time against initial pH on adsorption capacity for HA/Mn

4.4.2.2 Contact time.

(a) ***Colour removal***

The effect of contact time on colour removal for RA, HA and HA/Mn are shown in Figure 4.22, 4.23 and 4.24, respectively. In Figure 4.22, RA has a decrease in colour removal from 69 % to 65 % when the contact time is increased from 10 to 180 mins, at pH 2 and dye concentration of 0.3 g/L and adsorbent dosage of 2.75 g/L. However, an increased in colour removal for RA is observed for 180 mins when the pH is increased. The ANOVA analysis of RA for colour removal indicated contact time to be an insignificant variable. However, the highest colour removal for RA was recorded at 10 min of contact time. This is in line with previous studies, as all the active binding sites of the adsorbent are unoccupied at the start of the adsorption process, and as contact time increases, fewer vacant sites are available for adsorption process to occur (V. S. Munagapati et al., 2018; Prabakaran et al., 2022)

In Figure 4.23, the effect of contact time for HA in colour removal indicates highest colour removal for can be achieved at higher contact time. Unlike RA, HA has an increase in colour removal from 75 % to 94 % when time was increased from 10 to 180 mins at pH 2. Moreover, at pH 10, when the time was increased from 10 to 180 min, the complete colour removal was achieved at 80 min using dye concentration of 0.3 g/L and adsorbent dosage of 2.75 g/L. A slight decrease in the colour removal can be observed from 130 min to 180 min. This aligns with previous studies, where it has been observed that during the initial stages of the adsorption process, all the active binding sites of the adsorbent remain unoccupied. As the contact time increases, fewer binding sites are left vacant, thereby reducing the availability of binding sites for the adsorption process to take place (V. S. Munagapati et al., 2018; Prabakaran et al., 2022).

In Figure 4.24 for HA/Mn, when the contact time increased from 10 min to 180 min, colour removal increased from 84 % to 87 % at dye concentration of 0.3 g/L and adsorbent dosage of 2.75 g/L. The rapid increase in removal rate at the initial stage of contact time between 10 min to 44 min is due to the abundant availability of vacant active sites on the surface of adsorbent, resulting in instantaneous adsorption of dye molecules (Waghmare et al., 2023). Increasing the contact time from 44 min to 180 min, the adsorption performance increases slowly as the vacant sites become fully occupied, limiting the adsorption reaction and decreasing the adsorption rate (Hambisa et al., 2022). Although contact time is an insignificant variable in the ANOVA analysis for HA/Mn, the maximum dye removal is observed at 80 minutes and is within the range of fruit waste adsorbents for dye removal . A study conducted by Waghmare et. al. (2023) reported optimum contact time for fruit waste adsorbent as 90 mins, meanwhile a study conducted by Nipa et. al. (2023) which reported the optimum contact time to be 100 mins.

(b) ***Adsorption capacity***

Figure 4.25, 4.26 and 4.27 shows effect of contact time on adsorption capacity, for RA, HA and HA/Mn, respectively. The adsorption capacity of raw combined adsorbent was highest at lower contact time of 10 mins with 233.7 mg/g compared with 82.4 mg/g. However, when the time was increased to 180 mins, the adsorption capacity was 53.2 mg/g and 205 mg/g at pH 2 and 10, respectively. lower contact time of 10 min – 90 mins favours the highest adsorption capacity for RA. The ANOVA analysis of RA for adsorption capacity indicated the contact time to be an insignificant variable. The increases in contact time leads to a decrease in adsorption capacity because the adsorption equilibrium was reached (Tang et al., 2021).

As presented in Figure 4.26, the adsorption capacity for HA was increased 109.3 mg/g to138.3 mg/g at pH 2 and 10, respectively, when the contact time was increased to 180

mins. a higher contact time of 78 min – 180 mins were favoured for the highest adsorption capacity. Furthermore, when the time was increased from 10 to 180 mins, in initial pH of 10 the adsorption capacity increased from 100.3 mg/g to 140.0 mg/g. as contact time increases the adsorption increases at first, then the dye removal becomes stable, and no more adsorptions can be observed. This is because at the beginning of the adsorption process, all the active binding sites of the adsorbent will be vacant and with allowed time there will be fewer sites available (V. S. Munagapati et al., 2018).

Likewise, in Figure 4.27 for HA/Mn, increment in contact time from 10 min to 180 min increased the adsorption capacity, achieving 106.89 mg/g at pH 2 and 118.72 mg/g at pH 10. The rapid increase in removal rate at the initial stage of contact time between 10 min to 44 min is due to the abundant availability of vacant active sites on the surface of adsorbent, resulting in instantaneous adsorption of dye molecules (Waghmare et al., 2023). Increasing the contact time from 44 min to 180 min, the adsorption performance increases slowly as the vacant sites become fully occupied, limiting the adsorption reaction and decreasing the adsorption rate (Hambisa et al., 2022). Although contact time is an insignificant variable in the ANOVA analysis for HA/Mn, the maximum dye removal is observed at 80 minutes and is within the range of fruit waste adsorbents for dye removal as indicated in Table 4.12. The rapid increase in removal rate at the initial stage of contact time between 10 min to 44 min is due to the abundant availability of vacant active sites on the surface of adsorbent, resulting in instantaneous adsorption of dye molecules (Waghmare et al., 2023).

In summary, the effect of contact time on adsorption performance for the hybrid adsorbents indicate the rapid increase in the adsorption performance at the beginning of the experiment is due to the availability of active binding site. However, as the time is increased fewer active binding are aviable for the adsorption of methylene blue dye

molecules. Besides, the decrease in the adsorption performance after around midway through experiment is when the adsorption has reached its equilibrium. This is in line with previous studies using biomass-based adsorbents for cationic dye removal with optimum contact time of 90 mins (Afshin et al., 2018), date palm adsorbent for cationic dye with optimum contact time of 200 mins (Eniola et al., 2023) and coconut shell adsorbent for pharmaceutical removal with optimum contact time of 120 mins (Al-sareji et al., 2023).

4.4.2.3 Adsorbent dosage

(a) ***Colour removal***

The effect of adsorbent dosage on colour removal for RA, HA, and HA/Mn is presented in Figures 4.28, 4.29, and 4.30, respectively. The ANOVA analysis for all three adsorbents for both colour removal and adsorption capacity shows that adsorbent dosage is the most significant variable for the adsorbents. The adsorbent dosage of RA was increased from 25 mg (0.5 g/L) to 250 mg (5.0 g/L) at a concentration of 0.1 g/L, where colour removal was increased from 64 % to 90 % as shown in Figure 4.28. Furthermore, when the initial dye concentration is at 0.5 g/L for a maximum adsorbent dosage of 5.0 g/L, RA reached 82 % colour removal, while at 0.1 g/L, RA achieved 90 % colour removal. This suggests that increased doses of the adsorbent offer a greater number of active sites for successful adsorption at the fixed dye concentration. Thus, for RA, the highest colour removal was observed when the dosage was highest at 5 g/L. This is in line with previous studies using an optimum adsorbent dosage of 4 g/L of activated corn (Ismail et al., 2022), 5 g/L of coffee husk biochar, and 5 g/L of mimosa plant biochar (Cuong Nguyen et al., 2021) for wastewater treatment. After a specific adsorbent dose, the adsorption decreases gradually, this may be because the active sites are saturated with accumulated particles, which result in repulsion between the dye molecules and the adsorbent (Roy et al., 2018).

The effect of adsorbent dosage on colour removal for HA in Figure 4.29 shows when the dosage of HA was increased from 25 mg to 250 mg (0.5 g/L at a concentration of 100 mg/L where colour removal was increased from 81 % to complete colour removal. Similarly, an increasing trend was investigated in colour removal from 50 % to 100 % when the HA adsorbent dosage increased from 25 mg to 200 mg at a highest initial concentration of 0.5 g/L. The results are in good agreement with previous studies. For example, Danish and others (2018) reported the adsorption process was noted to be increased with increasing dosage for removal of methylene blue dye using banana waste. Like the research conducted by Prabakaran and others (2022) using avocado seed, dye removal was increased, attaining 95% colour removal with the increase in adsorbent dosage up to 1.5g/L. The results revealed that HA shows higher removal efficiency at higher adsorbent dosages due to the presence of more active sites available for adsorption (Jiang et al., 2021).

Figure 4.30 shows that when HA/Mn adsorbent dosage increases from 0.5 g/L to 5.0 g/L, complete colour removal was achieved at a dye concentration of 0.35 g/L. This suggests that increased doses of the adsorbent offer a greater number of active sites for successful adsorption at the fixed dye concentration. These observations align with previous studies on dye removal using biomass adsorbents (Dhaouadi et al., 2021; Leite et al., 2018b; Prastuti et al., 2019; Yu et al., 2018). For example, Iron-modified banana peel and HCL-activated papaya bark has an optimum adsorbent dosage of 2.5 g/L (Cathoglu et al., 2021; Nipa et al., 2023), while 1 g/L of adsorbent dosage is the optimum dosage for avocado seed biochar, raw orange peel, and raw banana peel (Dhaouadi et al., 2020; Maheshwari et al., 2023).

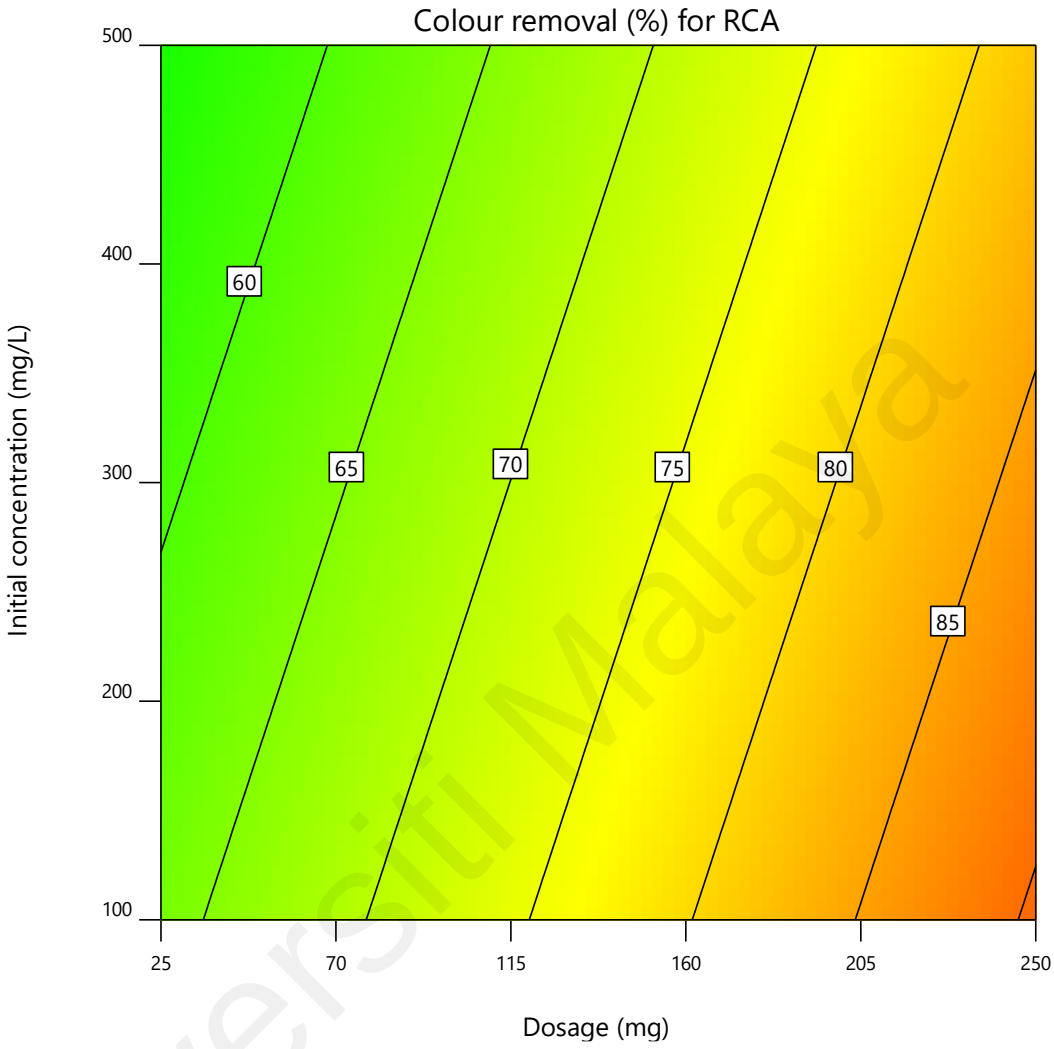

Figure 4.28 : 2D Contour for effect of initial dye concentration against adsorbent dosage on colour removal for RA

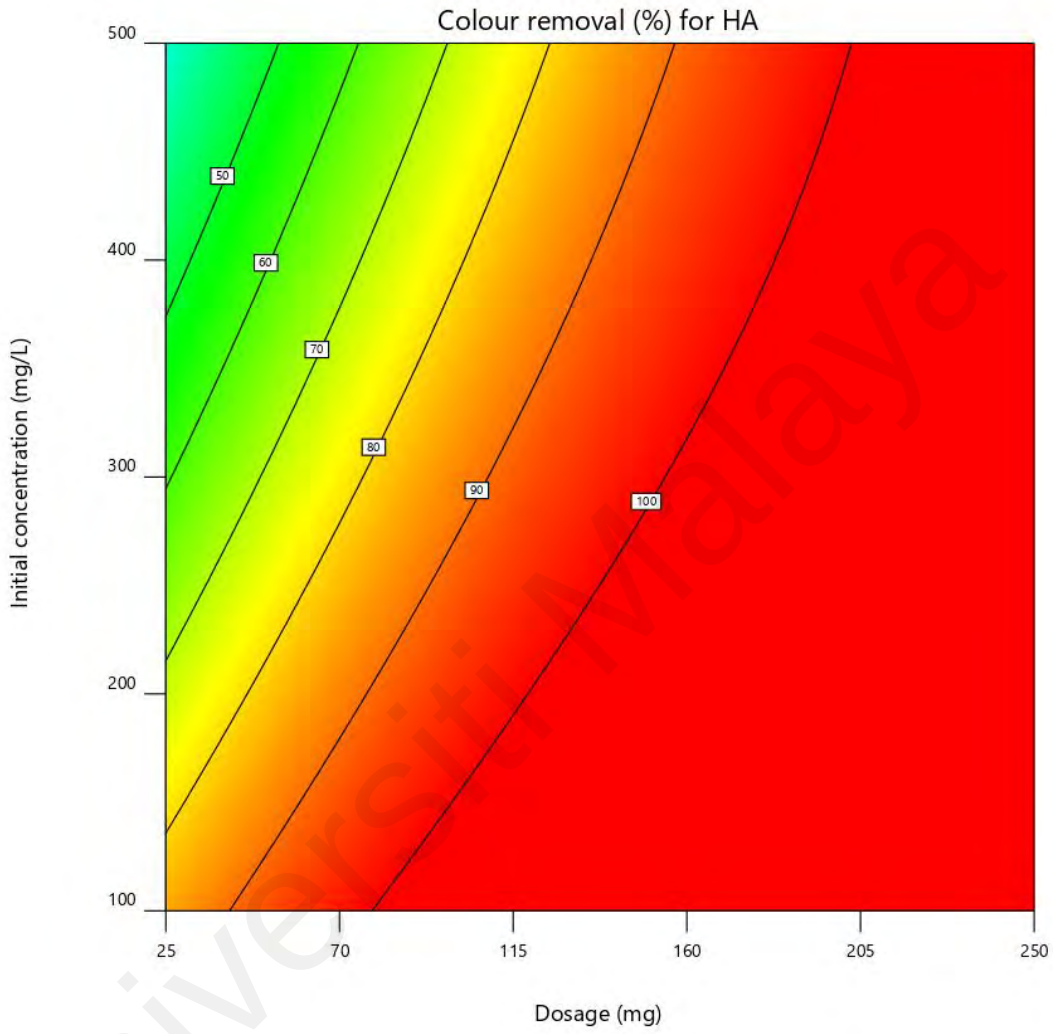

Figure 4.29 : 2D Contour for effect of initial dye concentration against adsorbent dosage on colour removal for HA

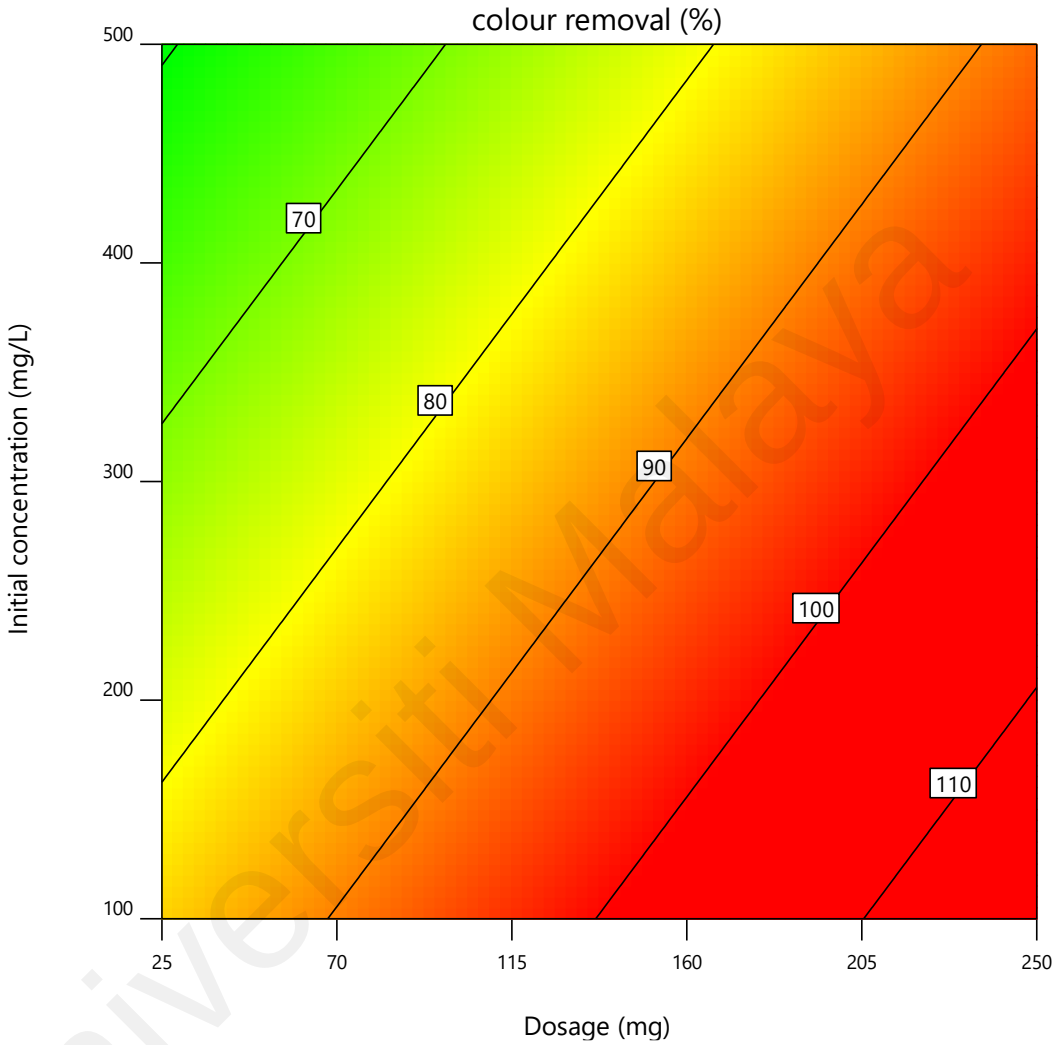

Figure 4.30 : 2D Contour for effect of initial dye concentration against adsorbent dosage on colour removal for HA/Mn

In summary, the optimum adsorbent dosage of HA/Mn for MB dye removal was determined to be 0.5 g/L, based on ANOVA analysis, which identified adsorbent dosage as the most significant operational parameter influencing both colour removal and adsorption capacity. The findings indicate that HA/Mn achieves high removal efficiency even at lower dosages, outperforming many conventional biomass-based adsorbents. This efficiency can be attributed to the enhanced surface area, improved pore structure, and increased availability of active sites resulting from hydrothermal activation and manganese oxide impregnation. Notably, the ability of HA/Mn to achieve substantial dye removal at a lower dosage also has practical benefits, as reducing the required adsorbent amount lowers the overall treatment cost and minimizes secondary waste generation, making the process more sustainable and economically viable.

(b) ***Adsorption capacity***

In Figure 4.31, RA has a decrease in adsorption capacity from 150 mg/g to lower than 50 mg/g when the dosage is increased from 25 mg to 160 mg/g. The maximum adsorption capacity reached for RA was at 300 mg/g at lower adsorbent dosages of 25 mg to 70 mg, between 0.4 g/L to 0.5 g/L of initial dye concentration. As for HA in Figure 4.32, the adsorption capacity is highest (163.7 mg/g) with the lowest adsorbent dosage of 25 mg and the initial concentration of 500 mg/L. With the same adsorbent dosage of HA at an initial concentration of 100 mg/L, a lower adsorption capacity was recorded at 156.9 mg/g. The lowest adsorption capacity for HA was recorded as 24.9 mg/g at 250 mg of adsorbent dosage and the lowest dye concentration at 95 min, indicating higher adsorption capacity occurs when low adsorbent dosages are used. Similar results were reported for biomass-based adsorbents for dye removal using high adsorbent dosage for higher efficiency (Ozdemir et al., 2023; Rose et al., 2023).

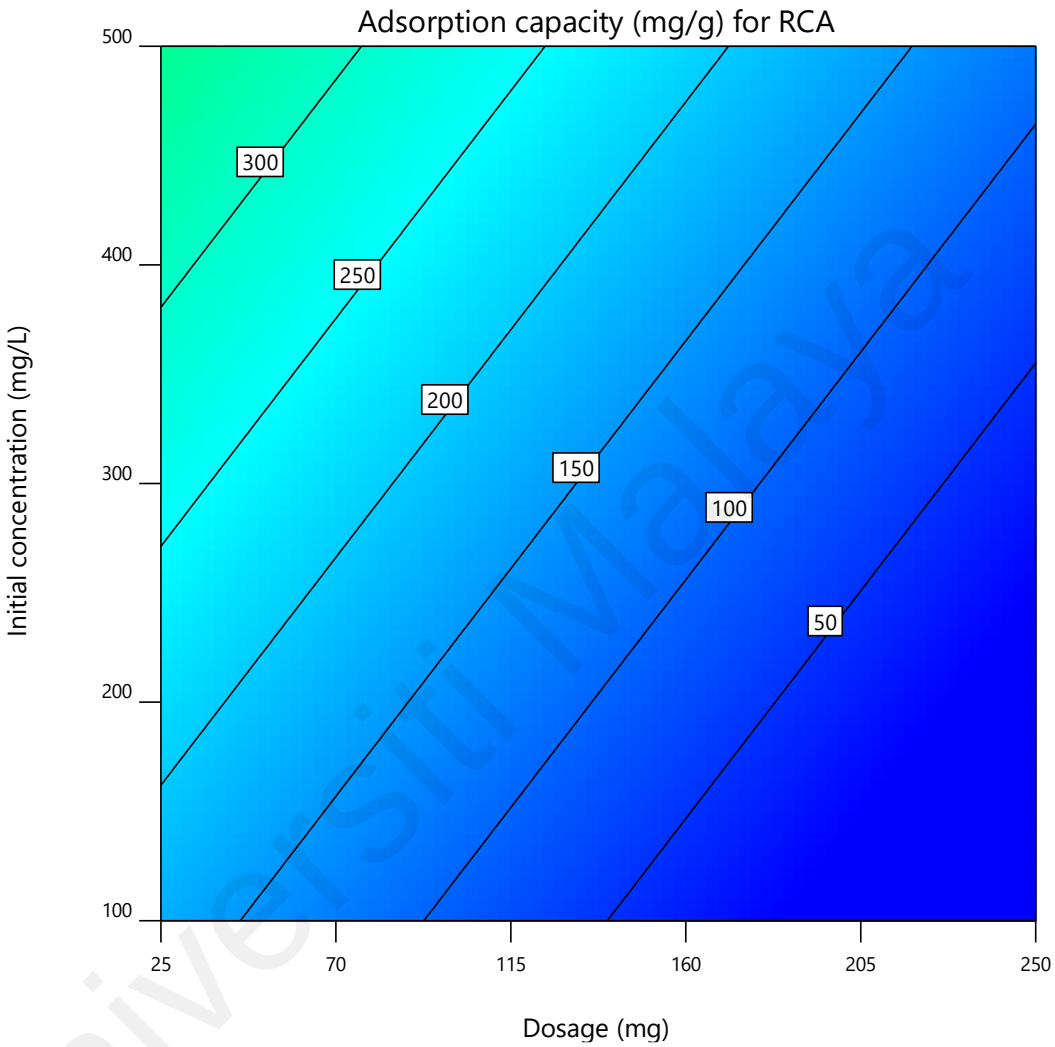

Figure 4.31 : 2D Contour for effect of initial dye concentration against adsorbent dosage on adsorption capacity for RA

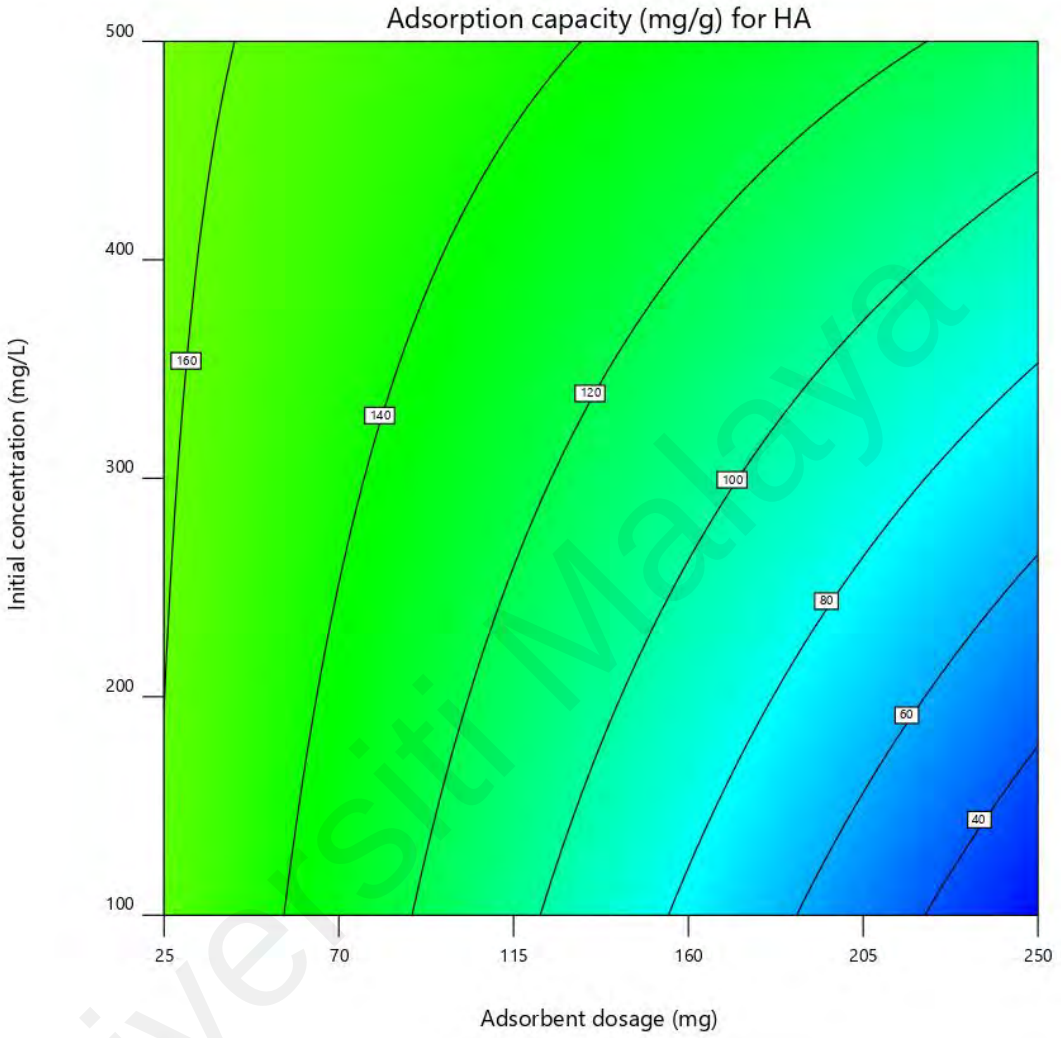

Figure 4.32 : 2D Contour for effect of initial dye concentration against adsorbent dosage on adsorption capacity for HA

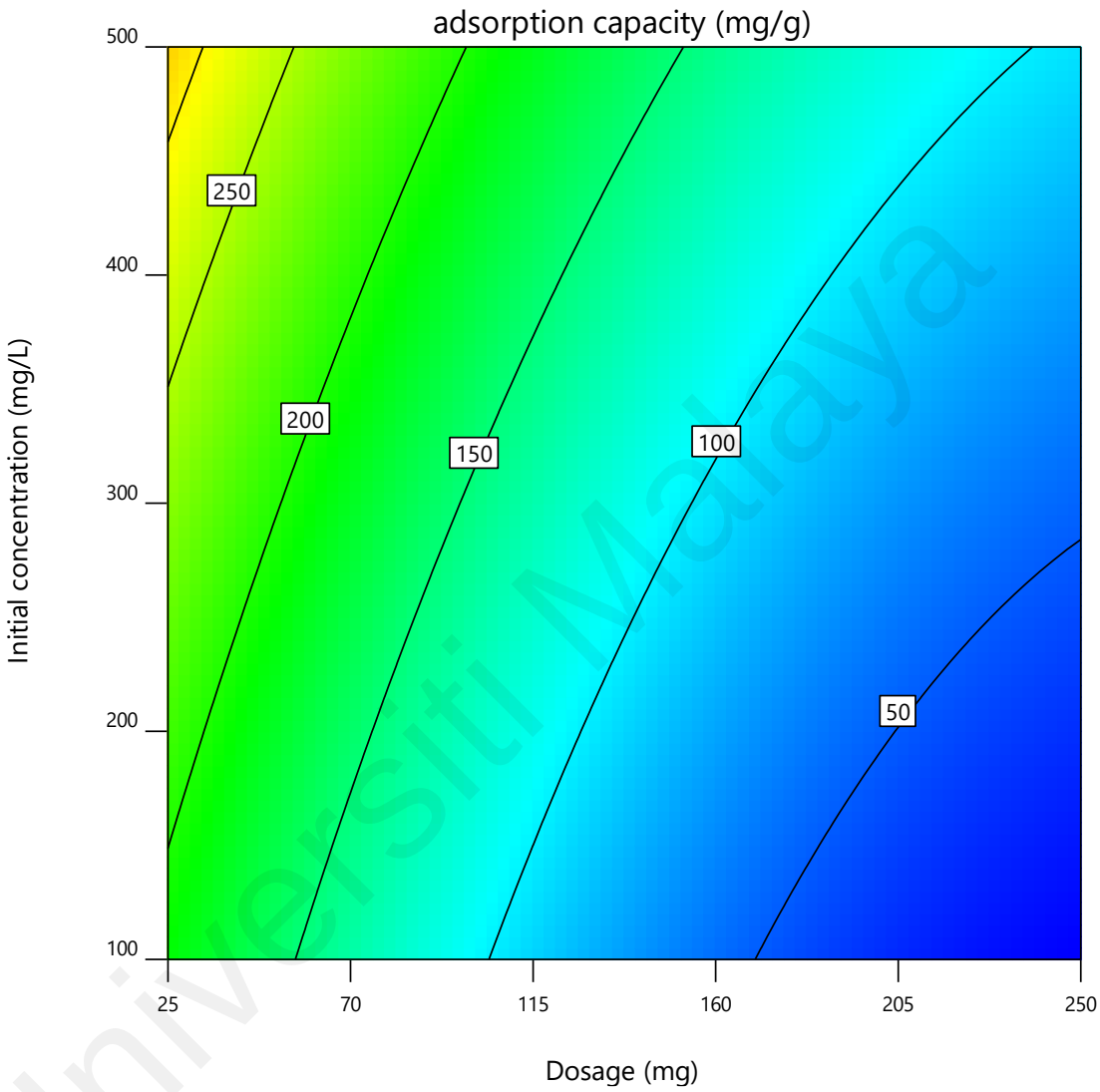

Figure 4.33 : 2D Contour for effect of initial concentration against adsorbent dosage on adsorption capacity for HA/Mn

For HA/Mn, as can be seen in Figure 4.33, using lowest initial concentration of 0.1 g/L, pH of 6, contact time of 95 minutes, an increase in the adsorbent dosage of HA/Mn to 5.0 g/L results in a decrease in adsorption capacity from 186.4 mg/g to 19.93 mg/g. The decrease in adsorption capacity from an increased adsorbent dosage is due to the reduced effective surface area and agglomeration (Batool & Valiyaveettil, 2021). The reduction in adsorption capacity as the adsorbent dosage is increased is in line with the study conducted by Batool et al. (Batool & Valiyaveettil, 2021), which noted a decrease in adsorption capacity from 94 mg/g to 23.4 mg/g as the adsorbent dosage increased. In this study, maximum removal efficiency for HA/Mn is observed at the lower adsorbent dosage of 0.5 g/L to 1.4 g/L, which is lower than most of the recent studies using biochar and hydrochar for cationic dye removal.

In summary, while the three hybrid adsorbents achieve higher colour removal in large adsorbent dosage, higher adsorption capacity was achieved from lower adsorbent dosage. This suggests that increasing the adsorbent dose provides a greater number of active sites for successful adsorption at a fixed dye concentration, while the decrease in adsorption capacity with increased adsorbent dosage is attributed to the reduced effective surface area and agglomeration.

4.4.2.4 Initial dye concentration

*(a) **Colour removal***

The effect of initial dye concentration on the colour removal using RA, HA, and HA/Mn are shown in Figures 4.28, 4.29, and 4.30, respectively. For RA, the colour removal was decreased from 90 % to 83 % when the initial dye concentration increased from 0.1 g/ l to 0.5 g/L using an adsorbent dosage of 250mg. A similar decreasing trend was investigated at an RA dosage of 25 mg, where colour removal decreased from 63 % to 57 % when the dye concentration was increased to 0.5 g/L. The colour removal was

observed to be higher under low initial dye concentration because more active sites are available for the adsorption of dye molecules. For HA, in Figure 4.29, when the concentration was increased from 100 mg/L to 500 mg/L, the colour removal decreased to 35 % at the lowest dosage (25 mg). At 500 mg/L of concentration and 250 mg of HA dosage, the removal was at 100 %, whereas at the lowest concentration (100 mg/L) and lowest adsorbent dosage (25 mg), the removal was recorded as 84%. Furthermore, 100 % removal can be achieved using HA using 0.1 g/L to 0.2 g/L of dye concentration and HA dosage in the range of 200 mg to 250 mg. While the ANOVA analysis indicated the initial concentration of dye to be insignificant for RA in colour removal, it is a significant variable for HA.

In HA/Mn for colour removal, the initial dye concentration is the second most significant operation parameter in this study based on the ANOVA analysis. As can be seen in Figure 4.30, when the concentration increases from 0.1 g/L to 0.5 g/L, the colour removal reduced from 83 % to 60 % when the adsorbent dosage of 25 mg is used. Similarly, when using a maximum adsorbent dosage of 250 mg, the colour removal for a dye solution concentration of 0.5 g/L was only 91.85 %. In contrast, when using a concentration of 0.3 g/L, almost complete colour removal of 99.9 % was achieved. However, when the dye concentration increases, the adsorbents could not provide sufficient active sites for the adsorption of dye molecules, which leads to decreases in colour removal. Besides that, surface complications can occur at high concentrations due to the adsorbents' surface and the dye molecules' interaction, which could affect the diffusion of dye molecules to adsorption sites (Khamwichit et al., 2022)

(b) ***Adsorption capacity***

In figure 4.31, unlike for colour removal, the adsorption capacity for RA is highest when the initial concentration is increased to 500 mg/L with 25 mg of adsorbent dosage.

With the same adsorbent dosage at 100 mg/L concentration, the adsorption capacity was recorded at 172.1 mg/g. When the concentration was increased from 300 mg/L to 500 mg/L at the highest adsorbent dosage of 250 mg, the adsorption capacity increased from 24.4 mg/g to 115.3 mg/g. The highest adsorption capacity for HA is 163. 7 mg/g was recorded at the highest initial concentration of 500 mg/L at 25 mg of adsorbent dosage. Similarly, for adsorption capacity in Figure 4.33 for HA/Mn, when the dye concentrations are lower, there are more active sites available for the dye molecules to be adsorbed. Higher concentrations can hinder adsorption because there are limited active sites and potential surface complications. These findings are consistent with previous studies on dye removal (Batool & Valiyaveettil, 2021; Prabakaran et al., 2022).

In summary, the effect of initial dye concentration on colour removal for RA, HA, and HA/Mn suggests higher colour removal in lower dye concentration. On the other hand, for higher adsorption capacity, higher dye concentration is required. The effect of concentration was similarly reported for dye removal using avocado and banana adsorbents (Dhaouadi et al., 2021; Leite et al., 2018a; Prastuti et al., 2019; Yu et al., 2018)

4.5 Optimization study

The optimization study was conducted using numerical optimization, with each of the operational parameters set to 'in range' and the response for colour removal and adsorption capacity set to 'maximum. ' The RSM model provides optimum values with simulated point prediction values, which was used for the validation of the model. To confirm the validity of the suggested models, verification experiments were conducted using the optimized conditions obtained. Validation experiments achieved 99.9 % colour removal and 199.0 mg/g adsorption capacity, while the numerical optimization predicted 99.4 % colour removal and 185.1 mg/g adsorption capacity. The optimal conditions for achieving

the highest adsorption performance were at a pH of 10, an adsorbent dosage of 0.5 g/L, a dye concentration of 0.1 g/L, and a contact time of 80 minutes.

In addition, the adsorption efficiency of HA/Mn was compared with HA and RA. HA obtained 81.1 % colour removal and 162.2 mg/g adsorption capacity at an initial pH of 10, 0.5 g/L adsorbent dosage, 0.1 g/L dye concentration, and contact time of 90 mins. At the optimum condition of pH 9, the adsorbent dosage of 1.1 g/L, dye concentration of 0.5 g/L, and 180 min of contact time, raw adsorbent resulted in 78.2 % colour removal and 71.1 mg/g adsorption capacity. The optimization study revealed that raw adsorbent requires a higher dosage and more contact time to reach maximum colour removal and adsorption capacity than HA and HA/Mn. Besides, HA/Mn is in line with the biomass-based adsorbents for methylene blue dye removal, as summarized in Table 4.13.

Based on the optimization study, higher adsorption performance can be obtained using HA/Mn, with lesser adsorbent dosage and lower contact time. Thus, HA/Mn is chosen over HA and RA as a potential adsorbent for methylene blue dye removal. Based on the adsorption study and physiochemical characteristics of HA/Mn is chosen as the best hybrid adsorbent dye to the high colour removal of 99.9 %, the adsorption capacity of 199 mg/g, increased porosity, high surface area of 666 m^2/g, additional oxygenated functional groups from acid activation (phosphate group) and metal impregnation (manganese groups). Therefore, HA/Mn was used for model validation for the adsorption kinetics and adsorption isotherms.

Table 4.13 : Biomass-based adsorbents for methylene blue dye removal

Adsorbent	Optimum conditions	Colour removal (%)	Adsorption capacity (mg/g)	Ref.
H_3PO_4 activated papaya peel	Initial pH: 6 Adsorbent dosage: 0.3g/L Dye conc: 0.01g/L Contact time: 90 min	96.2	47.0	(Waghmare et al., 2023)
HCL activated papaya bark	Initial pH: 11 Adsorbent dosage: 2.5g/L Dye conc: 0.10 g/L Contact time: 100 min	81.2	66.7	(Nipa et al., 2023)
Fe_3O_4 activated avocado peel	Initial pH: 8 Adsorbent dosage: 1.0g/L Dye conc: 0.015 Contact time: 120 min	99.5	62.1	(Prabakaran et al., 2022)
Na_2CO_3 activated avocado seed	Initial pH: 10 Adsorbent dosage: 1.0g/L Dye conc: 1.00 g/L	72.0	103.1	(Dhaouadi et al., 2020)
Iron Modified banana peel	Adsorbent dosage: 2.5g/L Dye conc: 0.05 g/L Contact time: 50 min	92.0	28.1	(Cathoglu et al., 2021)
HA/Mn	Initial pH: 10 Adsorbent dosage: 0.5g/L Dye conc: 0.10 g/L Contact time: 80 min	99.9	199.0	This study
HA	Initial pH: 10 Adsorbent dosage: 0.5g/L Dye conc: 0.10 g/L Contact time: 90 min	81.1	162.2	
RA	Initial pH: 9 Adsorbent dosage: 1.1g/L Dye conc: 0.50 g/L Contact time: 180 min	78.2	71.1	

4.5.1 Model validation

For the utilization of HA/Mn in industrial application, a validation study was conducted for COD removal. The effect of operational parameters on the COD removal using HA/Mn is in figure 4.34. When the contact time was increased from 10 min to 180 mins, the COD removal increased from 70 % to 86 %, with an adsorbent dosage of 137.5mg at 300mg/L initial dye concentration at acidic condition. Conversely, when the initial pH is increased, the COD removal increases to 95 % at pH 10 and a contact time of 180 mins. gradual increase of COD removal can be observed till the pH reaches 8 and at a contact time of 140, where COD removal is maximum with 98%. However, a 2 % decrease in COD removal is recorded when the pH is increased from 8 to 10. This aligns with previous studies conducted on COD removal using biomass materials, which reported that when the pH was above the neutral value of >70%, COD removal was achieved, followed by a decrease in the removal efficiency (Atiyah et al., 2024; Detho et al., 2022)

Similarly, in Figure 4.35, it can be observed that the higher COD removal is achieved at the highest adsorbent dosage of 250 mg (5 g/L) at an initial dye concentration between 250 mg/L and 500 mg/L. When the adsorbent dosage is 25 mg and the initial concentration is 100 mg/L, the COD removal is 77 %. It increased to 91% when the dosage is increased from 25 to 250 mg at 100 mg/L dye concentration, pH 6, and contact time of 95 mins. However, when the adsorbent dosage is maintained at 25 mg and when the concentration is increased to 500 mg/L, the COD removal gradually decreases, achieving just 47%. Complete COD removal can be achieved at higher concentrations and higher adsorbent dosage.

In conclusion, HA/Mn has efficient COD removal, which can be used for the industrial application. For higher COD removal, HA/Mn works best under alkaline conditions, at lower initial concentrations, and when in contact for around 120 mins. these results are in line with the adsorption performance of HA/Mn for colour removal and adsorption capacity. Thus, HA/Mn has the potential to remove COD from wastewater with a large amount of adsorbent dosage, increasing the active binding site.

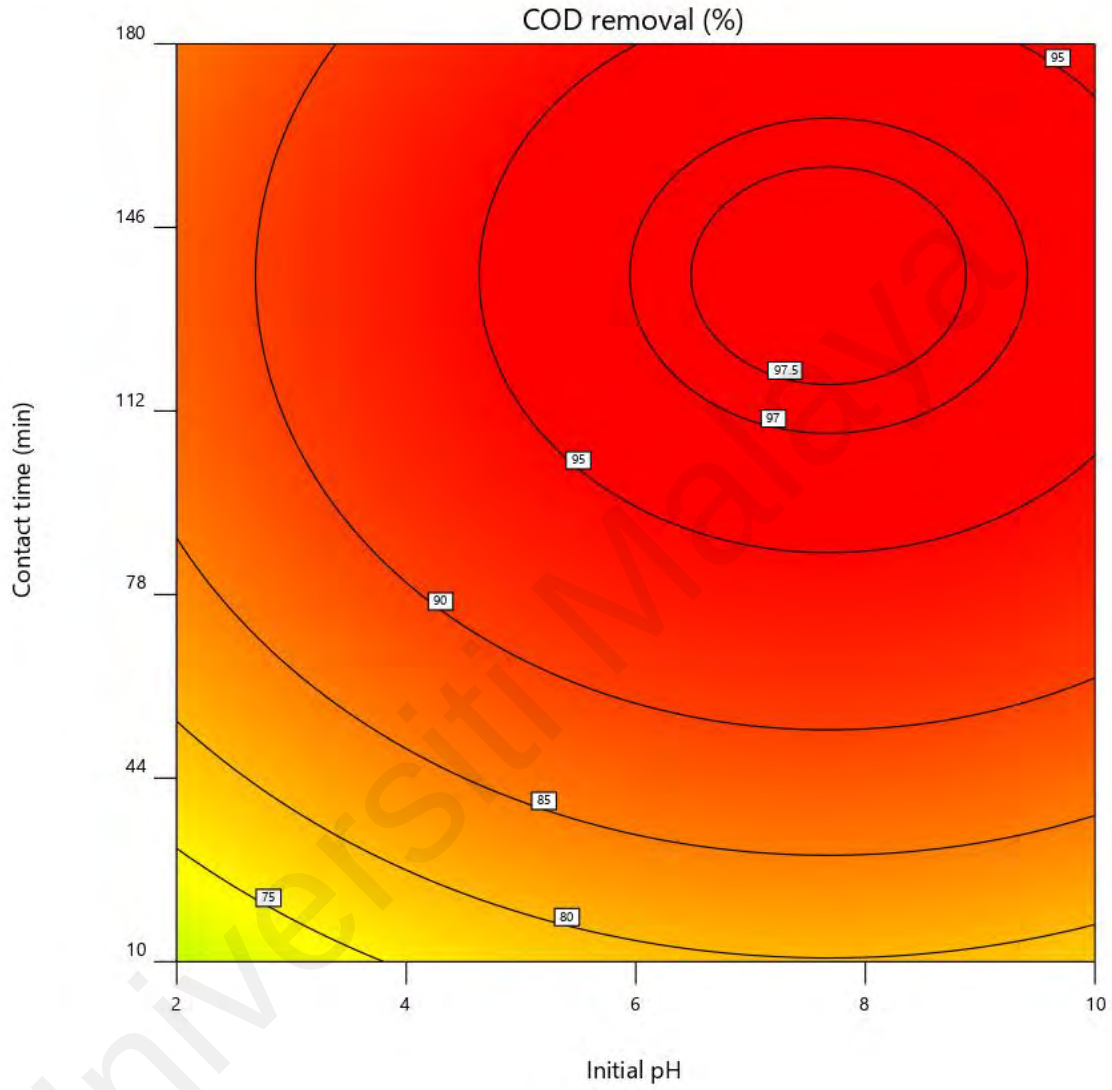

Figure 4.34 : 2D Contour for effect of contact time against initial pH on COD removal for HA/Mn

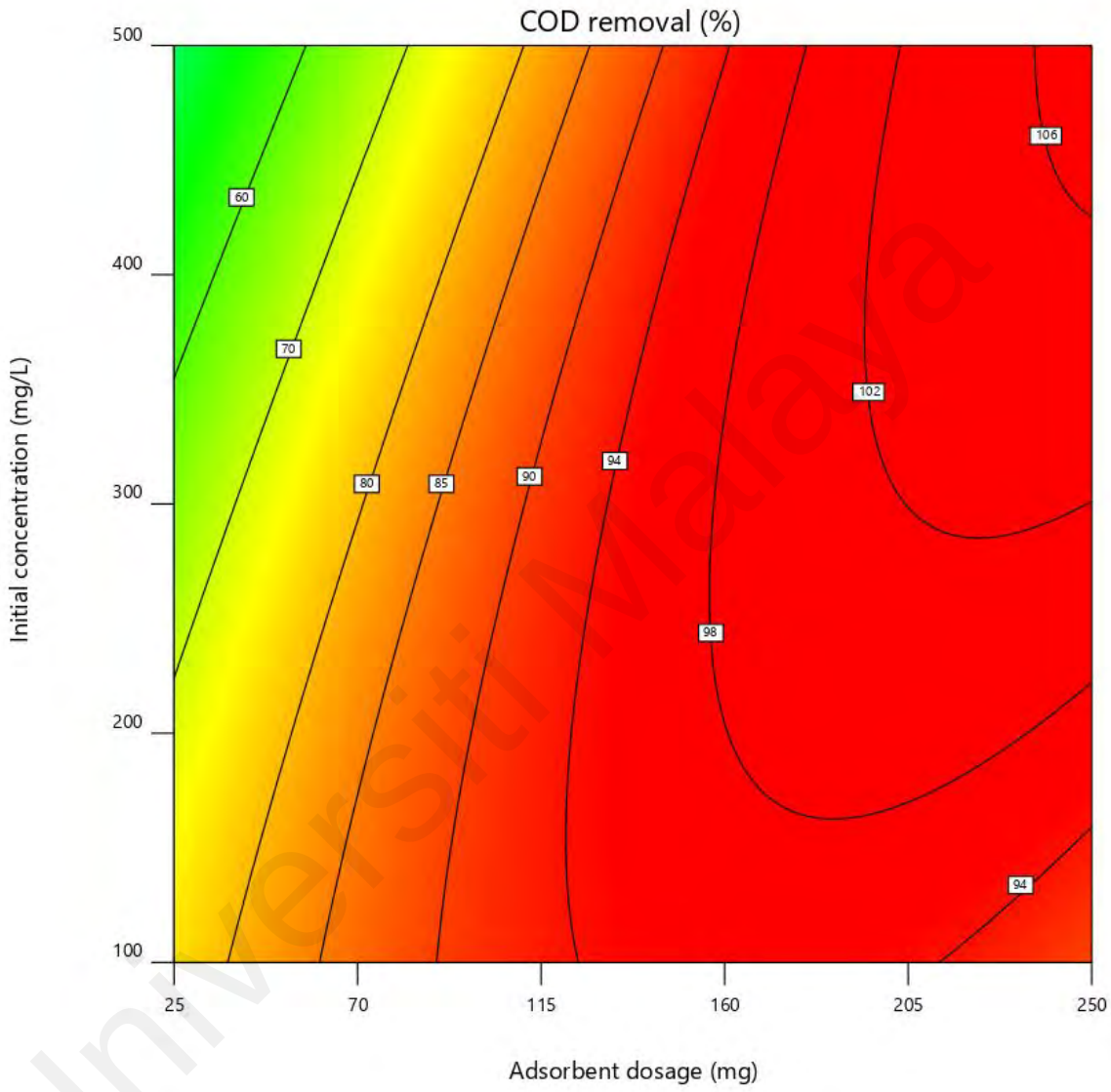

Figure 4.35 : 2D Contour for effect of initial dye concentration against adsorbent dosage on colour removal for RA

4.6 Modelling and prediction using machine learning

The prediction of methylene dye removal using HA/Mn was evaluated using the experimental data set. The prediction evaluation of removal efficiency utilized the Random Forest machine learning algorithm within Visual Studio Code, using Python (version 3.11.5). Random Forest, a widely used supervised learning method, is versatile in handling both regression and classification tasks with labelled target variables.

4.6.1 Random forest regression model analysis

The experimental data from DOE, including adsorbent dosage, pH, concentration, and contact time, were input variables to train the machine learning model, while the model outputs the COD removal, colour removal, and adsorption capacity as performance parameters. Two regression models were used to test the efficacy of the models. Assessing the efficacy of the model relies on evaluating MSE and R^2 values. The data from the experimental design for HA/Mn in Table 4.9 are utilized to train the RF ML model. Pandas, NumPy, Sklearn, and Random Forest Regressor modules from Python libraries are imported to create the RF regression model and evaluate the performance of the model. The module Pandas is utilized to load the data in a 2D array format and has various functions to analyse the model. The NumPy module can perform efficient computation tasks in a short time. The module Sklearn is utilized for data pre-processing in model development and evaluation. The "RandomForestRegressor" is the main regression model utilized for the ensemble learning in this article.

For the regression model, the recommended setting for the number of randomly selected predictors to choose from at each split for mtry ('k') is one-third of the number of predictors. For the classification model, the recommended setting mtry ('k') is the square root of the number of predictors. Another important tuning hyper-parameter is the decision trees' depth. Higher depth can result in overfitting to the training data but also

less correlation. It may improve the performance of the ensemble learning. Effective depth is in the range of 1 to 10. In this article, since the number of input features is only 4, the default setting by Python is adequate to create the efficient model.

In Table 4.14, where n estimators are 100 and max features are 6, the model with 20% data shows the highest R^2 value of 0.9671. The low value in the iterations is due to the randomness of the Bootstrapping in addition to the low available data sets of 30. It is in line with previous studies for cationic dye removal. In the study conducted by Kooh and others (2022), the modelling of malachite green dye adsorption using jackfruit seed exhibited high accuracy, with a reported predicted R^2 value of 0.986 (Kooh et al., 2022). Bootstrapping randomly performs row sampling and feature sampling from the dataset, forming sample datasets for every model. When the test data is increased to 30 %, there are improvements in the values of the R^2 test and the MSE test. However, there are decrements in the values of R^2 train and MSE train. This is due to the huge variance in the data set run numbers 2, 3, 8, 10, 16, 21, and 29 from the HA/Mn experimental dataset. The highest value of mean squared error, 8.0956, means that the predicted data of that specific model has 8 value differences from actual experimental data. This happens when the high variance data set is selected randomly in some iteration. Thus, the RF 20% is chosen as the regression model with a higher R^2 value of 0.9671.

Table 4.14 : Performance of the random forest regression model

	20% Test Data		**30% Test Data**	
	1st It	2nd It	1st It	2nd It
R^2 Train	0.9671	0.9189	0.9572	0.9517
R^2 Test	0.8511	0.4508	0.7023	0.7850
MSE Train	0.5497	0.5841	0.6979	1.2434
MSE Test	8.0956	7.8081	2.4520	1.1012

4.6.2 Validation of RF 20% regression model

RF 20% model validation considers various scores, including the bag score or OOB (out-of-bag) score, essential for validating the bagging algorithm. This score involves extracting a small portion of the validation data from the main dataset, making predictions on this subset, and comparing the results. The actual performance of the bagging algorithm is reflected by the true outcomes of the OOB score, set as True in the random forest regression model. As depicted in Table 4.15, the OOB score for raw data is 0.4652, while for clean data, it improves significantly to 0.8862. Enhancing the model's efficiency involves critical steps, such as data processing to remove high variance data sets. It is crucial in RF modelling to address anomalies and missing data points, which significantly impacting model performance due to overfitting and underfitting. Here, adequate dataset numbers and a simple RF algorithm are employed to mitigate these issues. For effective model training, accurate input variables representing fundamental factors influencing the target variable are utilized. During data preprocessing, features are precisely scaled, and no missing or noisy data exists. Consequently, the RF 20% model validates the RSM-CCD experimental dataset with an accuracy rate ranging from 70% to 90%.

Table 4.15 : OOB Score for clean data and raw data

	Clean Data	**Raw Data**
R^2 Train	0.9859	0.9126
R^2 Test	0.9981	0.7935
MSE Train	0.0010	1.0345
MSE Test	0.0001	0.6894
OOB Score	0.8862	0.4652

4.6.3 Predictive accuracy of Design-Expert and machine learning models

The significance of the Design-Expert, RSM-CCD model for COD removal, colour removal, and adsorption capacity have a coefficient of determination, R^2 value of 0.9676 (COD removal, 0.9717 (colour removal), and 0.9564 (adsorption capacity). Meanwhile, a higher R^2 value of 0.9981 can be observed for the Machine Learning, RF 20% model for the removal efficiency combining the three output parameters. The RSM-CCD prediction value is lower than the RF 20% value, suggesting that the RF 20% provides high accuracy in predicting the experimental results for HA/Mn dye removal (Fathalian et al., 2022). The RSM-CCD model provides predictions for identified parameters and generates an equation for the relationship between the input variables and outputs (Ahmad et al., 2024), whereas machine learning RF models can be used to predict the outcomes for any specific input value or combination of varied input and output values (Waqas et al., 2024). The RSM-CCD model has limitations, such as its inability to generate predictions for multiple variables or operational parameters using an output value for prediction. In contrast, the RF model allows predictions to be generated for multiple variables in both input and output values, providing greater flexibility and scope for prediction. The RSM-CCD model, along with ANOVA analysis, can preprocess the data by removing insignificant variables for the RF model. For example, in this study, significant independent variables such as adsorbent dosage and concentration of the dye solution can serve as input values for the RF model while maintaining constant levels of initial pH of the solution and contact time at their optimum values. However, the four variables that were used to design and evaluate the adsorption study using RSM-CCD were utilized in the RF model to maintain a uniform basis for both regression models using Design-Expert and Machine Learning.

Furthermore, for a comparative predictive study, five experiments predictions were selected from RSM-CCD simulated data generated using the experimental data for

HA/Mn. The five predictions from RSM-CCD were used for the RF 20% model as well to see the accuracy of the models as presented in Table 4.16. COD removal of HA/Mn for methylene blue dye removal had an accuracy of 99.4 % using RSM-CCD prediction while RF 20% had an accuracy of 99.7%. Though the prediction for the COD removal is very similar with just a 0.3 % difference, the comparative study revealed that the RF 20% model exhibited better accuracy at 99.2% compared to RSM, which had an accuracy of 98.1% for colour removal. Furthermore, the adsorption capacity demonstrates that the 20% RF model achieved the highest accuracy, with a prediction accuracy of 97.4%, followed by 94.8% for RSM. Consequently, the RF 20% model surpasses the RSM-CCD model in predicting data sets by 0.3% for COD removal, 1.1% for colour removal, and 4.3% for adsorption capacity.

In summary, the RF models developed in this study could reduce the time and cost of screening tests for different adsorbents used in various scenarios for dye removal, thus promoting cost-effective and cleaner production for sustainability. The initial experimental data set can be accurately evaluated and used to assess the significance of independent variables using RSM-CCD. Additionally, combining the RSM and RF models can improve predictability by eliminating insignificant variables. The dataset assessed with RSM-CCD can train and validate the machine learning RF regression models. Hence, the ML model, RF 20%, can be employed to predict efficiency more accurately compared to the RSM model. Furthermore, the developed regression model can be used to predict methylene dye removal using other adsorbents with similar physiochemical characteristics.

Table 4.16 : Prediction vs actual for HA/Mn

COD removal accuracy using HA/Mn			
No.	Actual (%)	RSM Prediction (%)	RF 20% Prediction (%)
1	92.3	94.9	94.8
2	89.4	97.8	93.4
3	93.8	96.3	94.3
4	95.2	97.1	92.8
5	89.1	95.9	95.6
Accuracy		**99.4 %**	**99.7 %**
Colour removal accuracy using HA/Mn			
No.	Actual (%)	RSM Prediction (%)	RF 20% Prediction (%)
1	98.3	97.2	99.4
2	99.4	100	99.3
3	97.8	97.7	97.9
4	98.6	97.9	95.2
5	95.8	94.1	95.6
Accuracy		**98.1 %**	**99.2 %**
Adsorption capacity accuracy using HA/Mn			
No.	Actual (mg/g)	RSM Prediction (mg/g)	RF 20% Prediction (mg/g)
1	196.6	194.2	181.6
2	159.9	198.2	172.1
3	195.5	199.0	197.4
4	197.3	197.7	188.3
5	191.6	185.2	188.2
Accuracy		**93.1 %**	**97.4 %**

4.6.4 Scale-up prediction RF 20% model validation

For the industrial application of the HA/Mn, a scale-up prediction was conducted using the RF 20 % model. For the scale-up prediction data collection, the initial pH, dye concentration, and contact time were kept constant at the optimized level of pH 10, concentration of 0.1 g/L, and contact time of 80 mins. The adsorbent dosage of HA/Mn and the volume of the solution varied from 1L to 5L. The predictions in Table 4.17 indicated that the volume of the solution used has no effect on the adsorption performance as the adsorption for 3L and 5L have significantly similar results. The validation of the predictions was determined by validation experiments under the same operation condition. The results of validation experiments for the selected predictions are summarized in Table 4.17 for fixed operation conditions of initial pH 10, contact time of 80 min, initial concentration of 0.1 g/L, and adsorbent dosage of 0.5 g/L. In summary, HA/Mn can potentially be used for dye removal in industrial applications. The predictions for dye removal using HA/Mn indicate >85% COD removal, >99% colour removal, and >100mg/g adsorption capacity.

Table 4.17 : Scale-up predictions vs actual for HA/Mn

	COD removal (%)		**Colour removal (%)**		**Adsorption capacity (mg/g)**	
Volume	**Prediction**	**actual**	**Prediction**	**actual**	**Prediction**	**actual**
3 L	99.8	99.9	99.5	99.5	86.2	86.1
5 L	99.9	86.1	100.0	99.9	86.1	89.5

4.7 Adsorption isotherms

Adsorption isotherms describe the interaction between the adsorbent and adsorbate, determining how adsorbate molecules distribute between the solid and liquid phases at equilibrium. Selecting an appropriate isotherm model is crucial for optimizing adsorbent utilization and designing effective adsorption systems. In this study, four non-linear isotherm models were applied to fit the HA/Mn experimental data: the two-parameter models of Temkin (1930), Freundlich (1906), and Langmuir (1918), and the three-parameter Redlich-Peterson model (1959).

The Freundlich isotherm is an empirical model that assumes a heterogeneous surface with a non-uniform distribution of adsorption heat. It describes multilayer adsorption and suggests that stronger binding sites are occupied first (Longchar et al., 2024). The model effectively captured the HA/Mn adsorption behaviour, achieving an R^2 value of 0.9200. The Freundlich constant, denoted by n = 10.35 (greater than 1), indicates a favourable adsorption process. The model provided a better fit than Langmuir, which had a lower R^2 value of 0.8988. The Langmuir isotherm assumes a homogeneous surface with uniform binding energies and monolayer adsorption. The model predicted a maximum adsorption capacity of 257 mg/g for MB dye removal. However, its lower value suggests that the adsorption process in HA/Mn leans more toward heterogeneous adsorption. Besides, the Temkin isotherm accounts for adsorbate-adsorbent interactions, assuming a linear decrease in adsorption heat with surface coverage. With an R^2 value of 0.9389, it highlights the significance of adsorption energy variations during the process. This model accurately describes adsorption by accounting for surface heterogeneity and interaction forces like van der Waals, especially in the early stages and under temperature effects (Al-Ahmed, 2024).

Among the four models, the Redlich-Peterson isotherm achieved the highest R^2 value (0.9529), followed by Temkin (0.9389), Freundlich (0.9200), and Langmuir (0.8988). These results suggest that HA/Mn exhibits both homogeneous and heterogeneous adsorption behaviour. The Redlich-Peterson model is a hybrid of the Langmuir and Freundlich models, adapting to different adsorption conditions (Munonde et al., 2023). The exponent β (ranging from 0 to 1) determines the model's behaviour. When β = 0, it follows Freundlich (heterogeneous adsorption), and when β = 1, the model follows Langmuir (homogeneous adsorption). Hence, it can be applied for either homogeneous or heterogeneous systems and may be used as a compromise between Langmuir and Freundlich models. For HA/Mn, β = 0.9412, indicating a predominantly homogeneous adsorption process. It indicates uniform, homogeneous adsorption sites on the mesoporous surface, where adsorption ceases once all active sites are occupied (Khan et al., 2023a).

Table 4.18: HA/Mn Adsorption isotherm study

Isotherm model	**Parameters**	**HA/Mn**
Langmuir	R^2	0.8988
	q_m (mg/g)	257.51
	K_l	14.65
Freundlich	R^2	0.9200
	K_f	184.09
	n	10.35
Temkin	R^2	0.9389
	AT	1.9513
	B	0.0945
Redlich-Peterson	R^2	0.9529
	β	0.9412
	αr	32.29

Overall, the results confirm that HA/Mn adsorption follows the Redlich-Peterson isotherm with predominantly homogeneous adsorption behaviour. This aligns with previous studies, such as Zhu et al. (2016), which found a similar trend using avocado seed adsorbents. The isotherm curves obtained for the HA/Mn are illustrated in Figure 4.36, further confirming the best-fitting model to be the Redlich-Peterson isotherm, confirming that the adsorption mechanism involves both homogeneous and heterogeneous characteristics. Moreover, from Figure 4.36, the maximum adsorption capacity is around 250-260 mg/g. This suggests that HA/Mn is an effective adsorbent for dye removal with strong adsorption properties.

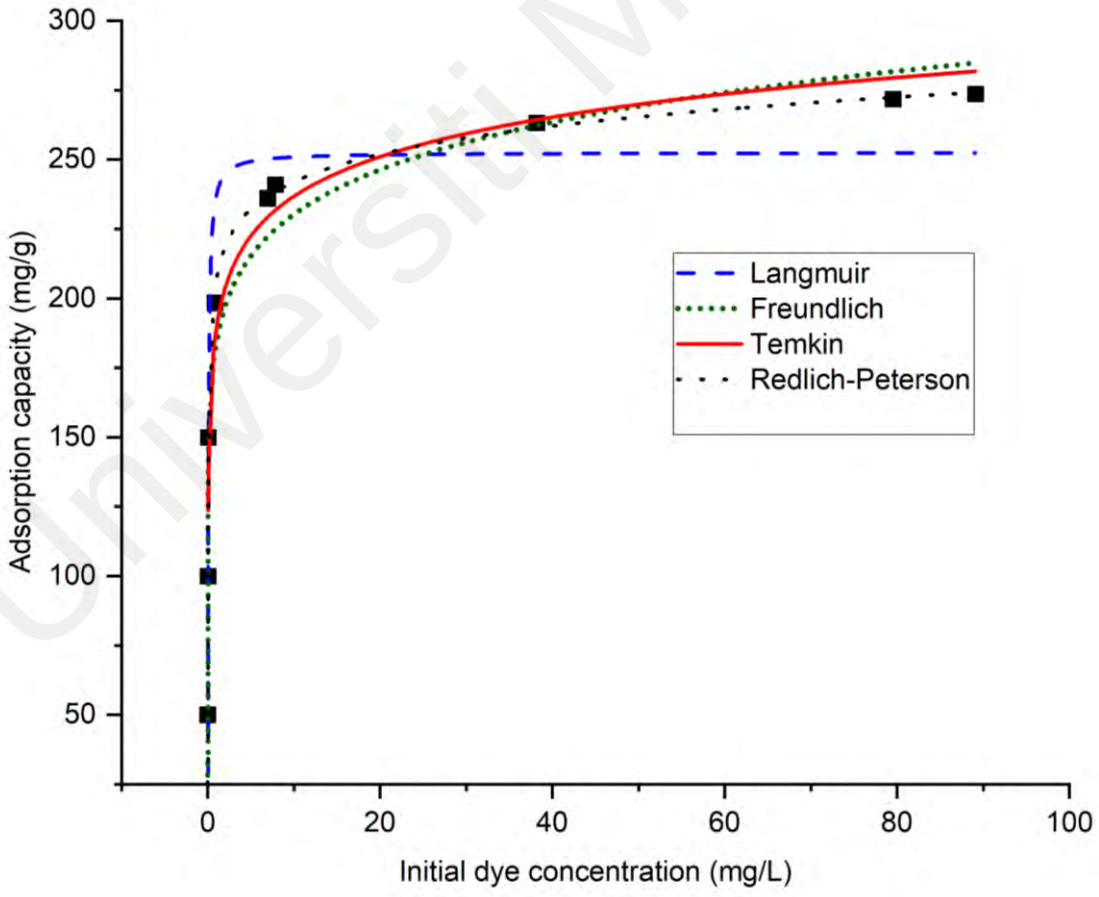

Figure 4.36 : Nonlinear plot of isotherm models

4.8 Adsorption kinetics

The adsorption kinetics of HA/Mn for MB dye removal were analysed using three non-linear kinetic models: Pseudo-First-Order, Pseudo-Second-Order, and Elovich under optimum conditions. Kinetic studies provide valuable insights into reaction pathways and adsorption mechanisms, helping to determine the dominant adsorption process (Mukkanti & Tembhurkar, 2021).

To identify the best-fitting model, correlation coefficients (R^2) were calculated, and the non-linear plots of all kinetic models are shown in Figure 4.37, while detailed results are presented in Table 4.19. The kinetic plots indicate that adsorption equilibrium is reached between 60 and 80 minutes, aligning with the optimum contact time for maximum adsorption at 80 minutes. The rapid initial adsorption phase suggests abundant active sites, but as these sites become occupied, the adsorption rate slows down until equilibrium is achieved (Tshemese et al., 2021).

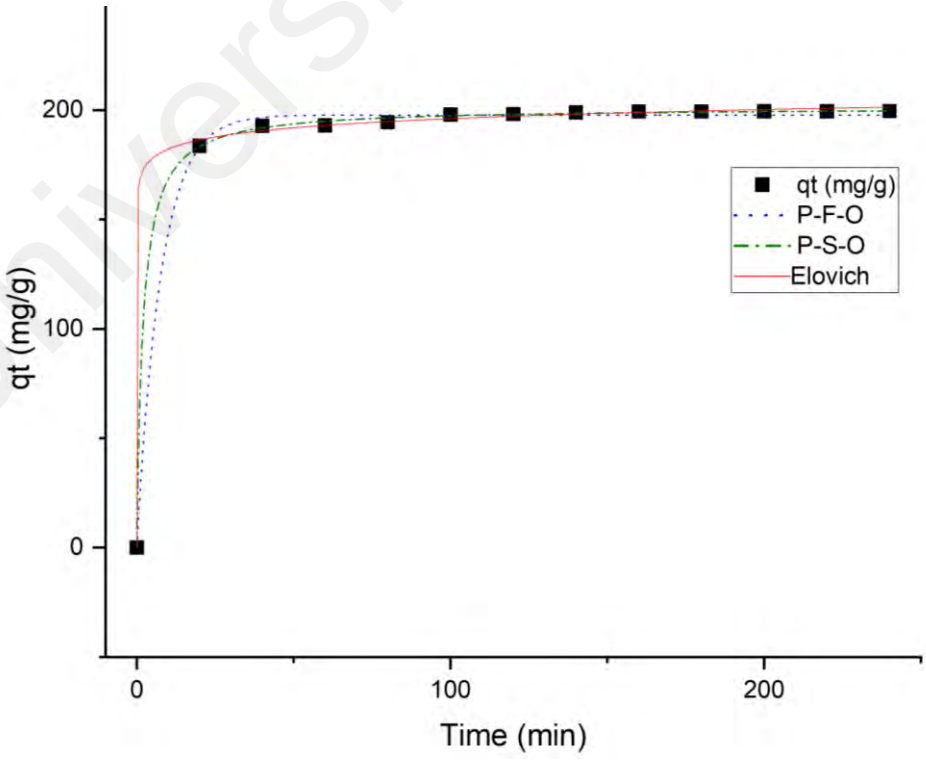

Figure 4.37 : Nonlinear plots of kinetic models

Among the models, the Pseudo-Second-Order model provides the best fit, closely following the experimental data points. This suggests that the adsorption process is primarily chemisorption, involving physiochemical interactions between HA/Mn and MB dye molecules (Rajoriya et al., 2021). Additionally, from the calculations in Table 4.19, the Pseudo-Second-Order model exhibits the highest R^2 value for HA/Mn, which is 0.9997, followed by Elovich (R^2 value of 0.9993) and pseudo-first order (R^2 value of 0.9982). Conversely, Table 4.19 also shows strong agreement between the experimental and the predicted adsorption capacity at equilibrium.

Table 4.19 : HA/Mn Adsorption kinetics study

Kinetics model	**Parameters**	**HA/Mn**
Pseudo-First-Order	K_1	0.1299
	q_e (Predicted)	197.61 mg/g
	q_e (Experimental)	199.49 mg/g
	R^2	0.9982
Pseudo-Second-Order	K_2	0.0026
	q_e (Predicted)	201.13 mg/g
	q_e (Experimental)	199.49 mg/g
	R^2	0.9997
Elovich	α	8.8891
	β	0.1665
	R^2	0.9993

These results are in line with previous studies where it follows the pseudo-second order of kinetics for cationic dye removal using avocado (Ukpong et al., 2023) and banana adsorbents (Rose et al., 2023). Additionally, the pseudo-second-order model further supports the idea that methylene blue adsorption onto HA/Mn involves a two-body

interaction, meaning adsorption depends on both the available adsorption sites and the number of dye molecules in the system(Watwe et al., 2023). In summary, HA/Mn exhibits both physisorption and chemisorption mechanisms. However, based on the non-linear plots and kinetic model calculations, chemisorption is the dominant adsorption mechanism in MB dye removal.

4.9 Adsorption mechanism

The adsorption mechanism of MB dye onto HA/Mn, illustrated in Figure 4.38 and the FTIR conducted after the adsorption process, as shown in Figure 4.38. The Pseudo-Second-Order model provided the best fit, indicating that the adsorption rate is dominated by chemisorption. The strong correlation with the Freundlich and Temkin isotherms suggests that adsorption occurs on both homogeneous and heterogeneous surfaces. Additionally, the high R^2 value (0.9529) for the Redlich-Peterson isotherm confirms this dual nature. However, the β value close to 1 in the Redlich-Peterson model indicates a predominantly homogeneous adsorption surface with some heterogeneity, likely due to surface modifications from manganese oxide impregnation.

As shown in Figure 4.38, chemisorption occurs via electrostatic attraction between the negatively charged functional groups, such as carboxyl and phosphate in HA/Mn, and the positively charged N^+ sites of MB dye ($C_{16}H_{18}N_3S$), facilitating ion-exchange interactions (Du et al., 2022). The optimum pH level of 10 for HA/Mn enhances adsorption efficiency after protonation as the HA/Mn surface gains a tendency to attract positively charged adsorbate ions in the solution through electrostatic forces (Qu et al., 2023). Additionally, hydrogen bonding between hydroxyl, amine, and carbonyl groups in HA/Mn and heteroatoms (N and S) in MB dye further stabilizes adsorption. The presence of manganese oxide (Mn–O) sites also enables surface complexation, providing additional binding sites and enhancing adsorption stability for MB dye removal (Wan et al., 2018).

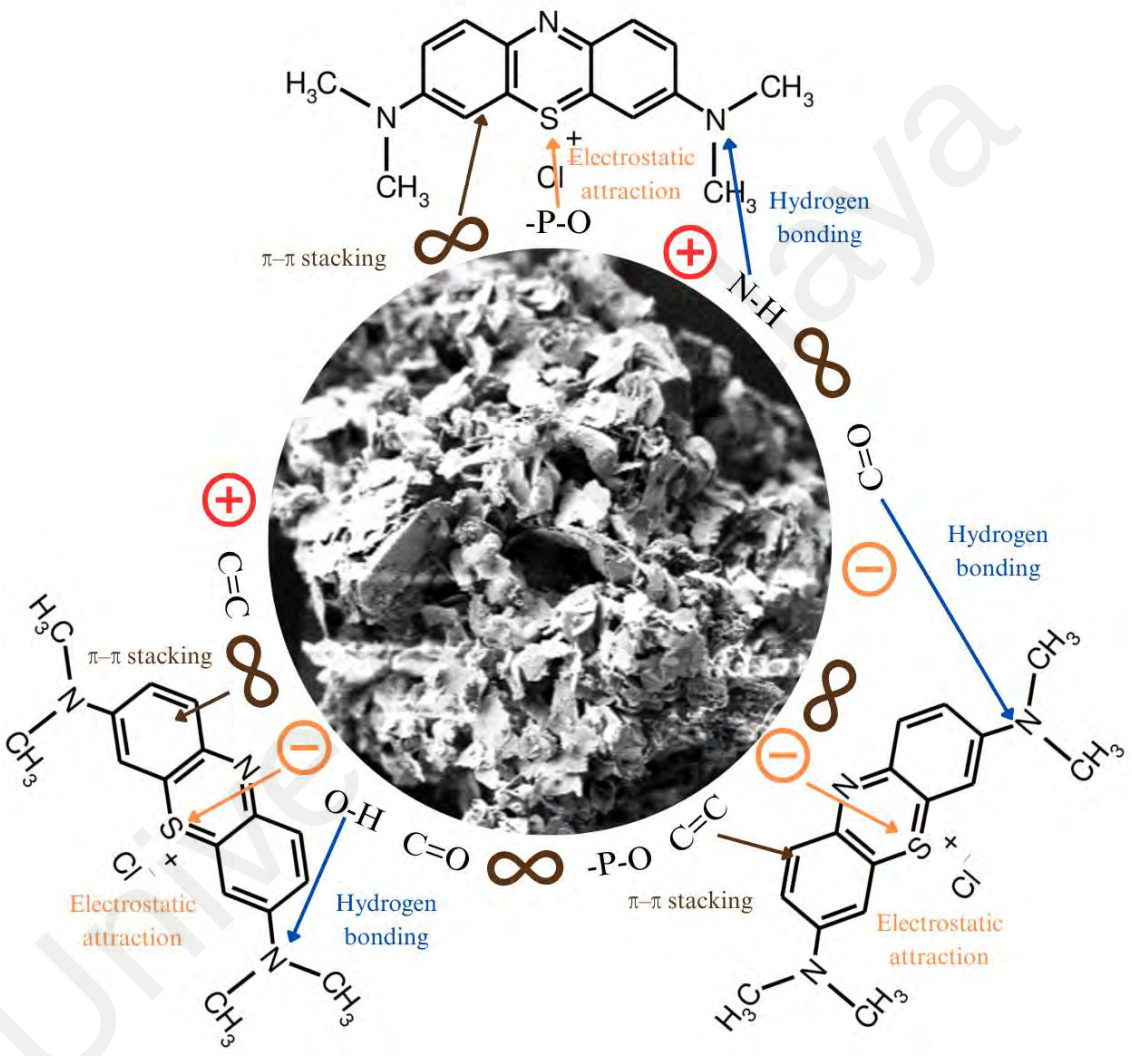

Figure 4.38 : Adsorption mechanism of MB dye onto HA/Mn

Beyond chemisorption, physisorption also plays a role through π–π interactions, where the aromatic rings of MB dye stack onto the aromatic structures in HA/Mn (Liu et al., 2025). The electrostatic attraction, hydrogen bonding, and the π–π interactions between the MB dye and the HA/Mn are further supported by the FTIR conducted after the adsorption process.

FTIR analysis before and after adsorption in Figure 4.39 confirms successful MB dye binding. The decrease in peak intensity for carboxyl between 1000–1300 cm^{-1} suggests successful hydrogen bonding of MB. It also reduced the free C–O availability, showing a decreased peak intensity. The slightly lower hydroxyl peak at 3200–3600 cm^{-1} and fluctuation in amine peaks at 3300–3500 cm^{-1} further confirm hydrogen bonding (T. Ahmad & M. Danish, 2022). Additionally, an increase in C–N peak intensity from 1200 cm^{-1} to 1350 cm^{-1} supports the electrostatic attraction between cationic MB dye and negatively charged HA/Mn sites.

The new S=O and C-S peak, from $-SO_3$ in MB dye, reflects electrostatic interactions, while a shift in C–O peaks (1000–1300 cm^{-1}) and an increase in C=C peak intensity (1400–1600 cm^{-1}) confirm π–π interactions between the π electrons of aromatic structure of the HA/Mn (Zhao et al., 2017). In summary, the adsorption of MB dye onto HA/Mn is predominantly driven by chemisorption mechanisms, with electrostatic attraction and hydrogen bonding as the main contributors. Additionally, physisorption through π–π stacking provides further contributions to the adsorption process. This combination of mechanisms ensures high adsorption efficiency and strong dye removal, making HA/Mn an effective adsorbent for cationic dyes like MB dye.

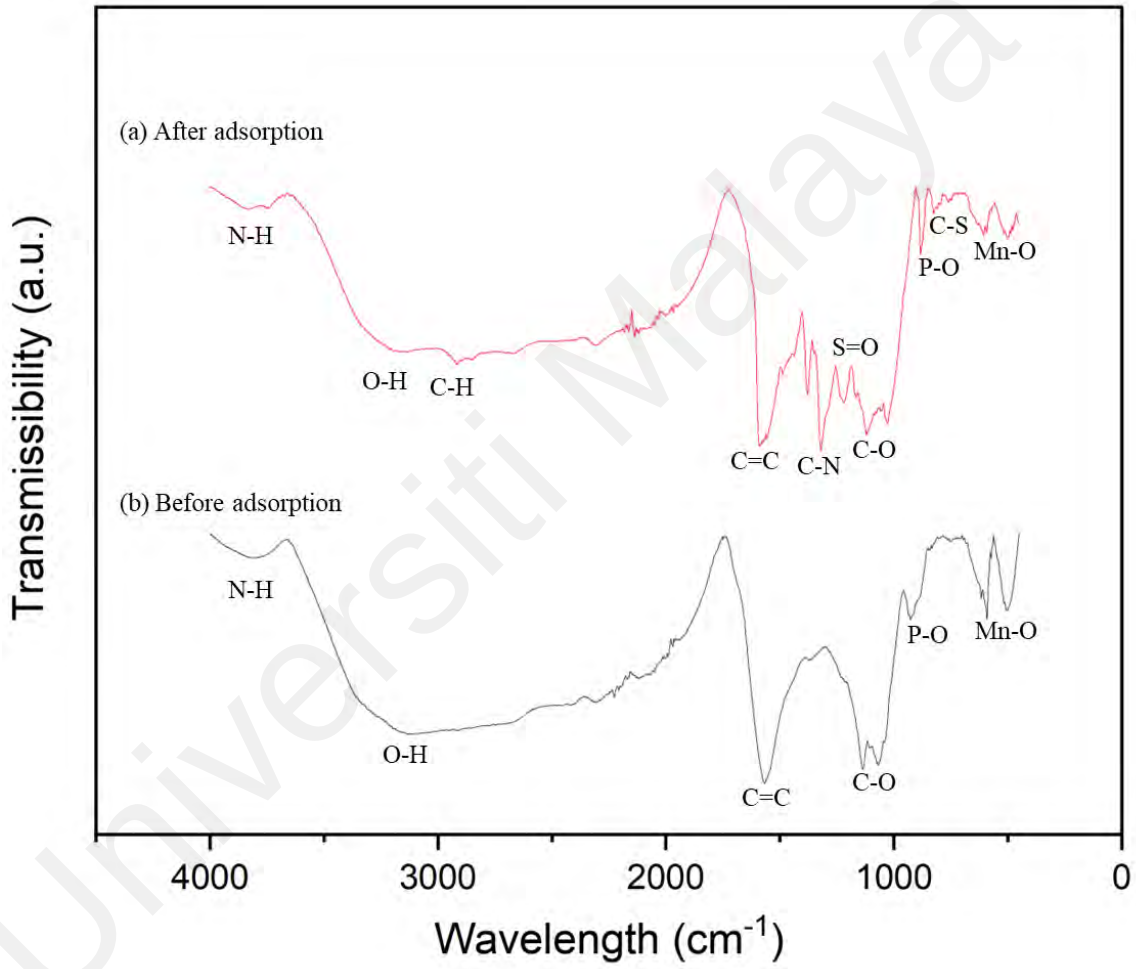

Figure 4.39 : FTIR spectra before and after the adsorption process

4.10 Economic evaluation

The economic evaluation of an adsorbent is essential for assessing its feasibility and commercial viability in industrial applications. Biomass-based adsorbents offer both economic and environmental benefits, making their cost-effectiveness a key factor in large-scale implementation. A critical aspect of economic evaluation is the regeneration study, which determines the reusability of the adsorbent, especially crucial for industries that generate millions of litres of wastewater daily. Additionally, assessing raw material costs, synthesis expenses, and overall production costs provides valuable insights into the feasibility of an adsorbent. This study evaluates the economic viability of the metal-impregnated hybrid adsorbent (HA/Mn) through a ten-cycle regeneration study, followed by a detailed cost analysis. Finally, the adsorbent's effectiveness was tested in real wastewater treatment applications to validate its practical industrial feasibility.

4.10.1 Regeneration study

The regeneration study evaluates the reusability of HA/Mn to minimize process costs and reduce the need for continuous adsorbent replenishment. Regeneration consists of two key stages: desorption, which removes adsorbed pollutants, and regeneration, which restores the adsorbent’s effectiveness for reuse. Effective regeneration directly influences the total cost of the adsorption process and waste generation (Skwierawska et al., 2022).

Successful desorption depends on the method used and the mechanical stability of the adsorbent. Industrial applications often favour weak solvents like ethanol and methanol due to their low boiling points and cost-effectiveness. Moreover, acidic solutions are commonly used as eluents to desorb cationic substances. Their acidic nature protonates the adsorbent surface, diminishing the electrostatic attraction between the cationic methylene blue molecules and the adsorbent (Chaima et al., 2024). Desorption not only

recovers contaminants but also prolongs the adsorbent's usability, making it a critical factor in industrial feasibility.

A ten-cycle regeneration study was conducted to assess HA/Mn's reusability. The first cycle was performed under optimum conditions, followed by desorption using 50 mL sulfuric acid and 50 mL ethanol. The adsorbents were then filtered, rinsed with distilled water, and oven-dried before reuse. As shown in Figure 4.38, HA/Mn exhibited an initial colour removal efficiency of 99.8%, while commercial activated carbon (COM-AC) achieved 98.0%. Over ten cycles, HA/Mn maintained 91.5% colour removal, demonstrating strong reusability. In contrast, COM-AC showed a steep decline, with removal efficiency dropping below 80% by the 3rd cycle and reaching only 34.5% by the 10th cycle.

The decline in adsorption at the end of the 10th cycle can be attributed to a combination of factors. The MB dye saturation on the HA/Mn adsorbent after continuous usage has reduced the available active sites (Telli et al., 2024). Additionally, the adsorbed MB molecules have partially formed permanent chemical bonds with the inner porous surface, which ethanol and sulfuric acid were unable to completely breakdown (Wang et al., 2024). Another significant factor is the structural degradation of HA/Mn over repeated adsorption-desorption cycles. The continuous exposure to acidic and thermal conditions may alter the porosity and mechanical integrity of the adsorbent, leading to a gradual loss of adsorption capacity. Furthermore, pore blockage caused by residual dye molecules or impurities from the desorption process may reduce the available surface area for adsorption (Chaima et al., 2024). These combined effects explain why HA/Mn maintained high efficiency for multiple cycles but showed a gradual decline by the 10th cycle.

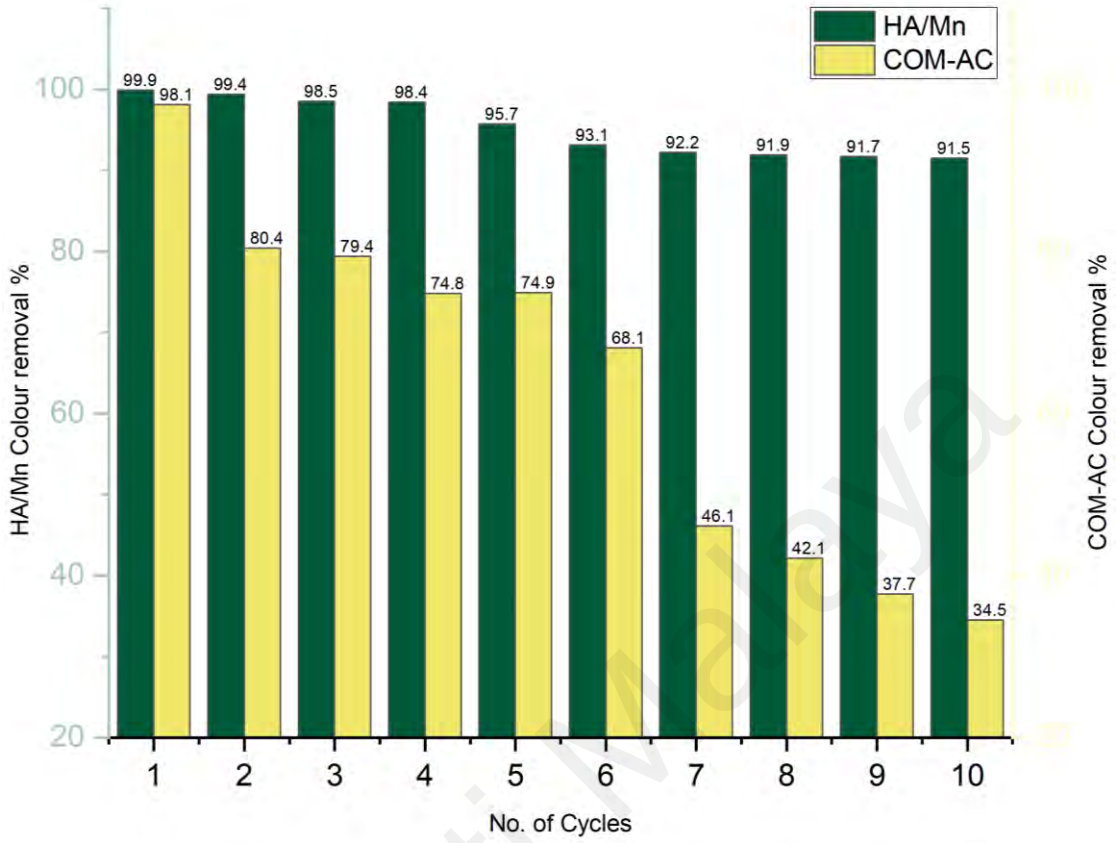

Figure 4.40 : Reusability of HA/Mn and commercial AC

These findings align with previous studies emphasizing the role of regeneration in cost minimization (Postai et al., 2016). For instance, Gao et al. (2023) achieved 88% desorption efficiency using 75% ethanol after three cycles for phenolic compounds. Similarly, iron oxide-loaded biochar maintained 99% methyl orange removal over five cycles. Other studies as summarized in Table 4.20 have reported a decline in adsorption performance after multiple cycles, such as H_3PO_4-modified papaya peel, which initially removed 92% methylene blue but dropped to 54.4% and 58.9% after three cycles using NaOH and HCl, respectively (Waghmare et al., 2023). Chen et al. (2023) observed that functionalized banana peel biochar had an initial adsorption capacity of 1790–2300 mg/g, which was reduced to 400–450 mg/g by the fifth cycle.

In conclusion, HA/Mn demonstrated superior regeneration capacity compared to commercial alternatives, confirming its cost-effectiveness and sustainability for industrial applications. The metal-impregnated hybrid structure retained high adsorption performance over multiple cycles, making it a viable long-term solution for wastewater treatment. These findings suggest that HA/Mn and similar hybrid adsorbents can be efficiently regenerated and reused, reducing overall operational costs and environmental impact.

Table 4.20 : Regeneration of biomass-based adsorbents

Adsorbent	**Adsorbate**	**Elution Solution**	**Cycles**	**Adsorption Efficiency**	**Ref.**
Modified avocado shell	Crystal violet	Ethanol	4	76.4 %	(Haki et al., 2022)
Magnetic avocado seed biochar	Methylene blue	HCL (0.1M)	4	46.0 %	(Prabakaran et al., 2022)
Sulphuric acid activated avocado seed biochar	Alizarin Red S	NaOH (0.1M)	4	61.0 %	(Bharath Balji et al., 2022)
H_3PO_4 activated papaya peel	Methylene blue	HCL (0.1M)	3	59.0 %	(Waghmare et al., 2023)
H_3PO_4 activated papaya peel	Methylene blue	NaOH (0.1M)	3	54.0 %	(Waghmare et al., 2023)
Banana peel biochar	Malachite green	Ethanol	5	90.0 %	(Chen et al., 2023)
HA/Mn	Methylene blue	Sulphuric acid and ethanol	10	91.5 %	This study

4.10.2 Cost analysis

The cost analysis of the metal-impregnated hybrid adsorbent (HA/Mn) includes expenses from raw materials, washing, drying, and chemical reagents, as detailed in Table 4.21. The cost in this research is represented as the amount required per litres of wastewater treated in US dollars (USD). The raw materials and chemical reagents cost USD 1.64/g, while the synthesis process costs USD 1.24/kg, accounting for 43% of the total production cost per kilogram of adsorbent. The overall production cost of HA/Mn sums up to USD 2.88/kg, while commercial activated carbon (COM-AC) is available in the market for USD 2.40/kg. However, it is important to note that COM-AC is synthesized through pyrolysis without additional chemical activation, while HA/Mn undergoes hydrothermal carbonization (HTC), activation, and manganese oxide functionalization. The synthesis process for HA/Mn is less expensive (USD 1.24/kg) than the pyrolysis process for commercial AC (USD 2.40/kg). This suggests that the additional cost of HA/Mn primarily arises from the use of chemical reagents rather than the synthesis method itself. According to a study conducted by Rangel et al (2021), collection of raw material, pretreatment, and activation sum up to USD 4.63/kg.

Although HA/Mn has a 16% higher initial production cost, its superior adsorption performance and reusability make it significantly more cost-effective over multiple cycles. HA/Mn requires an optimum dosage of 0.5 g/L for maximum adsorption capacity, while COM-AC requires 1.24 g/L, meaning that COM-AC requires more than double the dosage needed for HA/Mn. This difference in dosage efficiency directly affects the cost of wastewater treatment. The cost to treat 1000 litres of wastewater with HA/Mn is USD 1.44, compared to USD 2.98 for COM-AC. Over multiple adsorption cycles, the cost difference becomes even more significant. Treating 10,000 litres of wastewater in 10 cycles, assuming each cycle contains 1000L, HA/Mn costs only USD 1.44, whereas using COM-AC costs USD 11.92, leading to an 88% reduction in cost when using HA/Mn.

Moreover, considering the optimal conditions for HA/Mn, which achieves higher removal efficiency in alkaline conditions (pH 10), this presents a significant advantage. Most dye wastewater naturally falls within a pH range of 6–10, meaning that in many cases, no additional pH adjustment is required (Yaseen & Scholz, 2018). As a result, no extra chemical reagents are needed, effectively reducing operational costs and making HA/Mn a more cost-efficient option for industrial wastewater treatment.(Rangel et al., 2021; Yaseen & Scholz, 2018).

One of the key advantages of HA/Mn is its high regeneration efficiency, as it maintains its adsorption performance over 10 cycles without significant loss of efficiency. In contrast, COM-AC requires replacement every three cycles to maintain 80% colour removal efficiency, leading to a higher operational cost over time. This regeneration ability translates into substantial cost savings, making HA/Mn a more economical choice despite its higher initial production cost. However, additional cost factors related to the regeneration process should be evaluated, such as whether HA/Mn requires extra chemical or energy input for regeneration and whether its adsorption efficiency decreases with each regeneration cycle. These factors will influence the long-term cost-effectiveness of HA/Mn compared to COM-AC

The economic feasibility of HA/Mn becomes even more evident in large-scale wastewater treatment applications. For example, in the textile industry, daily wastewater discharge can reach 1.6 million litres (Jorge et al., 2023). Treating this volume would require approximately 800 kg of HA/Mn, costing USD 2,304 per day, whereas COM-AC would require 1,984 kg, costing USD 4,762 per day, more than twice the cost of HA/Mn. This substantial cost difference demonstrates that HA/Mn is not only viable for large-scale treatment but also provides a clear economic advantage over COM-AC.

In summary, while HA/Mn has a slightly higher initial production cost, its lower dosage requirement and superior reusability lead to substantial long-term cost savings compared to COM-AC. The potential cost reductions, particularly for large-scale wastewater treatment, highlight the economic feasibility of HA/Mn. However, further research is needed to evaluate transportation, storage, regeneration, and disposal costs to ensure its widespread industrial application.

4.11 Industrial wastewater treatment

The applicability of metal-impregnated hybrid adsorbent (HA/Mn) for real industrial wastewater treatment was evaluated alongside commercial activated carbon (Com-AC), as summarized in Table 4.22. Both adsorbents were tested on batik wastewater (800 mg/L), printing wastewater (490 mg/L), palm oil mill effluent (POME, 680 mg/L), and plastic fabrication wastewater (1500 mg/L) to assess the applicability of HA/Mn in industrial wastewater treatment.

The optimum conditions for methylene blue dye removal using HA/Mn adsorbent dosage of 0.5 g/L, contact time of 80 min, and initial pH of 10 were used as the comparative operating conditions for all wastewater treatments. To evaluate the potential of HA/Mn in wastewater treatment, the original solution concentrations were used without pre-treatment. A UV-spectrophotometer, along with a COD cell kit and a cuvette filled with a filtered wastewater sample, was used to determine the initial COD, colour, and concentration before treatment. All wastewater samples exhibited distinct visible colouration, with their respective maximum absorbance wavelengths (λmax) recorded. Batik wastewater appeared blue-purple with a λmax of 478 nm, printing wastewater was dark violet with a λmax of 646 nm, POME had a dark amber hue with λmax of 620 nm, and plastic fabrication wastewater was light blue with λmax of 297 nm.

Table 4.21: Cost estimation of HA/Mn and commercial AC

	Chemical and Materials	Unit Price (USD/ kg or L)	Usage	Cost (USD)	Total cost (USD)	Total cost (USD) to treat 1000 L	Total cost for 10 cycles
HA/Mn	Banana peel	-	5.00	-	2.88	1.44 (Optimum adsorbent dosage of 0.5 g/L)	1.44
	Avocado seed	-	5.00	-			
	Phosphoric acid	0.8	2.00	1.60			
	Manganese (II,III) oxide	0.15	0.25	0.04			
	Synthesis process						
	Washing						
	Grinding	0.05/kWh	1.10 kW, 1h	0.02			
	Hydrothermal carbonization	0.05/kWh	3.60kW, 2h at 200	0.36			
	Heating	0.05/kWh	1.70 kW, 1h	0.08			
	Carbonization	0.05/kWh	4.0 kW, 4h	0.78			
Commercial activated carbon					2.40	2.98 (Optimum adsorbent dosage of 1.24 g/L)	11.92

The results, summarized in Table 4.22, indicate that HA/Mn achieved a higher removal efficiency than the COM-AC. For batik wastewater, HA/Mn removed over 50% of the colour and 67 % COD removal with an adsorption capacity of 33 mg/g. In comparison, COM-AC achieved 64 % COD removal, 46 % colour removal, and an adsorption capacity of 32 mg/g. HA/Mn demonstrated significant performance for printing wastewater, achieving more than 50% COD removal and 60% colour removal with an adsorption capacity of 132 mg/g. COM-AC treating printing wastewater achieved 52 % COD removal, 47% colour removal, and an adsorption capacity of 106mg/g.

Among the four wastewater types, HA/Mn exhibited the highest adsorption performance for POME and plastic fabrication wastewater. HA/Mn achieved 75 % COD removal and over 85 % colour removal for POME, with an adsorption capacity of 268 mg/g. For plastic fabrication wastewater, HA/Mn removed 67 % of COD and 82 % of colour, with an adsorption capacity of 578 mg/g. In comparison, Com-AC removed 55 % of COD and 57 % of colour for POME, with an adsorption capacity of 178 mg/g. For plastic fabrication wastewater, COM-AC achieved 19 % COD removal, 64 % colour removal, and an adsorption capacity of 448 mg/g. The higher performance of HA/Mn in POME may be attributed to the presence of natural organic matter, which could interact favourably with HA/Mn, enhancing adsorption efficiency. Moreover, the high efficiency observed in plastic fabrication wastewater suggests that simpler dye structures or fewer interfering compounds allowed HA/Mn to perform more effectively.

In summary, HA/Mn outperformed COM-AC in COD and colour removal, as well as adsorption capacity. However, its removal efficiency was limited due to the complex composition of industrial wastewater, including organic matter, heavy metals, and varying pH, which can interfere with adsorption. Despite this, HA/Mn holds strong potential as an alternative adsorbent for industrial applications.

Table 4.22: Comparison of HA/Mn with COM-AC

Adsorbate	Adsorbent	COD removal (%)	Colour removal (%)	Adsorption capacity (mg/g)
Batik wastewater (800 mg/L)	HA/Mn	67	52	33
	COM-AC	64	46	32
Printing wastewater (490 mg/L)	HA/Mn	59	60	132
	COM-AC	52	47	106
Palm Oil Mill Effluent (680 mg/L)	HA/Mn	75	85	268
	COM-AC	55	57	178
Plastic Fabrication Wastewater (1500 mg/L)	HA/Mn	67	82	567
	COM-AC	19	64	448

CHAPTER 5: CONCLUSION

5.1 Conclusion

This study successfully developed a hybrid adsorbent from mixed fruit wastes, specifically banana peels and avocado seeds, using a two-step hydrothermal carbonization process. Optimal synthesis was achieved with a 1:1 mixing ratio of raw avocado seed (1.5 g) to raw banana peel (1.5 g). The highest carbonization yield and adsorption efficiency were obtained at 200 °C, while subsequent phosphoric acid activation (85% H_3PO_4, 1:1 ratio) and carbonization at 450 °C for 2 hours produced the most effective adsorbent.

The acid-activated and manganese-impregnated hybrid (HA/Mn) showed significantly enhanced physicochemical properties, with a surface area increase from 1.73 m^2/g (raw hybrid adsorbent) to 666 m^2/g and well-developed crater-like pores, resulting in superior adsorption performance compared to RA and acid-activated (HA) adsorbents. Among the three, HA/Mn demonstrated the highest removal efficiency, followed by HA and RA, making it the most effective formulation. ANOVA analysis confirmed that HA/Mn follows reduced quadratic models for colour removal, COD removal, and adsorption capacity. Under optimized conditions (initial pH 10, dye concentration 0.1 g/L, adsorbent dosage 0.5 g/L, and contact time of 80 minutes), HA/Mn achieved 99.9% colour removal, and an adsorption capacity of 199 mg/g. Validation tests further confirmed its effectiveness, with COD removal exceeding 85%.

Kinetic studies revealed that HA/Mn best fits the pseudo-second-order model, indicating chemisorption as the dominant mechanism. Isotherm analysis showed strong alignment with the Redlich–Peterson model, suggesting both monolayer and multilayer adsorption, while also indicating dominantly homogeneous surface interactions. The adsorption mechanisms involves electrostatic attraction, hydrogen bonding, and π–π

stacking, all contributing to the high performance of HA/Mn in methylene blue dye removal.

Moreover, the integration of machine learning using the Random Forest (RF) algorithm demonstrated high predictive accuracy. The 20% RF model achieved an R^2 value of 0.9671, while the 30% RF model reached 0.9572, indicating strong model performance for methylene blue dye removal. In terms of prediction accuracy, the 20% RF model achieved 99.7% for COD removal, 99.2% for colour removal, and 97.4% for adsorption capacity. In comparison, the RSM-CCD approach achieved a similar COD removal accuracy of 99.4%, but lower values for colour removal (98.1%) and adsorption capacity (93.1%). These results highlight the superior predictive performance and robustness of the Random Forest model over traditional statistical methods.

The scalability and reusability of HA/Mn were also validated. At 3 L and 5 L, it maintained over 85 % COD removal and 99 % colour removal efficiency, with adsorption capacities of 86.1 and 89.5 mg/g, respectively. In regeneration studies, HA/Mn retained 91.5% efficiency after 10 cycles, outperforming commercial adsorbent (COM-AC), which declined to 34.5% at the end of the 10^{th} cycle. Although HA/Mn has a slightly higher production cost (USD 2.88/kg vs. USD 2.40/kg for COM-AC), its extended reusability led to an 88% reduction in total treatment cost over 10,000 L of wastewater. Furthermore, in real industrial wastewater applications, including batik, printing, palm oil mill effluent (POME), and plastic fabrication, HA/Mn consistently outperformed COM-AC, achieving 6–18% higher removal efficiencies for COD, colour, and adsorption capacity.

In summary, HA/Mn exhibited excellent dye removal efficiency, strong reusability, enhanced surface and functional properties, and outstanding economic viability. Its performance in various real-world wastewater scenarios highlights its potential as a

sustainable, high-performance, and cost-effective alternative to conventional commercial adsorbents for industrial dye wastewater treatment.

5.2 Recommendations

This research has achieved significant results for the hybrid adsorbent, which demonstrates a high potential for removing recalcitrant pollutants from wastewater. However, several aspects require further discussion and investigation. For instance, the synthesis method can be optimized through a one-step hydrothermal carbonization process using wet biomass with chemicals, which would minimize the need for additional heating and moisture removal, as well as reduce the requirement for further activation and use of high-temperature furnaces.

Beyond wastewater treatment, hybrid adsorbents hold the potential for carbon capture in industrial settings. Quantum-level modelling and experimental studies could help understand CO_2 adsorption mechanisms and improve their efficiency for carbon sequestration. Additionally, their application in soil remediation should be explored, particularly for heavy metal immobilization and improving soil aeration, which could support agricultural and environmental restoration.

The management of spent adsorbents is another key research area. While hybrid adsorbents exhibit excellent regeneration capacity, long-term reuse may eventually lead to saturation, necessitating proper disposal or repurposing. Potential applications include their incorporation into cement and brick manufacturing to enhance mechanical strength. Additionally, a full life-cycle assessment (LCA) should be conducted to evaluate their environmental footprint, including greenhouse gas emissions, energy consumption, and overall sustainability.

Furthermore, a molecular-level study on the interactions between the adsorbent surface and the adsorbate could optimize targeted pollutant removal. Lastly, the incorporation of the hybrid adsorbent into membrane technology should be explored, as it could be used in advanced wastewater treatment filtration systems.

5.3 Novelty

This study presents a novel approach to developing a hybrid adsorbent from mixed fruit waste using two-step hydrothermal carbonization combined with acid activation and metal oxide impregnation. Unlike conventional biomass adsorbents, the optimized HA/Mn adsorbent exhibits a remarkably high surface area, well-defined pore structure, and enhanced functional groups, significantly improving its adsorption efficiency and stability. A key innovation lies in the integration of machine learning with Response Surface Methodology for precise optimization and prediction of methylene blue removal, demonstrating superior accuracy in adsorption performance modelling. Additionally, the study provides an economic analysis, proving that HA/Mn is not only more effective but also more cost-efficient than commercial activated carbon, maintaining high regeneration efficiency while reducing operational costs. Furthermore, the study aligns with circular economy principles, offering a sustainable, scalable alternative for industrial wastewater treatment. HA/Mn outperforms commercial absorbents in treating printing wastewater, palm oil mill effluent, and synthetic wastewater, making it a practical and eco-friendly solution for real-world applications. This research bridges the gap between waste valorisation, advanced adsorption technologies, and machine learning-driven optimization, setting a new benchmark for sustainable dye removal strategies.

5.4 Knowledge contribution and significance of the study

This study presents a significant advancement in sustainable wastewater treatment through the development of a novel hybrid adsorbent (HA/Mn), synthesized from avocado seeds and banana peels via a two-step hydrothermal carbonization process. Enhanced by acid activation and manganese oxide impregnation, this adsorbent demonstrates superior adsorption performance, high reusability, and cost-effectiveness, offering a practical alternative to commercial activated carbon. It contributes meaningfully to circular economy practices and sustainable resource management through the following key contributions:

1. Development and optimization of a hybrid adsorbent from agricultural waste using an innovative two-step hydrothermal carbonization approach, transforming biomass into value-added adsorbents with enhanced surface functionality and porosity.
2. Significant enhancement in physicochemical properties through manganese oxide impregnation, increasing the surface area from 1.73 m^2/g to 666 m^2/g and producing crater-like pore structures that significantly improve colour removal, COD reduction, and adsorption capacity.
3. The establishment of optimal adsorption conditions for methylene blue removal, including an initial pH of 10, dye concentration of 0.1 g/L, adsorbent dosage of 0.5 g/L, and 80-minute contact time, achieving up to 99.9% colour removal and 199 mg/g adsorption capacity.
4. Integration of machine learning with statistical optimization, where the Random Forest (RF) regression model demonstrated superior predictive performance over Response Surface Methodology (RSM-CCD), achieving higher accuracy in predicting COD removal (99.7%), colour removal (99.2%), and adsorption capacity (97.4%).

5. High reusability and operational stability, with HA/Mn maintaining 91.5% efficiency after 10 regeneration cycles, significantly outperforming commercial activated carbon, which dropped below 35% after just three cycles
6. Proven effectiveness in real-world wastewater treatment, including batik, printing, palm oil mill effluent (POME), and plastic fabrication effluents, where HA/Mn consistently achieved 6–18% higher removal efficiencies than commercial adsorbents.

The significance of this study lies in its comprehensive and novel approach to addressing both environmental pollution and biomass waste utilization. By combining advanced material synthesis with machine learning- driven process optimization, the study offers a scalable, cost-effective, and sustainable solution for industrial dye wastewater treatment. The integration of Random Forest algorithms into adsorption performance modelling sets a new benchmark for predictive accuracy in adsorption studies. This research bridges the gap between waste valorisation, advanced adsorption material development, and data-driven process optimization. It supports key Sustainable Development Goals by promoting responsible consumption, sustainable industrial processes, and the transformation of agricultural waste into value added materials for environmental remediation.

REFERENCES

Abdi, J., Hadavimoghaddam, F., Hadipoor, M., & Hemmati-Sarapardeh, A. (2021). Modeling of CO(2) adsorption capacity by porous metal organic frameworks using advanced decision tree-based models. *Sci Rep*, *11*(1), 24468. https://doi.org/10.1038/s41598-021-04168-w

Abdulfatai, J., Saka, A. A., Afolabi, A. S., & Micheal, O. (2013). Development of Adsorbent from Banana Peel for Wastewater Treatment. *Applied Mechanics and Materials*, *248*, 310-315. https://doi.org/10.4028/www.scientific.net/AMM.248.310

Abdulhameed, A. S., Hum, N. N. M. F., Rangabhashiyam, S., Jawad, A. H., Wilson, L. D., Yaseen, Z. M., AL-Kahtani, A. A., & AlOthaman, Z. A. (2021). Statistical modeling and mechanistic pathway for methylene blue dye removal by high surface area and mesoporous grass-based activated carbon using K2CO3 activator. *Journal of Environmental Chemical Engineering*, *9*(105530). https://doi.org/https://doi.org/10.1016/j.jece.2021.105530

Afroze, S., Sen, T. K., & Ang, H. M. (2016). Adsorption removal of zinc (II) from aqueous phase by raw and base modified Eucalyptus sheathiana bark: Kinetics, mechanism and equilibrium study. *Process Safety and Environmental Protection*, *102*, 336-352. https://doi.org/10.1016/j.psep.2016.04.009

Afshin, S., Mokhtari, S., A., Vousoughi, M., Sadhegi, H., & Rashtbari, Y. (2018). Data of adsorption of Basic Blue 41 dye from aqueous solutions by activated carbon prepared from filamentous algae. *Data in Brief*, *21*, 1008-1013. https://doi.org/https://doi.org/10.1016/j.dib.2018.10.023

Ahmad, A., Yadav, A. K., Singh, A., & Singh, D. K. (2024). A comprehensive machine learning-coupled response surface methodology approach for predictive modeling and optimization of biogas potential in anaerobic Co-digestion of organic waste. *Biomass and Bioenergy*, *180*. https://doi.org/10.1016/j.biombioe.2023.106995

Ahmad, T., & Danish, M. (2022). A review of avocado waste-derived adsorbents: Characterizations, adsorption characteristics, and surface mechanism. *Chemosphere*, 134036. https://doi.org/10.1016/j.chemosphere.2022.134036

Ahmad, T., & Danish, M. (2022). A review of avocado waste-derived adsorbents: Characterizations, adsorption characteristics, and surface mechanism. *Chemosphere*, *296*, 134036. https://doi.org/10.1016/j.chemosphere.2022.134036

Al-Ahmed, Z. A. (2024). Surface methodology for optimized adsorption of hazardous organic pollutant from aqueous solutions via novel magnetic metal organic framework: Kinetics, isotherm study, and DFT calculations. *Journal of Molecular Liquids*, *409*. https://doi.org/10.1016/j.molliq.2024.125507

Al-sareji, O. J., Meiczinger, M., Somogyi, V., Al-Juboori, R. A., Grmasha, R. A., Stenger-Kovács, C., Jakab, M., & Hashim, K. S. (2023). Removal of emerging pollutants from water using enzyme-immobilized activated carbon from coconut shell.

Journal of Environmental Chemical Engineering, *11*(3). https://doi.org/10.1016/j.jece.2023.109803

Alalid, W., Alseroury, F. A., Almeelbi, T., & Barakat, M. A. (2020). Manganese oxide-modified biochar (MBC) for arsenic and lead adsorption from groundwater. *International Journal of Innovations in Engineering and Technology*, *15*(4). https://doi.org/http://dx.doi.org/10.21172/ijiet.154.07

Alam G, Ihsanullah I, Naushad M, & Sillanpaa, M. (2022). Applications of artificial intelligence in water treatment for optimization and automation of adsorption processes: Recent advances and prospects. *Chemical Engineering Journal*, *427*(130011). https://doi.org/https://doi.org/10.1016/j.cej.2021.130011

Alam, M. G., Danish, M., Alanazi, A. M., Ahmad, T., & Khalil H.P.S, A. (2023). Response surface methodology approach of phenol removal study using high-quality activated carbon derived from H3PO4 activation of Acacia mangium wood. *Diamond and Related Materials*, *132*. https://doi.org/10.1016/j.diamond.2022.109632

Alorabi, A. Q., Hassan, M. S., & Azizi, M. (2020). Fe3O4-CuO-activated carbon composite as an efficient adsorbent for bromophenol blue dye removal from aqueous solutions. *Arabian Journal of Chemistry*. https://doi.org/http://doi.org/10.1016/j.arabjc.2020.09.039

Alpaydin, E. (2020). *Introduction to machine learning*. MIT press.

Amela, K., Hassen, M. A., & Kerroum, D. (2012). Isotherm and Kinetics Study of Biosorption of Cationic Dye onto Banana Peel. *Energy Procedia*, *19*, 286-295. https://doi.org/10.1016/j.egypro.2012.05.208

Aragaw, T. A., & Alene, A. N. (2022). A comparative study of acidic, basic, and reactive dyes adsorption from aqueous solution onto kaolin adsorbent: Effect of operating parameters, isotherms, kinetics, and thermodynamics. *Emerging Contaminants*, *8*, 59-74. https://doi.org/10.1016/j.emcon.2022.01.002

Araújo, R. G., Jasso, R. M. R., Ruiz, H. A., Pintado, M. M. E., & Aguilar, C. N. (2018). Avocado by-products: nutritional and functional properties. *Trends in Food Science & Technology*. https://doi.org/10.1016/j.tifs.2018.07.027

Asfaram, A., Fathi, M. R., Khodadoust, S., & Naraki, M. (2014). Removal of Direct Red 12B by garlic peel as a cheap adsorbent: kinetics, thermodynamic and equilibrium isotherms study of removal. *Spectrochim Acta A Mol Biomol Spectrosc*, *127*, 415-421. https://doi.org/10.1016/j.saa.2014.02.092

Atiyah, Z. Y., Muallah, S. K., & Abbar, A. H. (2024). Removal of COD from petroleum refinery wastewater by adsorption using activated carbon derived from avocado plant. *South African Journal of Chemical Engineering*, *48*, 467-483. https://doi.org/10.1016/j.sajce.2024.03.015

Avalos-Viveros, M., Santolalla-Vargas, C.-E., Santes-Hernández, V.-F., Martínez-Flores, H.-E., Torres-García, E., López-Meza, J.-E., Virgen-Ortiz, J.-J., Pérez-Calix, E., & García-Pérez, M.-E. (2023). Valorization of avocado peels by

conventional extraction and hydrothermal carbonization for cosmeceutical applications. *Sustainable Chemistry and Pharmacy*, *36*. https://doi.org/10.1016/j.scp.2023.101335

Avila, H., E,R., Castillo, D., I,M., Olumide, A., A., & Petriciolet, A., B. (2016). A survey of multi-component sorption models for the competitive removal of heavy metal ions using bush mango and flamboyant biomasses. *Journal of Molecular Liquids*, *224*, 1041-1054. https://doi.org/10.1016/j.molliq.2016.10.061

Ay, C. O., Ozcan, A. S., Erdogan, Y., & Ozcan, A. (2012). Characterization of Punica granatum L. peels and quantitatively determination of its biosorption behavior towards lead(II) ions and Acid Blue 40. *Colloids Surf B Biointerfaces*, *100*, 197-204. https://doi.org/10.1016/j.colsurfb.2012.05.013

Baloo, L., Isa, M., Sapari, N., Jabgaba, A., Wei, L., Yavari, S., Razali, R., & Vasu, R. (2021). Adsorptive removal of methylene blue and acid orange 10 dyes from aqueous solutions using oil palm wastes-derived activated carbons. *Alexandria Engineering Journal*, *60*, 5611-5629. https://doi.org/https://doi.org/10.1016/j.aej.2021.04.044

Batool, A., & Valiyaveettil, S. (2021). Chemical transformation of soya waste into stable adsorbent for enhanced removal of methylene blue and neutral red from water. *Journal of Environmental Chemical Engineering*, *9*(1). https://doi.org/10.1016/j.jece.2020.104902

Bharath Balji, G., Senthil Kumar, P., & Kooh, M. R. R. (2022). Adsorptive Removal of Alizarin Red S onto Sulfuric Acid-Modified Avocado Seeds: Kinetics, Equilibrium, and Thermodynamic Studies. *Adsorption Science & Technology*, *2022*, 1-13. https://doi.org/10.1155/2022/3137870

Bisiriyu, I., O., & Meijboom, R. (2020). Adsorption of Cu(II) ions from aqueous solution using pyridine-2,6-dicarboxylic acid crosslinked chitosan as a green biopolymer adsorbent. *International Journal of Biological Macromolecules*, *165*, 2484-2493. https://doi.org/https://10.1016/j.ijbiomac.2020.10.150

Boeykens, S., Redondo, N., Obeso, R., Caracciolo, N., & Vazquez, C. (2019). Chromium and Lead adsorption by avocado seed biomass study through the use of Total Reflection X-Ray Fluorescence analysis. *Applied Radiation and Isotopes*, *153*. https://doi.org/https://10.1016/j.apradiso.2019.108809

Boeykens, S. P., Redondo, N., Obeso, R. A., Caracciolo, N., & Vazquez, C. (2019a). Chromium and Lead adsorption by avocado seed biomass study through the use of Total Reflection X-Ray Fluorescence analysis. *applied Radiation and Isotopes*, *153*, 108809. https://doi.org/https://10.1016/j.apradiso.2019.108809

Boeykens, S. P., Redondo, N., Obeso, R. A., Caracciolo, N., & Vazquez, C. (2019b). Chromium and Lead adsorption by avocado seed biomass study through the use of Total Reflection X-Ray Fluorescence analysis. *Appl Radiat Isot*, *153*, 108809. https://doi.org/10.1016/j.apradiso.2019.108809

Brazil, T. R., Gonçalves, M., Junior, M. S. O., & Rezende, M. C. (2022). Sustainable process to produce activated carbon from Kraft lignin impregnated with H3PO4

using microwave pyrolysis. *Biomass and Bioenergy*, *156*. https://doi.org/10.1016/j.biombioe.2021.106333

Brocza, F. M., Foster, S. J., Peacock, C. L., & Jones, J. M. (2024). Synthesis and applications of manganese oxide - biochar composites: A systematic review across catalysis, capacitor and sorption applications. *Biomass and Bioenergy*, *184*. https://doi.org/10.1016/j.biombioe.2024.107201

Cathoglu, F., Akay, S., Turunc, E., Gozman, B., Anastopoulos, I., Kayan, B., & Kalderis, D. (2021). Preparation and application of Fe-modified banana peel in the adsorption of methylene blue: Process optimization using response surface methodology. *Environmental Nanotechnology, Monitoring & Management*, *16*(100517). https://doi.org/https://doi.org/10.1016/j.enmm.2021.100517

Cha Zhang, Y. M. (2012). *Ensemble Machine Learning*. Springer New York, NY. https://doi.org/https://doi.org/10.1007/978-1-4419-9326-7

Chaima, H., Eddine, B. C., Faouzia, B., Rana, H., Aymene Salah, B., Gil, A., Imene, B.-A., Ferhat, D., Riadh, B., & Mokhtar, B. (2024). Adsorptive removal of cationic dye from aqueous solutions using activated carbon prepared from Crataegus monogyna/sodium alginate/polyaniline composite beads: Experimental study and molecular dynamic simulation. *Journal of Molecular Liquids*, *408*. https://doi.org/10.1016/j.molliq.2024.125372

Chen, L., Mi, B., He, J., Li, Y., Zhou, Z., & Wu, F. (2023). Functionalized biochars with highly-efficient malachite green adsorption property produced from banana peels via microwave-assisted pyrolysis. *Bioresour Technol*, *376*, 128840. https://doi.org/10.1016/j.biortech.2023.128840

Chen, W., Tang, Q., Liu, Z., Luo, F., Liao, Y., Zhao, S., Zhang, K., Cheng, L., & Ma, D. (2020). Fabricating a novel chitosan-based adsorbent with multifunctional synergistic effect for Cu(II) removal: Maleic anhydride as a connecting bridge. *Chemical Engineering Research and Design*, *163*, 21-35. https://doi.org/https://10.1016/j.cherd.2020.08.023

Chen, Y., Wang, H., Zhao, W., & Huang, S. (2018). Four different kinds of peels as adsorbents for the removal of Cd (II) from aqueous solution: Kinetics, isotherm and mechanism. *Journal of the Taiwan Institute of Chemical Engineers*, 1–6. https://doi.org/10.1016/j.jtice.2018.03.046

Correia, I., Santos, P., Santana, C., Neris, J., Luzardo, F., & Velasco, F. (2018). Application of coconut shell, banana peel, spent coffee grounds, eucalyptus bark, piassava (Attalea funifera) and water hyacinth (Eichornia crassipes) in the adsorption of Pb2+ and Ni2+ ions in water. *Journal of Environmental Chemical Engineering*, *6*(2), 2319-2334. https://doi.org/https://doi.org/10.1016/j.jece.2018.03.033

Cuong Nguyen, X., Thanh Huyen Nguyen, T., Hong Chuong Nguyen, T., Van Le, Q., Yen Binh Vo, T., Cuc Phuong Tran, T., Duong La, D., Kumar, G., Khanh Nguyen, V., Chang, S. W., Jin Chung, W., & Duc Nguyen, D. (2021). Sustainable carbonaceous biochar adsorbents derived from agro-wastes and invasive plants

for cation dye adsorption from water. *Chemosphere*, *282*, 131009. https://doi.org/10.1016/j.chemosphere.2021.131009

Dang, X., Yu, Z., Yang, M., Woo, M. W., Song, Y., Wang, X., & Zhang, H. (2022). Sustainable electrochemical synthesis of natural starch-based biomass adsorbent with ultrahigh adsorption capacity for Cr(VI) and dyes removal. *Separation and Purification Technology*, *288*. https://doi.org/10.1016/j.seppur.2022.120668

De Miranda Ramos Soares, A. P., de Oliveira Carvalho, F., de Farias Silva, C. E., da Silva Gonçalves, A. H., & de Souza Abud, A. K. (2020). Random Forest as a promising application to predict basic-dye biosorption process using orange waste. *Journal of Environmental Chemical Engineering*, *8*(4). https://doi.org/10.1016/j.jece.2020.103952

Della-Flora, A., Wilde, M. L., Thue, P. S., Lima, D., Lima, E. C., & Sirtori, C. (2020). Combination of solar photo-Fenton and adsorption process for removal of the anticancer drug Flutamide and its transformation products from hospital wastewater. *J Hazard Mater*, *396*, 122699. https://doi.org/10.1016/j.jhazmat.2020.122699

Detho, A., Daud, Z., Almohana, A. I., Almojil, S. F., Alali, A. F., Memon, A. A., Samo, S. R., Rosli, M. A., Awang, H., Ridzuan, M. B., Kamaruddin, M. A., & Halim, A. A. (2022). Adsorption efficiency and isotherm of COD and NH3–N removal from stabilized leachate using natural low-cost adsorbent green mussel (Perna viridis). *Desalination and Water Treatment*, *245*, 191-201. https://doi.org/10.5004/dwt.2022.27978

Dhaouadi, F., Sellaoui, L., Dotto, G. L., Bonilla-Petriciolet, A., Erto, A., & Lamine, A. B. (2020). Adsorption of methylene blue on comminuted raw avocado seeds: Interpretation of the effect of salts via physical monolayer model. *Journal of Molecular Liquids*, *305*. https://doi.org/10.1016/j.molliq.2020.112815

Dhaouadi, F., Sellaoui, L., Hernández, L., Petriciolet, A., Castillo, D., Ávila, H., Ponce, H., Taamalli, S., Louis, F., & Lamine, A. (2021). Preparation of an avocado seed hydrochar and its application as heavy metal adsorbent: Properties and advanced statistical physics modeling. *Chemical Engineering Journal*, *419*. https://doi.org/10.1016/j.cej.2021.129472

Ding, Z., Ge, Y., Gowd, S. C., Singh, E., Kumar, V., Chaurasia, D., Kumar, V., Rajendran, K., Bhargava, P. C., Wu, P., Lin, F., Harirchi, S., Ashok Kumar, V., Sirohi, R., Sindhu, R., Binod, P., Taherzadeh, M. J., & Awasthi, M. K. (2023). Production of biochar from tropical fruit tree residues and ecofriendly applications - A review. *Bioresour Technol*, *376*, 128903. https://doi.org/10.1016/j.biortech.2023.128903

Dos Santos Escobar, O., Ferraz de Azevedo, C., Swarowsky, A., Adebayo, M. A., Schadeck Netto, M., & Machado Machado, F. (2021). Utilization of different parts of Moringa oleifera Lam. seeds as biosorbents to remove Acid Blue 9 synthetic dye. *Journal of Environmental Chemical Engineering*, *9*(4). https://doi.org/10.1016/j.jece.2021.105553

Du, P., Xu, L., Ke, Z., Liu, J., Wang, T., Chen, S., Mei, M., Li, J., & Zhu, S. (2022). A highly efficient biomass-based adsorbent fabricated by graft copolymerization: Kinetics, isotherms, mechanism and coadsorption investigations for cationic dye and heavy metal. *J Colloid Interface Sci*, *616*, 12-22. https://doi.org/10.1016/j.jcis.2022.02.048

Duan, F., Zhu, Y., Yu, H., & Wang, A. (2022). Facile fabrication of the porous adsorbent from natural plant Angelica Sinensis stabilized liquid foam for dye removal. *Green Chemical Engineering*, *3*(1), 83-91. https://doi.org/10.1016/j.gce.2021.10.001

Ecer, Ü., & Yılmaz, Ş. (2024). Fabrication of magnetic biochar-MIL-68(Fe)-supported cobalt composite material toward the catalytic reduction performance of crystal violet. *Journal of Water Process Engineering*, *57*. https://doi.org/10.1016/j.jwpe.2023.104574

Ecer, Ü., Yılmaz, Ş., & Şahan, T. (2020). Investigation of Mercury(II) and Arsenic(V) adsorption onto sulphur functionalised pumice: a response surface approach for optimisation and modelling. *International Journal of Environmental Analytical Chemistry*, *102*(19), 7779-7799. https://doi.org/10.1080/03067319.2020.1838495

Ecer, Ü., Yılmaz, Ş., & Şahan, T. (2023). Synthesis, Characterization, and application of Ag-Doped Mercapto-Functionalized clay for decolorization of Coomassie brilliant Blue: Optimization using RSM. *Chemical Physics Letters*, *825*. https://doi.org/10.1016/j.cplett.2023.140610

Edokpayi, J., & Makete, E. (2021). Removal of Congo red dye from aqueous media using Litchi seeds powder: Equilibrium, kinetics and thermodynamics. *Physics and Chemistry of the Earth, Parts*, *123*. https://doi.org/10.1016/j.pce.2021.103007

El Farissi, H., Lakhmiri, R., Albourine, A., Safi, M., & Cherkaoui, O. (2021). Adsorption study of charcoal of cistus ladaniferus shell modified by H3PO4 and NaOH used as a low-cost adsorbent for the removal of toxic reactive red 23 dye: Kinetics and thermodynamics. *Materials Today: Proceedings*, *43*, 1740-1748. https://doi.org/10.1016/j.matpr.2020.10.438

Elizalde-González, M. P., Mattusch, J., Peláez-Cid, A. A., & Wennrich, R. (2007). Characterization of adsorbent materials prepared from avocado kernel seeds: Natural, activated and carbonized forms. *Journal of Analytical and Applied Pyrolysis*, *78*(1), 185-193. https://doi.org/10.1016/j.jaap.2006.06.008

Eniola, J. O., Sizirici, B., Khaleel, A., & Yildiz, I. (2023). Fabrication of engineered biochar-iron oxide from date palm frond for the effective removal of cationic dye from wastewater. *Journal of Water Process Engineering*, *54*. https://doi.org/10.1016/j.jwpe.2023.104046

Fan, M., Shao, Y., Wang, Y., Sun, J., He, H., Guo, Y., Zhang, S., Wang, S., Li, B., & Hu, X. (2025). Evolution of pore structure and functionalities of activated carbon and phosphorous species in activation of cellulose with H3PO4. *Renewable Energy*, *240*. https://doi.org/10.1016/j.renene.2024.122151

Farghali, M. A., Selim, A. M., Khater, H. F., Bagato, N., Alharbi, W., Alharbi, K. H., & Taha Radwan, I. (2022). Optimized adsorption and effective disposal of Congo red dye from wastewater: Hydrothermal fabrication of MgAl-LDH nanohydrotalcite-like materials. *Arabian Journal of Chemistry*, *15*(11). https://doi.org/10.1016/j.arabjc.2022.104171

Fathalian, F., Aarabi, S., Ghaemi, A., & Hemmati, A. (2022). Intelligent prediction models based on machine learning for CO(2) capture performance by graphene oxide-based adsorbents. *Sci Rep*, *12*(1), 21507. https://doi.org/10.1038/s41598-022-26138-6

Feng, C., Zhang, S., Wang, Y., Wang, G., Pan, X., Zhong, Q., Xu, X., Luo, L., Long, L., & Yao, P. (2020). Synchronous removal of ammonium and phosphate from swine wastewater by two agricultural waste based adsorbents: Performance and mechanisms. *Bioresour Technol*, *307*, 123231. https://doi.org/10.1016/j.biortech.2020.123231

Fetimi, A., Dâas, A., Benguerba, Y., Merouani, S., Hamachi, M., Kebiche-Senhadji, O., & Hamdaoui, O. (2021). Optimization and prediction of safranin-O cationic dye removal from aqueous solution by emulsion liquid membrane (ELM) using artificial neural network-particle swarm optimization (ANN-PSO) hybrid model and response surface methodology (RSM). *Journal of Environmental Chemical Engineering*, *9*(5). https://doi.org/10.1016/j.jece.2021.105837

Fito, J., Abrham, S., & Angassa, K. (2020). Adsorption of Methylene Blue from Textile Industrial Wastewater onto Activated Carbon of Parthenium hysterophorus. *International Journal of Environmental Research*, *14*(5), 501-511. https://doi.org/10.1007/s41742-020-00273-2

Flora, J. F., Lu, X., Li, L., Flora, J. R., & Berge, N. D. (2013). The effects of alkalinity and acidity of process water and hydrochar washing on the adsorption of atrazine on hydrothermally produced hydrochar. *Chemosphere*, *93*(9), 1989-1996. https://doi.org/10.1016/j.chemosphere.2013.07.018

Francis, A. A., & Abdel Rahman, M. K. (2016). The environmental sustainability of calcined calcium phosphates production from the milling of eggshell wastes and phosphoric acid. *Journal of Cleaner Production*, *137*, 1432-1438. https://doi.org/10.1016/j.jclepro.2016.08.029

Genuino, D. A. D., de Luna, M. D. G., & Capareda, S. C. (2018). Improving the surface properties of municipal solid waste-derived pyrolysis biochar by chemical and thermal activation: Optimization of process parameters and environmental application. *Waste Manag*, *72*, 255-264. https://doi.org/10.1016/j.wasman.2017.11.038

Georgin, J., Marques, B., Salla, J., Foletto, E., Allasia, D., & Dotto, G. (2018). Removal of Procion Red dye from colored effluents using H2SO4-/HNO3-treated avocado shells (Persea americana) as adsorbent. *Environmental Science and Pollution Research*, *25*(7), 6429-6442. https://doi.org/10.1007/s11356-017-0975-1

Ghaedi, M., Ghaedi, A. M., Negintaji, E., Ansari, A., Vafaei, A., & Rajabi, M. (2014). Random forest model for removal of bromophenol blue using activated carbon

obtained from Astragalus bisulcatus tree. *Journal of Industrial and Engineering Chemistry*, *20*(4), 1793-1803. https://doi.org/10.1016/j.jiec.2013.08.033

Gonzales-Condori, E. G., Avalos-López, G., Gonzales-Condori, J., Mujica-Guzmán, A., Terán-Hilares, R., Briceño, G., Quispe-Avilés, J. M., Parra-Ocampo, P. J., & Villanueva-Salas, J. A. (2023). Avocado seed powder residues as a promising bio-adsorbent for color removal from textile wastewater. *Revista Mexicana de Ingeniería Química*, *22*(3), 1-23. https://doi.org/10.24275/rmiq/IA2370

Haki, M., Imgharn, A., Aarab, N., Hsini, A., Essekri, A., Laabd, M., El Jazouli, H., Elamine, M., Lakhmiri, R., & Albourine, A. (2022). Efficient removal of crystal violet dye from aqueous solutions using sodium hydroxide-modified avocado shells: kinetics and isotherms modeling. *Water Science & Technology*, *85*(1), 433-448. https://doi.org/10.2166/wst.2021.451

Hambisa, A. A., Regasa, M. B., Ejigu, H. G., & Senbeto, C. B. (2022). Adsorption studies of methyl orange dye removal from aqueous solution using Anchote peel-based agricultural waste adsorbent. *Applied Water Science*, *13*(1). https://doi.org/10.1007/s13201-022-01832-y

Hameed, B. H. (2009). Removal of cationic dye from aqueous solution using jackfruit peel as non-conventional low-cost adsorbent. *J Hazard Mater*, *162*(1), 344-350. https://doi.org/10.1016/j.jhazmat.2008.05.045

Hassan, M. A., Khalil, A., Kaseb, S., & Kassem, M. A. (2017). Exploring the potential of tree-based ensemble methods in solar radiation modeling. *Applied Energy*, *203*, 897-916. https://doi.org/https://doi.org/10.1016/j.apenergy.2017.06.104

Hastie, T., Tibshirani, R., Friedman, J. H., & Friedman, J. H. (2009). *The elements of statistical learning: data mining, inference, and prediction* (Vol. 2). Springer.

Hong, G., B., & Yang, J., X. (2017). Dye removal using the solid residues from Glossogyne tenuifolia based on response surface methodology. *Journal of Molecular Liquids*, *242*, 82-90. https://doi.org/http://10.1016/j.molliq.2017.07.007

Hu, Z., Ding, Y., Shao, Y., Cai, L., Jin, Z., Liu, Z., Zhao, J., Li, F., Pan, Z., Li, X., & Zhao, J. (2021). Banana peel biochar with nanoflake-assembled structure for cross contamination treatment in water: Interaction behaviors between lead and tetracycline. *Chemical Engineering Journal*, *420*. https://doi.org/10.1016/j.cej.2021.129807

Ibrahim, F. M., Najeeb, D. A., & ThamerSadeq, H. (2023). Green preparation of Cu nanoparticles of the avocado seed extract as an adsorbent surface. *Materials Science for Energy Technologies*, *6*, 130-136. https://doi.org/10.1016/j.mset.2022.12.006

Iheanacho, O., Nwabanne, J., Obi, C., & Onu, C. (2021). Packed bed column adsorption of phenol onto corn cob activated carbon: linear and nonlinear kinetics modeling. *South African Journal of Chemical Engineering*, *36*, 80-93. https://doi.org/10.1016/j.sajce.2021.02.003

Imad Rabichi, Kawtar Ezzahi, Fatima Ezzahra Yaacoubi, Zaina Izghri, Karima Ennaciri, Abdelaziz Ounas, Abdelrani Yaacoubi, Abdelaziz Baçaoui, Mohamed Hafidi, & Fels, L. E. (2025). Evaluating the fixed-bed column adsorption capacity of olive pomace biochar activated with KOH and H3PO4 for olive mill wastewater treatment: Insights from TOC and HPLC analysis. *Chemosphere*, *377*(144356). https://doi.org/https://doi.org/10.1016/j.chemosphere.2025.14435610.1016/j.chemosphere.2025.144356

Inglezakis, V. J., Kudarova, A., Guney, A., Kinayat, N., & Tauanov, Z. (2023). Efficient mercury removal from water by using modified natural zeolites and comparison to commercial adsorbents. *Sustainable Chemistry and Pharmacy*, *32*. https://doi.org/10.1016/j.scp.2023.101017

Inyinbor, A. A., Bankole, D. T., Adekola, F. A., Bello, O. S., Oreofe, T., Amone, K., & Lukman, A. F. (2023). Chemometrics validation of adsorption process economy: Case study of acetaminophen removal onto quail eggshell adsorbents. *Scientific African*, *19*. https://doi.org/10.1016/j.sciaf.2022.e01471

Ismail, M. S., Yahya, M. D., Auta, M., & Obayomi, K. S. (2022). Facile preparation of amine -functionalized corn husk derived activated carbon for effective removal of selected heavy metals from battery recycling wastewater. *Heliyon*, *8*(5), e09516. https://doi.org/10.1016/j.heliyon.2022.e09516

Ismail, U. M., Onaizi, S. A., & Vohra, M. S. (2024). Crystal violet removal using ZIF-60: Batch adsorption studies, mechanistic & machine learning modeling. *Environmental Technology & Innovation*, *33*. https://doi.org/10.1016/j.eti.2023.103456

Iwar, R. T., Ogedengbe, K., Katibi, K. K., & Oshido, L. E. (2021). Meso-microporous activated carbon derived from Raffia palm shells: optimization of synthesis conditions using response surface methodology. *Heliyon*, *7*(6), e07301. https://doi.org/10.1016/j.heliyon.2021.e07301

Jabar, J., Odusote, Y., Ayinde, Y., & Yılmaz, M. (2022). African almond (Terminalia catappa L) leaves biochar prepared through pyrolysis using H3PO4 as chemical activator for sequestration of methylene blue dye. *Results in Engineering*, *14*. https://doi.org/10.1016/j.rineng.2022.100385

Jabar, J. M., Adebayo, M. A., Owokotomo, I. A., Odusote, Y. A., & Yilmaz, M. (2022). Synthesis of high surface area mesoporous ZnCl(2)-activated cocoa (Theobroma cacao L) leaves biochar derived via pyrolysis for crystal violet dye removal. *Heliyon*, *8*(10), e10873. https://doi.org/10.1016/j.heliyon.2022.e10873

Jasri, K., Abdulhameed, A. S., Jawad, A. H., Alothman, Z. A., Yousef, T. A., & Al Duaij, O. K. (2023). Mesoporous activated carbon produced from mixed wastes of oil palm frond and palm kernel shell using microwave radiation-assisted K2CO3 activation for methylene blue dye removal: Optimization by response surface methodology. *Diamond and Related Materials*, *131*. https://doi.org/10.1016/j.diamond.2022.109581

Jiang, F., Cao, D., Hu, S., Wang, Y., Zhang, Y., Huang, X., ZHao, H., Wu, C., Li, J., Ding, Y., & Liu, K. (2022). High-pressure carbon dioxide-hydrothermal enhance

yield and methylene blue adsorption performance of banana pseudo-stem activated carbon. *Bioresource Technology*, *354*(127137). https://doi.org/https://doi.ord/10.1016/j.biotech.2022.127137

Jiang, W., Zhang, L., Guo, X., Yang, M., Lu, Y., Wang, Y., Zheng, Y., & Wei, G. (2021). Adsorption of cationic dye from water using an iron oxide/activated carbon magnetic composites prepared from sugarcane bagasse by microwave method. *Environ Technol*, *42*(3), 337-350. https://doi.org/10.1080/09593330.2019.1627425

Jiao, G. J., Ma, J., Li, Y., Jin, D., Ali, Z., Zhou, J., & Sun, R. (2021). Recent advances and challenges on removal and recycling of phosphate from wastewater using biomass-derived adsorbents. *Chemosphere*, *278*, 130377. https://doi.org/10.1016/j.chemosphere.2021.130377

Jjagwe, J., Olupot, P. W., Menya, E., & Kalibbala, H. M. (2021). Synthesis and Application of Granular Activated Carbon from Biomass Waste Materials for Water Treatment: A Review. *Journal of Bioresources and Bioproducts*, *6*(4), 292-322. https://doi.org/10.1016/j.jobab.2021.03.003

Jorge, A. M. S., Athira, K. K., Alves, M. B., Gardas, R. L., & Pereira, J. F. B. (2023). Textile dyes effluents: A current scenario and the use of aqueous biphasic systems for the recovery of dyes. *Journal of Water Process Engineering*, *55*. https://doi.org/10.1016/j.jwpe.2023.104125

Kabiru Bello, B. K. S., Badiadka Narayana, Anjali Rao, & Byrappa., K. (2018). A study on adsorption behavior of newly synthesized banana pseudo-stem derived superabsorbent hydrogels for cationic and anionic dye removal from effluents. *Carbohydr Polym*, *181*, 605-615. https://doi.org/https://doi.org/10.1016/j.carbpol.2017.11.106

Kaewtrakulchai, N., Chanpee, S., Pasee, W., Putta, A., Chutipaijit, S., Kaewpanha, M., Suriwong, T., Puengjinda, P., Panomsuwan, G., Fuji, M., & Eiad-ua, A. (2024). Valorization of horse manure conversion to magnetic carbon nanofiber for dye adsorption by hydrothermal treatment coupled with carbonization. *Case Studies in Chemical and Environmental Engineering*, *9*. https://doi.org/10.1016/j.cscee.2023.100563

Karaman, C., Karaman, O., Show, P. L., Karimi-Maleh, H., & Zare, N. (2021). Congo red dye removal from aqueous environment by cationic surfactant modified-biomass derived carbon: Equilibrium, kinetic, and thermodynamic modeling, and forecasting via artificial neural network approach. *Chemosphere*, *290*, 133346. https://doi.org/10.1016/j.chemosphere.2021.133346

Keikavousi Behbahan, A., Mahdavi, V., Roustaei, Z., & Bagheri, H. (2021). Preparation and evaluation of various banana-based biochars together with ultra-high performance liquid chromatography-tandem mass spectrometry for determination of diverse pesticides in fruiting vegetables. *Food Chem*, *360*, 130085. https://doi.org/10.1016/j.foodchem.2021.130085

Khamwichit, A., Dechapanya, W., & Dechapanya, W. (2022). Adsorption kinetics and isotherms of binary metal ion aqueous solution using untreated venus shell. *Heliyon*, *8*(6), e09610. https://doi.org/10.1016/j.heliyon.2022.e09610

Khan, M., Din, I., Aziz, F., Qureshi, I. U., Zahid, M., Mustafa, G., Sher, A., & Hakim, S. (2023a). Chromium adsorption from water using mesoporous magnetic iron oxide-aluminum silicate adsorbent: An investigation of adsorption isotherms and kinetics. *Current Research in Green and Sustainable Chemistry*, *7*. https://doi.org/10.1016/j.crgsc.2023.100368

Khan, M., Din, I., Aziz, F., Qureshi, I. U., Zahid, M., Mustafa, G., Sher, A., & Hakim, S. (2023b). Chromium adsorption from water using mesoporous magnetic iron oxide-aluminum silicate adsorbent: An investigation of adsorption isotherms and kinetics. *Current Research in Green and Sustainable Chemistry*. https://doi.org/10.1016/j.crgsc.2023.100368

Khan, T., Nouman, M., Dua, D., Khan, S., & Alharthi, S. (2022). Adsorptive scavenging of cationic dyes from aquatic phase by H3PO4 activated Indian jujube (Ziziphus mauritiana) seeds based activated carbon: Isotherm, kinetics, and thermodynamic study. *Journal of Saudi Chemical Society*, *26*(2). https://doi.org/10.1016/j.jscs.2021.101417

Khiam, G., Karri, R., Mubarak, N., Khalid, M., Walvekar, R., Abdullah, E., & Rahman, M. (2022). Modelling and optimization for methylene blue adsorption using graphene oxide/chitosan composites via artificial neural network-particle swarm optimization. *Materials Today Chemistry*, *24*. https://doi.org/10.1016/j.mtchem.2022.100946

Kiani Ghaleh sardi, F., Behpour, M., Ramezani, Z., & Masoum, S. (2021). Simultaneous removal of Basic Blue41 and Basic Red46 dyes in binary aqueous systems via activated carbon from palm bio-waste: Optimization by central composite design, equilibrium, kinetic, and thermodynamic studies. *Environmental Technology & Innovation*, *24*. https://doi.org/10.1016/j.eti.2021.102039

Kooh, M. R. R., Thotagamuge, R., Chou Chau, Y.-F., Mahadi, A. H., & Lim, C. M. (2022). Machine learning approaches to predict adsorption capacity of Azolla pinnata in the removal of methylene blue. *Journal of the Taiwan Institute of Chemical Engineers*, *132*. https://doi.org/10.1016/j.jtice.2021.11.001

Kumar, A., & Gupta, H. (2020). Activated carbon from sawdust for naphthalene removal from contaminated water. *Environmental Technology & Innovation*, *20*. https://doi.org/10.1016/j.eti.2020.101080

Kumar, V., Sharma, N., Panneerselvam, B., Dasarahally Huligowda, L. K., Umesh, M., Gupta, M., Muzammil, K., Zahrani, Y., & Malmutheibi, M. (2024). Lignocellulosic biomass for biochar production: A green initiative on biowaste conversion for pharmaceutical and other emerging pollutant removal. *Chemosphere*, *360*, 142312. https://doi.org/10.1016/j.chemosphere.2024.142312

Kumari, S., Verma, A., Sharma, P., Agarwal, S., Rajput, V. D., Minkina, T., Rajput, P., Singh, S. P., & Garg, M. C. (2023). Introducing machine learning model to response surface methodology for biosorption of methylene blue dye using

Triticum aestivum biomass. *Sci Rep*, *13*(1), 8574. https://doi.org/10.1038/s41598-023-35645-z

Lee, E.-H., Moon, S. Y., & Lee, S.-W. (2021). Removal of bovine serum albumin and methylene blue using a hybrid membrane of single walled carbon nanotube-banana peel protein: Fabrication and characterization. *Environmental Technology & Innovation*, *24*. https://doi.org/10.1016/j.eti.2021.101880

Leite, A., Saucier, C., Lima, E., Dos Reis, G., Umpierres, C., Mello, B., Shirmardi, M., Dias, S., & Sampaio, C. (2018a). Activated carbons from avocado seed: optimisation and application for removal of several emerging organic compounds. *Environ Sci Pollut Res Int*, *25*(8), 7647-7661. https://doi.org/10.1007/s11356-017-1105-9

Leite, A., Saucier, C., Lima, E., Dos Reis, G., Umpierres, C., Mello, B., Shirmardi, M., Dias, S., & Sampaio, C. (2018b). Activated carbons from avocado seed: optimisation and application for removal of several emerging organic compounds. *Environmental Science and Pollution Research*, *25*(8), 7647-7661. https://doi.org/10.1007/s11356-017-1105-9

Leite, A. J. B., Sophia, A. C., Diasa, S. L. P., Thue, P. S., Reis, G. S., Lima, E. C., Vaghettia, J. C. P., Pavan, F. A., & Alencar, W. S. (2017). Activated carbon from avocado seeds for the removal of phenolic compounds from aqueous solutions. *Desalination and Water Treatment*, *71*, 168–181. https://doi.org/10.5004/dwt.2017.20540

Li, H., Cao, X., Zhang, C., Yu, Q., Zhao, Z., Niu, X., Sun, X., Liu, Y., Ma, L., & Li, Z. (2017). Enhanced adsorptive removal of anionic and cationic dyes from single or mixed dye solutions using MOF PCN-222. *RSC Advances*, *7*(27), 16273-16281. https://doi.org/10.1039/c7ra01647f

Liu, C., Ngo, H., Guo, W., & Tung, K. (2012). Optimal conditions for preparation of banana peels, sugarcane bagasse and watermelon rind in removing copper from water. *Bioresoure Technology*, *119*, 349-354. https://doi.org/10.1016/j.biortech.2012.06.004

Liu, C., Ngo, H. H., Guo, W., & Tung, K. L. (2012). Optimal conditions for preparation of banana peels, sugarcane bagasse and watermelon rind in removing copper from water. *Bioresour Technol*, *119*, 349-354. https://doi.org/10.1016/j.biortech.2012.06.004

Liu, X.-J., Li, M.-F., & Singh, S. K. (2021). Manganese-modified lignin biochar as adsorbent for removal of methylene blue. *Journal of Materials Research and Technology*, *12*, 1434-1445. https://doi.org/10.1016/j.jmrt.2021.03.076

Liu, X., Peng, L., Deng, P., Xu, Y., Wang, P., Tan, Q., Zhang, C., & Dai, X. (2025). Co-hydrothermal carbonization of sewage sludge and rice straw to improve hydrochar quality: Effects of mixing ratio and hydrothermal temperature. *Bioresour Technol*, *415*, 131665. https://doi.org/10.1016/j.biortech.2024.131665

Longchar, I. T., Kumar, S., Umdor, R. S., Sharma, S., Bora, P., & Sinha, D. (2024). Evaluation of a novel activated carbon/graphene oxide as an efficient composite

adsorbent for the removal of herbicide 2,4-Dichlorophenoxyacetic acid: Adsorption isotherm and kinetics study. *Journal of Molecular Liquids*, *415*. https://doi.org/10.1016/j.molliq.2024.126406

M. Arias, E. López, A. Nuñez, D. Rubinos, B. Soto, M. T. Barral, & Díaz-Fierros, F. (1999). *Adsorption of Methylene Blue by Red Mud, An Oxide- Rich Byproduct of Bauxite Refining*. Springer, Boston, MA. https://doi.org/https://doi.org/10.1007/978-1-4615-4683-2_39

Ma, X., Xu, W., Su, R., Shao, L., Zeng, Z., Li, L., & Wang, H. (2023). Insights into CO2 capture in porous carbons from machine learning, experiments and molecular simulation. *Separation and Purification Technology*, *306*. https://doi.org/10.1016/j.seppur.2022.122521

Mahalaxmi, S., & Kumar, P. S. (2024). Hydrothermal carbonization of muskmelon exocarp for enhanced dye removal from an aqueous solution: A sustainable approach. *Desalination and Water Treatment*, *317*. https://doi.org/10.1016/j.dwt.2024.100259

Mahato, R. K., Kumar, D., & Rajagopalan, G. (2020). Biohydrogen production from fruit waste by Clostridium strain BOH3 *Renewable Energy*, *153*, 1368-1377. https://doi.org/https://doi.org/10.1016/j.renene.2020.02.092

Maheshwari, U., Thakur, R. V., Deshpande, D., & Ghodke, S. (2023). Efficiency evaluation of orange and banana peels for dye removal from synthetic industrial effluent. *Materials Today: Proceedings*, *76*, 170-176. https://doi.org/10.1016/j.matpr.2022.11.023

Mahmood Al-Nuaimy, M. N., Azizi, N., Nural, Y., & Yabalak, E. (2023). Recent advances in environmental and agricultural applications of hydrochars: A review. *Environ Res*, *250*, 117923. https://doi.org/10.1016/j.envres.2023.117923

Mbarki, F., Selmi, T., Kesraoui, A., & Seffen, M. (2022). Low-cost activated carbon preparation from Corn stigmata fibers chemically activated using H3PO4, ZnCl2 and KOH: Study of methylene blue adsorption, stochastic isotherm and fractal kinetic. *Industrial Crops and Products*, *178*. https://doi.org/10.1016/j.indcrop.2022.114546

Mehmandost, N., Goudarzi, N., Arab Chamjangali, M., & Bagherian, G. (2022). Application of random forest for modeling batch and continuous fixed-bed removal of crystal violet from aqueous solutions using Gypsophila aretioides stem-based biosorbent. *Spectrochim Acta A Mol Biomol Spectrosc*, *265*, 120292. https://doi.org/10.1016/j.saa.2021.120292

Mehmandost, N., Goudarzi, N., Arab Chamjangali, M., & Bagherian, G. (2023). Application of chemometrics tools for removal of crystal violet and methylene blue in binary solution by eco-friendly magnetic adsorbent modified on Heracleum persicum waste. *Spectrochim Acta A Mol Biomol Spectrosc*, *292*, 122415. https://doi.org/10.1016/j.saa.2023.122415

Misran, E., Bani, O., Situmeang, E., & Purba, A. (2021). Banana stem based activated carbon as a low-cost adsorbent for methylene blue removal: Isotherm, kinetics,

and reusability. *Alexandria Engineering Journal*. https://doi.org/https://doi.org/10.1016/j.aej.2021.07.022

Misran, E., Bani, O., Situmeang, E. M., & Purba, A. S. (2022). Banana stem based activated carbon as a low-cost adsorbent for methylene blue removal: Isotherm, kinetics, and reusability. *Alexandria Engineering Journal*, *61*(3), 1946-1955. https://doi.org/10.1016/j.aej.2021.07.022

Mohd Hanafiah, Z., Azmi, A. R., Ilham, Z., Wan Mohtar, W. H. M., Abdul Halim-Lim, S., Nafisyah, A. L., Show, P.-L., & Wan-Mohtar, W. A. A. Q. I. (2024). Treatment of the Textile Wastewater using Malaysian Ganoderma lucidum Mycelial Pellets. *Sains Malaysiana*, *53*(7), 1645-1660. https://doi.org/10.17576/jsm-2024-5307-13

Muhamad, N., Soontornnon Sinchai, P., & Tansom, U. (2023). Banana peel as bioremediation agent in textile dyes decolorization for wastewater management. *Biochemical Systematics and Ecology*, *106*. https://doi.org/10.1016/j.bse.2022.104582

Mujtaba, M., Fernandes Fraceto, L., Fazeli, M., Mukherjee, S., Savassa, S. M., Araujo de Medeiros, G., do Espírito Santo Pereira, A., Mancini, S. D., Lipponen, J., & Vilaplana, F. (2023). Lignocellulosic biomass from agricultural waste to the circular economy: a review with focus on biofuels, biocomposites and bioplastics. *Journal of Cleaner Production*, *402*. https://doi.org/10.1016/j.jclepro.2023.136815

Mukkanti, V. B., & Tembhurkar, A. R. (2021). Defluoridation of water using adsorbent derived from the Labeo rohita (rohu) fish scales waste: Optimization, isotherms, kinetics, and thermodynamic study. *Sustainable Chemistry and Pharmacy*, *23*. https://doi.org/10.1016/j.scp.2021.100520

Munagapati, V., Yarramuthi, V., Kim, Y., Lee, K., & Kim, D. (2018). Removal of anionic dyes (Reactive Black 5 and Congo Red) from aqueous solutions using Banana Peel Powder as an adsorbent. *Ecotoxicology and Environmental Safety*, *148*, 601-607. https://doi.org/https://doi.org/10.1016/j.ecoenv.2017.10.075

Munagapati, V. S., Yarramuthi, V., Kim, Y., Lee, K. M., & Kim, D. S. (2018). Removal of anionic dyes (Reactive Black 5 and Congo Red) from aqueous solutions using Banana Peel Powder as an adsorbent. *Ecotoxicol Environ Saf*, *148*, 601-607. https://doi.org/10.1016/j.ecoenv.2017.10.075

Munonde, T. S., Nqombolo, A., Hobongwana, S., Mpupa, A., & Nomngongo, P. N. (2023). Removal of methylene blue using MnO(2)@rGO nanocomposite from textile wastewater: Isotherms, kinetics and thermodynamics studies. *Heliyon*, *9*(4), e15502. https://doi.org/10.1016/j.heliyon.2023.e15502

Muñoz, L. L. D., Bonilla, P. H., & E.Reynel, Á., D, I. Mendoza, Castillo. (2016). Sorption of heavy metal ions from aqueous solution using acid-treated avocado kernel seeds and its FTIR spectroscopy characterization. *Journal of Molecular Liquids*(215), 555-564.

Murugesan, K., Tareke, K., Gezehegn, M., Kebede, M., Yazie, A., & Diyana, G. (2019). Rapid Development of Activated Carbon and ZnO Nanoparticles via Green Waste

Conversion Using Avocado Fruit Peel Powder and its High Performance Efficiency in Aqueous Dye Removal Application. *Journal of Inorganic and Organometallic Polymers and Materials*, *29*(4), 1368-1374. https://doi.org/10.1007/s10904-019-01101-7

Nallapan Maniyam, M., Hari, M., & Yaacob, N. S. (2020). Enhanced methylene blue decolourization by Rhodococcus strain UCC 0003 grown in banana peel agricultural waste through response surface methodology. *Biocatalysis and Agricultural Biotechnology*, *23*. https://doi.org/10.1016/j.bcab.2019.101486

Negrete, M. A. S., Ávila, H. E. R., Castillo, D. I. M., Petriciolet, A. B., & Valle, C. J. D. (2018). Water defluoridation with avocado-based adsorbents: Synthesis, physicochemical characterization and thermodynamic studies. *Journal of Molecular Liquids*. https://doi.org/10.1016/j.molliq.2018.01.084

Neolaka, Y. A. B., Riwu, A. A. P., Aigbe, U. O., Ukhurebor, K. E., Onyancha, R. B., Darmokoesoemo, H., & Kusuma, H. S. (2023). Potential of activated carbon from various sources as a low-cost adsorbent to remove heavy metals and synthetic dyes. *Results in Chemistry*, *5*. https://doi.org/10.1016/j.rechem.2022.100711

Nguyen, D., Zhao, W., Mäkelä, M., Alwahabi, Z. T., & Kwong, C. W. (2022). Effect of hydrothermal carbonisation temperature on the ignition properties of grape marc hydrochar fuels. *Fuel*, *313*. https://doi.org/10.1016/j.fuel.2021.122668

Nipa, S. T., Shefa, N. R., Parvin, S., Khatun, M. A., Alam, M. J., Chowdhury, S., Khan, M. A. R., Shawon, S. M. A. Z., Biswas, B. K., & Rahman, M. W. (2023). Adsorption of methylene blue on papaya bark fiber: Equilibrium, isotherm and kinetic perspectives. *Results in Engineering*, *17*. https://doi.org/10.1016/j.rineng.2022.100857

Nwabanne, J., Iheanacho, O., Obi, C., & Onu, C. (2022). Linear and nonlinear kinetics analysis and adsorption characteristics of packed bed column for phenol removal using rice husk-activated carbon. *Applied Water Science*, *12*(5). https://doi.org/10.1007/s13201-022-01635-1

Nyakang'i, C. O., Ebere, R., Marete, E., & Arimi, J. M. (2023). Avocado production in Kenya in relation to the world, Avocado by-products (seeds and peels) functionality and utilization in food products. *Applied Food Research*, *3*(1). https://doi.org/10.1016/j.afres.2023.100275

Obayomi, K., & Auta, M. (2019). Development of microporous activated Aloji clay for adsorption of lead (II) ions from aqueous solution. *Heliyon*, *5*(11), e02799. https://doi.org/10.1016/j.heliyon.2019.e02799

Obele, C., Ejimofor, M., Atuanya, C., & Ibenta, M. (2021). Cassava stem cellulose (CSC)Nanocrystal for optimal methylene BlueBio sorption with response surface design. *Current Research in Green and Sustainable Chemistry*, *4*(100067). https://doi.org/https://doi.org/10.1016/j.crgsc.2021.100067

Oladoye, P. O., Ajiboye, T. O., Omotola, E. O., & Oyewola, O. J. (2022). Methylene blue dye: Toxicity and potential elimination technology from wastewater. *Results in Engineering*, *16*. https://doi.org/10.1016/j.rineng.2022.100678

Oluwasina, O. O., Demehin, B. F., Awolu, O. O., & Igbe, F. O. (2020). Optimization of starch-based candy supplemented with date palm (Phoenix dactylifera) and tamarind (Tamarindus indica L.). *Arabian Journal of Chemistry*, *13*(11), 8039-8050. https://doi.org/10.1016/j.arabjc.2020.09.033

Ozdemir, N. C., Bilici, Z., Yabalak, E., Dizge, N., Balakrishnan, D., Khoo, K. S., & Show, P. L. (2023). Physico-chemical adsorption of cationic dyes using adsorbent synthesis via hydrochloric acid treatment and subcritical method from palm leaf biomass waste. *Chemosphere*, *339*, 139558. https://doi.org/10.1016/j.chemosphere.2023.139558

Pakalapati, H., Show, P., L., Chang, J., Liu, B., L., & Chang, Y., K. (2020). Removal of dye waste by weak cation-exchange nanofiber membrane immobilized with waste egg white proteins. *International Journal of Biological Macromolecules*, *165*, 2494-2507. https://doi.org/https://10.1016/j.ijbiomac.2020.10.099

Pandharipande, S., & Deshpande, R. (2013). Synthesis & Effectiveness Study Of Banana Peel Adsorbent & Artificial Neural Network Modeling In Removal Of Cu (II) Ions From Aqueous Solution. *Journal of Engineering Research and Applications*, *3*(6), 730-734.

Pandiarajan, A., Kamaraj, R., Vasudevan, S., & Vasudevan, S. (2018). OPAC (orange peel activated carbon) derived from waste orange peel for the adsorption of chlorophenoxyacetic acid herbicides from water: Adsorption isotherm, kinetic modelling and thermodynamic studies. *Bioresour Technol*, *261*, 329-341. https://doi.org/10.1016/j.biortech.2018.04.005

Patra, C., Suganya, E., Sivaprakasam, S., Krishnamoorthy, G., & Narayanasamy, S. (2021). A detailed insight on fabricated porous chitosan in eliminating synthetic anionic dyes from single and multi-adsorptive systems with related studies. *Chemosphere*, *281*, 130706. https://doi.org/10.1016/j.chemosphere.2021.130706

Pauletto, P. S., Moreno-Perez, J., Hernandez-Hernandez, L. E., Bonilla-Petriciolet, A., Dotto, G. L., & Salau, N. P. G. (2021). Novel biochar and hydrochar for the adsorption of 2-nitrophenol from aqueous solutions: An approach using the PVSDM model. *Chemosphere*, *269*, 128748. https://doi.org/10.1016/j.chemosphere.2020.128748

Peng, W., & Karimi Sadaghiani, O. (2023). Enhancement of quality and quantity of woody biomass produced in forests using machine learning algorithms. *Biomass and Bioenergy*, *175*. https://doi.org/10.1016/j.biombioe.2023.106884

Phonlam, T., Weerasuk, B., Sataman, P., Duangmanee, T., Thongphanit, S., Nilgumhang, K., Anantachaisilp, S., Chutimasakul, T., Kwamman, T., & Chobpattana, V. (2023). Ammonia modification of activated carbon derived from biomass via gamma irradiation vs. hydrothermal method for methylene blue removal. *South African Journal of Chemical Engineering*, *43*, 67-78. https://doi.org/10.1016/j.sajce.2022.10.004

Phouthavong, V., Hagio, T., Park, J.-H., Nijpanich, S., Srihirunthanon, T., Chantanurak, N., Duangkhai, K., Rujiravanit, R., Chounlamany, V., Phomkeona, K., Kong, L., Li, L., & Ichino, R. (2023). Utilization of Agricultural Waste to Herbicide

Removal: Magnetic BEA Zeolite Adsorbents Prepared by Dry-Gel Conversion Using Rice Husk Ash–Derived SiO2 for Paraquat Removal. *Arabian Journal of Chemistry*. https://doi.org/10.1016/j.arabjc.2023.104959

Pocha, C., Chia, S., Chia, W., Koyande, A., Nomanbhay, S., & Chew, K. (2022). Utilization of agricultural lignocellulosic wastes for biofuels and green diesel production. *Chemosphere*, *290*(133246). https://doi.org/https://doi.org/10.1016/j.chemosphere.2021.133246

Postai, D. L., Demarchi, C. A., Zanatta, F., Melo, D. C. C., & Rodrigues, C. A. (2016). Adsorption of rhodamine B and methylene blue dyes using waste of seeds of Aleurites Moluccana, a low cost adsorbent. *Alexandria Engineering Journal*, *55*(2), 1713-1723. https://doi.org/10.1016/j.aej.2016.03.017

Prabakaran, E., Pillay, K., & Brink, H. (2022). Hydrothermal synthesis of magnetic-biochar nanocomposite derived from avocado peel and its performance as an adsorbent for the removal of methylene blue from wastewater. *Materials Today Sustainability*, *18*. https://doi.org/10.1016/j.mtsust.2022.100123

Prastuti, O., Septiani, E., Kurniati, Y., Widiyastuti, & Setyawan, H. (2019). Banana Peel Activated Carbon in Removal of Dyes and Metals Ion in Textile Industrial Waste. *Materials Science Forum*, *966*, 204-209. https://doi.org/10.4028/www.scientific.net/MSF.966.204

Qu, J., Che, N., Niu, G., Liu, L., Li, C., & Liu, Y. (2023). Iron/manganese binary metal oxide-biochar nano-composites with high adsorption capacities of Cd2+: Preparation and adsorption mechanisms. *Journal of Water Process Engineering*, *51*. https://doi.org/10.1016/j.jwpe.2022.103332

Rainert, K. T., Nunes, H. C. A., Gonçalves, M. J., Helm, C. V., & Tavares, L. B. B. (2021). Decolorization of the synthetic dye Remazol Brilliant Blue Reactive (RBBR) by Ganoderma lucidum on bio-adsorbent of the solid bleached sulfate paperboard coated with polyethylene terephthalate. *Journal of Environmental Chemical Engineering*, *9*(2). https://doi.org/10.1016/j.jece.2020.104990

Raji, Y., Nadi, A., Mechnou, I., Saadouni, M., Cherkaoui, O., & Zyade, S. (2023). High adsorption capacities of crystal violet dye by low-cost activated carbon prepared from Moroccan Moringa oleifera wastes: Characterization, adsorption and mechanism study. *Diamond and Related Materials*, *135*. https://doi.org/10.1016/j.diamond.2023.109834

Rajoriya, S., Saharan, V. K., Pundir, A. S., Nigam, M., & Roy, K. (2021). Adsorption of methyl red dye from aqueous solution onto eggshell waste material: Kinetics, isotherms and thermodynamic studies. *Current Research in Green and Sustainable Chemistry*, *4*. https://doi.org/10.1016/j.crgsc.2021.100180

Ramalingam, G., Priya, A. K., Gnanasekaran, L., Rajendran, S., & Hoang, T. K. A. (2024). Biomass and waste derived silica, activated carbon and ammonia-based materials for energy-related applications – A review. *Fuel*, *355*. https://doi.org/10.1016/j.fuel.2023.129490

Ramutshatsha-Makhwedzha, D., Mavhungu, A., Moropeng, M. L., & Mbaya, R. (2022). Activated carbon derived from waste orange and lemon peels for the adsorption of methyl orange and methylene blue dyes from wastewater. *Heliyon*, *8*(8), e09930. https://doi.org/10.1016/j.heliyon.2022.e09930

Ranasinghe, S. H., Navaratne, A. N., & Priyantha, N. (2018). Enhancement of Adsorption Characteristics of Cr(III) and Ni(II) by Surface Modification of Jackfruit Peel Biosorbent. *Journal of Environmental Chemical Engineering*. https://doi.org/10.1016/j.jece.2018.08.058

Rangel, A. V., Becerra, M. G., Guerrero-Amaya, H., Ballesteros, L. M., & Mercado, D. F. (2021). Sulfate radical anion activated agro-industrial residues for Cr(VI) adsorption: is this activation process technically and economically feasible? *Journal of Cleaner Production*, *289*. https://doi.org/10.1016/j.jclepro.2021.125793

Raninga, M., Mudgal, A., Patel, V. K., Patel, J., & Kumar Sinha, M. (2023). Modification of activated carbon-based adsorbent for removal of industrial dyes and heavy metals: A review. *Materials Today: Proceedings*, *77*, 286-294. https://doi.org/10.1016/j.matpr.2022.11.358

Reyes Molina, E. A., Park, S., Park, S., & Kelley, S. S. (2023). Effective toluene removal from aqueous solutions using fast pyrolysis-derived activated carbon from agricultural and forest residues: Isotherms and kinetics study. *Heliyon*, *9*(5), e15765. https://doi.org/10.1016/j.heliyon.2023.e15765

Rezk, M. Y., Zeitoun, M., El-Shazly, A. N., Omar, M. M., & Allam, N. K. (2019). Robust photoactive nanoadsorbents with antibacterial activity for the removal of dyes. *Journal of Hazardous Materials*, *378*, 120679. https://doi.org/https://10.1016/j.jhazmat.2019.05.072

Rima, S. A. J., Paul, G. K., Islam, S., Akhtar-E-Ekram, M., Zaman, S., Abu Saleh, M., & Salah Uddin, M. (2022). Efficacy of Pseudomonas sp. and Bacillus sp. in textile dye degradation: A combined study on molecular identification, growth optimization, and comparative degradation. *Journal of Hazardous Materials Letters*, *3*. https://doi.org/10.1016/j.hazl.2022.100068

Rodrigues, L. A., da Silva, M. L. C. P., Alvarez-Mendes, M. O., Coutinho, A. d. R., & Thim, G. P. (2011). Phenol removal from aqueous solution by activated carbon produced from avocado kernel seeds. *Chemical Engineering Journal*, *174*(1), 49-57. https://doi.org/10.1016/j.cej.2011.08.027

Rose, P. K., Poonia, V., Kumar, R., Kataria, N., Sharma, P., Lamba, J., & Bhattacharya, P. (2023). Congo red dye removal using modified banana leaves: Adsorption equilibrium, kinetics, and reusability analysis. *Groundwater for Sustainable Development*. https://doi.org/10.1016/j.gsd.2023.101005

Rosly, N. Z., Ishak, S., Abdullah, A. H., Kamarudin, M. A., Ashari, S. E., & Alang Ahmad, S. A. (2022). Fabrication and optimization calix[8]arene-PbS nanoadsorbents for the adsorption of methylene blue: Isotherms, kinetics and thermodynamics studies. *Journal of Saudi Chemical Society*, *26*(1). https://doi.org/10.1016/j.jscs.2021.101402

Roy, K., Dey, T. K., Jamal, M., Rathanasamy, R., Chinnasamy, M., & Uddin, M. E. (2023). Fabrication of graphene oxide–keratin–chitosan nanocomposite as an adsorbent to remove turbidity from tannery wastewater. *Water Science and Engineering*, *16*(2), 184-191. https://doi.org/10.1016/j.wse.2022.12.003

Roy, U., Sengupta, S., Banerjee, P., Das, P., Bhowal, A., & Datta, S. (2018). Assessment on the decolourization of textile dye (Reactive Yellow) using Pseudomonas sp. immobilized on fly ash: Response surface methodology optimization and toxicity evaluation. *J Environ Manage*, *223*, 185-195. https://doi.org/10.1016/j.jenvman.2018.06.026

Salah omer, A., A.El Naeem, G., Abd-Elhamid, A. I., O.M. Farahat, O., A. El-Bardan, A., M.A. Soliman, H., & Nayl, A. A. (2022). Adsorption of crystal violet and methylene blue dyes using a cellulose-based adsorbent from sugercane bagasse: characterization, kinetic and isotherm studies. *Journal of Materials Research and Technology*, *19*, 3241-3254. https://doi.org/10.1016/j.jmrt.2022.06.045

Salazar-Lópeza, N., J., Domínguez-Avila, J., A., Yahia, E., M., Belmonte-Herrera, B., H., Wall-Medrano, A., Montalvo-González, E., & González-Aguilar, G. A. (2020). Avocado fruit and by-products as potential sources of bioactive compounds. *Food Research International*, *138*(109774). https://doi.org/https://doi.org/10.1016/j.foodres.2020.109774

Salih, S. J., Abdul Kareem, A. S., & Anwer, S. S. (2022). Adsorption of anionic dyes from textile wastewater utilizing raw corncob. *Heliyon*, *8*(8), e10092. https://doi.org/10.1016/j.heliyon.2022.e10092

Salomón-Negrete, M. Á., Reynel-Ávila, H. E., Mendoza-Castillo, D. I., Bonilla-Petriciolet, A., & Duran-Valle, C. J. (2018). Water defluoridation with avocado-based adsorbents: Synthesis, physicochemical characterization and thermodynamic studies. *Journal of Molecular Liquids*, *254*, 188-197. https://doi.org/10.1016/j.molliq.2018.01.084

Salomón, Y. L. d. O., Georgin, J., Franco, D. S. P., Netto, M. S., Grassi, P., Piccilli, D. G. A., Oliveira, M. L. S., & Dotto, G. L. (2020). Powdered biosorbent from pecan pericarp (Carya illinoensis) as an efficient material to uptake methyl violet 2B from effluents in batch and column operations. *Advanced Powder Technology*, *31*(7), 2843-2852. https://doi.org/10.1016/j.apt.2020.05.004

Schadeck Netto, M., da Silva, N. F., Mallmann, E. S., Dotto, G. L., & Foletto, E. L. (2019). Effect of Salinity on the Adsorption Behavior of Methylene Blue onto Comminuted Raw Avocado Residue: CCD-RSM Design. *Water, Air, & Soil Pollution*, *230*(8). https://doi.org/10.1007/s11270-019-4230-x

Selimin, M. A., Latif, A. F. A., Er, Y. C., Muhamad, M. S., Basri, H., & Lee, T. C. (2022). Adsorption efficiency of banana blossom peels (musa acuminata colla) adsorbent for chromium (VI) removal. *Materials Today: Proceedings*, *57*, 1262-1268. https://doi.org/10.1016/j.matpr.2021.10.502

Sellaoui, L., Yazidi, A., Taamalli, S., Bonilla-Petriciolet, A., Louis, F., El Bakali, A., Badawi, M., Lima, E. C., Lima, D. R., & Chen, Z. (2021). Adsorption of 3-aminophenol and resorcinol on avocado seed activated carbon: Mathematical

modelling, thermodynamic study and description of adsorbent performance. *Journal of Molecular Liquids*, *342*. https://doi.org/10.1016/j.molliq.2021.116952

Seyyedi, K., & Jahromi, M. A. F. (2014). Decolorization of Azo Dye C.I. Direct Black 38 by Photocatalytic Method Using TiO2 and Optimizing of Process. *APCBEE Procedia*, *10*, 115-119. https://doi.org/10.1016/j.apcbee.2014.10.027

Shahrokhi-Shahraki, R., Benally, C., El-Din, M. G., & Park, J. (2021). High efficiency removal of heavy metals using tire-derived activated carbon vs commercial activated carbon: Insights into the adsorption mechanisms. *Chemosphere*, *264*(Pt 1), 128455. https://doi.org/10.1016/j.chemosphere.2020.128455

Shalaby, N. H., Ewais, E. M. M., Elsaadany, R. M., & Ahmed, A. (2016). Rice husk templated water treatment sludge as low cost dye and metal adsorbent. *Egyptian Journal of Petroleum*. https://doi.org/10.1016/j.ejpe.2016.10.006

Shelke, B. N., Jopale, M. K., & Kategaonkar, A. H. (2022). Exploration of biomass waste as low cost adsorbents for removal of methylene blue dye: A review. *Journal of the Indian Chemical Society*, *99*(7). https://doi.org/10.1016/j.jics.2022.100530

Shirzad-Siboni, M., Jafari, S. J., Giahi, O., Kim, I., Lee, S.-M., & Yang, J.-K. (2014). Removal of acid blue 113 and reactive black 5 dye from aqueous solutions by activated red mud. *Journal of Industrial and Engineering Chemistry*, *20*(4), 1432-1437. https://doi.org/10.1016/j.jiec.2013.07.028

Shukla, A. K., Alam, J., Mallik, S., Ruokolainen, J., Kesari, K. K., & Alhoshan, M. (2024). Optimization and prediction of dye adsorption utilising cross-linked chitosan-activated charcoal: Response Surface Methodology and machine learning. *Journal of Molecular Liquids*, *411*. https://doi.org/10.1016/j.molliq.2024.125745

Silva, M., Spessato, L., Silva, T., Lopes, G., Zanella, H., Yokoyama, J., Cazetta, A., & Almeida, V. (2021). H3PO4–activated carbon fibers of high surface area from banana tree pseudo-stem fibers: Adsorption studies of methylene blue dye in batch and fixed bed systems. *Journal of Molecular Liquids*, *324*. https://doi.org/https://10.1016/j.molliq.2020.114771

Silva, M. C., Spessato, L., Silva, T. L., Lopes, G. K. P., Zanella, H. G., Yokoyama, J. T. C., Cazetta, A. L., & Almeida, V. C. (2021). H3PO4–activated carbon fibers of high surface area from banana tree pseudo-stem fibers: Adsorption studies of methylene blue dye in batch and fixed bed systems. *Journal of Molecular Liquids*, *324*. https://doi.org/10.1016/j.molliq.2020.114771

Singh, L. (2017). Biodegradation of Synthetic Dyes: A Mycoremediation Approach for Degradation/Decolourization of Textile Dyes and Effluents. *Journal of Applied Biotechnology & Bioengineering*, *3*(5). https://doi.org/10.15406/jabb.2017.03.00081

Sivaranjanee, R., Kumar, P. S., & Rangasamy, G. (2024). Hydrothermally produced activated carbon spheres from discarded maize cobs for efficient removal of rose bengal dye from water environment. *Desalination and Water Treatment*, *317*. https://doi.org/10.1016/j.dwt.2024.100123

Skwierawska, A. M., Blizniewska, M., Muza, K., Nowak, A., Nowacka, D., Zehra Syeda, S. E., Khan, M. S., & Leska, B. (2022). Cellulose and its derivatives, coffee grounds, and cross-linked, beta-cyclodextrin in the race for the highest sorption capacity of cationic dyes in accordance with the principles of sustainable development. *J Hazard Mater*, *439*, 129588. https://doi.org/10.1016/j.jhazmat.2022.129588

Solayman, H. M., Hossen, M. A., Abd Aziz, A., Yahya, N. Y., Leong, K. H., Sim, L. C., Monir, M. U., & Zoh, K.-D. (2023). Performance evaluation of dye wastewater treatment technologies: A review. *Journal of Environmental Chemical Engineering*, *11*(3). https://doi.org/10.1016/j.jece.2023.109610

Song, C., Chen, K., Chen, M., Jin, X., Liu, G., Du, X., Chen, D., & Huang, Q. (2022). Sequential combined adsorption and solid-phase photocatalysis to remove aqueous organic pollutants by H3PO4-modified TiO2 nanoparticles anchored on biochar. *Journal of Water Process Engineering*, *45*. https://doi.org/10.1016/j.jwpe.2021.102467

Sridhar, A., Ponnuchamy, M., Kapoor, A., & Prabhakar, S. (2022). Valorization of food waste as adsorbents for toxic dye removal from contaminated waters: A review. *J Hazard Mater*, *424*(Pt B), 127432. https://doi.org/10.1016/j.jhazmat.2021.127432

Subbaiah Munagapati, V., Wen, H.-Y., Wen, J.-C., Gollakota, A. R. K., Shu, C.-M., & Mallikarjuna Reddy, G. (2021). Characterization of protonated amine modified lotus (Nelumbo nucifera) stem powder and its application in the removal of textile (Reactive Red 120) dye from liquid phase. *Journal of Molecular Liquids*, *338*. https://doi.org/10.1016/j.molliq.2021.116486

Sulaiman, N. S., Hashim, R., Amini, M. H. M., Danish, M., & Sulaiman, O. (2018). Optimization of activated carbon preparation from cassava stem using response surface methodology on surface area and yield. *Journal of Cleaner Production*. https://doi.org/10.1016/j.jclepro.2018.07.061

Sun, Y.-t., Chen, J.-d., Wei, Z.-h., Chen, Y.-k., Shao, C.-l., & Zhou, J.-f. (2023). Copper ion removal from aqueous media using banana peel biochar/Fe3O4/branched polyethyleneimine. *Colloids and Surfaces A: Physicochemical and Engineering Aspects*, *658*. https://doi.org/10.1016/j.colsurfa.2022.130736

Tamer, T., Omar, K., Amin, F., & Hany, A. (2020). Equilibrium and Kinetic Study on the Biosorption of Trypan Blue from Aqueous Solutions using Avocado Seed Powder. *Biointerface Research in Applied Chemistry*, *11*(3), 11042-11053. https://doi.org/10.33263/briac113.1104211053

Tang, Y., Lin, T., Jiang, C., Zhao, Y., & Ai, S. (2021). Renewable adsorbents from carboxylate-modified agro-forestry residues for efficient removal of methylene blue dye. *Journal of Physics and Chemistry of Solids*, *149*. https://doi.org/10.1016/j.jpcs.2020.109811

Telli, S., Ghodbane, H., Nessaibia, M., Jalgham, R., Boublia, A., Benguerba, Y., Ouksel, L., Maouche, N., & Khalfaoui, M. (2024). Remediation of cationic dye from aqueous solution through adsorption utilizing natural Haloxylon salicornicum: An

integrated experimental, physical statistics and molecular modeling investigation. *Journal of Molecular Liquids*, *411*. https://doi.org/10.1016/j.molliq.2024.125777

Temesgen, F., Gabbiye, N., & Sahu, O. (2018). Biosorption of reactive red dye (RRD) on activated surface of banana and orange peels: Economical alternative for textile effluent. *Surfaces and Interfaces*, *12*, 151-159. https://doi.org/10.1016/j.surfin.2018.04.007

Tharayil, J. M., & Chinnaiyan, P. (2024). Optimization of Malachite green adsorption using Palmyra Palm fibre-Derived Biochar: A central composite design approach. *Materials Today: Proceedings*. https://doi.org/10.1016/j.matpr.2024.05.151

Thomas, P., Wei Lai, C., & Rafie Johan, M. (2023). Biosynthesis of multifunctional Fe3O4/cocoa pod carbon composite and its versatile role as sonoadsorbent in triphenylmethane textile dye remediation and potential cathode material for energy storage applications. *Sustainable Energy Technologies and Assessments*, *56*. https://doi.org/10.1016/j.seta.2023.103102

Tshemese, S. J., Mhike, W., & Tichapondwa, S. M. (2021). Adsorption of phenol and chromium (VI) from aqueous solution using exfoliated graphite: Equilibrium, kinetics and thermodynamic studies. *Arabian Journal of Chemistry*, *14*(6). https://doi.org/10.1016/j.arabjc.2021.103160

Tuli, F. J., Hossain, A., Fazle Kibria, A. K. M., Tareq, A. R. M., Mamun, S. M. M. A., & Atique Ullah, A., K, M. (2020a). Removal of methylene blue from water by low-cost activated carbon prepared from tea waste_ A study of adsorption isotherm and kinetics. *Environmental Nanotechnology, Monitoring & Management*, *14*(100354).

Tuli, F. J., Hossain, A., Fazle Kibria, A. K. M., Tareq, A. R. M., Mamun, S. M. M. A., & Atique Ullah, A., K, M. (2020b). Removal of methylene blue from water by low-cost activated carbon prepared from tea waste_ A study of adsorption isotherm and kinetics *Environmental Nanotechnology, Monitoring & Management*, *14*(100354).

Typical IR Absorption Frequencies for Common Functional Groups. Northern Illinois University, Department of Chemistry. https://www.niu.edu/clas/chembio/research/analytical-lab/ftir/ir-frequencies-table.shtml

Ukpong, A. A., Asuquo, E. O., & Edekhe, G. I. (2023). The Adsorption Equilibrium and Kinetic Studies for The Removal of Crystal Violet Dye (Methyl Violet 6b) from Aqueous Solution Using Avocado Pear Seed Activated Carbon. *International Journal of Research and Scientific Innovation*, *X*(IV), 154-164. https://doi.org/10.51244/ijrsi.2023.10419

Ullah, S., Hussain, S., Sidra, Shah, N. A., Ahmad, W., & Akitsu, T. (2024). Graphene oxide and hydroxyapatite-based composite extracted from fish scales: Synthesis, characterization and water treatment application. *Journal of Molecular Liquids*. https://doi.org/10.1016/j.molliq.2024.126577

Van Thuan, T., Quynh, B. T. P., Nguyen, T. D., Ho, V. T. T., & Bach, L. G. (2017). Response surface methodology approach for optimization of Cu2+, Ni2+ and Pb2+ adsorption using KOH-activated carbon from banana peel. *Surfaces and Interfaces*, *6*, 209-217. https://doi.org/10.1016/j.surfin.2016.10.007

Vargas, M., Contreras, M., & Castro, E. (2020). Avocado-Derived Biomass as a Source of Bioenergy and Bioproducts. *Applied Sciences*, *10*(22). https://doi.org/10.3390/app10228195

Vasconcelos, K. C., Alencar, S. G., Ferro, A. B., Oliveira, L. F. A. M., Fonseca, E. J. S., Bernardo, V. B., Zanta, C. L. P. S., Duarte, J. L. S., & Oliveira, L. M. T. M. (2023). Novel kapok pods (Ceiba pentandra (l.) Gaerth) adsorbent and its reusability by transformation on hydrochar with an outstanding adsorptive capacity for Rhodamine B removal. *Separation and Purification Technology*, *326*. https://doi.org/10.1016/j.seppur.2023.124787

Vinayagam, R., Nagendran, V., Murugesan, G., Goveas, L. C., Varadavenkatesan, T., Samanth, A., & Selvaraj, R. (2024). In-situ one-pot synthesis, characterization of magnetic hydrochar and its application as Fenton-like catalyst for the degradation of methylene blue dye. *Materials Chemistry and Physics*, *317*. https://doi.org/10.1016/j.matchemphys.2024.129160

Waghmare, C., Ghodmare, S., Ansari, K., Dehghani, M. H., Amir Khan, M., Hasan, M. A., Islam, S., Khan, N. A., & Zahmatkesh, S. (2023). Experimental investigation of H(3)PO(4) activated papaya peels for methylene blue dye removal from aqueous solution: Evaluation on optimization, kinetics, isotherm, thermodynamics, and reusability studies. *J Environ Manage*, *345*, 118815. https://doi.org/10.1016/j.jenvman.2023.118815

Wan, S., Wu, J., Zhou, S., Wang, R., Gao, B., & He, F. (2018). Enhanced lead and cadmium removal using biochar-supported hydrated manganese oxide (HMO) nanoparticles: Behavior and mechanism. *Sci Total Environ*, *616-617*, 1298-1306. https://doi.org/10.1016/j.scitotenv.2017.10.188

Wang, D., Wang, L., Li, X., Zuo, J., & Cai, J. (2024). Adsorptive behavior of Rhodamine B dye over hierarchical N-doped carbons from hexamine-based complexes: Equilibrium and kinetics. *Journal of Molecular Liquids*, *414*. https://doi.org/10.1016/j.molliq.2024.126091

Wang, H. S.-H., & Yao, Y. (2023). Machine learning for sustainable development and applications of biomass and biomass-derived carbonaceous materials in water and agricultural systems: A review. *Resources, Conservation and Recycling*, *190*. https://doi.org/10.1016/j.resconrec.2022.106847

Wanja, N. E., Murungi, J., Wanjau, R., & Ali, A. H. (2016). Application of chemically modified avocado seed for removal of Copper (II), Lead(II), and Cadmium(II) ions from aqueous solutions. *International Journal of Research in Engineering and Applied Sciences*, *6*(8), 1-15.

Waqas, S., Harun, N. Y., Arshad, U., Laziz, A. M., Sow Mun, S. L., Bilad, M. R., Nordin, N. A. H., & Alsaadi, A. S. (2024). Optimization of operational parameters using

RSM, ANN, and SVM in membrane integrated with rotating biological contactor. *Chemosphere*, *349*, 140830. https://doi.org/10.1016/j.chemosphere.2023.140830

Watwe, V., Kulkarni, S., & Kulkarni, P. (2023). Development of dried uncharred leaves of Ficus benjamina as a novel adsorbent for cationic dyes: Kinetics, isotherm, and batch optimization. *Industrial Crops and Products*, *195*. https://doi.org/10.1016/j.indcrop.2023.116449

Xue, H., Wang, X., Xu, Q., Dhaouadi, F., Sellaoui, L., Seliem, M. K., Ben Lamine, A., Belmabrouk, H., Bajahzar, A., Bonilla-Petriciolet, A., Li, Z., & Li, Q. (2022). Adsorption of methylene blue from aqueous solution on activated carbons and composite prepared from an agricultural waste biomass: A comparative study by experimental and advanced modeling analysis. *Chemical Engineering Journal*, *430*. https://doi.org/10.1016/j.cej.2021.132801

Yan, M., Chen, F., Li, T., Zhong, L., Feng, H., Xu, Z., Hantoko, D., & Wibowo, H. (2023). Hydrothermal carbonization of food waste digestate solids: Effect of temperature and time on products characteristic and environmental evaluation. *Process Safety and Environmental Protection*, *178*, 296-308. https://doi.org/10.1016/j.psep.2023.08.010

Yaseen, D. A., & Scholz, M. (2018). Textile dye wastewater characteristics and constituents of synthetic effluents: a critical review. *International Journal of Environmental Science and Technology*, *16*(2), 1193-1226. https://doi.org/10.1007/s13762-018-2130-z

Ying, C. L., Jiang, L., Qunhui, Y., Hui, T., Feng, Y., & Xin, L. (2016). A green adsorbent derived from banana peel for highly effective removal of heavy metal ions from water. *the Royal Society of Chemistry*. https://doi.org/10.1039/C6RA07460J

Yu, D., Wang, L., & Wu, M. (2018). Simultaneous removal of dye and heavy metal by banana peels derived hierarchically porous carbons. *Journal of the Taiwan Institute of Chemical Engineers*, *93*, 543-553. https://doi.org/10.1016/j.jtice.2018.08.038

Yusuff, A. S., Ajayi, O. A., & Popoola, L. T. (2021). Application of Taguchi design approach to parametric optimization of adsorption of crystal violet dye by activated carbon from poultry litter. *Scientific African*, *13*. https://doi.org/10.1016/j.sciaf.2021.e00850

Yusuff, A. S., Popoola, L. T., & Igbafe, A. I. (2022). Response surface modeling and optimization of hexavalent chromium adsorption onto eucalyptus tree bark-derived pristine and chemically-modified biochar. *Chemical Engineering Research and Design*, *182*, 592-603. https://doi.org/10.1016/j.cherd.2022.04.007

Zafar, L., Khan, A., Kamran, U., Park, S.-J., & Bhatti, H. N. (2022). Eucalyptus (camaldulensis) bark-based composites for efficient Basic Blue 41 dye biosorption from aqueous stream: Kinetics, isothermal, and thermodynamic studies. *Surfaces and Interfaces*, *31*. https://doi.org/10.1016/j.surfin.2022.101897

Zagklis, D. P., Vavouraki, A. I., Kornaros, M. E., & Paraskeva, C. A. (2015). Purification of olive mill wastewater phenols through membrane filtration and resin

adsorption/desorption. *J Hazard Mater*, *285*, 69-76. https://doi.org/10.1016/j.jhazmat.2014.11.038

Zayed, A. M., Metwally, B. S., Masoud, M. A., Mubarak, M. F., Shendy, H., Petrounias, P., & Abdel Wahed, M. S. M. (2023). Facile synthesis of eco-friendly activated carbon from leaves of sugar beet waste as a superior nonconventional adsorbent for anionic and cationic dyes from aqueous solutions. *Arabian Journal of Chemistry*, *16*(8). https://doi.org/10.1016/j.arabjc.2023.104900

Zhang, T., Wang, W., Zhao, Y., Bai, H., Wen, T., Kang, S., Song, G., Song, S., & Komarneni, S. (2020). Removal of heavy metals and dyes by clay-based adsorbents : From natural clays to 1D and 2D nano-composites. *Chemical Engineering Journal*. https://doi.org/http://doi.org/j.cej.2002.127574

Zhang, W., Duo, H., Li, S., An, Y., Chen, Z., Liu, Z., Ren, Y., Wang, S., Zhang, X., & Wang, X. (2020). An overview of the recent advances in functionalization biomass adsorbents for toxic metals removal. *Colloid and Interface Science Communications*, *38*. https://doi.org/10.1016/j.colcom.2020.100308

Zhao, N., Zhao, C., Lv, Y., Zhang, W., Du, Y., Hao, Z., & Zhang, J. (2017). Adsorption and coadsorption mechanisms of Cr(VI) and organic contaminants on H(3)PO(4) treated biochar. *Chemosphere*, *186*, 422-429. https://doi.org/10.1016/j.chemosphere.2017.08.016

Zhu, Y., Kolar, P., Shah, S. B., Cheng, J. J., & Lim, P. K. (2017). Simultaneous mitigation of p-cresol and ammonium using activated carbon from avocado seed. *Environmental Technology & Innovation*. https://doi.org/10.1016/j.eti.2017.10.006

Zourou, A., Ntziouni, A., Adamopoulos, N., Roman, T., Zhang, F., Terrones, M., & Kordatos, K. (2022). Graphene oxide-CuFe2O4 nanohybrid material as an adsorbent of Congo red dye. *Carbon Trends*, *7*. https://doi.org/10.1016/j.cartre.2022.100147

Zuo, X., Liu, Z., & Chen, M. (2016). Effect of H2O2 concentrations on copper removal using the modified hydrothermal biochar. *Bioresour Technol*, *207*, 262-267. https://doi.org/10.1016/j.biortech.2016.02.032